Stony Brook University

Effects of Blood Glucose Elevation on the Structure and Function of Microvascular Networks of Skeletal Muscle in Mice

A Dissertation Presented

by

Melissa Katherine-Barrell Georgi

to

The Graduate School

in Partial Fulfillment of the

Requirements

for the Degree of

Doctor of Philosophy

in

Biomedical Engineering

Stony Brook University

May 2010

Stony Brook University

The Graduate School

Melissa Katherine-Barrell Georgi

We, the dissertation committee for the above candidate for the Doctor of Philosophy degree, hereby recommend acceptance of this dissertation.

Dr. Mary D. Frame – Dissertation Advisor
Associate Professor
Department of Biomedical Engineering

Dr. Peter Brink – Chairperson of Defense
Chairman, Department of Physiology and Biophysics

Dr. Helmut Strey
Associate Professor
Department of Biomedical Engineering

Dr. Mohammad Kiani – Outside Member
Chairman, Department of Mechanical Engineering
Temple University

This dissertation is accepted by the Graduate School

Lawrence Martin
Dean of the Graduate School

Abstract of the Dissertation

Effects of Blood Glucose Elevation on the Structure and Function of Microvascular Networks of Skeletal Muscle in Mice

by

Melissa Katherine-Barrell Georgi

Doctor of Philosophy

in

Biomedical Engineering

Stony Brook University

2010

Diabetes Mellitus and its precursor, pre-diabetes, are metabolic disorders that are characterized by high levels of elevated blood glucose. This work addresses the effects of these diseases on the microvasculature of the peripheral cardiovascular system including endothelial dysfunction and capillary rarefaction, which lead to circulation problems and secondary complications. The purpose of this study is to develop an understanding of the arteriolar network architecture and function in peripheral skeletal muscle in the normal mouse and to investigate the effects of alterations in blood glucose.

We demonstrate that only two hours of elevated glucose concentration decreases dilatory responses in both endothelium dependent and endothelium independent pathways in normal mice. Additionally, two hours elevation of glucose concentration shows early evidence of shear dysregulation in the networks. To investigate the effects of chronic full-blow diabetes, two leptin-challenged models of metabolic syndrome were used. Baseline non-fasting blood glucose differs between strains; The ob/ob mice had an elevated non-fasting blood glucose level as compared with the wild type mice, and the diabetic

mice had an extremely elevated non-fasting blood glucose level. Architecture was significantly different in the metabolic models. Total network length was decreased in the db/db model and increased in the ob/ob model as compared to C57 animals. C57 and ob/ob animals had a similar number of bifurcations per network, while the db/db animals had fewer. The feed diameter of the db/db mice were significantly smaller than normal C57 mice overall when bifurcation sequence was not taken into account. Additionally, when analyzed by bifurcation sequence, the db/db strain had significantly smaller diameters (feed and branch) than both the C57 and the ob/ob mice at only the first bifurcation. Changes in cytokine expression are distinct between the three mouse strains which may be related to architecture. Patterns in blood flow and flux are altered in the metabolic models as compared to metabolically normal mice.

These data suggest that a brief elevation in glucose has effects that may be related to the significant changes in structure and function seen in the metabolically challenged models of diabetes.

Table of Contents

List of Figures

List of Tables

List of Abbreviations

Ach: acetylcholine
η : fluid viscosity
AGEs: Advanced glycation endproducts.
AVI: audio video interleave – digital video format
cGMP: cyclic guanylyl monophosphate
D : diameter
ECM: Extracellular Matrix
F_{in} : Flow into a section of vessel
F_{out} : Flow out of a section of vessel
GLUT**:** Glucose transporter
ICCD: Intensified charge coupled device
LNNA: N^{ω}-nitro-L-arginine
mg/dl: milligrams per deciliter – clinical measurement of blood glucose concentration
NA: numerical aperture
NO: nitric oxide
NTSC: National Television Standards Committee – standard analog broadcast television signal in the US.
PDGF: platelet derived growth factor
r : radius
R : Flow resistance
RBC: Red blood cell
SNP: Sodium Nitroprusside
SWI: Salt water immersion
T : Shear stress
$\bar{u}$: mean axial fluid velocity
V_{in} : Velocity into a section of vessel
V_{out} : Velocity out of a section of vessel
VEGF: vascular endothelial growth factor
VSM: Vascular smooth muscle
XRITC: tetramethyl rhodamine isothiocyanate

Acknowledgements

To call this work the product of a single individual would be failing to acknowledge all of the people who made it possible for me to complete it. To try and name each and every person who had a hand in this undertaking is, in point of fact, impossible. I will however acknowledge those that had a particularly large part and to whom I owe great thanks.

First and foremost, I will ever be indebted to my advisor, Dr. Molly Frame, for teaching me everything I know, putting up with my stubbornness, my tears, and all of the wrenches I threw in the works over these last several years.

As for the contents of these pages, the contributions of many undergraduates and graduate students who passed through the lab cannot be ignored. To Warda Zaman, Jackie Vigilance, Anthony Dewar, Kevin De los Reyes, Irfan Asam, Michael Wong, Zia Sardar, and Alia Rizvi I say thank you for your hours of work, sometimes boring and repetitive, always appreciated. I would be remiss however, if I failed to offer special thanks to Saumya Sharma, without whose contribution this dissertation would never have been finished and my sanity would not have been maintained. Your countless hours and dedication to helping me make the most of the data collected has not gone unnoticed. Thank you so much, for all you have done.

To the Biomedical Engineering department at Stony Brook and their captain, Dr. Clint Rubin: Every member of this department went out of their way to make sure I succeeded. A more supportive group of teachers and administrators could not be wished for. And of course, to the two people who really make the department work, Anne Marie Dusatko and Wendy Scharf: Thank you for staying on top of all the red tape that is needed to make anything happen, and for making it possible for me to finish this work from a great distance without a hitch.

To all of my colleagues, friends and family who offered everything from the

inspiration to go to graduate school in the first place, to content advice, to a shoulder to cry on when times got tough: Ann and Howard Georgi, Geoff and Sara Georgi, James Nason, Suzanne Barrell, Dr. Sarah Nichols, Dr. Andrew Farke, Joe Groenke, Jessica Stanton, Gina Sorrentino, Dr. Suzanne Ferreri and oh so many others that are too many to enumerate: Thank you all.

To my parents, Sandra B. Nason and William A. Barrell: Thank you for supporting me through all my decisions, whether you understood them or not. You have made me who I am today and I owe a great deal of my success to you.

To my patient husband, Dr. Justin Georgi: Thank you for, well, everything. I love you more than you could ever imagine. Without you, I would never have managed to complete such an enormous undertaking or had quite as much fun as I did along the way.

And to my son Russell, who isn't yet old enough to understand what a great ride he is taking me on: Thank you for showing me why all of this matters.

I offer each of you my sincerest appreciation and undying gratitude for all you have shared with me. Thank you, from the bottom of my heart.

May 2010

Chapter I

Introduction

Clinical Background

Diabetes mellitus and its precursor, pre-diabetes, are metabolic disorders that affect the body's production or processing of insulin[1]. There are an estimated 17.9 million people in the United States with diabetes, and an additional 5.7 million with pre-diabetes. In total these estimates indicate that over 7% of the United States population is affected by diabetes with numbers increasing every year[2]. Complications of diabetes are known in most major organ systems, and often severely impact patient quality of life[2]. In the peripheral cardiovascular system, two of the most common complications are endothelial cell dysfunction and capillary rarefaction. Together, these complications lead to circulation problems including flow mismatch, in which blood flow is dysregulated over time, creating localized areas of hyper- and hypo-perfusion[3]. Poorly perfused tissue beds then suffer from secondary complications such as tissue necrosis and higher rates of infection.

Epidemiologically, impaired fasting glucose (indicating early stage metabolic disorder) and impaired endothelial cell function are correlated[4], but little is known about whether there is a causal relationship between the two, and if so, by what mechanism glucose acts to affect endothelial cell function. Similarly, there is no understanding of whether endothelial cell dysfunction alone can be held responsible for the development of flow heterogeneity within peripheral tissues in the diabetic or whether other mechanisms are present.

Statement of the Problem

While it is clear that patients with metabolic disorders suffer from a range of complications, both primary and secondary, there are several missing links

between the change in metabolic state and the development of those complications. It is the goal of this dissertation to investigate endothelial cell dysfunction and blood flow heterogeneity in the microcirculation in normal mice under acute elevations of glucose and in two models of metabolic disease, the diabetic (db/db) and obese (ob/ob) mice. This will be achieved by describing the phenotypic characteristics in a diabetic model and determining whether acute glucose elevation in a metabolically normal model elicits precursors to those changes.

Purpose of the Study

The purpose of this study is to develop an understanding of the arteriolar network architecture and flow in peripheral skeletal muscle in the normal mouse and in leptin deficient murine models of diabetes, and to investigate architectural changes and blood flow heterogeneity as potential consequences of alterations in blood glucose.

Specific Aims

This study has four specific aims,

Aim 1: To determine the effects of elevated glucose on the vasodilative responses of peripheral skeletal arteriolar networks.

A hallmark of metabolic disorder is endothelial cell dysfunction, typically characterized by impaired nitric oxide mediated dilation. In a recent epidemiological study, endothelial cell dysfunction, measured by diminished flow mediated dilation (FMD), has been shown to positively correlate with impaired fasting glucose[4]. These results may indicate that the early stages of cardiovascular disease are concurrent with the early stages of type 2 diabetes. Whether the elevation in blood glucose in the early stages of diabetes is responsible for the endothelial cell dysfunction has yet to be determined.

Flow mediated dilation in the arterioles requires a functional endothelium. It utilizes endogenously produced nitric oxide, produced from the action of

endothelial nitric oxide synthase, to increase the concentration of cGMP within the cells. On the other hand, exogenous nitric oxide elicits a dilatory response regardless of the function of the endothelium.

Hypothesis 1.1: Peripheral arteriolar networks in normal mice will have a consistent and predictable vasodilatory response to sodium nitroprusside (SNP) and acetylcholine (Ach).

Hypothesis 1.2: In normal mice, two hours of acute elevated glucose treatment will reduce the vasodilatory response to acetylcholine, but not SNP.

Hypothesis 1.3: In the db/db and ob/ob mouse models, vasodilatory response to SNP will not be altered. Vasodilatory response to Ach will be damped.

Hypothesis 1.4: In normal mice with acutely induced endothelial dysfunction, the SNP dilatory response will remain unchanged, and the Ach response will be entirely removed.

Aim 2: To determine the effects of acute elevated glucose and chronic metabolic disease on the architecture of peripheral skeletal arteriolar networks.

Clinical studies have shown that structural vascular rarefaction, a decrease in the number of blood vessels per tissue area, is seen in the skeletal muscles of diabetic patients[5,6]. Sustained low blood flow is linked to impaired vascular remodeling and rarefaction[7,8]. Arteriolar network flow may be affected by the architecture of the network, including parameters such as branch angles[9] and variations in diameter axially along vessel segments[10]. In order to understand the role of rarefaction in the diabetic pathology, arteriolar network architecture first must be defined in the normal state, and then compared to networks from diabetics. This aim will define normal terminal arteriolar network structural architecture and characterize the changes in the architecture brought about by chronic metabolic disease. Diameters, number of branches, branch angles and network lengths will be used to define network architecture. This aim addresses the following four hypotheses:

Hypothesis 2.1: Peripheral skeletal arteriolar networks in normal mice will have a consistent and predictable architecture, with branch angles and length of the feed section between branches dependent on sequential branch order. Diameters will be statistically similar for homologous segments across networks.

Hypothesis 2.2: In normal mice, two hours of acute elevated glucose treatment will not change the architecture of the peripheral skeletal arteriolar networks.

Hypothesis 2.3: In the db/db and ob/ob mouse models, peripheral skeletal arteriolar networks will be altered compared to normal mice; the length of feed between branches will be lengthened due to a smaller number of branches present, and diameters will decrease.

Hypothesis 2.4: In normal mice with acutely induced endothelial dysfunction, the only architectural change to the network will be slightly decreased average resting diameters, as compared to normal mice.

Aim 3: To determine the effects of acute elevated glucose and chronic metabolic disease on red blood cell (RBC) distribution within peripheral skeletal arteriolar networks.

When taken as a whole, normal peripheral vascular flow is homogeneous with respect to solute delivery to the tissues. However, at individual microvascular locations, a normal time and metabolism dependent heterogeneity of flow is observed[11,12]. One rheological mechanism that may be responsible for local heterogeneity of flow is plasma skimming, a phenomenon in which there is a differential distribution of red blood cells at a branch point[13]. Secondly, within a network, flow is distributed to sequential terminal branch arterioles in a prescribed pattern[14], which can be disrupted in a pathological state[15]. Specifically, this disruption involves shunting of flow through the arteriolar network to the anatomically larger terminal branch of the network[15]. Of course, red blood cell distribution affects the distribution of oxygen to the capillary beds. The impact of elevated glucose levels on the distribution of red blood cells has not previously been investigated and may be a key factor in the dysregulation of

blood flow seen in the microcirculation of diabetics. This aim addresses the question of how red blood cell distribution is affected by elevated glucose levels by the following four hypotheses:

Hypothesis 3.1: Red blood cell distribution in normal mice will have a predictable pattern based on network geometry, including the curvature of the bifurcation at the point of flow split, with more red blood cells being distributed to the first branch of the network and fewer being distributed downstream.

Hypothesis 3.2: In normal mice, two hours of acute excess glucose treatment will dysregulate red blood cell distribution, with upstream branches receiving fewer red blood cells and a higher flux of red cells will pass to the downstream branches.

Hypothesis 3.3: In the diabetic and obese mouse models, red blood distribution will be dysregulated, characterized by shunting of all red blood cells to the last branch.

Hypothesis 3.4: In normal mice with induced endothelial dysfunction, red blood cell distribution will be identical to elevated glucose effects, with upstream branches receiving reduced red blood cell flux and a higher red blood cell flux being passed to the downstream branches.

Aim 4: To determine the effects of acute elevated glucose and chronic metabolic disease on velocity and shear stress distribution within peripheral skeletal arteriolar networks.

Endothelial cells are believed to be the primary mechanotransducer of shear stress in the microcirculation[16,17,18], and as such are responsible for the regulation of tone and flow. Clinically, significant alterations in microvascular blood flow regulation and vasoresponsivity are reported in the extremities of diabetic patients as measured with various laser doppler methods[19]. An alteration such as a decrease in diameter will result in a decreased velocity for the same mass flow. This, in turn, will reduce the shear rate sensed along the vessel walls. The decrease in shear rate would alter the signals transduced, which would result in a further reduction in diameters. Alternately, an increase in

velocity would be caused by a decrease in diameter. For either mechanism, homeostasis maintained by the sensing, transducing, and regulatory mechanisms of the vessels become increasingly disturbed. This aim addresses the question of whether elevated glucose causes a dysregulation of shear within the vessels, and if that dysregulation is associated with endothelial cell function by the following four hypotheses:

Hypothesis 4.1: Velocity distribution and axial shear rate distribution in normal mice will have a predictable pattern, with velocities and shear rate similar across branches. Within individual branch junctions, the highest velocity will be found along the apical wall at the junction of the bifurcation, resulting in the highest shear rate.

Hypothesis 4.2: In normal mice, two hours of acute excess glucose treatment will dysregulate velocity and shear rate distribution, with upstream branches experiencing a uniform drop in velocity and shear and downstream branches experiencing near normal velocity and shear. Within individual branch junctions, the peak shear at the apical wall will be reduced as compared to normal mice. The point of highest shear will no longer be consistent across branches.

Hypothesis 4.3: In the diabetic and obese mouse models, velocity and shear rate distribution will be dysregulated, with upstream branches experiencing very low velocities, and downstream branches near normal. Within individual bifurcations, shear rate at the apical wall will be reduced to the levels along the rest of the network, eliminating the point of highest shear at the apical wall of the junction altogether. Shear will be uniform along each bifurcation.

Hypothesis 4.4: In normal mice with induced endothelial dysfunction, velocity and shear rate distribution will be identical to that seen with acute excess glucose, with upstream branches experiencing a drop in velocity and shear and downstream branches experiencing near normal velocity and shear. Within individual branch junctions the shear at the apical wall will be reduced as compared to normal mice.

Relevance of the Study

With over twenty percent of the US population affected by metabolic diseases including diabetes, the loss of quality of life caused by peripheral cardiovascular complications is a significant health issue. The results from this study will further the understanding of how these complications develop by determining whether a direct link exists between elevations in blood glucose, endothelial dysfunction, and flow heterogeneity. As a result, the findings of this study will form a critical component of the knowledge base needed for development of clinical methodologies to both prevent and treat these complications in the affected population.

Scope of the Study

Diabetes Mellitus and metabolic disorder are complex and multifaceted diseases. This dissertation focuses on the structure and function of terminal arteriolar networks, comparing the effects of brief glucose exposure to that found in animals models of diabetes and obesity. Both positive and negative controls are included. The following statements are intended to define the focus of the study and the scope of possible interpretation of the results.

Vascular size and type: It is well established that the macrovasculature and microvasculature, commonly described as vessels larger or smaller than 100 microns respectively, are quite different both in structure and function. Similarly, the difference in structure and function between the veins and arteries are quite different at each scale. The subject of this study is solely the vessels within the arteriolar microcirculation.

Tissue Bed: Vascular research has shown that even at the same level of the circulation and in the same type of vessels, vascular behavior varies dependent upon the tissue type in which the vessels are found. To that end, this project has narrowed its scope to the skeletal microcirculation only.

Metabolic disease risk factor: There are dozens of physiological changes that are characteristic of metabolic syndrome and diabetes mellitus, blood sugar levels, cytokine levels, insulin production, level of tissue adiposity and high triglyceride levels, to name a few. This study isolates elevations in blood glucose levels as a study factor, while attempting to maintain as broad an applicability of results as possible.

Animal Model: There is variability in physiology across all mammalian species, and response to metabolic changes is no exception. These studies are performed in murine models, both metabolically normal inbred background mice (C57/bl6) and in two different leptin compromised strains (db/db and ob/ob). The db/db mice were selected as the test group with chronically elevated blood glucose, whereas ob/ob mice were selected as a leptin control that did not posses elevated blood glucose levels. These are common models in pre-clinical basic research, and the results will be a first step towards understanding the mechanisms of elevated glucose. It is also accepted however, that murine physiology and human physiology vary and in order for clinical applicability to be achieved, all studies must eventually be extended to human physiology.

Summary

Endothelial cell dysfunction and capillary rarefaction (loss of capillary density) are common microvascular complications in diabetics; both are precursors to poor wound healing and tissue necrosis. Elevated blood glucose is the hallmark of diabetes. It is unknown whether elevated glucose is the cause of the development of microvascular complications associated with diabetes. This study examines the effects of acute elevated glucose and chronic metabolic disease on several aspects of the peripheral microcirculation including the architecture, vascular reactivity and flow regulation. The effects on diameters flux and velocity of elevated glucose acutely (over two hours) are compared to the same parameters in animals with chronic diabetes. In this way, we will investigate early effects of elevations in glucose as potential initiators of

endothelial dysfunction and flow heterogeneity. The specific aim of this study is to understand arteriolar network flow in peripheral skeletal muscle in the normal mouse and in leptin compromised murine models of diabetes, and to investigate glucose induced endothelial dysfunction as a rheological phenomenon. Understanding the relationship between the acute and chronic effects of endothelial dysfunction on the blood flow in the skeletal peripheral microvasculature may lead to better treatment of complications seen clinically in diabetics by allowing early treatment intervention.

References Cited

1. American Diabetes, A. (2006). "Diagnosis and Classification of Diabetes Mellitus." Diabetes Care **29**(suppl_1): S43-48

2. Centers for Disease Control and Prevention. (2007) “National diabetes fact sheet: general information and national estimates on diabetes in the United States.” Atlanta, GA: U.S. Department of Health and Human Services, Centers for Disease Control and Prevention.

3. Utriainen, T., Nuutila, P., et al. (1997). “Intact insulin stimulation of skeletal muscle blood flow, its heterogeneity and redistribution, but not of glucose uptake in non-insulin-dependent diabetes mellitus.” J. Clin. Invest. **100**(4): 777-785

4. Rodriguez, C., Miyake, Y., et al. (2005). “Relation of plasma glucose and endothelial function in a population-based multiethnic sample of subjects without diabetes mellitus.” Am J. Cardiol. **96**(9): 1273-1277

5. Marin, P., B. Andersson, et al. (1994). "Muscle fiber composition and capillary density in women and men with NIDDM." Diabetes Care **17**(5): 382-386.

6. Mathieu-Costello, O., A. Kong, et al. (2003). "Regulation of skeletal muscle morphology in type 2 diabetic subjects by troglitazone and metformin: Relationship to glucose disposal." Metabolism **52**(5): 540.

7. Wang, D. H. and R. L. Prewitt (1993). "Alterations of mature arterioles associated with chronically reduced blood flow." Am J Physiol Heart Circ Physiol **264**(1): H40-44.

8. Buus, C. L., F. Pourageaud, et al. (2001). "Smooth Muscle Cell Changes During Flow-Related Remodeling of Rat Mesenteric Resistance Arteries." Circ Res **89**(2): 180-186.

9. Noren, D., H. J. Palmer, et al. (2000). "Predicted wall shear rate gradients in T-type arteriolar bifurcations." Biorheology **37**(5-6): 325-40.

10. Rossitti, S. and J. Lofgren (1993). "Vascular dimensions of the cerebral arteries follow the principle of minimum work." Stroke **24**(3): 371-377.

11. Laine, H., M. J. Knuuti, et al. (1998). "Preserved Relative Dispersion but Blunted Stimulation of Mean Flow, Absolute Dispersion, and Blood Volume by Insulin in Skeletal Muscle of Patients With Essential Hypertension." Circulation **97**(21): 2146-2153.

12. De Backer, D., J. Creteur, et al. (2002). "Microvascular Blood Flow Is Altered in Patients with Sepsis." Am. J. Respir. Crit. Care Med. **166**(1): 98-104.

13. Kiani, M. F., A. R. Pries, et al. (1994). "Fluctuations in microvascular blood flow parameters caused by hemodynamic mechanisms." Am J Physiol Heart Circ Physiol **266**(5): H1822-1828.

14. Koller, A. and G. Kaley (1991). "Endothelial regulation of wall shear stress and blood flow in skeletal muscle microcirculation." Am J Physiol Heart Circ Physiol **260**(3): H862-868.

15. Frame, M., Sarelius, I., (1993) “Regulation of capillary perfusion by small arterioles is spatially organized.” Circulation Research **73**(1):155-163

16. Mustafa, S., Rivers, R., (1999) “Microcirculatory basis for nonuniform flow delivery with intravenous nitroprusside.” Anesthesiology **91**(3):723-731.

17. Secomb, T. W., R. Hsu, et al. (2001). "Effect of the endothelial surface layer on transmission of fluid shear stress to endothelial cells." Biorheology **38**: 143 - 150.

18. Weinbaum, S., X. Zhang, et al. (2003). "Mechanotransduction and flow across the endothelial glycocalyx." PNAS **100**(13): 7988-7995.

19. Belcaro, G., S. Vasdekis, et al. (1989). "Evaluation of skin blood flow and venoarteriolar response in patients with diabetes and peripheral vascular disease by laser Doppler flowmetry." Angiology **40**(11): 953-7.

Chapter II

The Structure and Function of the Microcirculation and the Effects of Diabetes: A Review

Introduction

Diabetes mellitus and its precursor, pre-diabetes, are metabolic disorders that affect the body's production or processing of insulin[1]. In 2007 there were an estimated 17.9 million people in the United States with diabetes, and an additional 5.7 million with pre-diabetes. In total these estimates indicate that over 7% of the United States population is affected by diabetes with numbers increasing every year[1]. Complications of diabetes are known in most major organ systems, and often severely impact patient quality of life.

The microcirculation is a target for diabetic complications. This chapter is an overview of the structure and function of the microcirculation under physiologically normal conditions including descriptions of the relevant fluid mechanics. Following this is a brief summary of the pathology associated with diabetes and the known effects of diabetes upon the microcirculation.

Microvascular Biology

Microvascular Anatomy and Basic Function: Three major types of vessels are found in the circulatory system: arteries, veins and capillaries. Arteries take flow away from the heart, and are responsible for the maintenance of blood pressure. Arteries are composed of three distinct layers, the intima, the media, and adventitial layers. The intima, made up of endothelial cells, lines the inside of the vessels and is in direct contact with the blood. The media is made up of vascular smooth muscle (VSM) cells wrapped circumferentially around the vessel, and is responsible for the maintenance of vessel tone, or the amount of dilation and constriction that the vessel undergoes. The adventitial layer is comprised of connective tissue and encircles the vessel on the abluminal

surface. In the circulatory system, larger arteries branch into smaller arteries, and finally into arterioles. Arterioles regulate blood to the capillary networks. In order to facilitation nutrient exchange with the tissues, capillaries have only an endothelial layer and a thin connective tissue layer. Without a smooth muscle layer, there is little diameter regulation within the capillaries, resulting in passive blood flow. From the capillaries, blood flows to venules (the smallest veins) which run together into larger and larger veins until finally returning to the heart. Veins have a thinner vessel wall with less vascular smooth muscle, and much less connective tissue.

Angiogenesis and vascular remodeling: Angiogenesis is the process by which new blood vessels are formed. In a hypoxic tissue, an existing vessel will form a new branch that grows in the direction of the low-oxygenation signal[3]. Angiogenesis occurs in three steps: 1) dissociation of cellular connections of existant vessel tissue 2) proliferation and migration of endothelial cells and 3) assembly and lumen formation[4]. The process of angiogenesis is often triggered by release of nitric oxide (NO), which causes vasodilation as well as upregulation of vascular endothelial growth factor (VEGF) transcription[4]. Primarily, control of angiogenesis is through the action of vascular endothelial growth factor[5,6]. The release of VEGF is responsible for the earliest stages of angiogenesis including an increase in vascular permeability and the subsequent extravasation of plasma proteins, necessary for creating an extravascular support structure for migrating cells[4,7]. Subsequently VEGF acts to increase the proliferation and migration of endothelial cells[5,7]. Several other molecules are responsible for mediating angiogenesis, for a full review see Conway[4]. The processes of vasculogenesis, growth of blood vessels without previous vessels present, and arteriogenesis, growth of new blood vessels as sprouts or branching off of old vessels, both occur through similar processes, the distinctions between the two are not yet well understood[8,9]. Vascular remodeling is initiated by apoptosis of vascular cells. Apoptosis is a mechanism by which cells undergo pre-programmed death. Pathologic levels of apoptosis can be triggered by any number of stimuli,

including a loss of functional ECM[10,11] and loss of hemodynamic forces generated by flow[12]. Following apoptosis, it appears that a process similar to angiogenesis or arteriogenesis occurs. The important caveat is that in normal healthy tissue, the microcirculation is continually remodeling, presumably to meet the changing metabolic needs of the tissue[58]. These processes all work in concert to determine vascular architecture in response to environment.

Extracellular matrix (ECM) interaction with blood vessels: The ECM plays a key role in the development survival and function of vascular endothelial cells. An ECM is necessary for angiogenic development of the vasculature both initially and in remodeling[13]. Loss of ECM induces apoptosis and therefore eliminates EC survival[10,11,14]. Mechanically, the ECM is required for shear sensing and mechanotransduction by ECs[15-18] and vascular tone maintenance through the myogenic response[16]. Additionally the ECM affects the transmission of remote responses along the vascular network[20].

Factors affecting microvascular flow

Rheology of blood flow: Fluid flow through cylindrical tubes is well characterized. For an incompressible viscous fluid, laminar flow through a tube can be described mathematically using the Hagen–Poiseuille equation (commonly referred to as the Poiseuille equation). The Hagen-Poiseuille equation is shown below, where ΔP is the pressure drop across the tube, η is the viscosity of the fluid, L is the tube length, Q is the volumetric flow rate and r is the radius of the tube.

$$\Delta P = \frac{8\eta L Q}{\pi r^4} \qquad \text{(equation 2.1)}$$

This equation highlights the important fact that for any tube, the flow will be proportional to the radius of the tube to the fourth power, whereas all of the other factors are only to the first power and less influential.

Resistance: Within the circulation, resistance to blood flow is a major determinant of cardiac function and of blood flow. Resistance is determined by the size of individual vessels (length and diameter), the organization of the vascular network (series and parallel arrangements), physical characteristics of the blood (viscosity, laminar flow versus turbulent flow), and extravascular mechanical forces acting upon the vasculature. Mathematically, resistance can be calculated by a rearranged version of Poiseuille's Law that corresponds to Ohm's law, seen in equation 2.2, where Q is the volumetric flow rate, ΔP is the pressure drop across the vessel and R is the resistance.

$$Q = \frac{\Delta P}{R} \qquad \text{(equation 2.2)}$$

By comparing equation 2.2 to equation 2.1, we can see that R is equal to $8\mu L/\pi r^{4.}$ It is then apparent that resistance to blood flow within a vascular network is predominantly a factor of vessel radius. Changes in vessel diameter, particularly in small arteries and arterioles, enable organs to adjust their own blood flow to meet the metabolic requirements of the tissue. Therefore, if an organ needs to adjust its blood flow (and therefore, oxygen delivery), cells surrounding these blood vessels release vasoactive substances that can either constrict or dilate the resistance vessels.

Shear stress: The flow of a viscous fluid through a tube will always be fastest at the centerline of the tube and zero along the tube walls due to friction between the flowing fluid and the static wall. The differential velocities of the layers of fluid cause a force to be generated between those layers. This force is termed shear stress. For a Newtonian fluid flowing through a tube, shear stress, T, is calculated by the equation below where η is the viscosity of the fluid, v is the velocity of the fluid at a distance, r from the wall of the tube.

$$\mathrm{T} = \eta \frac{dv}{dr} \qquad \text{(equation 2.3)}$$

Equation 2.3 calculates the shear stress as a function of the flow velocity profile, regardless of the shape of that profile. In the case of the microcirculation, where the viscosity of the blood is indeterminate, calculating shear stress is often discarded in favor of calculating shear rate at the wall, as shown below in equation 2.4.

$$\dot{\gamma} = \frac{dv}{dr} \qquad \text{(equation 2.4)}$$

If you can assume a parabolic velocity profile, there is a second equation available for the approximation of shear rate, shown as equation 2.5, where D is the diameter of the vessel, and $\overline{u}$ is the mean axial fluid velocity.

$$\dot{\gamma} = \frac{8\overline{u}}{D} \qquad \text{(equation 2.5)}$$

Equation 2.5 allows the approximation of shear rate when you cannot get dv/dr, taking into account the entire flow field.

Viscosity: When fluids flow the internal friction between the flowing layers of fluid is called viscosity. Viscous fluids also exert friction on the surfaces over which they flow. This results in a gradient of velocity that goes from zero at the surface-to-fluid interface, to a maximum at the maximum distance from the surface. For a cylindrical tube, that maximum is the centerline. Viscosity is independent of the speed of flow for a Newtonian fluid. If the viscosity is not independent of the speed of flow, the fluid is termed non-Newtonian. Blood is a non-Newtonian fluid, because the particulate matter within the plasma distributes differentially throughout the fluid (see below).

Reynold's number: Reynold's number is a dimensionless term that describes the relative inertial forces to the viscous resistance forces in a system. In the microcirculation, the viscous forces predominate, as opposed to the macro-circulation where inertial forces predominate. In engineering terms, the Reynold's number (Re) is well above unity for the macro-circulation and below unity in the microcirculaton. This has important implications for the predicted

shear gradients at bifurcations, or as fluid travels through a curving section of the blood vessel. In high Reynold's flow, where inertial forces predominate, flow along the wall of a curved vessel will be higher on the branching wall of the vessel just after the bifurcation[21]. On the other hand, in low Reynold's flow, it would be expected that the highest shear gradients would be on the branching wall of the feed just prior to the bifurcation[22]. The Re value will also predict whether the flow will travel along its streamlines (laminar flow, Re<2300) or not (turbulent flow, Re>4000[21]) therefore affecting the flow behavior along the wall, for intermediate Reynold's numbers, the flow field has both laminar and turbulent properties, with characteristic eddies and vortices. The low Re conditions, with the non-Newtonian two-phase nature of microvascular flow has interesting consequences for how red blood cells distribute at branch points, as noted next.

Two Phase flow: (RBC flow vs. Bulk Flow): Blood is a two-phase fluid. The fluid phase is plasma, a protein rich fluid in which the solid phase is suspended. The solid phase is made of up red blood cells, white blood cells and platelets. Red blood cells are responsible for oxygen transport, white blood cells are integral in the immune response, and platelets play a key role in clotting[23].

Because blood has two phases, it has a viscosity that is dependent upon the shearing rate and is therefore classified as non-Newtonian. Non-Newtonian flow is not well understood, and often impossible to treat mathematically from first principles. Computational estimations are sometimes possible, but more often, relationships are derived empirically[24].

Additionally, when in the microcirculation, the ratio of the radius of the red blood cells to the radius of the blood vessels approaches unity. This fact causes some of the interesting fluid flow characteristics of the microcirculation (see Fahraeus Effect, below). This phenomenon begins when the tube diameter is approximately 20x the RBC diameter.

The primary purpose of the circulation is the delivery of oxygen to the tissues. To that end, it is not flow volume, but rather the number of red blood cells (RBC) that is important for a functional circulatory system. This measure is

referred to as RBC flux. RBC flux is easily approximated by volumetric flow rate in the larger vessels in the circulatory system. However, in the microcirculation, the high particle to tube diameter ratios change distribution of red cells significantly.

One rheological mechanism that may be responsible for local heterogeneity of flux is plasma skimming, a phenomenon in which there is a differential distribution of red blood cells at a branch point and a resultant change in the local apparent viscosity of the blood[25]. Variations in local apparent viscosity would act to alter flux patterns by altering the concentration of red blood cells within each streamline of flow.

Fahraeus and Fahraeus-Lindquist effects:The large particle to tube diameter ratio that is seen in the microcirculation is responsible for a number of microcirculation-specific phenomena. The Fahraeus effect is one such phenomenon. The Fahraeus effect describes the apparent decrease in the tube hematocrit (the fraction of RBCs per total blood volume) within the smallest vessels as compared to the systemic hematocrit, or discharge hematocrit, that would be collected for a typical blood sample. When flowing through microvessels, the red blood cells travel faster than the plasma. Since the RBCs travel faster than the plasma, proportionately fewer are present within a single microvessel at one instant in time – hence the tube hematocrit is lower than the systemic hematocrit. In contrast, the systemic hematocrit (discharge hematocrit) reflects the correct proportion of the volume of RBC relative to the volume of plasma within the stationary fluid. As the hematocrit of blood is one of the chief determinants of its apparent viscosity, a consequence of the Fahraeus effect is that the viscosity continually changes within the microcirculation, making it difficult to estimate.

Another phenomenon resulting from the large particle to tube diameter ratio in the microcirculation is the Fahraeus-Lindqvist effect. Due to the Fahraeus effect (above), the particles are carried along the midline of flow. This leaves the region of fluid immediately adjacent to the walls nearly particulate free.

A layer of particulate free flow at the wall reduces the apparent viscosity of the fluid by decreasing the particle concentration at the point of wall contact, and increases the particle concentration in the centerline[26]. The consequence is that apparent viscosity decreases as the tube diameter approaches the size of the red blood cell.

One rheological consequence of the Fahraeus-Lindquist effect is plasma skimming, a phenomenon in which there is a differential distribution of red blood cells at a branch point due to the layer of fluid at the branching wall having fewer RBC than the fluid in the center of the tube. As a result, there is a change in the local apparent viscosity of the blood[25]. By altering the local concentration of red blood cells within each streamline of flow, flux distribution within the networks will be affected.

Permeability: Blood flow is also regulated by permeability within the vasculature. A sudden increase in permeability will cause an increase in the volume of fluid that leaves the capillaries, drawing increased flow through the vessel

Osmolarity: In addition to permeability, hydrostatic and osmotic forces also determine the amount of fluid movement across the capillary walls according to Starling's equation. Starling's equation is shown below where (equation 2.6) J_v is the net fluid movement from the capillary to the interstitial space, S is the surface area, L_p is the hydraulic conductivity of the capillary wall, P_c is the capillary hydrostatic pressure, P_i is the interstitial capillary hydrostatic pressure, π_c is the capillary oncotic pressure, π_i is the interstitial oncotic pressure, and σ is the reflection coefficient[23].

$$J_v / S = L_P \left([P_c - P_i] - \sigma [\pi_c - \pi_i] \right) \qquad \text{(equation 2.6)}$$

Blood Flow Regulation

The hydrostatic pressure within the capillaries is dictated by many factors, the dilation state of the precapillary arterioles being the most important. The majority of the other factors are, under normal conditions, relatively constant[23].

Blood flow to the capillaries is mostly regulated by the arterioles, with as much as 60% of control handled by the terminal arterioles[27]. Terminal arterioles are the smallest arterioles located immediately upstream of the capillary beds. These vessels have one to two layers of vascular smooth muscle that provides an active control of vessel tone. These vessels form discrete networks of predictable shape which respond to a number of signals: chemical, electrical and mechanical which control the dilation of the individual arteriole segments in a manner that is dependent on the location of that segment within the network[28].

Endothelial Cell Function and FMD: The endothelial cells within the microcirculation perform a multitude of functions. The endothelial cells not only serve as a selective barrier for transport of proteins but also participate in the coagulation and inflammation responses, regulate vascular tone, and actively participate in angiogenesis[29]. From a rheological perspective, the endothelial cells serve two significant functions, maintenance of vascular tone, and the mechanotransduction of the shear stress signal generated by the flowing blood.

Arterioles with a functional endothelium readily exhibit flow mediated dilation (FMD). FMD is a mechanotransduction response to sudden elevations in flow (fluid shear stress) causing activation of endothelial nitric oxide synthase (eNOS) within endothelial cells to endogenously produce nitric oxide (NO)[30]. NO diffuses to the vascular smooth muscle cells, increasing the concentration of cyclic guanosine monophosphate (cGMP), causing intracellular calcium sequestration within the vascular smooth muscle cells, and dilation[31]. Through this mechanism, the shearing forces generated by the blood flow through the vessels are a key factor in the regulation of vascular tone. Acetylcholine (Ach) is one of several pharmacological agents to trigger this set of pathways. This

phenomenon is completely endothelium dependent[32], and can be bypassed by pharmacological NO donors such as sodium nitroprusside (SNP).

Vascular Smooth Muscle Function: The VSM layer in the arterioles is responsible for the control of vascular tone in the arterial microcirculation. There are a number of pathways that lead to the contraction of VSM, all of which ultimately lead to an increase in the calcium concentration within the muscle cell. Calcium binds to calmodulin and subsequently activates myosin light chain kinase. Myosin light chain kinase is the enzyme responsible for the phosphorylation of myosin light chains which, when phosphorylated, create the crossbridges to actin necessary for contraction of the muscle. These signal transduction pathways act locally within the tissue and therefore may be affected by the local pharmacological state of the tissues.

Vasomotor function and regulation of network flow distribution: In the peripheral tissues of the body, the delivery of nutrients and oxygen is dependent on a number of anatomical, chemical and mechanical factors, including the number of capillaries, transport distance from the microvessels (source) to the tissues (sink), the volume and velocity of the flow, the type of transport (active or passive) required to deliver nutrients to the cells that make up the tissues and the amount of nutrients in the oxygen within the blood stream.

It is widely believed that the network regulation of blood flow to the capillaries is handled in the terminal arterioles, the vessels immediately upstream of the capillaries. These vessels form discrete networks of predictable shape which respond to a number of signals, chemical, electrical and mechanical, that control the dilation of the individual arteriole segments in a manner that is dependent on the location of that segment within the network[33].

Diabetes

Clinical aspects of diabetes mellitus: The single most important indicator of diabetes is an elevated blood glucose level. In the normal non-diabetic patient, ideal fasting capillary blood glucose levels are below 90 mg/dl[35]. According to the American Diabetes Association, to be diagnosed as pre-diabetic, a patient's fasting capillary blood glucose levels are between 100 and 125 mg/dl, while diabetics have fasting capillary blood glucose levels above 125 mg/dl[1]. There are many reasons why blood glucose elevations can occur. The two most common are insulin deficiency (type I diabetes) and insulin resistance (type II diabetes).

Elevated blood glucose levels increase interstitial glucose[35-37], leading to systemic hyperglycemic exposure. Short term hyperglycemia has not been shown to cause direct damage to organ function. It does have number of clinical symptoms, such as sensations of fatigue, weakness, and blurred vision. Elevations in blood also significantly affect fluid balance, increasing thirst and frequency of urination which in turn can lead to dehydration, and electrolyte imbalance in some patients. In addition, epidemiological studies have demonstrated that hyperglycemia is the primary factor associated with vascular complications in diabetics[38]. In tissues that do not require insulin for glucose uptake, including small blood vessels, elevated interstitial glucose levels cause glycation[39].

Time course of tissue glycation: Nonenzymatic glycation is a series of spontaneous chemical reactions which cause fructosamine formation from glucose by binding to the terminal amine groups of surface proteins[40]. This process is also known as the Maillard reaction[41]. Over time, these reactions yield chemical byproducts, known as advanced glycation endproducts (AGEs). AGEs have been demonstrated to be responsible for some of the symptoms and complications of diabetes, including stiffening of the cardiac wall, retinopathy, neuropathy, nephropathy and impaired wound healing[39-42].

The reversibility of the glycation process is directly proportional to the duration of the elevation of fluid glucose levels. In the normal patient, short bursts of elevated blood glucose, such as those that are present after a large meal, do not allow time for significant chemical reactions with exposed tissue proteins. However, elevation over longer periods, even as little as a half an hour, can cause nucleophilic addition of reducing sugars to exposed amino groups on tissue proteins, forming chemical products known as Schiff Bases[41]. This process is freely reversible, and with the return to normal blood glucose levels the sugars dissociate from the proteins without further chemical reactions.

If the elevation of blood glucose is a persistent event, lasting for a number of days, as is the case of metabolic syndrome, there is a rearrangement of the Schiff Bases, and formation of Amadori Products begins[39,41]. This process is effectively irreversible. The subsequent breakdown or further reactions of the Amadori products is one of the main sources of AGEs.

Chronic diabetics, patients with blood glucose levels remaining elevated for months or longer, accumulate AGEs systemically. The buildup of AGEs has been implicated in a number of diabetic complications e.g. retinal neuropathy and renal dysfunction[38,39].

Short term effects of glycation are less well understood. One study has focused on the effects of short term glycation on the changes in mechanical properties of the extracellular matrix[43]. Glycation inhibits actin organization, cellular migration and changes the mechanical properties of the ECM. Tang et. al. have recently shown that short term elevated glucose levels increase the production of collagen types I and III in the ECM[44]. Since collagen is one of the primary structural proteins in the ECM, changes in collagen production may lead to a change in mechanical properties in tissues throughout the body, and ultimately affect functions mediated by the ECM such as angiogenesis, apoptosis and mechanotransduction of shear sensing in the endothelial cells.

Cardiovascular complications of diabetes: There are several complications of diabetes seen clinically that affect the microcirculation. These include:

Endothelial dysfunction: Endothelial dysfunction is a condition in which the blood vessels demonstrate impaired endothelial mediated dilation. In addition to removing one of the most important regulators of blood flow, endothelial dysfunction has been demonstrated to be key in the development of many vascular processes and a early step in the development of atherosclerosis[45]. Elevations in blood glucose have been correlated with endothelial dysfunction[46,47,48]. The mechanism behind development of endothelial dysfunction in diabetics is still unknown. What is known is that endothelial cells are sensitive to elevated glucose levels[46], as they do not require insulin for the uptake of glucose. Glucose uptake is facilitated by a glucose transporter (GLUT) 1, the expression of which is independent of glucose levels[45].

Rarefaction: In chronic metabolic disorders, vascular density per tissue area is decreased as compared to normal tissue, a condition referred to as structural rarefaction[51,52]. Structural rarefaction is distinguished from functional rarefaction, where vessels are present but not perfused. A reduction in vascular density decreases perfusion to the tissues and results in poor wound healing and ulcer formation[53].

Inflammation and cytokines: Diabetes is a disease characterized by a chronic pro-inflammatory state. Clinically, patients with diabetes exhibit elevated markers of low-grade inflammation[54]. These markers are cytokines or cytokine-like molecules such as chemokines, or growth factors. The primary function of cytokines is to mediate the immune response. Several, however, have other roles and effects within the cardiovascular system, and changes in their expression due to chronic inflammation may have secondary effects on blood flow and vascular maintenance. These effects include acute manipulation of tone as vasoactive agents as well as long term initiators of remodeling and new vessel growth. A complete discussion of these cytokines is given in chapter V.

Leptin metabolism and diabetes

Leptin is an adipokine (a cytokine-like protein secreted from adipose tissue), and is primarily responsible for indicating energy sufficiency (satiety)[55]. There are 6 splice variants of the leptin receptor gene: the long-form LRb, four short-forms, LRa, c, d and f, and the secreted form LRe. LRb is linked to glucose and insulin metabolism[56]. The functions of the short forms and the secreted form are less well understood[57]. The LRb receptor splice variant is linked to glucose and insulin metabolism, as well as a number of other important functions[3]. Two murine models of diabetes have been bred with defects to Leptin processing. The db/db mouse possesses the LRb^{-}/LRb^{-} genotype and the ob/ob possesses the Lep^{-}/Lep^{-} (Leptin deficient) genotype. These models are discussed in greater detail in chapter V.

Summary

This dissertation examines both the physical forces of blood flow movement in the murine microcirculation, and the pathophysiological alterations in cellular function for the disease state of diabetes in mice. In specific, we have examined whether high glucose alone can induce endothelial cell dysfunction, and next defined the architectural and rheological changes that are induced by high glucose, and those that occur normally in a leptin deficient variety of type II diabetes.

References Cited

1) American Diabetes Assn. (2006). "Diagnosis and Classification of Diabetes Mellitus." Diabetes Care **29**(suppl_1): S43-48

2) Centers for Disease Control and Prevention. (2007) “National diabetes fact sheet: general information and national estimates on diabetes in the United States.” Atlanta, GA: U.S. Department of Health and Human Services, Centers for Disease Control and Prevention.

3) Pugh, C., Ratcliffe, P., (2003) “Regulation of angiogenesis by hypoxia: Role of the HIF system.” Nature Medicine **9**(6):677-684.

4) Conway, E., Collen, D., et. al. (2001) “Molecular mechanisms of blood vessel growth.” Cardiovascular Research **49**:507-521.

5) Carmeliet, P., (2003) “Angiogenesis in health and disease.” Nature Medicine **9**(6):653-660.

6) Ferrara, N., T. Davis-Smyth. (1997). “The Biology of Vascular Endothelial Growth Factor.” Endocrine Reviews **18**(1): 4-25.

7) Ferrara, N. (2001). “Role of vascular endothelial growth factor in regulation of physiological angiogenesis.” Am J Physiol Cell Physiol **280**: C1358-C1366.

8) Carmeliet, P., Collen, D., (1997) “Molecular analysis of blood vessel formation and disease.” Am. J. Physio. Heart Circ. Physiol. **273**:2091-2104.

9) Tkachuk, V., Plekhanova, O., et. al. (2009) “Regulation of arterial remodeling and angiogenesis by urokinase-type plasminogen activator.” Can. J. Physiol. Pharmacol. **87**: 231–251

10) Wu, W., Peng, H., et. al. (2003) “Disintegrin causes proteolysis of β-catenin and apoptosis of endothelial cells Involvement of cell—cell and cell—ECM interactions in regulating cell viability “ Experimental Cell Research **286**:115–127

11) Re, F., Zanetti, A., (1994) “Inhibition of Anchorage-dependent Cell Spreading Triggers Apoptosis in Cultured Human Endothelial Cells.” The Journal of Cell Biology **127**(2):537-546

12) Kaiser, D., Freyberg., M., et. al. (1997) “Integrin-mediated mechanotransduction requires its dynamic interaction with specific

extracellular matrix (ECM) ligands." Biochemical And Biophysical Research Communications. **231**: 586–590

13) Feng, X., Clark, R., et. al. (1999) "Fibrin and collagen differentially regulate human dermal microvascular endothelial cell integrins: Stabilization of αv/β3 mRNA by Fibrin." J. Invest. Derm. **113**: 913-919.

14) Meredith, J., Fazeli, B., et. al. "The Extracellular Matrix as a Cell Survival Factor." Molecular Biology of the Cell **4**: 953-961.

15) Takahashi, M., Berk, B., (1996) "Mitogen-activated Protein Kinase (ERK1/2) Activation by Shear Stress and Adhesion in Endothelial Cells Essential Role for a Herbimycin-sensitive Kinase" J. Clin. Invest. **98**:2623–2631

16) Davies, P., Tripathi, S., (1993) "Mechanical Stress Mechanisms and the Cell: An Endothelial Paradigm" Circulation Research **72**:239-245.

17) Shyy, J., Chien, S., (2002) "Role of Integrins in Endothelial Mechanosensing of Shear Stress." Circ. Res. **91**:769-775

18) Jalili, S., Pozo, M., et. al. (2001) Integrin-mediated mechanotransduction requires its dynamic interaction with specific extracellular matrix (ECM) ligands." PNAS **98**(3):1042-1046.

19) Davis, J., Wu, X., et. al. (2001) "Integrins and mechanotransduction of the vascular myogenic response." Am J Physiol Heart Circ Physiol **280**: H1427–H1433

20) Frame, M., Rivers R., et. al. (2007) "Mechanisms initiating integrin-stimulated flow recruitment in arteriolar networks." J Appl Physiol. **102**(6):2279-87.

21) Fox, R., McDonald, A., et. al. (2004) Introduction to Fluid Mechanics John Wiley and Sons Inc. USA

22) Noren, D., H.J. Palmer, et al. (2000). "Predicted wall shear rate gradients in T-type arteriolar bifurcations." Biorheology **37**(5-6): 325-40.

23) Berne, Robert M., Matthew N. Levy, Bruce M. Koeppen, and Bruce A. Stanton. Berne & Levy Physiology. Philadelphia, PA: Mosby/Elsevier, 2008. Print.

24) Pries, A., Secomb., et. al. (1994) "Resistance to blood flow in microvessels in vivo" Circ. Res.**75**;904-915

25) Kiani, M. F., A. R. Pries, et al. (1994). "Fluctuations in microvascular blood flow parameters caused by hemodynamic mechanisms." Am J Physiol Heart Circ Physiol **266**(5): H1822-1828

26) Fahraeus, R. and T. Lindqvist (1931). "The viscosity of the blood in narrow capillary tubes." Am J Physiol **96**(3): 562-568.

27) Pohl, U., DeWit, C., et. al. (2000) “Large arterioles in the control of blood flow: role of endothelium-dependent dilation.” Acta Physiol Scand, **168**: 505-510

28) Jin, Z., Ueba, H, et. al. (2003) “Ligand-independent activation of vascular endothelial growth factor receptor 2 by fluid shear stress regulates activation of endothelial nitric oxide synthase.” Circ Res. **93**(4):354-63

29) Michiels, C., (2003) “Endothelial Cell Functions.” Journal of Cellular Physiology **196**:430–443

30) Vanhoutte, P., (2009) “Endothelial dysfunction and vascular disease,” Acta Physiologica **196**(2):193-222.

31) Lee, J. H. and L. Ragolia (2006). "AKT Phosphorylation Is Essential For Insulin-induced Relaxation of Rat Vascular Smooth Muscle Cells." Am J Physiol Cell Physiol:

32) Abularrage, C. J., A. N. Sidawy, et al. (2005). "Evaluation of the microcirculation in vascular disease." Journal of Vascular Surgery **42**(3): 574-581.

33) Segal, S. S. (2005). "Regulation of Blood Flow in the Microcirculation." Microcirculation **12**: 33-45.

34) Renard, E. (2005). "Monitoring glycemic control: the importance of self-monitoring of blood glucose." The American Journal of Medicine **118**(9, Supplement 1): 12-19.

35) Moberg, E., E. Hagström-Toft, et al. (1997). "Protracted glucose fall in subcutaneous adipose tissue and skeletal muscle compared with blood during insulin-induced hypoglycaemia." Diabetologia **40**(11): 1320.

36) Aussedat, B., M. Dupire-Angel, et al. (2000). "Interstitial glucose concentration and glycemia: implications for continuous subcutaneous glucose monitoring." Am J Physiol Endocrinol Metab **278**(4): E716-728.

37) Kulcu, E., J. A. Tamada, et al. (2003). "Physiological Differences Between Interstitial Glucose and Blood Glucose Measured in Human Subjects." Diabetes Care **26**(8): 2405-2409.

38) Jakus, V. and N. Rietbrock (2004). "Advanced Glycation End-Products and the Progress of Diabetic Vascular Complications." Physiological Research **53**(2): 131-142.

39) Ahmed, N. (2005). "Advanced glycation endproducts-role in pathology of diabetic complications." Diabetes Research and Clinical Practice **67**: 3-21.

40) Ahmed, N. and P. J. Thornalley (2003). "Quantitative screening of protein biomarkers of early glycation, advanced glycation, oxidation and nitrosation in cellular and extracellular proteins by tandem mass spectrometry multiple reaction monitoring." Biochemical Society Transactions **31**(6): 1417-1422.

41) Beisswenger, P. J., B. S. Szwergold, et al. (2001). "Glycated Proteins in Diabetes." Clinics in Laboratory Medicine **21**(1): 53 - 78.

42) Avendano, G. F., R. K. Agarwal, et al. (1999). "Effects of glucose intolerance on myocardial function and collagen-linked glycation." Diabetes **48**(7): 1443-1447.

43) Rana, S. (2007). Short Term Exposure to High Glucose Has Multiple Adverse Effects on Wound Provisional Matrix Molecules and a Bioengineered Matrix. Biomedical Engineering. Stony Brook, NY, University of Stony Brook. **Doctor of Philosophy:** 138.

44) Tang, M., W. Zhang, et al. (2007). " Molecular and Cellular Biochemistry High glucose promotes the production of collagen types I and III by cardiac fibroblasts through a pathway dependent on extracellular-signal-regulated kinase 1/2." Molecular and Cellular Biochemistry **301**(1-2): 109-114.

45) Schafer A, and Bauersachs J.(2008) “Endothelial dysfunction, impaired endogenous platelet inhibition and platelet activation in diabetes and atherosclerosis.” Curr. Vasc. Pharm. **6**:52-60.

46) Rodriguez, C., Miyake, Y., et al. (2005). “Relation of plasma glucose and endothelial function in a population-based multiethnic sample of subjects without diabetes mellitus.” Am J. Cardiol. **96**(9): 1273-1277

47) Schaefer, C., Biermann, T., et. al. (2009). “Early Microvascular Complications of prediabetes in mice with impaired glucose tolerance and dyslipidemia.” Acta Diabetol. (Epub ahead of print)

48) Su, Y., Liu, X., et. al. (2008). “The relationship between endothelial dysfunction and oxidative stress in diabetes and prediabetes.” Int. J. Clin. Pract. **62**(6): 877-882.

49) Rask-Madsen, C. and G. L. King (2007). "Mechanisms of Disease: endothelial dysfunction in insulin resistance and diabetes." Nature Clinical Practice Endocrinology and Metabolism **3**(1): 46-56.

50) Giardino, I., D. Edelstein, et al. (1996). "BCL-2 Expression or Antioxidants Prevent Hyperglycemia-induced Formation of Intracellular Advanced Glycation Endproducts in Bovine Endothelial Cells." J. Clin. Invest. **97**(6): 1422-1428.

51) Marin, P., B. Andersson, et al. (1994). "Muscle fiber composition and capillary density in women and men with NIDDM." Diabetes Care **17**(5): 382-386.

52) Mathieu-Costello, O., A. Kong, et al. (2003). "Regulation of skeletal muscle morphology in type 2 diabetic subjects by troglitazone and metformin: Relationship to glucose disposal." Metabolism **52**(5): 540.

53) Junger, M., Steins, A., et. al. “Microcirculatory Dysfunction in Chronic Venous Insufficiency (CVI)” Microcirculation 76(6)S3-S12 2000.

54) Dandona, P., (2002) “Endothelium, Inflammation and Disease” Current Diabetes Reports. **2**:311-315.

55) Vettor, R., Milan, G., et. al. “Review article: adipocytokines and insulin resistance.” Aliment Pharmacol Ther **22**(Suppl. 2): 3–10.

56) Banks, A., Davis, S., et. al. “Activation of Downstream Signals by the Long Form of the Leptin Receptor.” (2000) **275**(19):14563-14572.

57) Patel, S., Garry, M., et. al. “Leptin: Linking Obesity, the Metabolic Syndrome, and Cardiovascular Disease.” Current Hypertension Reports. **10**:131-137.

58) Hudlicka, O., M. Brown, et al. (1992). “Angiogenesis in Skeletal and Cardiac Muscle.” Physiological Reviews **72(**2): 369-417.

Chapter III

Materials and Methods

For these studies, each experimental animal was used to test multiple hypotheses. The methods applicable to all experiments are described first. Methods and protocols specific to particular experiments are described second, with the pertinent chapter given in parentheses.

Animal Preparation

With university IACUC approval, male mice, 97±19 days of age (n=45, weight 32.4 ± 1.4g), were anesthetized with intraperitoneal injection of pentobarbital sodium (50 mg/kg). A constant level of anesthesia was maintained throughout the experiment by constant infusion of pentobarbital sodium. Tracheostomy was performed to ensure a patent airway. Temperature of the animal was maintained between 37º and 38 ºC by conductive and convective heat sources. Immediately post induction, blood samples were taken in triplicate via toe clip for blood glucose and systemic hematocrit measurements. Additionally, in a subset of animals a blood sample taken for cytokine measurement at this time. Blood glucose was measured using a commercially available blood glucose meter (OneTouch Basic, LifeScan, Milpitas, CA). Systemic hematocrit was measured using a commercially available micro-hematocrit reader (Hemata Stat-II, Separation Technology Inc., Altamonte Springs, FL). For plasma cytokine measurements, blood plasma was isolated by centrifugation, and diluted in serum standard diluent to optimal incubation conditions for detection. Analysis was run using a commercially available analysis kit (Beadlyte Mouse 21-Plex Cytokine Detection System, Upstate Cell Signaling Solutions, Lake Placid, NY) and run on a Bio-Plex 200 System (Bio-Rad, Hercules, California). Cytokine measurements were performed by Mr. Anthony Dewar (Master's candidate in the Frame Laboratory). Blood glucose

and systemic hematocrit measurements were repeated from fresh blood samples (toe clip) at the end of the experimental day.

The right cremaster muscle was prepared for direct observation of the microvascular network, using the method of Baez[1]. Briefly, after being freed from the scrotum, the cremaster muscle was incised longitudinally, separated from the testis and epididymis, cleared of connective tissue and gently extended over a glass pedestal by means of several insect pins secured in SylGard 34 (Dow Corning, Midland, MI). The testis and epididymis were retracted through the inguinal canal. The preparation was continuously superfused with bicarbonate-buffered saline (control suffusate) containing (in mmol) 132 NaCl, 4.7 KCl, 2.0 $CaCl_2$, 1.2 $MgSO_4$, and 20 $NaHCO_3$ (equilibrated with gas containing 5% CO_2-95% N_2 gas, pH 7.4 at 34°C). All chemicals were obtained from Sigma Chemical (St. Louis, MO), unless otherwise noted. Three different strains of mice were used in these protocols, C57/bL6 (inbred, normal metabolism), ob/ob (obese, leptin deficient mice), or db/db (diabetic, leptin receptor deficient mice, LRb-). All mice were obtained from Harlan Laboratories (Somerville, NJ).

Site selection and Vessel Nomenclature: All observations were made at defined locations along terminal arteriolar networks, shown schematically in Figure 3.1. These networks were functionally defined using the description of Sweeny and Sarelius[2]. The terminal arteriole (branch) is defined as the most distal arteriolar segment to respond actively to topical application of 10^{-4} M adenosine. The terminal arteriolar network (network) is defined as the collection of vessels that includes only terminal arterioles that are directly fed by a single unifying vessel, and includes the unifying vessel. The unifying vessel is defined as the terminal arteriolar feed (feed), which is itself fed by an arcading arteriole.

During a 60-min stabilization period, arteriolar tone was verified by dilation to topically applied 10^{-4} M adenosine (used to obtain maximal diameters) and constriction to topically applied 10^{-4} M phenylepherine (used to obtain minimum diameters). At least 30 minutes were allowed after adenosine and

phenylepherine application prior to nitroprusside (SNP) and acetylcholine (ACh) exposures, to ensure recovery from exposure to these agents.

Treatment groups: For all experiments with C57/bl6 mice, there were four treatment groups defined by the composition of the suffusate used as a tissue bath. The bath solutions were control suffusate (n=9), glucose added to control suffusate (15 mM, 270 mg/dl, n=8). 15mM mannitol added to control suffusate (osmolar control, n=9) or 10^{-4}M N^{ω}nitro-L-arginine (LNNA, to induce endothelial cell dysfunction, n=8) added to control suffusate.

The optimal dose of LNNA was determined in six additional animals, using three concentration of LNNA (10^{-6}M, 10^{-5}M, 10^{-4}M, n=2 each) in the tissue bath, and testing micropipette applied ACh (10^{-8} – 10^{-4} M) 20 minutes or 2 hours later. Our criterion for optimal concentration selection was to induce a significant decrease in the acetylcholine (Ach) maximal dilation within 20 minutes. These data are shown in Figure 3.2. After 20 minutes exposure to LNNA, only 10^{-4}M LNNA had significantly decreased dilation to maximal [ACh] (10^{-4}M or 10^{-5}M) (p=0.03, unpaired t-test). This dose of LNNA also significantly decreased dilation to lower doses of ACh, and persisted to 2 hours. Lower tissue bath treatments with LNNA did not significantly decrease 10^{-4}M or 10^{-5}M ACh by 20 minutes (for LNNA 10^{-5}M, p=0.11; LNNA 10^{-6}M, p=0.28). In fact, at 2 hours, 10^{-5}M LNNA (p=0.01), but not 10^{-6}M LNNA (p=0.60) had significantly decreased the ACh maximal dilation. Thus, for this study, we chose 10^{-4}M LNNA to induce endothelial cell dysfunction within 20 minutes. This concentration of LNNA in the superfusate is comparable to that reported in other studies where nitric oxide production is blocked in the terminal arteriolar networks of the cremaster[3].

Image acquisition and Processing

The microcirculation was observed with transillumination using a modified Nikon upright microscope (Nikon, Tokyo, Japan), with a 25x objective (Leitz, NA 0.35), with secondary magnification of 1.5x (total magnification 37.5x) or with a 60x salt water immersion objective (Nikon, NA 0.90) with no secondary

magnification. Video images were produced by using an intensified charge-coupled device (ICCD) video camera (Solamere Technologies Group, INC., XR/ABF, Pal Alto, CA) and video recorded (Panasonic SVHS AG7350). All observations were made at defined locations along the network, shown schematically in Figure 3.1.

Vasoreactivity methods (chapter IV)

All vasoreactivity protocols were performed on C57/bl6 mice. Responses were measured to either sodium nitroprusside (SNP) or acetylcholine (Ach) along the feed arteriole two feed diameters downstream from the arcade before the first bifurcation. Each agent was applied locally to the observation region of the vessel using a micropipette as previously described[4,5]. Area of application was determined visually, using a fluorescent tracer (fluorescein isothiocyanate dextran, 40 kDa, 10^{-4} M) to ensure application area and measurement area were concurrent. The concentration of this tracer has been confirmed to be non-vasoactive[4]. Each test agent was applied in increasing concentrations (SNP 10^{-7} – 10^{-3} M; Ach 10^{-8} – 10^{-4} M), with 10 minutes recovery time between doses. Each animal was used for only one of the two agents. Initial diameter measurements were averaged for 30 seconds prior to application of the test agent, and response measurements were averaged over 30 seconds of continuous agent application. After control responses were recorded, measurements were repeated for responses after 20 minutes and 2 hours of exposure to one of the four treatments.

Arteriolar diameter measurements were taken from bitmap format files using freeware available for digital image analysis (ImageJ, NIH).

Architecture measurements (chapter VI)

Five different architectural measurements were taken on each network: total network length, interbranch length, diameter, locations of the apex and center of mass of the bifurcation, and number of bifurcations. The procedures for measuring diameter, angle and length are given in Appendix II.

Total network length and interbranch length were measured directly from the video using a ruler on the image display. Images were calibrated using video images of a micrometer taken on each experiment date. Network length was defined from the intersection of the feed arteriole and the arcade to the bifurcation point of the last branch. Interbranch length was measured from the intersection point of a branch with the feed at a bifurcation to the intersection point of the previous branch with the feed. For the first branch, this distance is measured back to the feed intersection with the arcade.

Diameter and the locations of the apex and center of mass of each bifurcation were measured using bmp format images and freeware available for digital image analysis (ImageJ, NIH). The angle of bifurcation, radius of curvature and angle slope ratio was all calculated from those measurements. Those calculations are described in chapter VI.

Flow protocol for velocity and flux measurements (chapter VII)

For velocity and flux measurements, all animal models were used (C57/bl6 with all four treatment suffusates, as well as ob/ob and db/db). Following preparation of the cremaster muscle and site identification as described above, ICCD camera gain was optimized so that the walls of the vessels (bright field illumination) and the fluorescently labeled RBCs (epi-illumination) were visible. The entire network was video recorded, starting at the arcade, and moving distally down the network, ensuring that each bifurcation is recorded for 30 seconds to acquire baseline data. Baseline data was only taken if the network was in steady state; steady state refers to no vasomotion along the vessel being recorded for the complete 30 seconds. After the entire network was recorded, an additional video was taken at the entrance for 30 seconds. At the completion of baseline data measurements, the control suffusate was changed to the test suffusate, which bathed the tissue for two hours, during which time network recording was repeated at 20 minutes and at 2 hours. (Figure 3.3)

Fluorescent labeling of RBCs for use as flow markers (chapter VII)

Red blood cells (RBCs) were fluorescently labeled using modified methods of Sarelius[6]. With university and IACUC approval, mice (male C57/bl6 90-112 days) were obtained and anesthetized with pentobarbital sodium (50 mg/kg). Blood collection was performed via a heart puncture into evacuated tubes, each containing 10mg lyophilized Heparin (standard 7ml green top tube, Becton-Dickinson). Plasma was then be separated by centrifugation, (2000 rpm, 5 min) and aspirated from the solids. The solids were then washed with HEPES buffered saline (HBS, pH 7.4), centrifuged, and the HBS supernatant aspirated. Remaining solids were mixed with 0.05 µg substituted tetramethyl rhodamine isothiocyanate (XRITC, Molecular Probes, Eugene OR) first dissolved in 60 µL DMSO and then combined with 25 mL Hepes buffered saline (pH 8.1) and incubated at room temperature for 1 hour. After stirring, the RBCs were washed seven times using HBS (pH 8.1) with bovine serum albumin (0.5g%) and stored at 4°C in HBS (pH 8.1) with bovine serum albumin (0.5g%) and used within three days. On the day of the experimental protocol, the final hematocrit of the solution was adjusted to at least 60% using phosphate buffered saline (pH 7.4). Approximately 0.05 mL of RBCs in solution was injected into the right jugular catheter. Total volume injected into the animal was never more than 0.075 mL which is 4% of the total blood volume of a C57/bl6 mouse or 2% of an ob/ob or db/db mouse. Total blood volume (mL) of a mammal is approximately 7% of the weight (grams) of the animal[7].

Data processing methods for RBC tracking using XCAP and Proanalyst

Video images were converted from analog NTSC signal (stored on SVHS) to uncompressed AVI 1.0 files using a commercially available video capture program (XCAP, Epix Inc, Buffalo Grove IL) in 10 second segments. Each 30 second data file consisted of three consecutive AVI files. Each of these files was then analyzed using a custom automated particle tracking program (Proanalyst, Xcitex, Cambridge MA). For each file, a region of interest (ROI) was selected such that it enclosed the vessels being analyzed and minimized the amount of

background analyzed (Figure 3.4). Each wall of those vessels was then traced manually within the ROI. The ROI and wall tracing data was saved and used for each of the three AVI files that make up a single 30 second data set. For each ten second AVI, a threshold value and a minimal particle size value were selected to optimize the data collection for that file (Figure 3.5). Each file was then processed by the program and was output in text format. Calibration of the data was achieved by videorecording the image of a micrometer prior to each experiment, and using the image as a reference for ProAnalyst to generate a pixel to distance ratio (Figure 3.6).

Each output data file contained the following parameters for each frame of each cell: Frame, Time, Particle number, size (area), the location of the leading edge of each cell, and the coordinates of the boundaries on either side of that cell. These measured data points were used to calculate the desired results for each experiment.

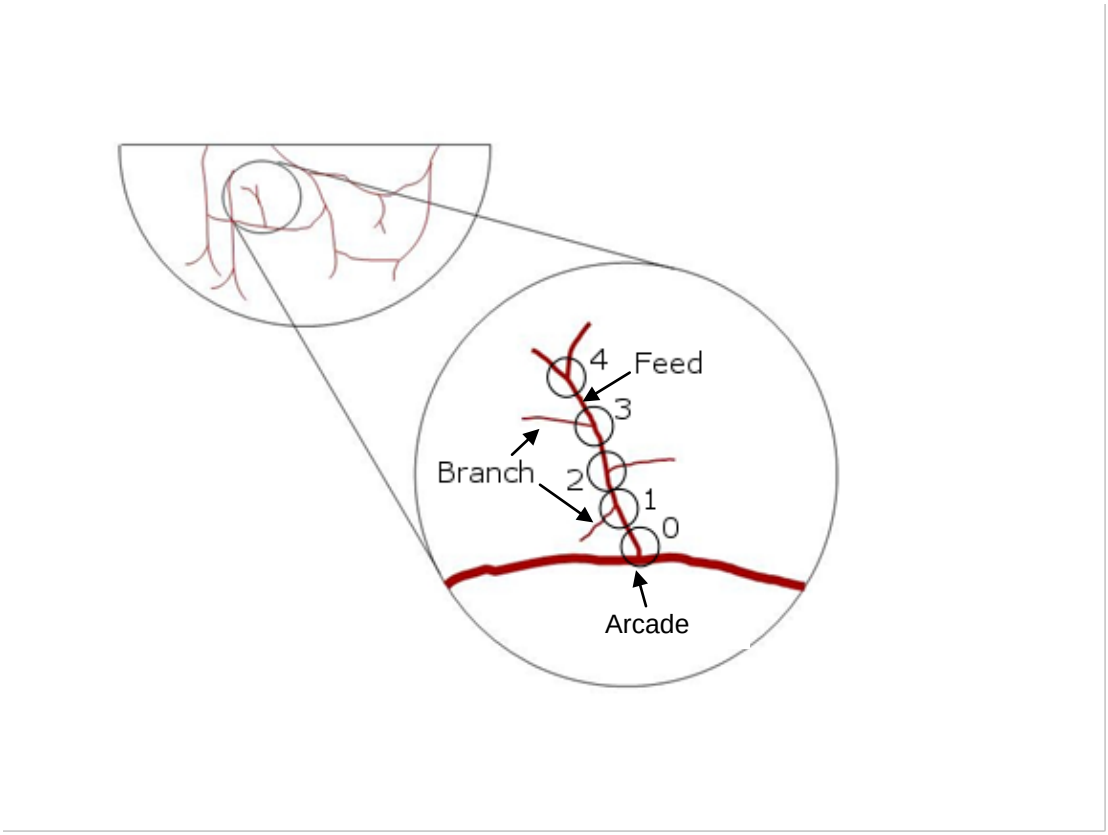

Figure 3.1: Schematic representation of a terminal arteriolar network and observation sites. The feed of the terminal arteriolar network comes off of an arcade vessel. Each branch feeds one or more capillary modules. Data was obtained at sequential branch points along the central feed. Branches were assigned numerical order (1, 2, 3) as they arose from the feed. The characteristic last branch (here designated 4) was determined by visually inspecting that each downstream branch fed only capillaries. Video was acquired at the entrance to the network from the arcade (site 0) as well as at each bifurcation along the network (sites 1-4).

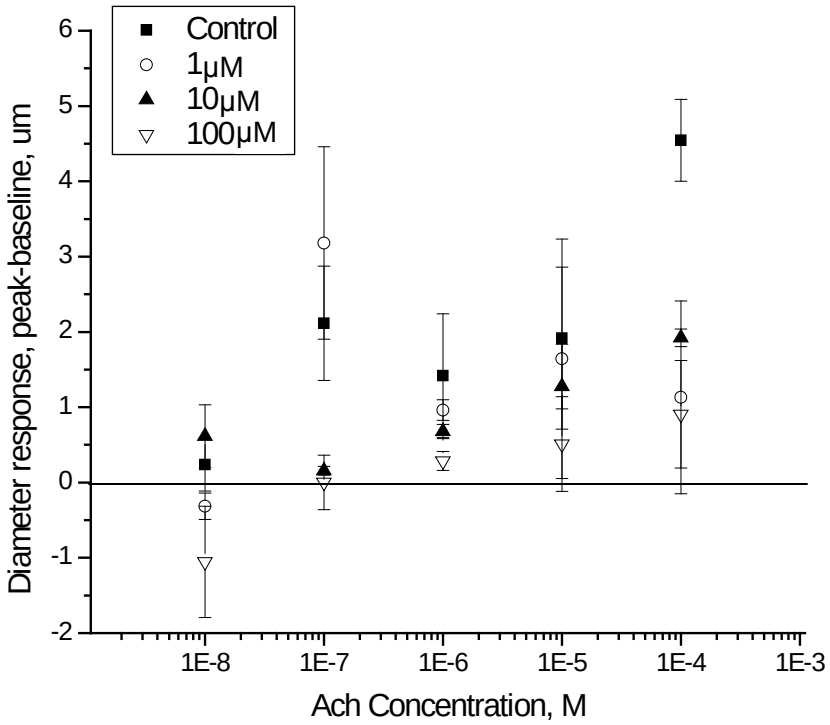

Figure 3.2: Determination of effective LNNA suffusate concentration. Dilation responses to acetylcholine were tested under four suffusate LNNA concentrations, no LNNA (control, filled squares), 10^{-6} LNNA (open circles), 10^{-5} LNNA (filled triangles) and 10^{-4} micromolar LNNA (open triangles). Only 10^{-4} micromolar concentrations of suffusate LNNA suppressed dilation to acetylcholine at the highest doses.

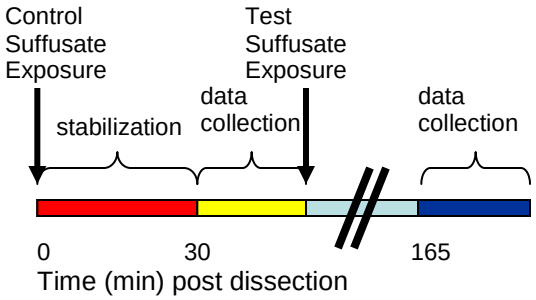

Figure 3.3: Time course of the experiments. The dissected tissue is topically superfused with physiological buffered saline solution. At the completion of dissection the tissue is allowed a stabilization period of 30 minutes before any data is recorded. The first data collection occurs at 30 minutes, and includes 30 seconds of recording at the entrance to the network, 30 seconds of recording at each bifurcation, and an additional five minutes of recording at the entrance. At the completion of the first data set, the control suffusate is exchanged for test suffusate (15 mM glucose or 15 mM mannitol.) After 2 hours of test suffusate exposure, the data collection pattern is repeated.

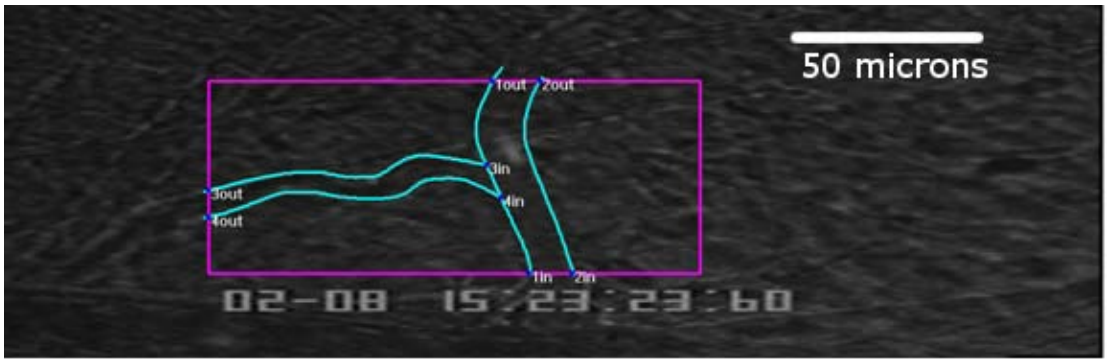

Figure 3.4: Preprocessing with ProAnalyst. The region of interest (ROI) (magenta) indicates the area of the image that will be processed by the program. The walls are traced manually (cyan). These parameters are used for an entire 30 second data set. This sample image is deinterlaced (actual y distance is twice image distance) and are taken at 37.5x magnification.

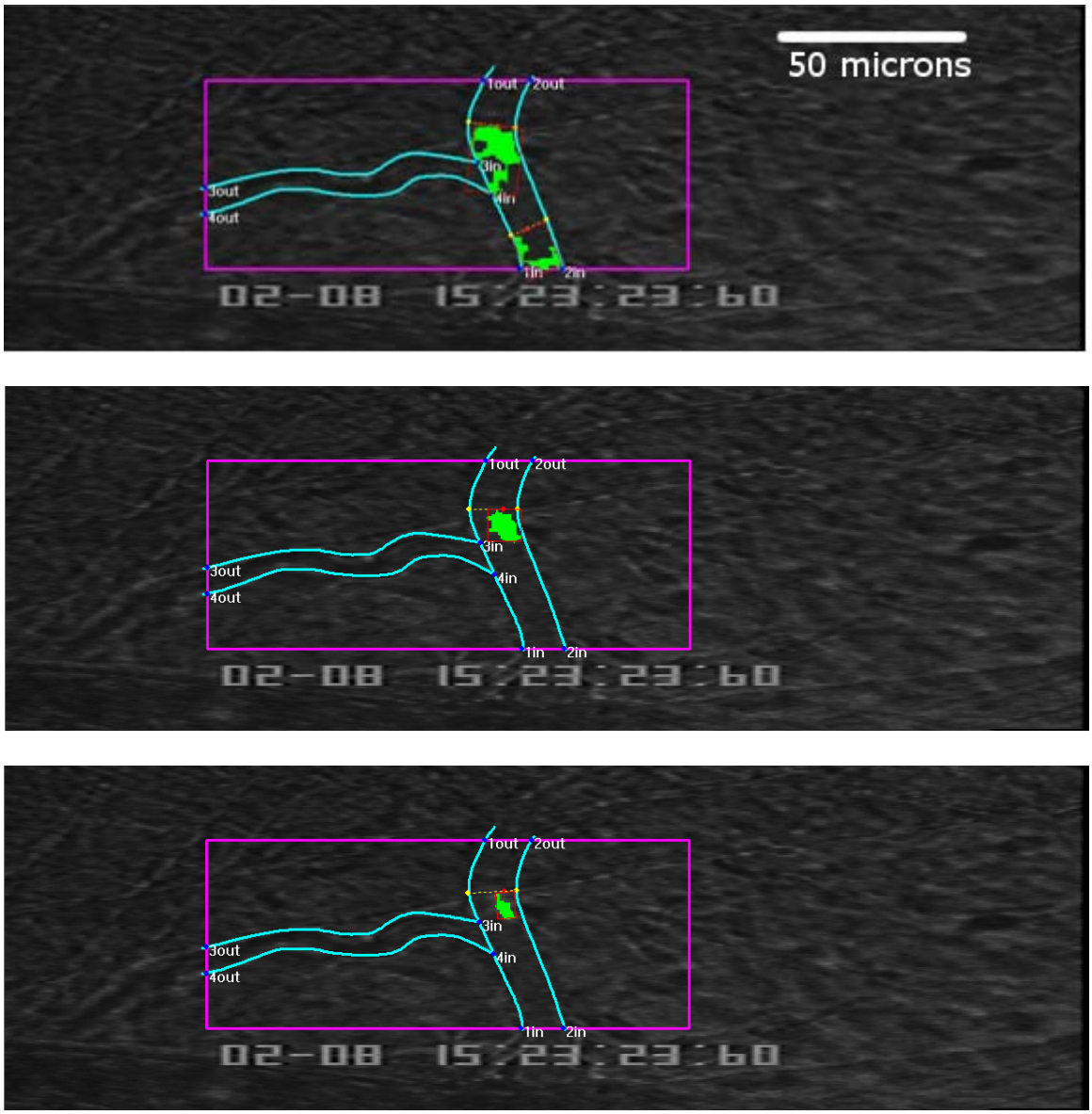

Figure 3.5: Thresholding an image in ProAnalyst. The center image is the ideal threshold for this experiment (52 grayscale). The top image demonstrates the errors generated with a threshold value that is too low (42 grayscale), including inaccurate identification of the leading edge of the cell and identification of a cell that does not exist. The bottom image demonstrates the type of errors generated when the threshold is too high (72 grayscale), including improper identification of the leading edge of the cell. If the threshold value is set even higher (75 grayscale) the cell will be not be identified at all. These sample images are deinterlaced (actual y distance is twice image distance) and are taken at 37.5x magnification.

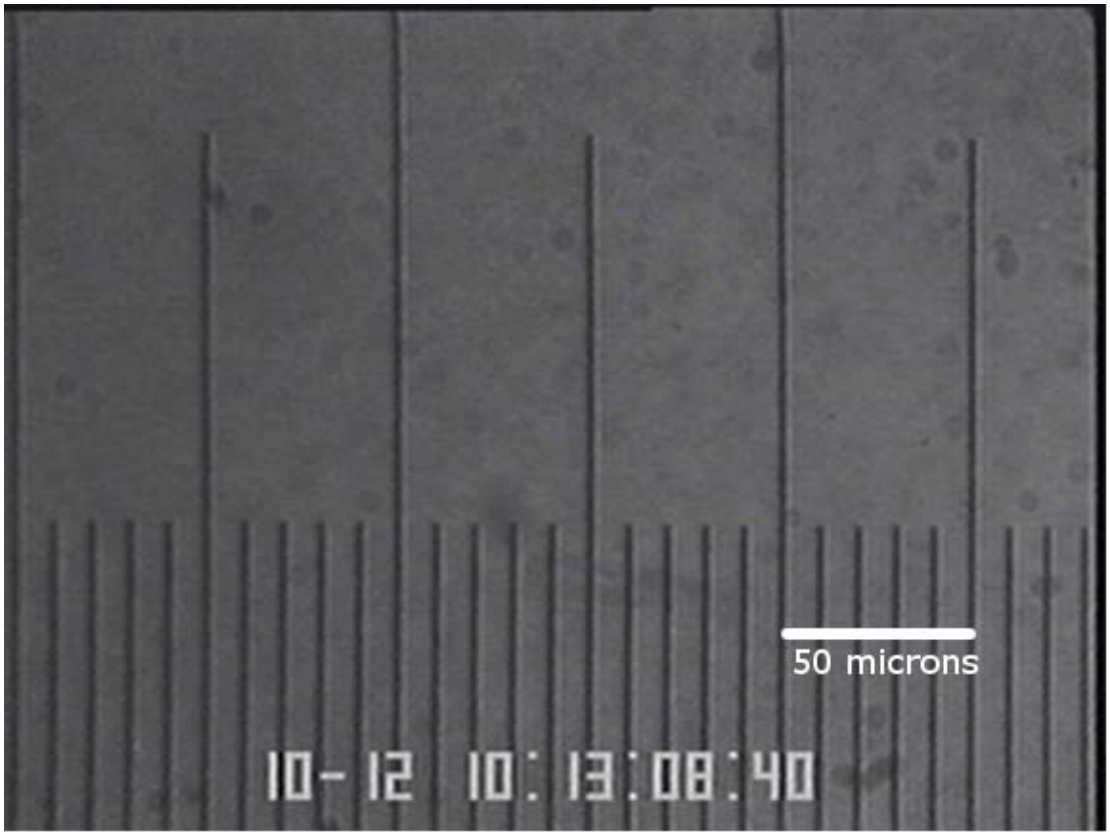

Figure 3.6: Calibration image (full frame), minor micrometer lines are spaced 10 microns apart; major lines are 50 microns apart. Sample image is taken at 37.5x magnification.

References Cited

1. Baez, S. (1973). "An open cremaster muscle preparation for the study of blood vessels by in vivo microscopy." Microvascular Research **5**(3): 384-94.

2. Sweeney, T., and Sarelius, I. (1989). “Arteriolar control of capillary cell flow in striated muscle.” Circ. Res. **64**(1): 112-120.

3. Cohen, K., and Sarelius, I. (2002). “Muscle contraction under capillaries in hamster muscle induces arteriolar dilatation via K(ATP) channels and nitric oxide.” J. Physiol. **539**(Pt. 2): 547-555.

4. Frame, M., and Sarelius, I. (1995). “L-arginine-induced conducted signals alter upstream arteriolar responsivity to L-arginine.” Circ. Res. **77**(4): 695-701

5. Cohen, K., and Berg, B. et. al. (2000). “Remote arteriolar dilations in response to muscle contraction under capillaries.” Am J Physiol Heart Circ Physiol **278**(6): H1916-1923.

6. Sarelius, I. H. and B. R. Duling (1982). "Direct measurement of microvessel hematocrit, red cell flux, velocity, and transit time." Am J Physiol Heart Circ Physiol **243**(6): H1018-1026.

7. Courtice, F. C. (1943). "The blood volume of normal animals." J Physiol **102**: 290-3-5.

Chapter IV

Vasoactive Responses of the Microvasculature to Locally Applied Sodium Nitroprusside and Acetylcholine with Elevated Glucose

Introduction

Endothelial dysfunction is a hallmark of type II diabetes and related metabolic disorders, and is manifest by impaired endothelial mediated dilation. There are two stages of type II diabetes, pre-diabetes and diabetes[1]. Distinction between the two is identified by the severity of loss of blood glucose control[1]. Pre-diabetics have an impaired fasting glucose or glucose tolerance when challenged by an oral glucose test, but not continuously elevated glucose levels[1]. In studies of pre-diabetics with elevated fasting glucose, there was a loss of endothelial cell flow mediated dilation (FMD)[2,3,4]. This patient population thus retains some control over glycemic state, yet shows signs of cardiovascular disease. This would suggest that periodic and uncontrolled elevated glucose may contribute to attenuate NO mediated dilation, even if blood plasma glucose levels never reach the levels necessary for a diabetic diagnosis. Many studies focus on whether this occurs through glycation of the extracellular matrix, or other mechanisms linked to glycosylation of proteins in vivo[5,6,7,8]. Alternately, as interstitial glucose levels mirror plasma levels, periodically increased osmolarity alone may be involved in the early changes in endothelial function. A plasma level of glucose of 270 mg/dl, for instance, adds 15mM to the normal 150mM concentration, raising the normal 290-300 mOsm to ~315 mOsm. While this seems trivial, the effect of a brief osmolar increase on other microvascular function is evident through the clinical practice of i.v. injection of mannitol to disrupt the blood brain barrier for specific treatment of elevated intracranial pressure[9]. The periodic presence of elevated osmolar content on endothelial dysfunction (NO mediated dilation) has not been reported. In this study, we chose to focus on the effects of elevated glucose on the vasoreactivity within the

peripheral vasculature. We hypothesized that elevated interstitial glucose, but not osmolar content per se, would adversely affect endothelial cell mediated dilation.

Arterioles with a functional endothelium readily exhibit flow mediated dilation (FMD). FMD is a mechanotransduction response to sudden elevations in flow (fluid shear stress) causing activation of endothelial nitric oxide synthase (eNOS) within endothelial cells to endogenously produce nitric oxide (NO)[10]. NO diffuses to the vascular smooth muscle cells, increasing the concentration of cGMP, causing intracellular calcium sequestration within the vascular smooth muscle cells, and dilation. Acetylcholine, through binding to the endothelial cell M_3 receptors, causes NO release and dilation through this pathway. Alternately, when the endothelium is compromised, acetylcholine causes constriction by acting preferentially through the vascular smooth muscle cell M_3 receptors[11]. Exogenous nitric oxide (i.e., nitroprusside) elicits a dilatory response regardless of the function of the endothelium though direct action on the smooth muscle cells, targeting guanylyl cyclase. The responses to acetylcholine and nitroprusside (SNP) thus allow the functional state of the endothelium to be characterized under a variety of conditions.

The primary purpose of this study was to investigate microvascular (terminal arteriolar) responses to endogenous and exogenous nitric oxide with brief elevated glucose (or mannitol, as an osmolar control) in the tissue bath. This would mimic local elevated interstitial levels only, without causing a systemic elevation in plasma glucose. The two exposure times (20 minutes and 2 hours) allowed a comparison between early glycation (Schiff's base formation) and complete glycation, which clinically correlates to the metabolically normal state of elevated post-prandial glucose levels and the metabolically pathological state of extended chronic glucose levels. As a positive control, we investigated responses with induced endothelial dysfunction with N^{ω}nitro-L-arginine (LNNA) to block eNOS. We hypothesized that acute elevated glucose (and not mannitol) would reduce the endothelial cell dependent dilation response to acetylcholine (Ach), yet not effect dilation to exogenous nitric oxide (SNP). We expected that

tissue exposed to two hours of glucose would have parallel responses to two hours of induced endothelial dysfunction.

Research Design

Anesthetized (pentobarbital sodium, 50 mg/kg i.p.) mice were prepared for intravital microscopy of the cremaster muscle microvasculature as described in chapter III. Observations were made at the entrance to terminal arteriolar networks, prior to the first branch, shown schematically in Figure 4.1.

Treatment groups were tissue bath solutions of control suffusate only (n=12), 15mM glucose added to control suffusate (n=13), 15mM mannitol added to control suffusate (osmolar control, n=12), or 10^{-4}M LNNA (endothelial dysfunction control, n=8) added to control suffusate. Diameter change in response to local micropipette applied (pneumatic pressures of 0.2 psi or less) SNP and Ach were determined before treatments (baseline), and then repeated after 20 minutes and again after 2 hours continuous exposure to the treatment tissue bath solutions; only one test agent (SNP or Ach) was tested per animal. Each agent was applied in increasing concentrations (SNP 10^{-7} – 10^{-3} M; Ach 10^{-8} – 10^{-4} M), with 10 minutes recovery time between doses. Recovery was defined as a return to baseline diameter. Initial diameter was the average for 30 seconds prior to application of the test agent, and the peak response was determined over 30 seconds of continuous application.

Population parameters are expressed as the mean and standard deviation. Diameter changes in response to test agents are given as the difference between peak and initial diameters (peak-initial) and standard error. Differences by concentration over time and between treatments are determined by ANOVA for repeated measures[12]. The EC50 and maximal responses were determined for each concentration response relationship (weighted by standard deviations), using Origin Lab software. Differences between the EC50 or maximal responses between treatments were determined by unpaired t-test.

Results

We first confirmed that glucose treatment in the tissue bath did not raise blood glucose levels. Initial blood glucose values were 135±24 mg/dl, and hematocrit values were 50±3%. Post experiment (6.2±0.8 hours later) blood glucose values were 63±36 mg/dl; hematocrit values were 47±3%. There was no significant difference between treatment groups for hematocrit values. Pre-glucose was significantly higher than post-glucose, equally for each group, as expected for these pentobarbital anesthetized animals that had been fasting for approximately 6 hours. All animals were experiencing the same glycemic status.

Initial baseline diameters did not differ by treatment group. Initial arteriolar diameters for all treatments combined were 9.5±3.6 µm; minimum diameters with 10^{-4}M phenylephrine were 6±2.5 µm, and maximal diameters with 10^{-4}M adenosine were 15.8±5.4 µm. The maximal diameter for each day was 19.4±5.7 µm. Change in diameter was evaluated across time using paired comparisons (Table 4.1). Baseline diameters changed differently with treatments, with the control group tending to constrict by 20 minutes with a return to the initial diameter by 2 hours. Glucose induced a significant dilation by 20 minutes that persisted over 2 hours, while LNNA induced a significant dilation by 20 minutes with a return to the initial diameter by 2 hours. Mannitol had no effect on baseline diameter at these time points. These changes in baseline diameters did not differ between the SNP vs. ACh exposure groups. Based on these findings, we used the simple test statistic of paired raw differences in diameter from baseline to peak response to evaluate the concentration response relationships.

EC50 and maximal responses values with SNP or ACh exposure are given in Table 4.2. Figure 4.2 shows the initial baseline responses for the treatment groups of control, glucose or mannitol. The EC50 values and maximal responses did not differ between these 3 groups.

The responses to SNP and ACh are shown after 20 minutes (Figure 4.3) or 2 hours (Figure 4.4) exposure. Timed controls showed that the maximal response to SNP was unchanged over 2 hours, but by 20 minutes the EC50 was significantly decreased. With glucose treatment, the maximal dilation to SNP was

significantly attenuated by 20 minutes, and the EC50 value was decreased. With ACh, timed controls showed a decrease in maximal response by 2 hours, with a decreased EC50 value. Glucose or mannitol treatment significantly decreased the maximal response to ACh by 20 minutes. At 2 hours, both the maximal dilation and EC50 values for glucose or mannitol groups were significantly different from controls, showing that the treatment alone further suppressed maximal dilation to ACh. Thus, by 20 minutes exposure, there was evidence of a diminished dilation capacity, with both endothelial dependant and endothelial independent pathways affected by glucose exposure, and only receptor dependent dilation affected by mannitol exposure. Additionally, the decrease in EC50 indicates more efficient NO production.

To determine whether endothelial dysfunction would alter the dilation capacity to only ACh, we tested 20 minutes and 2 hours exposure to LNNA (10^{-4}M) (Figure 4.5). The initial maximal dilation to SNP in this group of animals was decreased, as compared to the other control groups; the EC50 values were not different. Baseline responses to ACh were not different from the other control groups (see Table 4.1). The response to SNP was preserved over time. After 20 minutes exposure to LNNA, the maximal response to ACh was significantly decreased. The effect on EC50 is variable, as the curve flattens. This shows that deliberately induced endothelial dysfunction affected only the ACh dilation, and not receptor independent dilation with SNP.

Conclusions

There are two main findings of this study. First, two hours of exposure to elevated interstitial glucose decreases dilation through both endothelial cell dependent and endothelial cell independent mechanisms. Blocking the endothelial cell dependent response is mimicked by inducing endothelial dysfunction with LNNA. Second, an increase in osmotic stress of only 15mM significantly decreased dilation through only the endothelial cell dependent pathway.

Dilation to acetylcholine has been shown to be decreased in a variety of vascular beds by non-isotonic elevations in glucose in the rat[13-16], rabbit[17,18] and dog[19], and in diabetic models of the rat and mouse[12,20-24]. A number of possible mechanisms have been investigated to explain this change. Several studies have focused on oxidative damage caused by reactive oxygen species as the effector, focusing on the L-arginine metabolism (NO production) as the target[16,18,21,25-26]. Free radical production and oxidative stress are commonly seen in elevations in glucose in as little as 2 hours[27,28]. This time period is comparable to the exposure time in these experiments (less than two hours) and occurs prior to Schiff's base formation in the glycation cascade, thus ruling out the effect as a direct result of protein glycation or AGE byproducts. Two studies have demonstrated that the decrease in endothelium dependent dilation can be recovered with IL-2 treatment, suggesting that inflammation plays a significant role in the process[18,29]. In combination with our results above, this suggests that there is an immediate change in L-arginine metabolism due to inflammation that occurs before permanent glycation due to oxidative stress. This change is functionally different from the change in dilation seen with a non-metabolically active osmotic increase such as mannitol. While osmolarity may play a role in the change in endothelial dependent dilation, it is demonstrated through these results that it is not the only factor. Comparing our findings to those in the literature, we see an attenuated endothelial dependent dilation that may have at least two different mechanisms.

The secondary observation that there is a response to endothelium independent (NO-donor) dilation after only 20 minutes of glucose treatment in metabolically normal animals is novel, although it is in line with published results in murine models of metabolic disorders. Both diabetic (db/db) and obese (ob/ob) models are well documented to have reduced dilation to exogenous NO donors within peripheral vascular beds[24,30,22]. The mechanism for this action has yet to be determined. Our results suggest that an osmolar mechanism can be eliminated, and suggest that the effect occurs before permanent glycation.

The change in endothelial cell dependent dilation seen in both mannitol and glucose treated animals may be related to osmolar changes. However, what that mechanism is remains unclear. Mannitol is not the ideal osmolar control for glucose. Glucose is readily transported across cell membranes via the facilitator glut1[31,32], and mannitol is not. Therefore, with glucose the osmolar gradient will be zero across the membrane and in mannitol the osmolar gradient will be high, with the mannitol excluded from the cytoplasm. This may result in cellular water loss in the mannitol system and not in the glucose system. However, the mismatch in cellular uptake means that the condition held in common between the cells exposed to high glucose and high mannitol is a high osmolarity outside the cell. This suggests that the osmolar mechanism behind the alteration in endothelium dependent dilation may be on the external cell surface.

Assumptions and Limitations of the Study

This study uses a two dimensional method of visualization of the microvessels that permits a clear view of the vessels as they are still being perfused and maintained by the experimental animal. This methodology includes a few fundamental assumptions with regards to the data being collected. Most importantly, this method of vessel measurement assumes that the vessels in question dilate and constrict uniformly about the axis and along the length of the vessel. Since the vascular smooth muscle cells that cause dilation and contraction of the vessel diameter are wrapped around the vessel, constriction uniformly about the axis is likely at any one location along the vessel. However, individual muscle cells account for only about 2 microns of length along the tissue at any point[33]. Dilation could theoretically vary every 2 microns along the length of the vessel segments studied. Distinct dilation changes between separate cells cannot be distinguished. The measured diameter changes along the vessel appear consistent within the area of reagent application to the eye.

Additionally, the calculations assume that the vessels dilate maximally to the highest doses of agent applied, in order to fit a sigmoid curve and obtain the EC50 of the response. The maximum doses of each reagent were chosen within

the range that the application did not adversely affect the tissue, as such higher doses were not tested. The dose response curves however, were consistent with previously published sources. On the low end of the dose response range, the natural variability of response prevented a plateau at the minimum end of the range, and therefore fit of the sigmoid curves to the LNNA data produced an estimation of the EC50 values.

Summary

In normal mice, dilation to both the endothelium dependent and endothelium independent pathways was decreased with a brief elevation of interstitial glucose. However, it is clear that there are separate mechanisms acting on the two pathways, since osmolar control only affected one of the two pathways. This data presents evidence that the effects of glucose do not only act to induce endothelial dysfunction, they also affect the smooth muscle dilation as well, which we suggest works through an osmolar mechanism.

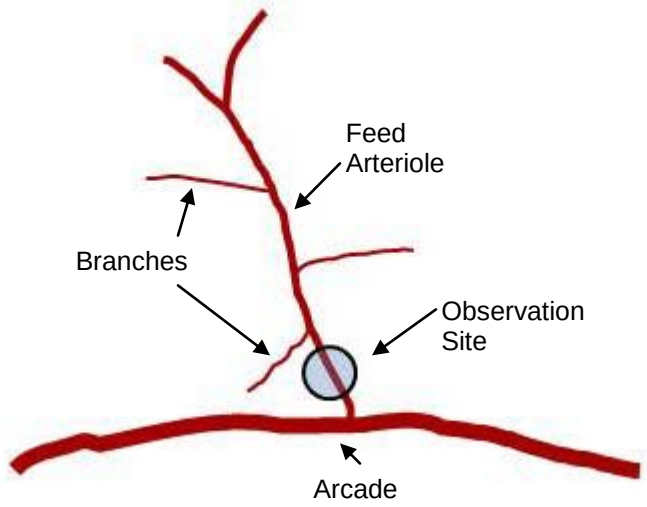

Figure 4.1: Schematic of observation site for vasoactivity measurements. Site of agent application was co-localized with observation site.

Table 4.1. Diameter changes with treatments.

	20min		2hour	
Control	-1.53	±3.6	+0.51	±4.2
Glucose	+1.83	±4.3 [a]	+2.43	±4.4 [b]
Mannitol	+0.82	±2.2 [c]	-0.05	±2.4
LNNA	+2.34	±2.2 [a,d]	+0.95	±2.9

Entries are the mean±SD for the raw change in baseline diameter; LNNA data is for 10^{-4}M (N=9).
[a]differs from control at same time period, $p<0.05$
[b]$p=0.09$, baseline glucose vs 2 hour glucose
[c]$p=0.06$, control 20 min vs mannitol 20 min
[d]significantly different from baseline for the same treatment, $p<0.05$

Table 4.2. Maximal Response and EC50 values.

SNP (10^{-7} to 10^{-3}M)

Maximal Response (peak-initial) µm

	Baseline		20min		2hour	
control	10.7	±1.4	11.3	±1.6	7.2	±0.2
Glucose	9.9	±1.4	5.0	±0.7[a]	4.2	±1.2[a]
Mannitol	12.3	±1.1	9.5	±1.2	8.6	±4.3
LNNA	5.3	±0.4[b]	6.3	±0.9	6.8	±0.6
All	10.9	±0.5				

EC50 Values ($x10^6$) M

	Baseline		20min		2hour	
Control	13.8	±7.1	2.2	±5.9[a]	1.2	±0.3[a]
Glucose	13.2	±10.1	0.3	±0.9[a]	1.2	±1.3[a]
Mannitol	8.6	±3.8	1.6	±2.1[a]	0.7	±4.3[a]
LNNA	12.6	±5.5	12.1	±0.8	11.0	±0.4[c]
All	10.7	±2.5				

Acetylcholine (10^{-9} to 10^{-4}M)

Maximal Response (peak-initial) µm

	Baseline		20min		2hour	
Control	9.0	±1.3	6.7	±1.5	6.2	±0.5[a]
Glucose	9.6	±2.8	4.2	±1.2[a]	2.4	±0.5[a,c]
Mannitol	11.2	±3.1	4.1	±2.8[a]	2.2	±0.5[a,c]
LNNA	9.0	±1.0	1.2	±0.2[a,c]	0.7	±6.1[a,c]
All	9.2	±2.4				

EC50 Values ($x10^6$)

	Baseline		20min		2hour	
Control	2.7	±1.6	2.2	±1.8	0.4	±0.2[a]
Glucose	4.4	±1.2	1.0	±1.2	0.09	±1.6[a,c]
mannitol	6.5	±1.7	0.7	±2.1	0.06	±1.6[a,c]
LNNA	11.1	±11	1.7	±1.4	15.6	±4.5
All	3.1	±3.4				

Entries are the mean±SD values from the fitted data; LNNA data is for 10^{-4}M (N=8 for each group).

[a]significantly different from baseline for the same treatment.

[b]baseline maximal response is significantly less than other 3 treatments.

[c]differs from control at same timepoint.

Figure 4.2.

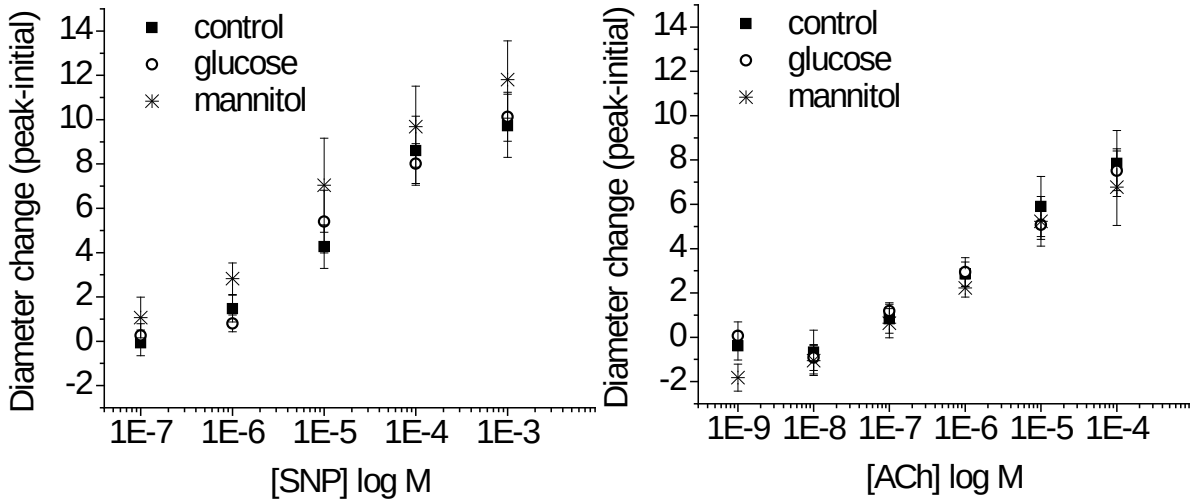

Figure 4.2. Shown are the baseline responses (mean±sem) to nitroprusside (SNP) or acetylcholine (ACh) prior to treatment, for the control, glucose (15mM) and mannitol (15mM) treatment groups. There were no differences in maximal response or EC50 values between groups; see Table 4.1(N=8).

Figure 4.3.

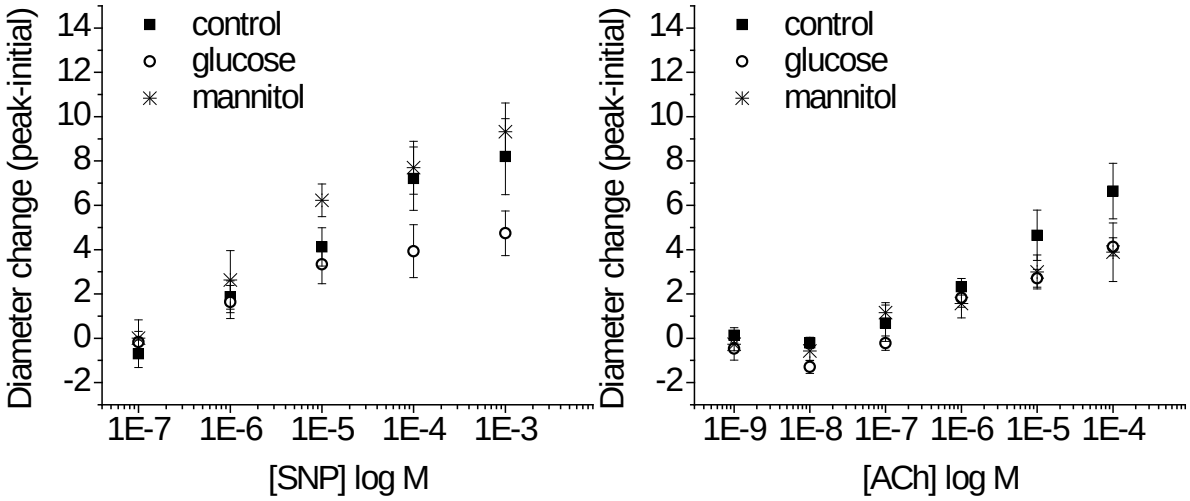

Figure 4.3. Shown are the responses to nitroprusside (SNP) or acetylcholine (ACh) after 20 minutes exposure to control, glucose (15mM) and mannitol (15mM). Maximal response and EC50 values differ between groups; see Table 4.1.

Figure 4.4.

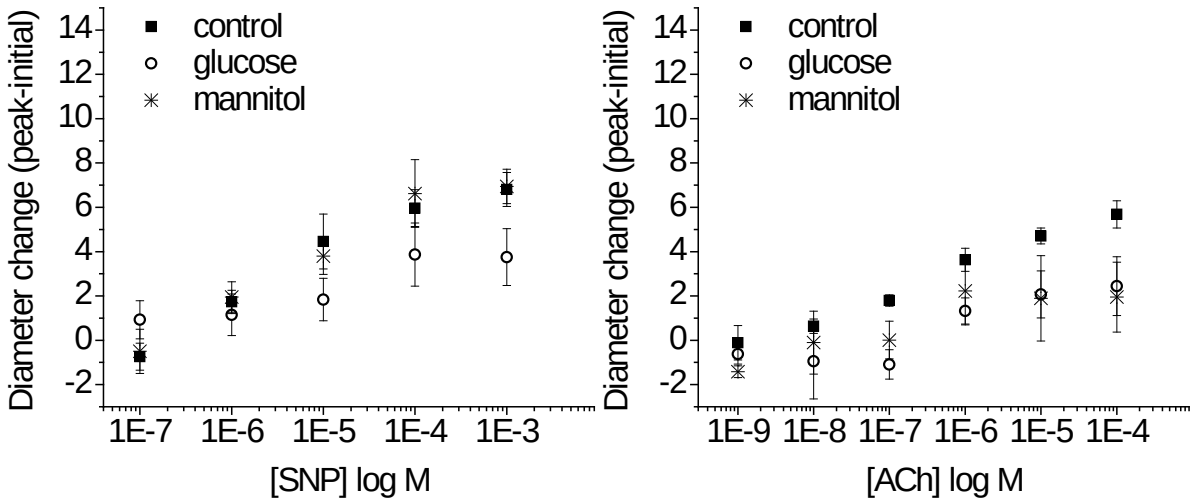

Figure 4.4. Shown are the responses to nitroprusside (SNP) or acetylcholine (ACh) after 2 hours exposure to control, glucose (15mM) and mannitol (15mM). Maximal response and EC50 values differ between groups; see Table 4.1.

Figure 4.5.

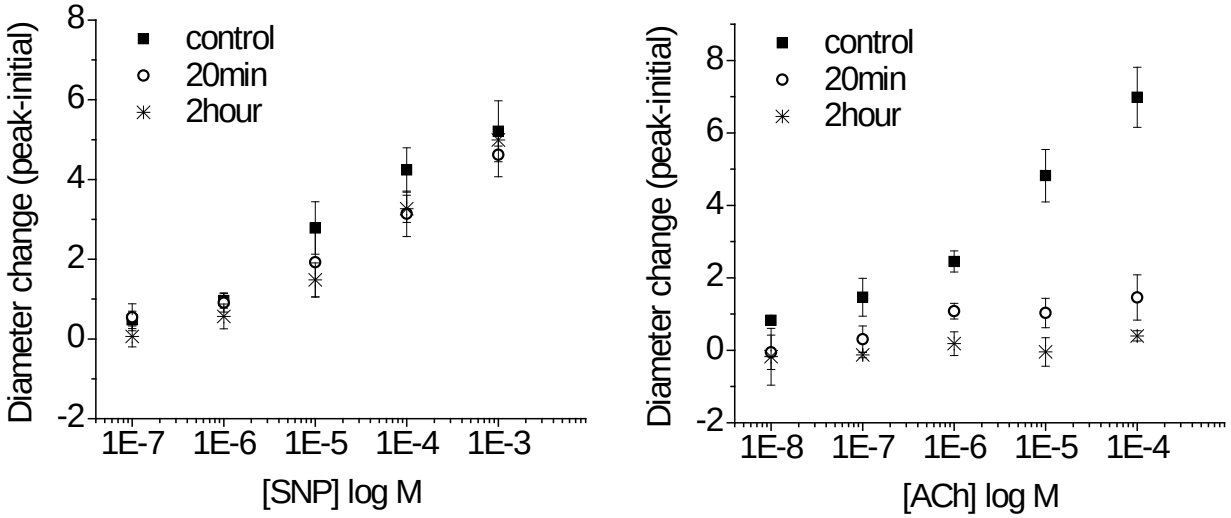

Figure 4.5. Shown are the responses to nitroprusside (SNP) or acetylcholine (ACh) to N^{ω}-nitro-L-arginine (10-4M LNNA). Maximal response and EC50 values differ between times of exposure; see Table 4.1.

References Cited

1. American Diabetes, A. (2006). "Diagnosis and Classification of Diabetes Mellitus." Diabetes Care **29**(suppl_1): S43-48.

2. Rodriguez, C., Miyake, Y., et al. (2005). “Relation of plasma glucose and endothelial function in a population-based multiethnic sample of subjects without diabetes mellitus.” Am J. Cardiol. **96**(9): 1273-1277

3. Schaefer, C., Biermann, T., et. al. (2009). “Early Microvascular Complications of prediabetes in mice with impaired glucose tolerance and dyslipidemia.” Acta Diabetol. (Epub ahead of print)

4. Su, Y., Liu, X., et. al. (2008). “The relationship between endothelial dysfunction and oxidative stress in diabetes and prediabetes.” Int. J. Clin. Pract. **62**(6): 877-882.

5. Toma, L., Stancu, C. et. al. (2009). “Irreversibly glycated LDL induce oxidative and inflammatory state in human endothelial cells; added effect of high glucose.” Biochemical and Biophysical Research Communications **390:** 877-882.

6. McDonald, D., Coleman, G. et. al. (2009). Advanced glycation of the Arg-Gly-Asp (RGD) tripeptide motif modulates retinal microvascular endothelial cell dysfunction.” Molecular Vision **15**:1509-1520.

7. Cszizar, A., and Ungvari, Z. (2008) “Endothelial dysfunction and vascular inflammation in Type 2 diabetes: interaction of AGE/RAGE and TNF-□ signaling.” Am J Physiol Heart Circ. Physiol. **295**: 475-476.

8. Goldin, A., Beckman, J., et. al. (2006). “Advanced Glycation End Products Sparking the Development of Diabetic Vascular Injury.” Circulation **114**: 597-605.

9. Rapoport, S. (1998) “Osmotic Opening of the Blood–Brain Barrier: Principles, Mechanism, and Therapeutic Applications.” Cellular and Molecular Neurobiology **20**(2): 217-230.

10. Rubanyi, G., Romero, J.C., et. al. (1986) “Flow induced release of endothelium-derived relaxing factor” Am. J. Physiol. Heart Circ. Physiol. **250**(6):H1145-H1149

11. Furchgott, R., (1983) “Role of endothelium in responses of vascular smooth muscle.” Circulation Research **53**(5):557-573.

12. Sokol, R. and Rohlf, J. (1994) Biometry: The Principles and Practices of Statistics in Biological Research Third Edition. W.H.Freeman pub.

13. Lash, J., Bohlen, G., (1991) “Structural and functional origins of suppressed acetylcholine vasodilation in diabetic rat intestinal arterioles.” Circulation Research 69:1259-1268

14. Massett, M., Michael, P., et. al. (2000) “Hyperosmolality dilates rat skeletal muscle arterioles: role of endothelial KATP channels and daily exercise.” J Appl Physiol **89**: 2227–2234

15. Yakubu, M., Sofola, O., et. al. (2004) “Link between free radicals and protein kinase C in glucose-induced alteration of vascular dilation” Life Sciences **75**: 2921–2932

16. Wang, S., Xiong, X, et. al. (2005) “Protective effects of cariporide on endothelial dysfunction induced by high glucose.” Acta Pharmicological Sinica **26**(3): 329-333.

17. Gomes, M., Affonso, F., et. al.(2004) “Glucose levels observed in daily clinical practice induce endothelial dysfunction in the rabbit macro- and microcirculation.” Fundamental and Clinical Pharmacology **18**(3): 339-346

18. Guo, X., Lin, W., et. al. (2000) “High glucose impairs endothelium-dependent relaxation in rabbit aorta.” Acta Pharmacol Sin **21**(2):169-73

19. Kocis, E., Pacher, P., (2000) “Hyperglycaemia alters the endothelium-dependent relaxation of canine coronary arteries.” Acta Physiol Scand. **169**(3): 183-7.

20. Su, J., Lucchesi, P., et. al. (2008) “Role of advanced glycation end products with oxidative stress in resistance artery dysfunction in type 2 diabetic mice.” Arterioscler Thromb Vasc Biol. **28**(8):1432-8

21. Bagi, Z., Koller, A., et. al. (2003) “Superoxide-NO interaction decreases flow- and agonist-induced dilations of coronary arterioles in Type 2 diabetes mellitus.” Am JPhysiol Heart Circ Physiol **285**: H1404–H1410

22. Gao X., Zhang, H., et. al. (2008) “AGE/RAGE produces endothelial dysfunction in coronary arterioles in Type 2 diabetic mice.” Am J Physiol Heart Circ Physiol **295:** H491–H498.

23. Park, Y., Capobianco, S, et. al. (2008) “Role of EDHF in type 2 diabetes-induced endothelial dysfunction.” Am J Physiol Heart Circ Physiol **295**: H1982–H1988

24. Howarth, A., Wiehler, W., (2006) “A Nonthiazolidinedione Peroxisome Proliferator-Activated Receptor γ Agonist Reverses Endothelial Dysfunction in Diabetic (db/db-/-) Mice” The Journal of Pharmacology and Experimental Therapeutics **316**(1):364-370.

25. Tesfamariam, B., Cohen, R., (1992) “Free radicals mediate endothelial cell dysfunction caused by elevated glucose.” Am J Physiol Heart Circ Physiol **263**: H321–H326.

26. Picchi A., Gao, X., et. al. (2006) “Tumor necrosis factor-alpha induces endothelial dysfunction in the prediabetic metabolic syndrome.” Circulation Research **99**:69-77

27. Esposito, K., Nappo, F., et. al. (2002) “Inflammatory Cytokine Concentrations Are Acutely Increased by Hyperglycemia in Humans.” Circulation **106**: 2067-2072.

28. Marfella, R., Quagliaro, L., et. al. (2001) “Acute Hyperglycemia induces an oxidative stress in healthy subjects.” The Journal of Clinical Investigation **108**(4):635-636.

29. Qian, L., Wang, H., et. al. (2006) ” Interleukin-2 protects against endothelial dysfunction induced by high glucose levels in rats.” Vascular Pharmacology **45**: 374-382.

30. Bohlen, H., Niggl, B., (1979) “Adult microvascular disturbances as a result of juvenile onset diabetes in Db/Db mice.” Blood Vessels.**16**(5):269-76.

31. Stenina, O., (2005) “Regulation of Vascular Genes by Glucose”, Current Pharmaceutical Design. **11**:2367-2381

32. Hruz, P., and Mueckler, M., (2001) "Structural Analysis of the Glut1 facilitative glucose transporter." Mol. Membr. Biol. **18**(3) :183-193.

33. Miller, B., Gattone, V., et. al. (1986) “Morphological Evaluation of Vascular Smooth Muscle Cell: Length and Width From a Single Scanning Electron Micrograph of Microvessels.” The Anatomical record **216**: 95-103.

Chapter V

Demographics, Phenotype and Metabolic State of the Experimental Animal Population

Introduction

This chapter provides novel phenotypic data for the three strains (genotypes) of mice used in this study. The data are in addition to the microvascular findings reported in the remainder of the document. The data are informative with regard to the inflammatory state and glucose handling capabilities of the animals before and after the surgical procedures.

Diabetes (or pre-diabetes) represents a disease state that is clinically defined by elevated blood glucose levels alone, yet clearly many physiological processes are affected by this disease state. In order to better understand our primary data (architecture and function of the microvasculature with elevated glucose) we collected supporting population data for key physiological parameters such as age, weight, blood plasma cytokine levels, and systemic blood glucose levels.

Animal models:

Three animal genotypes were examined. As a normal control animal we used metabolically normal C57/bl6 mice, which are the genetic background for both of the metabolic syndrome strains used. To look at the effects of high glucose and metabolic syndrome, we used a diabetic strain of mouse (BKS.Cg-+ $Lepr^{db}$/+$Lepr^{db}$/OlaHsd, also designated db/db) and an obese strain of mouse (B6.V-Lep^{ob}/OlaHsd, also designated ob/ob).

Both of the metabolic syndrome models of mice have altered leptin metabolisms. The ob/ob animals are leptin deficient and the db/db animals are leptin resistant because they lack a key leptin receptor (the LRb subtype[1]).

Leptin deficient vs. leptin resisitant:: Leptin is an adipokine (a cytokine-like protein secreted from adipose tissue), and is primarily responsible for indicating satiety[2]. There are 6 splice variants of the leptin receptor gene: the long-form LRb, four short-forms, LRa, c, d and f, and the secreted form LRe. LRb is linked to glucose and insulin metabolism[3]. The functions of the short forms and the secreted form are less well understood[4].

The LRb receptor splice variant is linked to glucose and insulin metabolism, as well as a number of other important functions[3]. It is altered in db/db animals, making it a short-form variant that resembles the LRa splice variant and therefore inactivates all of the characteristics that are associated with the LRb form[3]. As a result, db/db animals have a distinct Type II diabetes pheonotype. Metabolically, they express progressive weight gain around 3-4 weeks of age, elevation of plasma insulin at 10-14 days, hyperglycemia at 4-8 weeks of age, hyperleptinemia, proteinuria, and insulin resistance[5-13]. Mean blood pressure for the db/db mouse as measured by tail cuff is 110 mmHg[14]. They have also been shown to express elevated inflammatory cytokine levels (IL-1β, IL-6, TNF-α, and INF-γ)[12] and diminished cytokine and growth factor release (VEGF)[8,15]. Some studies have shown that the expression of the hyperinsulinemic phenotype begins to decrease again at 14 weeks[16].

In comparison, the ob/ob lack leptin entirely, and display a phenotype distinct form the db/db animals. These animals express the obesity phenotype at 4 weeks of age, hyperinsulinemia, moderate hyperglycemia, hyperlipemia, and are leptin protein deficient and insulin-resistant7,12,[17-29,31]. Mean blood pressure for the ob/ob mouse is 92 mmHg[33]. Additionally, endothelial nitric oxide synthase expression is reduced[12]. Increased levels of inflammatory cytokines, in particular TNFα, have also been reported for this strain[32].

While the ob/ob and db/db animals have individual differences in phenotype, both the ob/ob and db/db strains of mice exhibit increased weight and insulin resistance[2], a pair of characteristics that make these excellent models of type two diabetes. Throughout this and all subsequent chapters, the terms obese and diabetic will be used interchangeably with the terms ob/ob and db/db respectively.

Cytokines and metabolic disease: Part of the systemic disease process in diabetes is characterized by a chronic pro-inflammatory state. Clinically, patients with diabetes exhibit elevated markers of low-grade inflammation. These markers are cytokines or cytokine-like molecules such as chemokines or growth factors. The term cytokines will be used to encompass all of these subtypes throughout this and all subsequent chapters.

The primary function of cytokines is to mediate the immune response. Several, however, have additional roles within the cardiovascular system. In order to test the hypothesis that architectural changes seen in db/db and ob/ob mice were associated with corresponding changes in angiogenic cytokines, plasma levels of 10 specific cytokines were determined. These are: interleukin-1 (IL-1), interleukin-2 (IL-2), interleukin-6 (IL-6), interleukin-10 (IL-10), interleukin-17 (IL-17), the mouse ortholog of interleukin-8 (KC), granulocyte macrophage colony stimulating factor (GM-CSF), interfeuron gamma (IFNγ), tumor necrosis factor alpha (TNFα) and vascular endothelial growth factor (VEGF). These have known interactions with processes that pertain to vascular architecture and flow. Two processes that affect the vascular architecture (and their related cytokines) are angiogenesis (IL-6, GM-CSF, IFNγ, TNFα, KC, and VEGF) and ECM maintenance (IL-1 and GM-CSF). The two key processes that affect vascular flow (and their related cytokines) are permeability (IL-6, IL-2, TNFα, and VEGF) and vasomotor regulation (IL-6, IL-10, IL17, and TNFα). These key cytokines measured are summarized in Table 5.1, where supporting references are noted.

Cytokines

Cytokine regulation of vascular architecture: Angiogenesis: Angiogenesis is the process by which new blood vessels are formed. In brief, low tissue oxygen is considered to be the initiating signal that stimulates budding off of new vessels from existing vessels toward the low-oxygenation signal[35]. Cytokines that are intimately involved in angiogenesis include: IL-6, GM-CSF, IFNγ, TNFα, KC, and VEGF[40]. Primarily, control of angiogenesis is through the action of vascular endothelial growth factor (VEGF)[36]. VEGF acts to increase proliferation and migration of endothelial cells[36]. The action of VEGF is augmented by interleukin 6 (IL-6)[40]. IL-6 is a cytokine with a myriad of functions that primarily stimulates growth and differentiation of B lymphocytes[40]. One of those functions is to induce VEGF expression, playing a role in the regulation of angiogenesis.

Tumor necrosis factor alpha (TNFα) initiates signaling cascades for cell proliferation and apoptosis, and is a key angiogenic control molecule[40]. It has been shown to trigger inflammation which activates the release of VEGF.

Other cytokines affect angiogenesis through non-VEGF mechanisms. GM-CSF and IL-8 enhance angiogenesis by facilitating cell migration and proliferation[40]. The two work separately, with GM-CSF inducing migration and proliferation of endothelial cells, and IL-8 acting on vascular smooth muscle cells (VSM)[40].

Finally, IFN-γ may act to reduce angiogenesis, as it has been shown to suppress cell growth of all types[40].

Cytokines and extracellular matrix maintenance.: The interactions between the extra cellular matrix (ECM) and the cells that make up the vessels (EC and VSM) are also an important determinant of the architecture of the vascular network. As noted above, enhancements to cellular migration can influence angiogenesis, and changes to the composition of the ECM itself will directly affect the conditions for cell mobility. IL-1 and GM-CSF are two cytokines with major effects on the ECM:. IL-1 in particular downregulates collagen production and

upregulates collagenase production in VSM cells, and thus is critical for maintaining the ECM. This changes the composition of the ECM surrounding the VSM cells and their connection to it.

GM-CSF is of particular relevance to the effects of elevated glucose on the ECM as it has been shown to improve wound healing in diabetics through the up-regulation of IL-6 and other cytokines[37]. Wound healing processes are dependent upon ECM remodeling and re-growth because fibroblasts and vascular cells have to be able to migrate to the site of the wound and establish connections once there that allow stable tissue to develop.

Cytokine and blood flow regulation: Chapter VII investigates the effects of blood flow, shear stress and RBC flux by elevations in glucose and diabetes. There are a number of different mechanisms on which cytokines can elicit a change in these phenomena. We have chosen to measure cytokine levels that affect permeability and endothelial function via nitric oxide production. The former may affect flow and flux velocity within the network and the latter affects dilation state and therefore shear stress within the network.

Cytokines and Microvascular Permeability: Inflammation is known to cause an increase in microvascular permeability, as evidenced by tissue swelling at the site of an infection[41]. Four cytokines in particular play a role in vascular permeability changes: IL-6, IL-2, TNFα, and VEGF. TNFα and VEGF both act to increase vessel permeability and IL-2 has been shown to increase capillary leak. As presented above, IL-6 may indirectly play a role, as it acts to increase VEGF expression.

Cytokines and Vasomotor Function: Endothelial cell function is also affected by the expression of cytokines seen in inflammation and diabetes. TNFα has been shown to impair endothelial dependent dilation in humans via the suppression of Ach mediated dilation[38]. In contrast, IL-10 has been shown to decrease diabetic endothelial dysfunction by reducing superoxide production[39].

Two other cytokines have been shown to affect vascular dilation state. IL-17 modulates endothelial cell function by increasing EC production of NO[39]. Finally, IL-6 is a potent vasodilator acting through the endothelial cell endothelin-B receptors (ongoing work in the Frame laboratory by Jacqueline Vigilance). Additionally, IL-6 modulate vascular resistance by impairing smooth muscle constriction via enhanced cyclic AMP synthesis. This action is augmented by the presence of IL-17, which induces expression of IL-6[40]. Additionally, in this lab and others, it has been shown that VEGF can stimulate both local and remote dilations both through gap junction signaling and through flow recruitment[42,43].

The following results represent the population from our lab. The animals measured included all of the mice that underwent surgical cremaster preparation within a three year period. This population includes animals that were treated the same as the experimental animals in chapters VI and VII, but were used for for other studies. Hematocrit, plasma cytokine and glucose levels were measured as outlined in chapter III. All data presented in this chapter are mean ± SD with significance determined at a p value less than 0.05. Standard deviation was chosen to describe the population.

Results

Table 5.2 shows the average age and weight of all three strains of mice. C57/bl6 wild type mice were older than the db/db and ob/ob strains with no significant difference in age between the two metabolic syndrome models. Additionally the wild type mice were heavier than the metabolic syndrome models as well, and the obese mice were heavier than their diabetic counterparts.

Baseline non-fasting blood glucose differs between strains (Table 5.3). A normal blood glucose range for a mouse is between 60 and 175 mg/dl[44], which encompasses the normal human range which is between 80 and 120 mg/dl[45], both assume measurements four hours after eating. The C57/bl6 mice had a normal average blood glucose, whereas it was elevated in the obese mice, and further elevated in the diabetic mice. By the end of the acute experimental procedure, the control animals showed lower blood glucose levels, as expected

for a normal fasting mouse. However, both the ob/ob and db/db animals showed a continued elevation in blood glucose.

Hematocrit values for each three strain are shown in Table 5.4. These values were compared before and after the experimental protocol as an indicator of hydration state. No change in hematocrit would indicate that the mouse was properly hydrated via the i.p. anesthetic fluid line. The obese strain had a significantly higher hematocrit at the start of the experiments vs. control animals. Post experimental measurements show a significant decrease from baseline for both the C57/bl6 (0.48±0.06) and ob/ob (0.48±0.07) strains, and no change for the db/db strain (0.49±0.08). This resulted in all three strains ending with similar hematocrits at the end of the experiment.

The plasma protein concentration of all 10 cytokines is given in Table 5.5. First we compared between strains the cytokines that are related to angiogenesis, IL-6, GM-CSF, IFNγ, TNFα, KC, and VEGF. TNFα and KC were not different across strains, and GM-SCF was lower in both metabolic syndrome models than in control. All three of the others, IL-6, IFNγ, and VEGF were lower in the db/db animals, while they were higher (IL-6 and VEGF) or had no change (IFNγ) in the ob/ob animals as compared to the normal C57/bl6 animals. In fact, there was also a significant difference between the db/db and ob/ob concentrations of VEGF as compared to each other. Thus a general suppression of cytokine levels in angiogenesis can be seen in the db/db animals, whereas a dysregulation with no overall direction is seen in the ob/ob animals.

The protein concentration of the cytokines related to ECM maintenance, on the other hand, showed similar behaviors in the diabetic and obese mice. GM-CSF, as mentioned above, showed a decrease in both metabolic syndrome models as compared to the metabolically normal mice, and IL-1α showed an increase in both metabolic strains as compared to the C57/bl6 mice. Both metabolic strains had similar patterns of ECM related cytokine dysregulation.

Cytokines that affect flow through the vascular networks by altering permeability display a similar pattern to that of the angiogenic cytokines group. As mentioned above, TNFα did not show any differences across strains, whereas

IL-2 decreased for both metabolic syndrome models as compared with controls. Both strains were lower than the metabolically normal animals, the obese animals were significantly higher than the diabetic animals. Both of the remaining two cytokines in this group behaved differently in the two metabolic syndrome strains, decreasing in the diabetic animals as compared to C57/bl6 and increasing in the obese animals as compared to the C57/bl6.

The final group of cytokines affected the vasomotor tone of the vessels and therefore flow through the network In this group we had IL-6 and TNFα. TNFα, as reported above, increased and did not change for both metabolic syndrome strains respectively. IL-10 and IL-17 both decreased in the diabetic mice and did not change in the obese mice, as compared to the metabolically normal C57/bl6 mice.

Conclusions

These three strains of mice are related by their background genetics; both the db/db and the ob/ob strains were bred from a C57/bl6 background. The db/db model was bred to be lacking the leptin receptor to mimic closely the diabetic pathology. On the other hand, the ob/ob mouse was bred with a leptin deficiency. These mice are a model for obesity, without many of the phenotypic characteristics common to the diabetic pathology. The data presented here quantify several key phenotype differences between these two models and the C57/bl6 controls in order to provide supporting information to the results of our microvascular studies that follow.

We chose each the age ranges for each group of animals to maximize phenotype expression. The C57/bl6 animals used in all of these studies were young adults. The db/db and ob/ob populations used in these studies are younger than the C57/bl6 population. Both of the metabolic disease strains are bred to express their respective disease phenotypes early in the course of their lifespan, with the db/db phenotype beginning to revert to normal at 14 weeks of age[16]. As a result, we chose to perform our experiments at the peak of the

phenotype expression, rather than precise age matching with the C57/bl6 animal cohort.

The differences in weight between the three strains were expected, and in fact are part of the phenotype definitions for the two strains. The diabetic animals are heavier than their background counterparts as a direct result of their poor leptin and blood sugar handling. Even further along the continuum are the obese animals, which are the heaviest of the three strains. As such, this population was representative of the published phenotypes pertaining to these animals.

Another arena in which the three strains were in line with published phenotype data was in their blood glucose handling. The wild-type population demonstrated a normal blood glucose level of 144mg/dl. This average is at the high end of normal, which may be a result of the fact that our blood glucose measurements were taken post-induction. Our initial expectation was that the pentobarbital anesthetic was acting to raise blood sugar levels. However, a search of the literature proved that this widely held belief to be untrue[47]. Anxiety and stress can induce a slight elevation of blood glucose, and the handling of the animals necessary to inject the anesthetic may be mildly stress inducing. However, over the course of the experiment (up to 6 hours maximum) the animal's blood sugar drops due to a lack of food intake over that period. The maintenance injection did not contain nutritive glucose to avoid confounding glucose related results. By the conclusion of the experiment the average blood glucose was at the low end of normal, but still within the normal range.

The diabetic animals, on the other hand, had a significantly elevated blood glucose that was three times normal. This is one of the phenotypic characteristics of these animals, that makes them a good model of type two diabetes. Unlike the C57/bl6 animals, this level was constant over the course of the experiments, despite extended fasting.

Finally, the obese animals had a starting blood glucose that was larger than the metabolically normal mice and smaller than the diabetics. Instead of falling however, over the course of the experiment, these animals have a blood

glucose level that increases to be similar to that of the diabetics. The mechanism behind the increase is unknown. We postulate that the differences in blood sugar handling over the duration of the experiment protocol is tied to the differences between impaired fasting glucose and impaired glucose tolerance. These two metabolic impairments are recognized clinically through specialized glucose testing[45]. Impaired fasting blood glucose, which we postulate is happening in the db/db animals represents an inability to utilize the blood sugar in the blood stream over time[45]. Impaired glucose tolerance, which we postulate is happening in the ob/ob animals, represents an inability to reduce blood glucose levels after a load[45]. Post-protocol blood glucose measurements can be seen as a function of time in Figure 5.1. It is clear from this figure that while C57/bl6 animals have a blood sugar level that will be lower with time, the diabetic and obese animals have blood sugar levels that are unaffected by fasting.

The C57/bl6 animals showed a decrease in hematocrit over the course of the experimental protocol. This is likely due to continuous infusion of maintenance anesthetic suspended in saline over the extended time period of experimentation they experienced. This indicates increased hydration over the course of the experiment. In contrast, the db/db animals showed no change over their experimental time periods. The ob/ob animals initially had a higher hematocrit. We postulate that the ob/ob animals may have been dehydrated, perhaps because they showed limited mobility (although their mobility was not documented). Future work with this strain will include a modification to the water bottle height for easier access. The ob/ob animals also saw a decrease in hematocrit over the period that they were under anesthesia, indicating that they were being hydrated as well as the other two strains.

No single study could achieve a complete investigation of cytokines in diabetes and metabolic syndrome. We focused our cytokine expression measurements on the core studies of this project: architecture and flow regulation. A brief discussion of the cytokine results is below. Each point of interest will be treated in context in the chapters to follow.

Architecture changes are driven by angiogenesis and vascular remodeling. VEGF is the molecule most highly connected to the induction and modulation of angiogenesis. However, GM-CSF, IL-8, IL-6, and TNFα have also been shown to enhance the process. Of the cytokines we measured, only IFNγ has been shown to counteract it. VEGF expression was altered as compared to wild-type controls in both strains, though it showed a decrease in the db/db strain and an increase in the ob/ob strain. This expression pattern was mimicked in the IL-6 expression data. In contrast, GM-CSF and IFNγ decreased in both strains, IL-8 increased in both strains (we report the levels of KC, the mouse ortholog of human IL-8), and TNFα showed no change across the strains. These differential changes may be linked to differential architectural phenotypes. This supposition is supported by the data presented in chapter VI.

Architectural phenotypes may also be affected by the cytokines responsible for ECM maintenance. Both metabolic models of diabetes saw an increase in the IL-1 expression as compared to the wild type controls. An increased IL-1 expression will lead to collagen destabilization in the ECM. Both metabolic strains also saw a decrease in GM-CSF expression, indicating an unhealthy ECM environment for cellular migration. These results are consistent with an impaired ECM, and may explain some architectural changes seen with diabetes.

Flow regulation in the terminal arteriolar networks is largely controlled through local stimuli, but two significant stimuli can be altered by systemically circulating cytokines: capillary permeability and dilation state. VEGF is a key modulator of permeability. VEGF expression changed differentially in both metabolic syndrome models. Both IL-2 and IL-6 expression followed the same pattern. TNFα, which also increases permeability, was unchanged.

The other significant component to flow regulation is vascular resistance, which will affect shear stress locally and blood pressure systemically. Vascular resistance is largely controlled by EC function and dilation state of the vessels. No change in TNFα and a decrease in IL-10 in only the db/db strain (as compared with controls) indicate little to no cytokine driven impairment of

endothelial dependent dilation. In contrast, cytokines that affect VSM constriction show a downward trend, with IL-17 decreased in the db/db strain and no change in the ob/ob strain. Paradoxically, IL-6 expression, which should upregulate IL-17 and augment the suppression of VSM constriction, is decreased in the db/db and increased in the ob/ob strains as compared to the control strain. These results suggest that there are more significant control mechanisms at work for the vasoreactivity of the vessels.

Summary

There are significant differences as well as similarities in the basic phenotypes of the three mouse strains used in this lab. Importantly, there is a significant difference in blood glucose handling in the two metabolic disorder models as compared to the wildtype mice. Additionally, changes in cytokine expression are distinct between the three mouse strains. These differences will become important reference points as we look at the data for the following chapters, in order to inform our analyses and any conclusions drawn.

Table 5.1. Physiological Effects of Key Cytokines

	Angiogenesis	ECM	Permeability	Vasoreactivity
IL-1	Stimulates smooth muscle cell proliferation[39]	Downregulates collagen production upregulates collagenase production[40]		
IL-2			Induces capillary leak[40]	
IL-6	Induces VEGF[40]		Induces VEGF[40]	Induces dilation via ET-B[49] Impairs smooth muscle constriction via cAMP[40]
IL-10				Decreases diabetic endothelial dysfunction[39]
IL-17				Increases EC production of NO (also induces IL-6)[39]
GM-CSF	Migration and proliferation of EC[46]	Improves wound healing in diabetics[37]		
IFNγ	Inhibits cell growth (general)[40]			
TNFα	Triggers inflammation which yields VEGF release		Increases vascular permeability[42]	Impairs endothelial dependent dilation[38]
KC[#]	Migration and proliferation of VSM[39]			Induces dilation via ET-B[@]
VEGF	Primary mediator[36]		Increases vascular permeability[44]	Induces local and remote dilations[43]

[#]KC is the murine analog of IL-8

[@] ongoing work in the Frame Lab by Jackie Vigilance

Table 5.2. Age and weight of experimental animals.

	N	Age (days)	Weight (g)
C57/bl6	167	106.94± 27.16	28.28± 3.61
db/db	29	88.58± 18.92*	44.33 7.82*
ob/ob	25	80.44± 13.40*	49.54± 5.74* **

Entries are mean±SD

* p<0.05 vs. control **p<0.05 db/db vs. ob/ob

Table 5.3. Blood glucose measurements

	Post induction (mg/dl)	Post protocol (mg/dl)
C57/bl6[a]	142.83± 28.78	75.25± 47.56^
db/db	410.10± 122.73* **	442.14± 143.50*
ob/ob	239.28± 86.67* **	404.58± 101.21* ^

Entries are mean±SD

* p<0.05 vs. control **p<0.05 db/db vs. ob/ob ^p<0.05 post induction vs. post protocol

[a] Both post induction and post protocol values are within normal blood glucose range for mice

Table 5.4. Fractional hematocrit measurements

	Post induction	Post protocol
C57/bl6	0.51± 0.05	0.48± 0.06^
db/db	0.52± 0.08	0.49± 0.08
ob/ob	0.54± 0.07*	0.48± 0.07^

Entries are mean±SE

* p<0.05 vs. control **p<0.05 db/db vs. ob/ob ^p<0.05 post induction vs. post protocol

Table 5.5. Cytokine measurements

	C57/bl6	db/db	ob/ob
IL-1alpha	29.64± 3.32	50.22± 3.56*	65.80± 18.97
IL-1beta	154.51± 14.19	61.38± 14.14*	288.58± 90.63
IL-2	28.01± 2.29	7.36± 1.27*	182.88± 117.50
IL-6	10.57± 1.46	7.07± 0.96*	21.045± 5.24*
KC[#]	39.68± 6.05	134.96± 68.52	303.70± 171.57
IL-10	52.98± 7.99	9.85± 3.80*	42.44± 16.61
IL-17	31.32± 9.32	9.53± 1.46*	29.28± 10.32
GM-CSF	43.01± 4.03	11.56± 1.99*	20.86± 4.74*
IFNgamma	27.60± 3.07	9.05± 1.51*	17.76± 4.50
TNFalpha	13.94± 2.13	10.16± 2.11	13.77± 2.64
VEGF	11.59± 1.04	3.04± 0.35*	19.90± 4.15* **

Entries are mean±SE

Concentrations shown in picograms/ml plasma, mean+/-se

* p<0.05 vs. control **p<0.05 db/db vs. ob/ob [#] KC is the murine analog of IL-8

Figure 5.1: Post-protocol blood sugar levels vs. the duration of the experiment

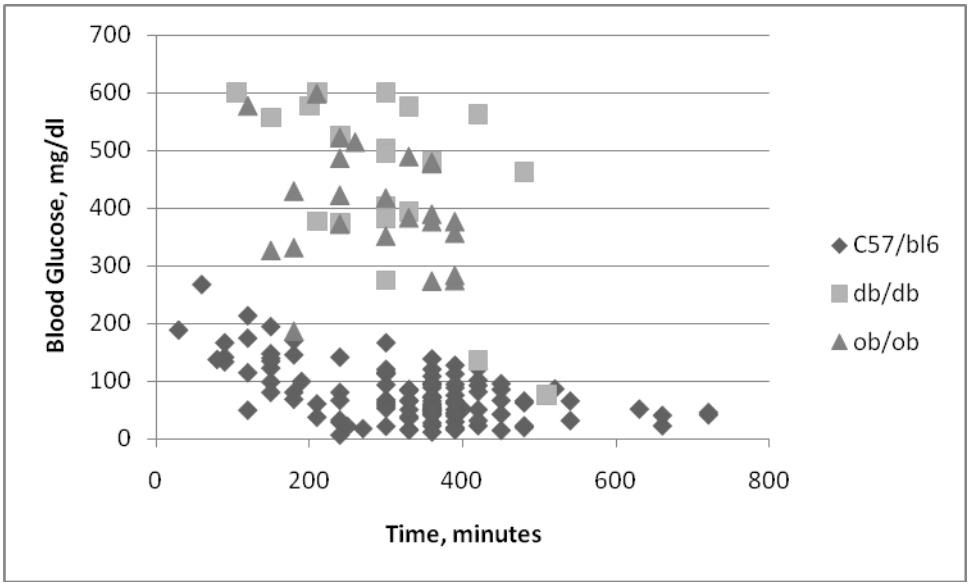

References Cited

1. del Carmen Garcia, M., Casanueava, F., et. al. (2000) “Gestational Profile of Leptin Messenger Ribonucleic Acid (mRNA) Content in the Placenta and Adipose Tissue in the Rat, and Regulation of the mRNA Levels of the Leptin Receptor Subtypes in the Hypothalamus During Pregnancy and Lactation.” Biology of Reproduction **62**: 698-703.

2. Vettor, R., Milan, G., et. al. “Review article: adipocytokines and insulin resistance.” Aliment Pharmacol Ther **22**(Suppl. 2): 3–10.

3. Banks, A., Davis, S., et. al. “Activation of Downstream Signals by the Long Form of the Leptin Receptor.” (2000) **275**(19):14563-14572.

4. Patel, S., Garry, M., et. al. “Leptin: Linking Obesity, the Metabolic Syndrome, and Cardiovascular Disease.” Current Hypertension Reports. **10**:131-137.

5. Hafstad, A. D., Solevåg, G. H., et. al.(2006) “Perfused hearts from 2 Type1 diabetic (db/db) mice show metabolic responsiveness.to insulin.” Am J Physiol Heart Circ Physiol, **290:** H1763-H1769.

6. Oakes, N. D., Thalén, P., et. al.(2006).”Cardiac metabolism in mice: Tracer method developments and in vivo application revealing profound metabolic inflexibility in diabetes.” Am J Physiol Endocrinol Metab, **290**: 870-881.

7. Takahashi, N., Waelput, W., et. al. (1999). ”Leptin is an endogenous protective protein against the toxicity exerted by Tumor Necrosis Factor.” J Exp Med, **189**:207-212.

8. Rodgers, K., Ellefson, D., et. al. (2006). “Expression of intracellular filament, collagen, and collagenase genes in diabetic and normal skin after injury.” Wound Rep Reg, **14**(298-305).

9. Schneider, J. G., Finck, B. N., et. al. (2006). “ATM-dependent suppression of stress signaling reduces vascular disease in metabolic syndrome.” Cell Metabolism **4**: 377-389.

10. Carley, A., Semeniuk, L., et al. (2004). “Treatment of type 2 diabetic db/db mice with a novel PPARγ agonist improves cardiac metabolism but not contractile function.” Am J Physiol Endocrinol Metab, **286**:E449-E455.

11. Jones, S., Girod, W., et. al. (1999). “Reperfusion injury is not affected by blockade of P-selectin in the diabetic mouse heart.” Am J Physiol Heart Circ Physiol **277**:763-769.

12. Brun, P., Castagliuolo, I., et al. (2007). “Increased intestinal permeability in obese mice: New evidence in the pathogenesis of nonalcoholic steatohepatitis.” Am J Physiol Gastrointest Liver Physiol, **292**:G518-G525.

13. del Rey, A., Besedovsky, H. (1989). “Antidiabetic effects of interleukin 1.” PNAS **86**:5943-5947.

14. Koya, D., Haneda, M., et. al. (2000) “Amelioration of accelerated diabetic mesangial expansion by treatment with a PKCβ inhibitor in diabetic db/db mice, a rodent model for type 2 diabetes.” FASEB J. **14**:439-447.

15. Anis, Y., Leshem, O., et al. (2004). “Antidiabetic effect of novel modulating peptides of G-protein-coupled kinase in experimental models of diabetes.” Diabetologia, **47**:1232-1244

16. Hoffman, S., Dong, H., et. al. (2002) “Improved Insulin Sensitivity Is Associated With Restricted Intake of Dietary Glycoxidation Products in the db/db Mouse.” Diabetes **51**: 2082-2089.

17. Igel, M., Becker, W., et. al. (1997) “Hyperleptinemia, leptin resistance, and polymorphic leptin receptor in the New Zealand obese mouse.” Endocrinology **138:**4234-4239.

18. Igel, M., Lindenthal, B., et. al. (2002). “Evidence that leptin contributes to intestinal cholesterol absorption in obese (ob/ob) mice and wild-type mice.” Lipids **37:**153-157.

19. Priestman, D., van der Spoel, A., et. al. (2008). “N-butyldeoxynojirimycin causes weight loss as a results of appetite suppression in lean and obese mice.” Diabetes, Obesity and Metabolism **10:**159-166.

20. Tarzi, R., Cook, H, et. al. (2004). “Leptin-deficient mice are protected from accelerated nephrotoxic nephritis.” Am J Pathology **164**:385-390.

21. Wiegman, C., Bandsma, R., et al. (2003). “Hepatic VLDL production in ob/ob mice is not stimulated by massive de novo lipogenesis but is less sensitive to the suppressive effects of insulin.” Diabetes **52**:1081-1089.

22. Bandsma, R., Grefhorst, A., et. al. (2004). “Enhanced glucose cycling and suppressed de novo synthesis of glucose-6-phosphate result in a net unchanged hepatic glucose output in ob/ob mice.” Diabetologia, **47**:2022-2031.

23. Bjursell, M., Gerdin, A-K., et al. (2006). “Melanin-Concentrating Hormone Receptor 1 deficiency increases insulin sensitivity in obese leptin-deficient mice without affecting body weight.” Diabetes **55**:725-733.

24. Liu, Y., Connoley, I., et. al. (2005). “Effects of the cannabinoid CB1 receptor antagonist SR141716 on oxygen consumption and soleus muscle glucose uptake in Lepob/Lepob mice.” International Journal of Obesity **29**:183-187.

25. Rafael, J., Herling, A. (2000). “Leptin effect in ob/ob mice under thermoneutral conditions depends not necessarily on central satiation.” Am J Physiol Regulatory Integrative Comp Physiol, **278**:R790-R795.

26. Kharitonenkov, A., Shiyanona, T., et al. (2005). “FGF-21 as a novel metabolic regulator.” The Journal of Clinical Investigation **115:**1627-1635.

27. Waterman, I., Zammit, V. (2002). “Activities of overt and latent diacylglycerol acyltransferases (DGATs I and II) in liver microsomes of ob/ob mice.” International Journal of Obesity **26**:742-743.

28. Calderan, L., Marzola, P., et al. (2006). “In vivo phenotyping of the ob/ob mouse by magnetic resonance imaging and 1H-magnetic resonance spectroscopy.” Obesity **14**:405-414.

29. Grefhorst, A., van Dijk, T., et al. (2005). “Differential effects of pharmacological liver X receptor activation on hepatic and peripheral insulin sensitivity in lean and ob/ob mice.” Am J Physiol Endocrinol Metab **289**:829-838.

30. Matarese, G., Di Giacomo, A., et al. (2001). “Requirement for leptin in the induction and progression of autoimmune encephalomyelitis.” The Journal of Immunology **166**: 5909-5916.

31. Höppener, J., Oosterwijk, C., et al. (1999) “Extensive islet amyloid formation is induced by development of Type II diabetes mellitus and contributes to its progression: Pathogenesis of diabetes in a mouse model.” Diabetologia **42**:427-434.

32. Roche, H., Noone, E., et al. (2002). “Isomer-dependent metabolic effects of conjugated linoleic acid.” Diabetes **51:**2037-2044.

33. Mark, A., Shaffer, R., et. al. (1999) “Contrasting blood pressure effects of obesity in leptin-deficient ob/ob mice and agouti yellow obese mice” J. Hypertension **17**:1949-1953.

34. Valerio, A., Cardile, A., et al. (2006). “TNF-α downregulates eNOS expression and mitochondrial biogenesis in fat and muscle of obese rodents.” The Journal of Clinical Investigation **116**:2791-2798

35. Pugh, C., Ratcliffe, P., (2003). :”Regulation of angiogenesis by hypoxia: role of the HIF system.” Nature Medicine **9**(6)677-684.

36. Carmeliet, P., (2003). “Angiogenesis in health and disease.” Nature Medicine 9(6)653-660.

37. Fang, Y., Shen, J., (2009) “Granulocyte-macrophage colony-stimulating factor enhances wound healing in diabetes via upregulation of proinflammatory cytokines.” British Journal of Dermatology Epub ahead of print

38. Chia, S., Qadan, M., et. al. (2003) “Intra-Arterial Tumor Necrosis Factor- Impairs Endothelium-Dependent Vasodilatation and Stimulates Local Tissue Plasminogen Activator Release in Humans.” Arterioscler Thromb Vasc Biol. **23**:695-701.

39. Fisman, E., Motro, M., et. al. (2003) “Cardiovascular diabetology in the core of a novel interleukins classification: the bad, the good and the aloof.” Cardiovascular Diabetology **12**:2-11.

40. Curfs, J., Meis, J., (1997) “A Primer on Cytokines: Sources, Receptors, Effects and Inducers.” Clinical Microbiology Reviews **10**(4):742-780.

41. Williams, T., and Moreley, J., (1973) “Prostaglandins as Potentiators of Increased Vascular Permeability in Inflammation”, Nature **246**:215-217.

42. Jin ZG, Ueba H, Tanimoto T, Lungu AO, Frame MD, Berk BC. Ligand-independent activation of vascular endothelial growth factor receptor 2 by fluid shear stress regulates activation of endothelial nitric oxide synthase. Circ.Res. 2003; **93:** 354-63.

43. Georgi, M., Dewar, A., et. al. (2010) “Downstream Exposure to Growth Factors Causes Elevated Velocity and Dilation in Arteriolar Networks.” Journal of Vascular Research In Press

44. Davies, M., Lund, R., (2005) “Low Turnover Osteodystrophy and Vascular Calcification are Amenable to Skeletal Anabolism in an Animal Model of Chronic Kidney Disease and the Metabolic Syndrome” Journal of the American Society of Nephrology **16**(4):917-928

45. American Diabetes, A. (2006). "Diagnosis and Classification of Diabetes Mellitus." Diabetes Care **29**(suppl_1): S43-48

46. Rajavashisth, T., Andalibi, A., et. al. (1990) “Induction of endothelial cell expression of granulocyte and macrophage colony-stimulating factors by modified low-density lipoproteins.” Nature **344**:254-257

47. Tanaka, K., Kawano, T., et al (2009) “Mechanisms of Impaired Glucose Tolerance and Insulin Secretion during Isoflurane Anesthesia” Anesthesiology **111**:1044-1051

48. Angelini, D., Hyun, S-W., et. al. (2006) “TNF-α increases tyrosine phosphorylation of vascular endothelial cadherin and opens the paracellular pathway through fyn activation in human lung endothelia.” Am J Physiol Lung Cell Mol Physiol **291**:1232-1245

49. Ferrera. N., Gerber, H., et. al. (2003) “The biology of VEGF and its receptors.” Nature Medicine **9**(6):669-676.

Chapter VI

Elevated Blood Glucose Affects Microvascular Architecture

Introduction

Regulation of the flow of blood to the capillary beds is primarily achieved by the terminal arterioles. These vessels form branching networks (terminal arteriolar networks) such that each terminal branch feeds a separate group of capillaries, where the majority of O_2 and nutrient exchange with the tissue occurs. The control mechanisms for regulation of blood flow are of significant interest, particularly in disease states where blood flow is impaired, such as obesity related metabolic disorders, including diabetes and its precursors metabolic syndrome and pre-diabetes.

The simple presence or absence of blood vessels is the main determinant of blood flow. In chronic metabolic disorders, vascular (typically capillary) density per tissue area is decreased as compared to normal tissue, a condition referred to as structural rarefaction[1,2]. Structural rarefaction is distinguished from functional rarefaction, where vessels are present but not perfused.

Vascular growth and remodeling come under the general heading of angiogenesis. Angiogenesis is regulated by a combination of mechanical and chemical stimuli. The mechanical signal of shear stress within the vessel stimulates growth and remodeling; or, in the opposite case, a lack of shear stress causes rarefaction[3]. Additionally, a few studies have shown that increasing muscular contraction (which increases both metabolism and flow) increases angiogenesis within skeletal muscle[4,5,6]. Chemically, there are several known pro-angiogenic growth factors and cytokines. One of the most significant of these factors is VEGF (vascular endothelial cell growth factor), which causes cell proliferation, tube formation, and differentiation in both in vivo and in vitro studies[7,8]. Additional cytokines that affect angiogenesis action were introduced

in chapter V and include GM-SCF, IL-6, IL-8 and TNFα. Angiogenesis is impaired in diabetics[9].

Apoptosis (programmed cell death) also plays a role in structural rarefaction. Absence of blood flow (lack of shear stress stimulus) induces apoptosis in endothelial cells[10]. (Flow phenomena including loss of flow and functional rarefaction are treated in more detail in chapter VII.) Elevated blood glucose has been demonstrated to either upregulate or suppress apoptosis dependent on tissue bed and conditions[11].

The cause of diabetic rarefaction has yet to be determined. Though many studies have suggested that structural rarefaction is a consequence of hypertension (a common co-morbidity of diabetes and metabolic disorders) Frisbee et al., have shown that microvascular remodeling and rarefaction occur before the onset of hypertension in obese Zucker rates (OZR) indicating that obesity and insulin resistance in the absence of hypertension are sufficient to cause rarefaction via a nitric oxide mediated mechanism[12].

Structural rarefaction is defined as a loss of vascular density per tissue area. Vascular density has historically been measured as the number or lengths of vessels per unit area of tissue, with little regard to branching complexity. This methodology, while instructive regarding capillary density (since capillaries are functionally similar with respect to nutrient exchange) hides interesting functional information about the terminal arteriolar networks. From a functional standpoint, a larger number of networks where each terminal arteriole feeds one capillary module is not necessarily the same as fewer networks where each terminal arteriole feeds many capillary modules. Assuming an identical capillary module off of each branch and a Krogh cylinder of diffusion[13], the smaller number of networks with more modules each would be required to deliver nutrients to a larger tissue area. Further, with increased metabolism, there would be a greater likelihood that the post-capillary vessels would be oxygen and nutrient depleted.

Other than structural rarefaction, both volume flow and red blood cell flux, are primary determinants of nutrient blood flow in terminal arteriolar networks. From a structural or architectural standpoint, volume of flow is determined by the

resistance in the blood vessel network. There are two architectural factors that affect resistance in a blood vessel, the radius of the vessel and its length. (Flow rate is discussed in chapter VII).

Vascular diameter is regulated by a myriad of mechanical and biological forces. The most important of these factors from an architectural perspective is vessel stiffness, or how easily the vessels are predisposed to dilation. Frisbee et al., have shown that in explanted vessels microvessel stiffening and a resultant decrease in passive diameter occurs in the microvasculature of the OZR[14]. These phenomena may be related to increased sensitivity to intraluminal pressure (the myogenic tone response) also seen in the OZR. Microvessel stiffening, therefore, may mechanically reduce the reactivity of microvessels under high glucose. Significant biological controls of vascular tone are discussed in chapter IV (vasoreactivity) and chapter VII (flow mediated dilation).

An additional architectural element to affect O_2 delivery that we studied was the geometry of the bifurcation region. In the large vessel circulation, the effect of the geometry on flow patterns within the bifurcations has been extensively studied. Overall, the geometry of the flow region has been found to significantly impact flow distribution in these large vessels. However, there are a number of mechanical differences between the macro- and micro-circulation that affect blood flow. In the microcirculation, the viscous forces predominate, as opposed to the macro-circulation where inertial forces predominate. In engineering terms, the Reynold's number (Re) is well above unity for the macro-circulation and below unity in the microcirculaton. The Re number can be calculated by equation 6.1, where ρ is the fluid density, V is the fluid velocity, L is the relevant length scale, for flow in a tube this is the radius, and μ is the viscosity of the fluid.

$$\mathrm{Re} = \frac{\rho V L}{\mu} \qquad \text{(equation 6.1)}$$

For the terminal arteriolar networks studied here, we estimated Re to be approximately 0.0027 to 0.0379 according to the equation 6.2 below, where ρ is the density of whole blood[15], V is the average velocity of flow through the

terminal arteriolar networks for this study (see chapter VII), L is the average diameter of the network feed for this study (see Table 6.1), and μ is the viscosity of blood plasma[16].

$$\begin{aligned} \mathrm{Re} &= \frac{\rho V L}{\mu} = 0.0027 - 0.0379 \\ \rho &= 1050 kg/m^3 \\ V &= 0.00029 - 0.003972 m/s \\ L &= .00001 m \\ \mu &= 0.0011 kg/m \cdot s \end{aligned}$$ (equation 6.2)

While the macrocirculation with high Re has inertial driven flow, the microcirculation with low Re exhibits viscous driven flow. For viscous driven flow conditions, the network architecture, especially at bifurcations, is important in two regards. First, within the bifurcation junction, the fluid expansion region with its decreased resistance, exhibits a characteristic increased gradient in shear along the wall leading to the branch[17]. Second, previous studies have shown that bifurcation shape itself is linked to red blood cell flux distribution at branch points[18]. Additionally, the tube diameter (arteriole) to particle diameter (RBC) ratio will dictate cell behavior and distribution through the vessels (Fahraeus Effect, chapter VII). The present chapter examines the architecture of the bifurcations and networks. The relationship between shape and red blood cell distribution will be explored in chapters VII and VIII.

There are two architectural measures we used to characterize the geometry of the junction region: the angle of bifurcation and the curvature of the wall at the point of flow division into the bifurcation, often referred to as the radius of curvature (Figure 6.1). A detailed summary on how angles of bifurcation and the radius of curvature are measured is given in Appendix II and Appendix III respectively. Some studies have shown that RBC distribution, and therefore O_2 distribution, is influenced by the shape of the junction between arteriolar network feed and branch[18,19], while others have shown that branch angles affect rheological behaviors such as shear rate and particle velocity[19,20]. The extent to which it affects flow and flux in systems with low Reynolds numbers is debated.

Additionally, bifurcation angle is not believed to be fixed in the microcirculation. Frame and Sarelius showed that the branch angle in the terminal arteriolar networks of the hamster cheek pouch were dynamic and could change as much as 50° with a change in vasoactive tone[18]. Radius of curvature on the other hand has been modeled in the large vessels, but to the best of our knowledge, no microvascular radius of curvature data has been reported.

Terminal arteriolar network structure is impaired clinically in patients with metabolic disorders; this is chiefly seen as rarefaction. Function is also shown to be impaired with significantly decreased oxygen supply capacity. In order to understand the role of the architecture changes in the diabetic pathology, arteriolar network architecture first must be understood in the normal state. This study defines normal terminal arteriolar network structural architecture in normal mouse cremaster and characterizes the changes in the architecture brought about by elevated glucose, both acutely and in two murine models of chronic metabolic syndrome.

Research Design

Using the methods presented in chapter III, five different measurements were taken from the network: total network length, interbranch length, diameter, and number of bifurcations. Architectural analyses are described below. Angle of bifurcation was calculated using the methods shown in Appendix II using the measurements from chapter III, and reflects the angle within one tube diameter of the bifurcation point. An estimate of the curvature of the apical wall for each bifurcation, radius of curvature, was calculated by fitting a circle to the three points that defined the apex of the bifurcation. The radius of the inscribed circle is the radius of curvature. (The complete methodology can be seen in Appendix III). Finally, an estimation of the volume of the vessel at the bifurcation point was made using the projected 2-dimensional diameter values of both the feed and the branch at the point of bifurcation; this reflects the intravascular volume within 1-tube diameter of the junction. This calculation assumes a circular cross-sectional

area for the 3 intersecting blood vessel segments. The calculation is given in Appendix IV.

A power analysis was done prior to the start of the experiments to determine the number of animals needed, with a ß value of 0.40. It was determined that six animals would be required for each condition. Comparisons were made across treatment types and time of treatment for all C57/bl6 animals. Additional comparisons were made across strains and glucose states. All data are expressed as the mean and standard error. All comparisons were done using ANOVA analysis for repeated measures with an α value of 0.05.

Results

Average normal terminal arteriolar network shape: From the baseline data of all C57/bl6 mice, we determined that the average terminal arteriolar network in murine cremaster muscle is 464.9 ± 35.5 μm long with 3.5 branches. A schematic of a typical network can be seen in Figure 6.2 including average inter-branch lengths. Feed diameter averaged 11 ± 1 μm and branch diameter averaged 7 ± 1 μm (Table 6.1). Feed diameters trended smaller along the network, with the difference between first and last being statistically significant. Branch diameters, on the other hand, did not show a trend along the network (Figure 6.3). Apical branch angles ranged from 17.1 – 137.7º, lateral angles ranged from 43.3 – 177.8°, and continuation angles ranged from 108.2 – 207.3º (Figure 6.4). The lateral angles at the last bifurcation were significantly more obtuse and the continuation angles were significantly more acute at the last bifurcation than at all other bifurcations (Figure 6.5), likely because most last bifurcations were a Y-shape as opposed to a T-shape for upstream branch points. Apical angles demarking the shape of the flow divider did not differ by position (Figure 6.6). The average calculated apical radius of curvature was 4 ± 1 μm and likewise showed no dependence on bifurcation sequence. The estimated bifurcation volume was also independent of bifurcation number and had a network average of 2.213 ± 0.199 pL.

Total network length and number of branches varied by strain (Table 6.2). Interbranch lengths were statistically similar, due to large standard deviations in the ob/ob animals (Figure 6.7). The low occurrence of branch 2 and complete lack of branch 3 in the db/db animals made comparisons at these branches impossible.

Diameters: With two hours of acute exposure, there were no significant changes in average branch or feed vessel diameter for any treatment (Table 6.3). However, two hours of elevated glucose exposure caused an increase in the magnitude of the variance which was two to four times that of the other three groups. When the data were analyzed by bifurcation sequence, a trend began to emerge (Figures 6.6 – 6.9). Overall, glucose and mannitol induced changes that were manifest at the second bifurcation moreso than at other bifurcations; the lack of significance of these changes may be attributable to the increase in variability.

In the two models of metabolic syndrome, the feed diameter of the db/db mice were significantly smaller than metabolically normal C57/bl6 mice overall (Table 6.4). Yet, when analyzed by bifurcation sequence, the db/db strain had significantly smaller diameters (feed and branch) than both the C57/bl6 and the ob/ob mice at only the first bifurcation (Figure 6.10). Further analysis of the first bifurcation diameters, demonstrated that the all four segments were significantly smaller in the db/db mice as compared to the C57/bl6s (Table 6.5). Segment diameter did not differ between bifurcations.

Angles of bifurcation: In the acute study, over two hours of treatment, there was no change in the average of the bifurcation angles with any treatment (Figure 6.11 - 6.14). Once again, the second bifurcation demonstrated trends in angles changes with glucose that highlight the second bifurcation. For instance, there is a decrease in apical angle and increase in lateral angle with glucose at the

second bifurcation only. The apical angle trends follow the same pattern seen in the branch diameter data.

In the comparisons of the two metabolic syndrome models with the metabolically normal C57/bl6, only the apical angle at the last bifurcation was different among the three strains, and was bigger in the db/db strains than in the other two (Table 6.6). Again the relatively small number of data points for the second and third branches in the db/db animals makes a complete statistical analysis impossible.

Radius of Curvature (ROC): Radius of Curvature for the and the comparison between metabolic syndrome strains is given in Tables 6.7 and 6.8 respectively. No significant trends were seen when glucose or mannitol was applied for 2 hours. The ROC value for the db/db mice at the first bifurcation however, was significantly smaller than that of the wild type mice, with no change in the ROC value for the ob/ob mice.

Bifurcation Volume: Bifurcation volume for both the two hour exposure experiments and the metabolic strain comparison is given in Tables 6.9 and 6.10 respectively. Again, no patterns of significance were found in either set of data. Further linear regression analysis also showed that bifurcation volume was not dependent on apical angle.

Conclusions

This study addresses the effect on the terminal arteriolar networks in the mouse cremaster muscle of exposure to glucose for two hours as compared to the chronic metabolic syndrome states for diabetes and obesity. We have shown significant and distinct rarefaction-like architectural changes in both diabetic and obese mouse models including changes in the network lengths and number of branches. Additionally, we have demonstrated that resting diameters in diabetic animals are smaller than in both the metabolically normal and obese strains.

It is generally accepted that diabetic patients have significant rarefaction of the microvasculature leading to insufficient blood flow and nutrient delivery. However, the architectural changes in the terminal arteriolar networks have never been characterized. Characterization of the networks would elucidate the effects on local regulation of blood flow and how those effects might lead to the development of complications seen in vascular disease such as rarefaction and decreased tissue perfusion. This is the first description of normal mouse terminal arteriolar networks that includes not only the lengths and number of branches, but the angles of bifurcation and a description of the curvature of the wall at the location of flow division for each bifurcation. Partial descriptions have been produced in the hamster and the rat, and show comparable network organization (e.g. networks arise from arcade arteries, branch sequence is spatially organized the same, each branch feeds one capillary module, etc.) as shown here[18,22]. The consistency of these descriptions indicates that these networks are similar across strains and tissue types, which is to be expected as the architecture of the networks is a key component in the function of these networks.

Acute effects of glucose elevation: Acute changes in blood glucose are common in mammalian organisms with blood sugar increasing as much as 50% after a meal (postprandial glucose) in a metabolically normal individual[22]. However, blood glucose levels in a metabolically normal individual should return to normal levels (maximum 120 mg/dl in humans) by two hours. In fact, this physiological response is the basis for the diagnostic test used to identify patients with impaired glucose tolerance. As such, it would be expected that at 20 minutes, there would be little effect of elevated glucose on microvascular remodeling. Our results support this fact, with no significant effects in any measure at 20 minutes of elevated glucose exposure. This does not include vasoactive changes in diameter, which are much more rapid responses and therefore effects of glucose act in the shorter time frame, see chapter IV.

Two hours of elevated glucose however, marks the very beginning of pathological impairment of glucose handling. The effects seen at this point are

examples of the earliest changes the tissues undergo. These effects may be the trigger that eventually leads to long-term effects and lead to the complications seen in diabetes and other metabolic disorders. Identifying these early effects is therefore a key first step in elucidating the progression of that disease state from normal conditions.

In these studies, two hours of glucose exposure had no significant effects on the architecture in any measure. This may be a reflection of the study design. As explained above, we are at the earliest temporal limit of glucose metabolism dysfunction, by choice, in order to be able to ask the question, "What happens at the earliest stages of elevated glucose?" We have addressed that question directly, and demonstrated that no significant architectural effects happen immediately.

However, the data still hold information of the earliest effects of elevations of glucose and of network function. In both the diameter data (Figure 6.8) and the bifurcation angle data (Figure 6.12) the initial effects seen after two hours of glucose exposure begin to display a pattern below the level of statistical significance. The responses in both diameter and bifurcation angle, however small, appear to happen exclusively at the second bifurcation. This suggests that the second branch may be more sensitive to changes in conditions as compared to the other bifurcations. In particular, the junction region of the second branch seems to be particularly sensitive, and it dilates under both an elevated glucose (Figure 6.8) and a high osmolar (mannitol, Figure 6.8) conditions. The sensitivity of the second bifurcation may indicate a location of importance. We postulate that a location of higher sensitivity to metabolic conditions could be a location of regulatory control. More work will need to be done to test these hypotheses.

One additional observation to come out of the acute studies is the fact that elevated glucose increased the variability of the diameter data disproportionately to the other three treatment groups (Figure 6.8). This increase in variability suggests that glucose disturbs the regulatory mechanisms for diameter and vascular tone in a non-specific manner. This observation agrees with the results of chapter IV, which demonstrate suppressed NO dependent dilation under high

glucose conditions, with different mechanisms for endothelial cell dependent vs independent dilation.

Chronic effects of elevations in glucose as seen in metabolic syndrome models: There are several significant findings resulting from the comparisons between the two metabolic syndrome mouse strains and the metabolically normal C57/bl6 animals. First, we demonstrate different phenotypes of apparent microvascular rarefaction in the two different metabolic disorder models. In this study we did not measure vascular density directly; observationally however, we noted that both the db/db and ob/ob models have a lower density of terminal arteriolar networks in the tissue than in the C57/bl6 wild-type animals. The network architecture data showed a distinct difference between the two strains. In the db/db animals, the networks were shortened and possessed fewer branches per network. On the other hand, the ob/ob animals had the same number of branches as the wild type C57/bl6 animals, but were significantly longer in total network length. While the interbranch lengths were not statistically different between the three strains for any single branch, the variability within the ob/ob animals were primarily responsible for this. Looking at Figure 6.7 demonstrates that the interbranch length for branches 2, 3 and last were longer than the other two strains. If we assume a constant number of networks, it follows that there are larger areas without branches, and potentially larger areas without capillary beds than in wild-type mice. Both of these architectural changes results in an effective reduction in the number of capillary beds being fed per network, but with much different phenotypes.

The differences in terminal arteriolar network phenotype between the two strains may be related differential cytokine expression reported in chapter V. VEGF, a pro-angiogenic factor, was decreased in the diabetic animals as compared to the obese animals, as was IL-6 which induces VEGF expression. The reduction in VEGF expression is consistent with the reduced vessel length and/or the reduced number of branches in the db/db animals. In contrast, the elevation in VEGF for the ob/ob mice is consistent with both the increased length

of the central feed arteriole and the increased diameter. However, as the ob/ob mice did not have an increased number of branches over the longer length, perhaps the role of VEGF to induce migration was unhindered, while the role to induce new vessel sprouting was hindered by other factors.

The reduction in the number of branches in the db/db animals is particularly interesting if we consider the phenomena in conjunction with the results from our acute studies. The patterns of sub-significant effects seen in the diameter and angle data seen in the 2 hour glucose treatments in C57 animals suggested that the second branch was the most sensitive to changes to suffusate composition. In all but one of the db/db animals, there were no existent second branches, and no third branches in any. This allows us to speculate that there is the possibility of a pattern of vessel loss in the diabetic animals where the second branch is lost over time due to changes in environment, changing the third to the second and so forth, until the networks are left with only the first and last branch (the configuration of branches most commonly seen in the db/db mice that we measured). Chronic studies that measure vessel density over time would be needed to substantiate this. Additionally, the loss of intermediate branches in the db/db animals must be kept in mind while performing our analyses on the other architectural measurements.

The phenotypes of the two metabolic mouse models continued to be distinct when looking at the diameter measurements. The feed diameter of the db/db mice was significantly smaller than normal mice when averaged over the entire network (Table 6.4). No decrease in diameter was seen in the ob/ob animals. When analyzed by bifurcation sequence, the db/db strain had significantly smaller diameters (feed and branch) than both the C57/bl6 and the ob/ob mice at only the first bifurcation (Figure 6.10). This however, is affected by a sample size of only one at the second bifurcation and a sample size of zero at the third bifurcation for the db/db mice. Obviously, the absence of the second and third bifurcations in the diabetic mice indicates a significant difference between the strains. Therefore we can conclude that the first branch (reduction in diameter) the second branch (near complete absence) and the third branch

(complete absence) are all adversely affected by the diabetic pathology. This consideration serves to further highlight the fact that despite the fact that we see major changes in vessel diameter between the db/db and the C57/bl6 animals at most of points of bifurcation, there is no difference in diameter at the last bifurcation. We speculate that the mechanism for control of diameters and/or angles differs for the last bifurcation compared to the others, and this may be related to some as of yet unknown difference in rheologic environment between them. In fact, data presented in chapter VII shows that there is significant shunting to the last branch. The continued flow to the last branch due to shunting may be responsible for the lack of change in the architecture of the last branch.

In terms of oxygen delivery, the reduction in branch number and diameter to the first three branches potentially indicates a reduced capacity for oxygen delivery to the tissue. A rough estimation of oxygen delivery in each species is made in chapter VIII. We analyzed the first bifurcation diameter data further, in order to see if the changes are localized within the bifurcation. We found that all four segments were significantly smaller in the db/db mice as compared to the C57/bl6 animals. There remained however, no differences in segment diameters at the last bifurcation. What the mechanism is that seems to protect the last bifurcation is as of yet unknown, and may be a result of the distinct bifurcation shape differences at the last bifurcation. Whatever the mechanism, the last bifurcation remains unaffected by chronic elevations in glucose as seen in mice with metabolic syndrome.

From a fluid dynamics perspective, the curvature of the wall at the point of flow division, referred to as the apex throughout this study, is a point of interest. At the apex, the division of streamlines to separate downstream branches in a high Reynold's flow is well known. Following streamlines, the way the convective flow would be divided would be dictated by the angle of the bifurcation and by the pressure head across the section of vessel in question. However, with a low Reynold's number flow, and in a 2-phase non-Newtonian fluid, the behavior at the bifurcation is theoretically less well understood. A full description of the geometry at the apex may help elucidate the mechanisms of flow division.

The shape of the curvature of the apical wall in low Re flow conditions has not been extensively reported. In computational models of flow through arteriolar network bifurcations, the radius of curvature is often a fixed parameter, and is usually considered to be the sharp corner that results from the intersection of two tubes. The present study shows that the apex of in vivo branch points is not always sharp, nor fixed. In addition, these results show no correlation of ROC with other architectural measurements.

One of the reasons for a lack of measurement data on the curvature at the apical wall of the bifurcation is that all means of quantification have inherent limitations. We have chosen to quantify the shape of the apex by approximating the radius of curvature from the 2D image. That is, we approximated the radius of a circle described by three functionally defined points along the apical wall: the apex (the point of inflection at the apical wall), a point half of one feed diameter up the feed wall from the center of mass of the bifurcation, and a point one half of a branch diameter up the branch wall from the center of mass of the bifurcation. The circle described by these points would be larger for rounded apices and smaller for sharper apices. The ROC did not vary at all along the network by bifurcation or under any of the treatments in the acute study. This methodology for approximating the curvature of the apex did not return any evidence that the ROC was varied by group within the networks at all.

Assumptions and Limitations of the Study

These results highlight the importance of the methodology used to measure angles of bifurcation. The methodology used here measures the angles at the midline of each vessel and the midline is determined at one tube diameter down each vessel, one tube diameter was selected as it represents the entrance length for the flow (see Appendix II for full calculation methodology). Whether the angles are measured at the wall or midline, and how far down to measure those angles however, could significantly alter the results, as the vessels are not perfectly straight nor of perfectly constant diameter.

In the interest of knowing how different the angles would be if we were to measure them at different points along the bifurcation, we calculated two alternate angles to compare to the apical angle measurements. All three angles are shown in Figure 6.16. All three angles correlate. The apical angle along the midline and the outside wall angle are in near perfect agreement (Figure 6.16a). The apical angle along the midline and the inside wall angle do not correlate as strongly (Figure 6.16b). This suggests that measuring angles along the wall will be affected by the curvature of the apex if measured too closely to the apex. On the other hand, if we were to go even further out, we get beyond the functional region of flow division after flow has passed its entry length and reestablished the velocity profile. These points need to be kept in mind when comparing data from the literature or in taking future measurements.

Additionally, as with the data presented in chapter IV, this data is taken from a 2 dimensional image of the vessels and networks. In the native tissue, these vessels can run in three dimensions, and as such a certain amount of information is lost when characteristics in the third dimension are reduced to two dimensional space. This results in network length measurements that are slightly shorter than the actual measurements since we do not see distance along the z axis, as well as potentially smaller angle measurements in the event that they are slightly rotated in the xz or yz plane. However, in the cremaster muscle these limitations are minimal, as the tissue itself is only 400-500 μm thick, the distances lost are often within measurement error.

Summary

This study shows that the terminal arteriolar networks of normal mice are spatially organized in a consistent manner, and that the spatial organization of those networks is significantly affected by metabolic disease. These findings may be related to a change in function of the networks also seen in the diabetic pathology. Furthermore, short term elevations of glucose suggest evidence of an important mechanosensory role for the second bifurcation within the network that

that may be related to the long term changes seen in the metabolic syndrome mouse models.

Figure 6.1

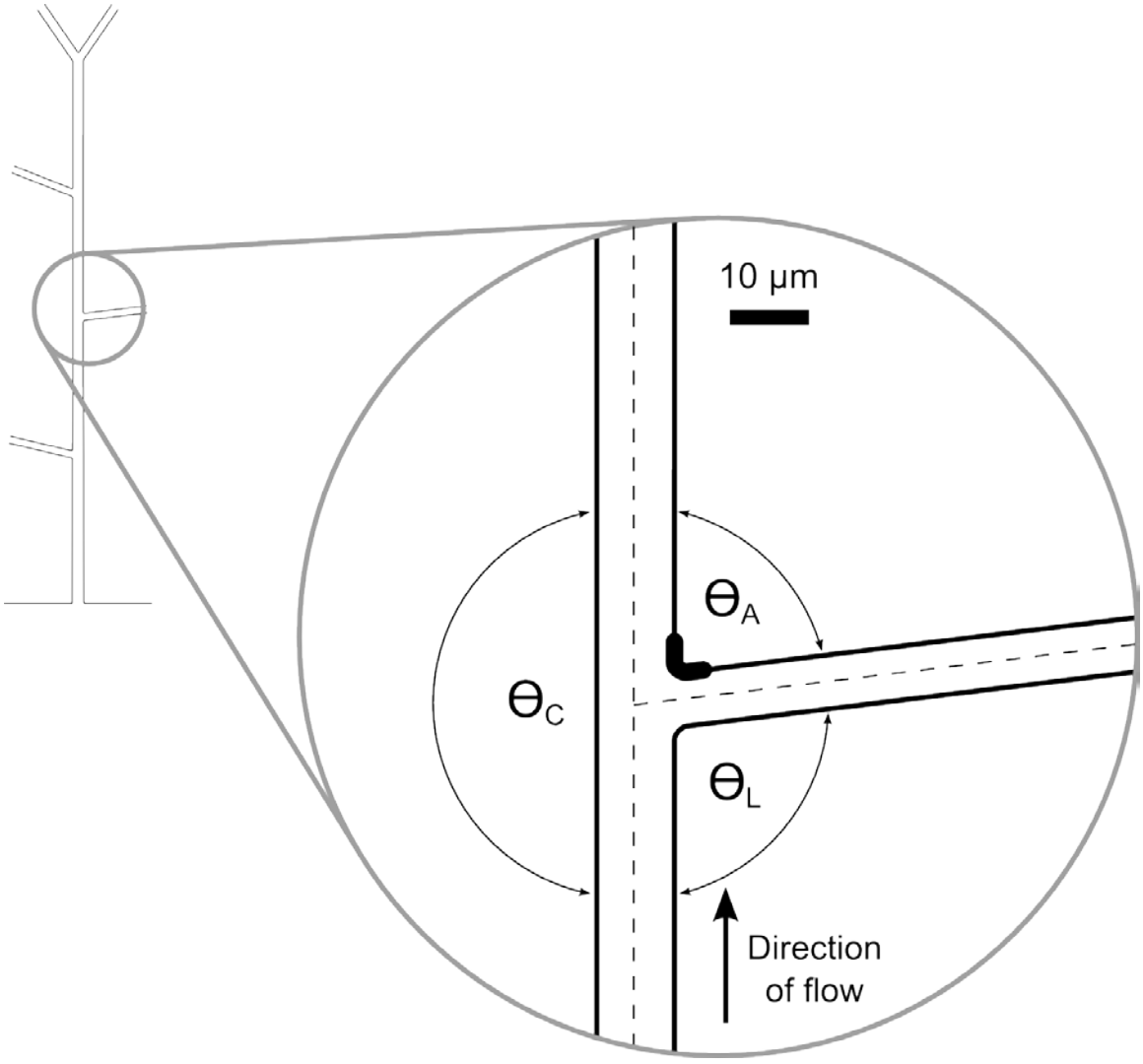

Schematic representation of the location of the apical bifurcation angle (θ_A), lateral bifurcation angle (θ_L), continuation angle (θ_C), and the location of measurement for the radius of curvature (bold line). A full description of the methodology for angle measurement can be found in Appendix II.

Figure 6.2

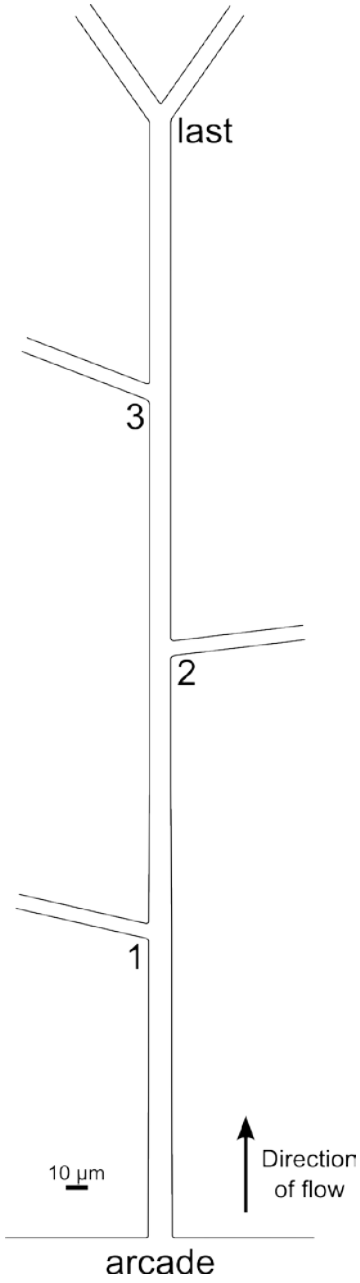

To scale representation of the average normal mouse terminal arteriolar network detailing relative interbranch lengths and angles of bifurcation. Bifurcations are numbered starting proximally and increase axially along the network. Branching direction (to the right or to the left) was random.

Table 6.1

Bifurcation	Interbranch Length (µm)	Feed Diameter (µm)	Branch Diameter (µm)
1	141.5 ± 15.3	11 ± 3	7 ± 1
2	143.4 ± 19.5	10 ± 2	7 ± 2
3	112.5 ± 19.7	10 ± 3	7 ± 1
Last	136.0 ± 17.1	9 ± 2	8 ± 1
Total Network	464.9 ± 34.5	10 ± 1	7 ± 1

Bifurcation	Apical Angle (°)	Lateral Angle (°)	Continuation Angle (°)
1	77.0 ± 5.9	112.4 ± 5.8	167.6 ± 3.4
2	83.1 ± 6.6	105.2 ± 7.1	167.6 ± 3.7
3	68.9 ± 7.9	121.9 ± 7.9	169.3 ± 3.0
Last	69.9 ± 3.7	135.3 ± 3.8	154.9 ± 4.1
Total Network	75.03 ± 2.93	118.84 ± 3.17	164.20 ± 1.93

Bifurcation	ROC (µm)	Bifurcation Volume (pL)
1	3 ± 1	2.546 ± 0.357
2	4 ± 1	2.049 ± 0.390
3	5 ± 2	2.236 ± 0.648
Last	5 ± 2	1.873 ± 0.310
Total Network	4 ± 1	2.183 ± 0.200

Architectural measurements in terminal arteriolar networks of the normal mouse. All data presented as mean ± SE.

Figure 6.3

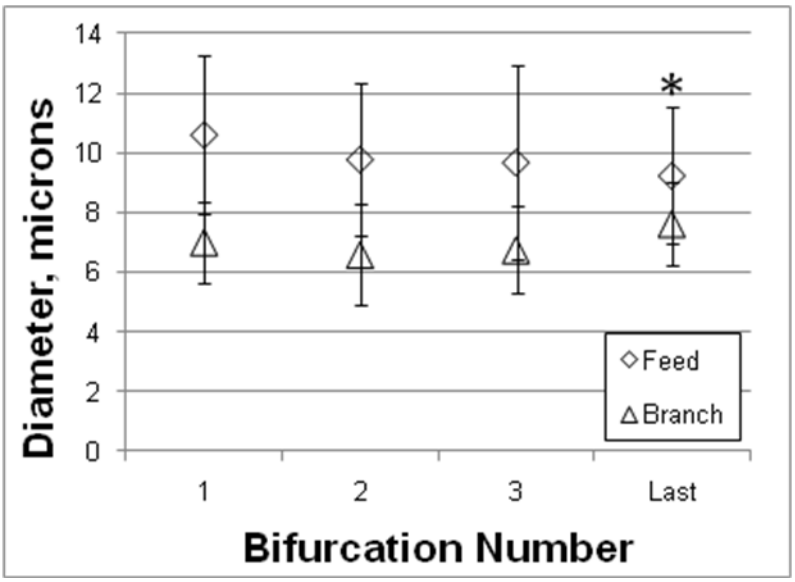

Diameter measurements in a normal mouse terminal arteriolar networks. Feed (open diamonds) and branch (open triangles) diameters by bifurcation number for C57/bl6 mice at baseline conditions. Data are mean ± SE. No significant differences were found among the branch diameters. Feed diameter decreases along the network with the diameter at the first bifurcation significantly larger than that at the last bifurcation. ($p < 0.05$)

Figure 6.4

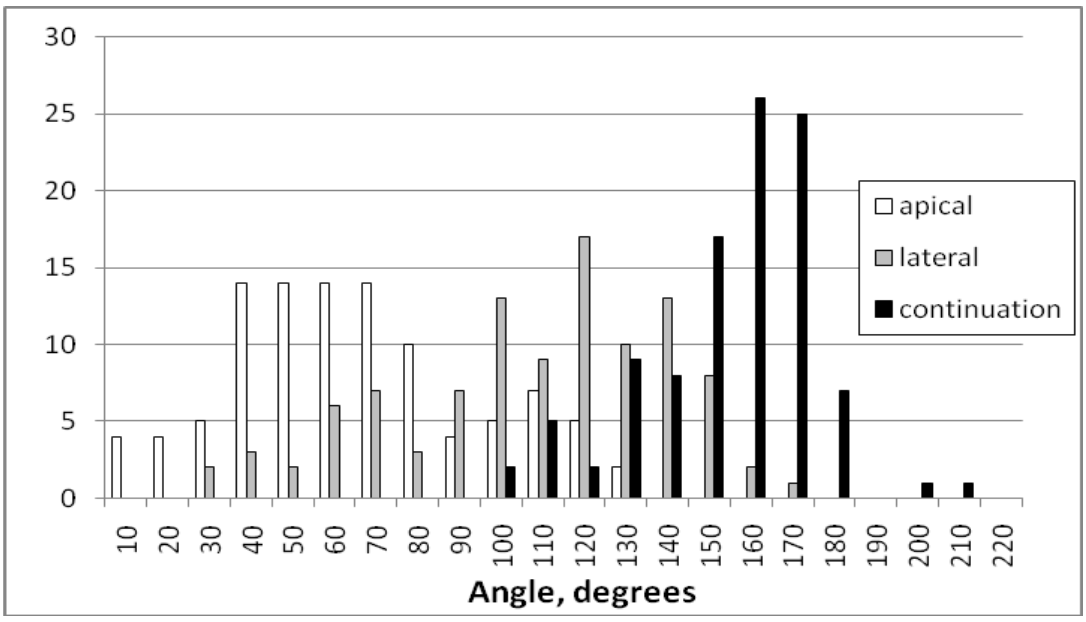

Histogram of angle distribution in C57/bl6 mice at baseline conditions, all bifurcations are pooled. See Figure 6.1 for schematic of angle locations.

Figure 6.5

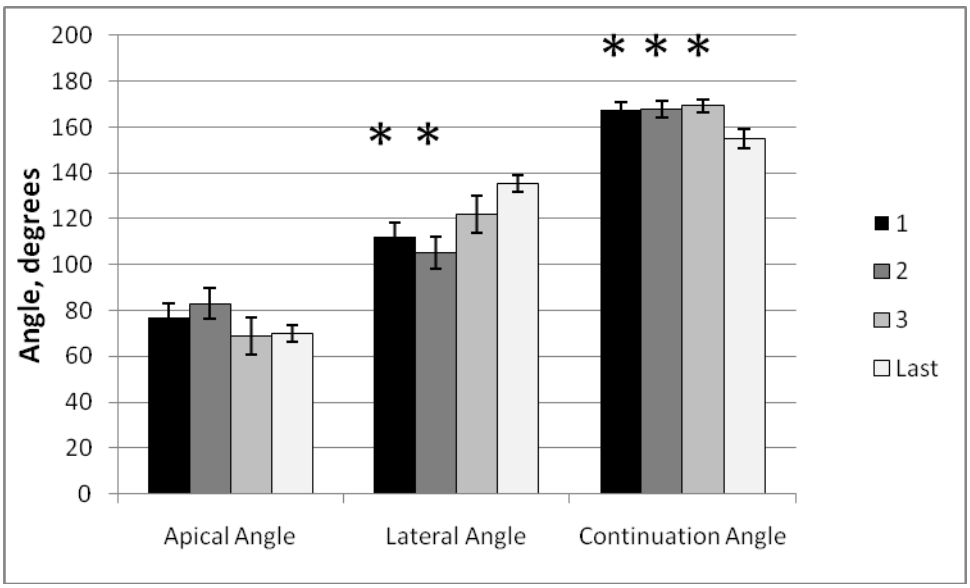

Angle distribution by bifurcation number along the terminal arteriolar networks of metabolically normal C57/bl6 mice. Data are presented as mean ± SE. Apical angle does not vary along the network. For both the lateral and continuation angles, upstream angles are significantly different from the last angle. ($p < 0.05$) For a schematic of angle locations, refer to Figure 6.1.

Figure 6.6

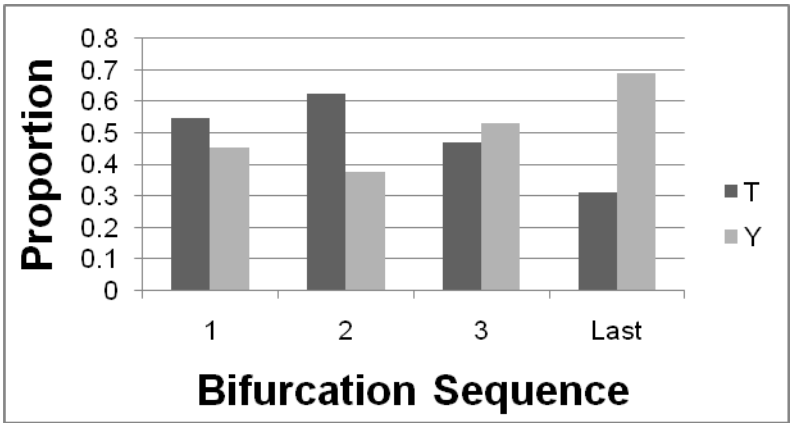

Distribution of branch shape by bifurcation number in metabolically normal mice. The vertical axis is proportion of total branches. Y shape is defined as having both the lateral and continuation angles greater than 120 degrees. Both the first and the third bifurcations have nearly equal distribution of T and Y bifurcations. The last bifurcation along the network is predominantly Y shaped, and the second bifurcation is predominantly T shaped.

Table 6.2

Strain	Number of Branches				Total Network Length			
C57/bl6	3.5	±	0.2		464.9	±	34.5	
db/db	2.0	±	0.3	*	206.5	±	32.0	*
ob/ob	3.7	±	0.3	**	761.6	±	247.9	*, **

* vs. C57/bl6 ** vs. db/db $p<0.05$

Comparison of network measurements in the terminal arteriolar networks of C57/bl6, diabetic, and obese mouse strains. Diabetic mice have significantly shorter networks with a smaller number of branches than C57/bl6. Obese mice have significantly longer networks as compared to both the diabetic and C57/bl6 mice, with a comparable number of branches to the C57/bl6 mice. All data are presented as mean ± SE.

Figure 6.7

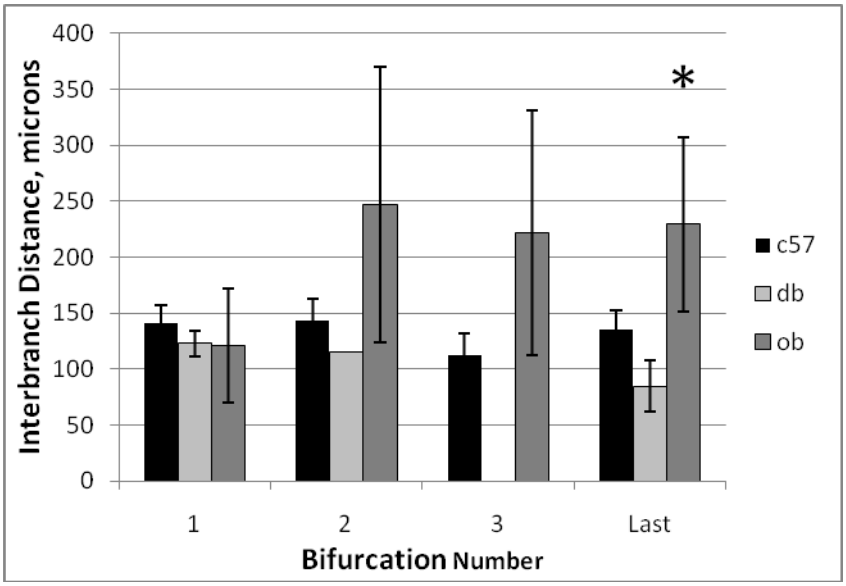

* vs. C57/bl6 $p<0.05$

Comparison of interbranch lengths by strain. At the last branch, obese mice have a significantly longer interbranch distance compared to the C57/bl6 cohort. Diabetic mice had only a single sample point at the second bifurcation and no animals with third bifurcations. All data are presented as mean ± SE.

Table 6.3

	Baseline	20 Minutes Exposure	2 Hours Exposure
	Feed Diameter		
control	10.31 ± 0.87	10.04 ± 0.92	10.04 ± 0.75
glucose	13.04 ± 1.28	12.46 ± 1.81	12.11 ± 2.02
mannitol	9.92 ± 0.46	9.62 ± 0.50	9.63 ± 0.69
Lnna	9.44 ± 0.61	10.25 ± 1.15	10.05 ± 0.77
	Branch Diameter		
control	6.83 ± 0.37	6.33 ± 0.42	6.15 ± 0.35
glucose	7.94 ± 0.68	7.10 ± 0.75	7.23 ± 0.83
mannitol	6.90 ± 0.55	6.94 ± 0.31	6.07 ± 0.37
Lnna	6.51 ± 0.27	6.28 ± 0.34	6.47 ± 0.43

Network diameters for 20 minute treatment exposure experiments, with all bifurcations pooled. No significant differences were found. All data are presented as mean ± SE.

Figure 6.6: Patterns of dilation in acute control experiments. (page 1 of 2)

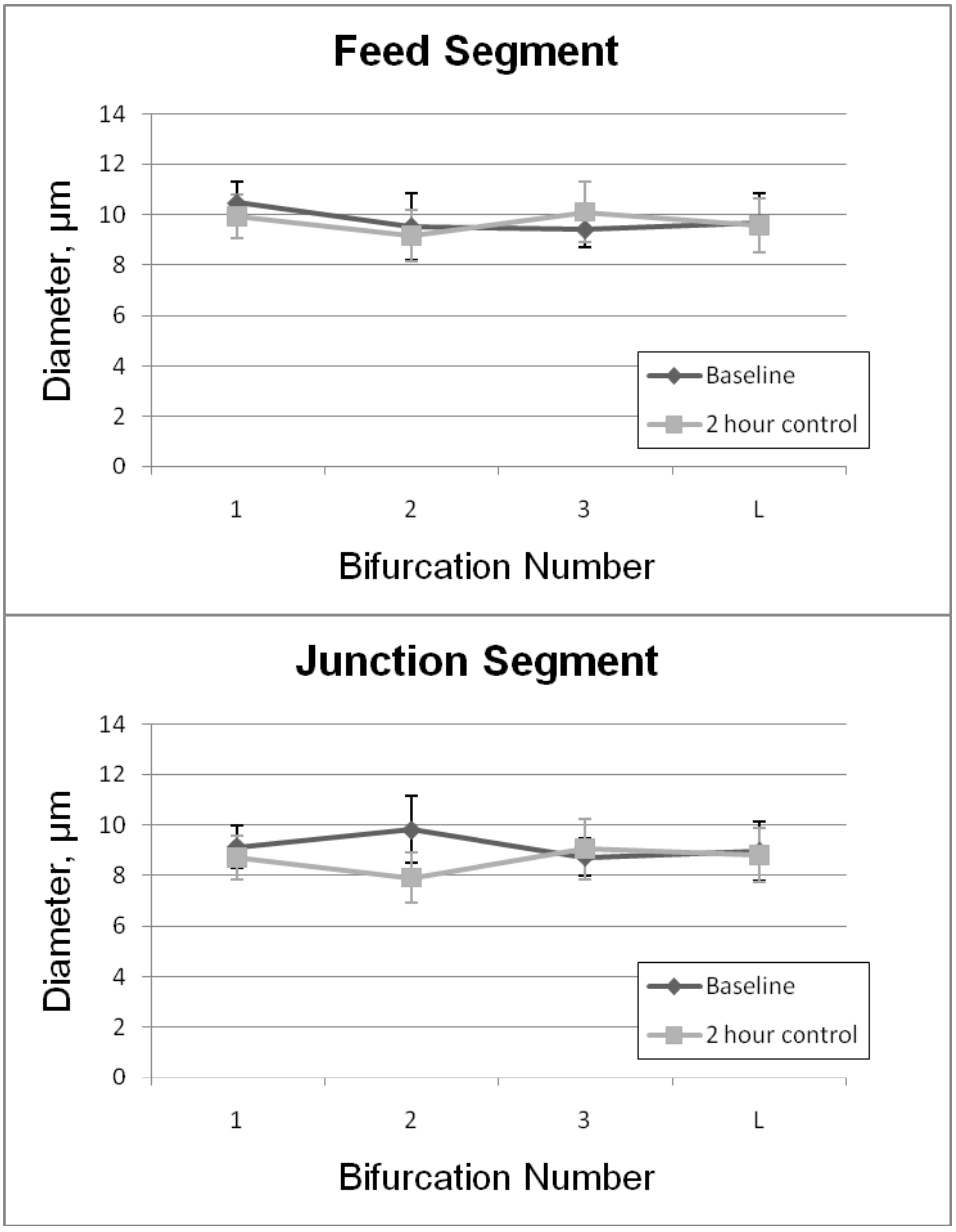

Figure 6.6 (Page 2 of 2)

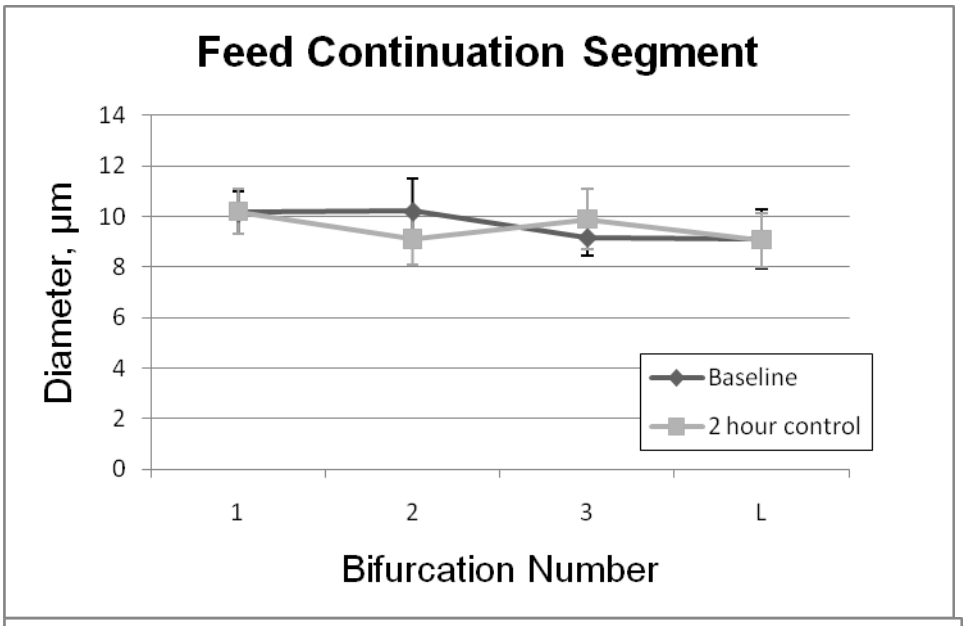

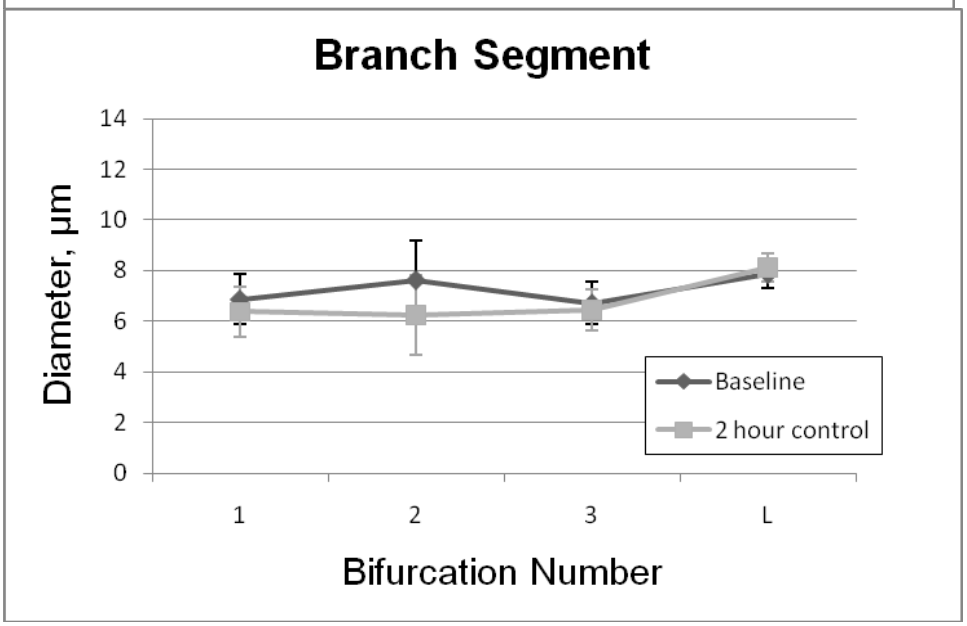

Patterns of dilation in acute experiments. C57/bl6 mice at baseline and at 2 hours of control suffusate exposure. There is a slight decrease in diameter at the second bifurcation within the junction, feed continuation, and branch segments, with almost no change at all other bifurcations at two hours of treatment. The feed segment showed no change at all. These changes are not statistically significant at p=0.05, but serve to illustrate that there is a behavior that is localized to the second bifurcation. Data are presented as mean ± SE

Figure 6.7: Patterns of dilation in acute glucose experiments.(page 1 of 2)

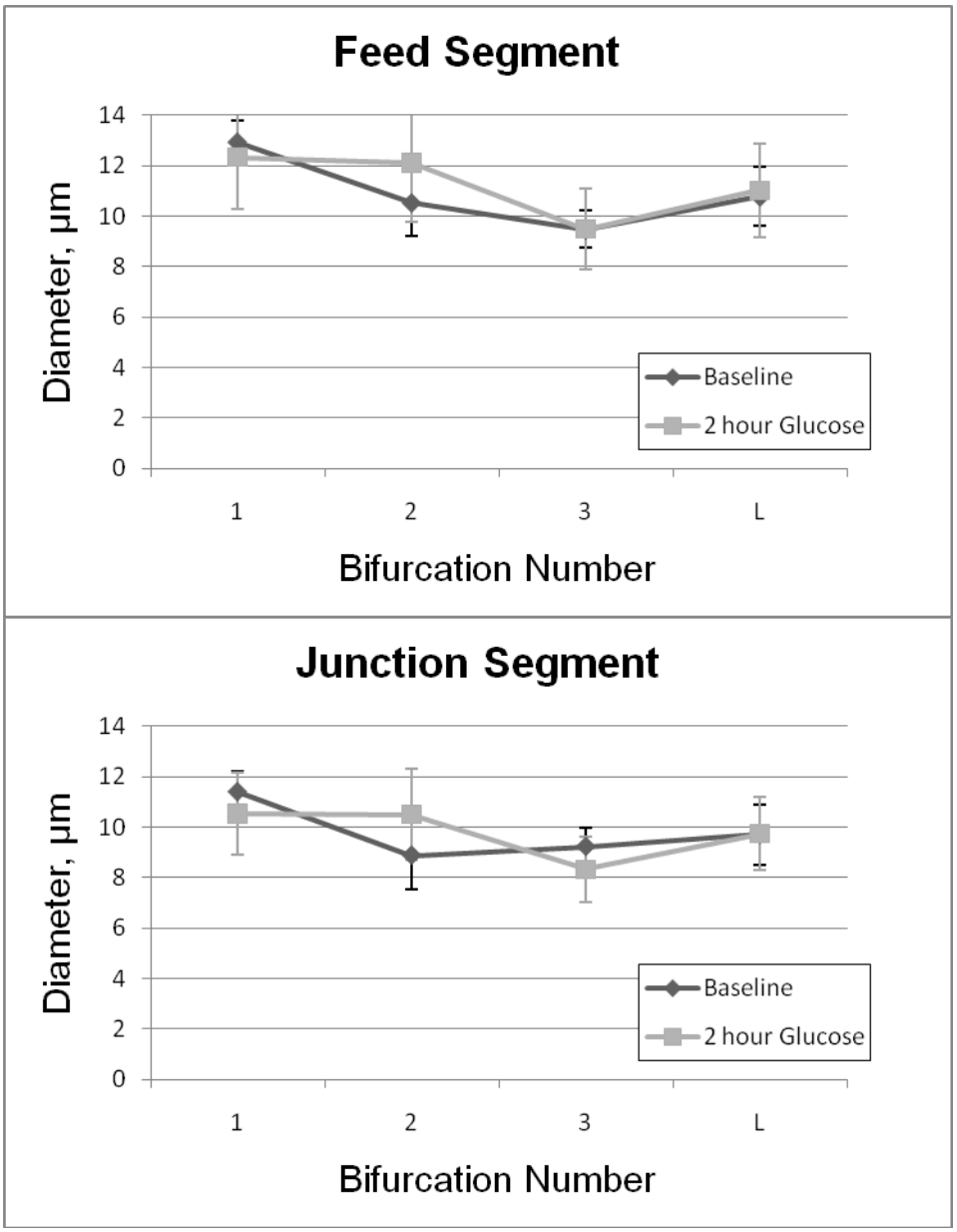

Figure 6.7 (page 2 of 2)

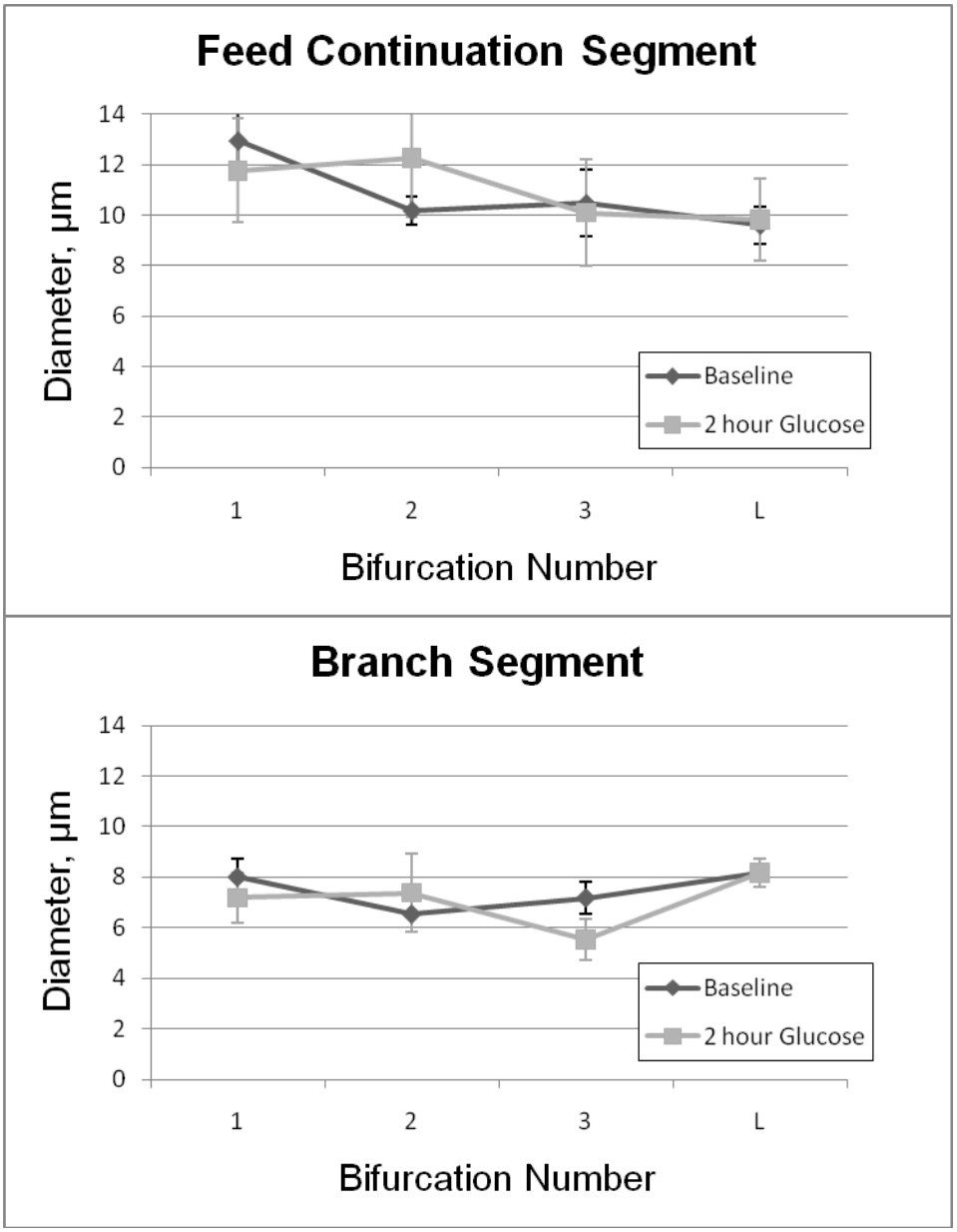

Patterns of dilation in acute experiments. C57/bl6 mice at baseline and at 2 hours of elevated glucose suffusate exposure. With two hours of glucose treatment there is a slight increase in diameter at the second bifurcation in all four regions. The only other locations with changes are the first bifurcation of the feed continuation and the third bifurcation in the junction segment. These changes are not statistically significant at p=0.05, but serve to illustrate that there is a behavior that is localized to the second bifurcation. Data are presented as mean ± SE

Figure 6.8: Patterns of dilation in acute osmolar control (mannitol) experiments. (page 1 of 2)

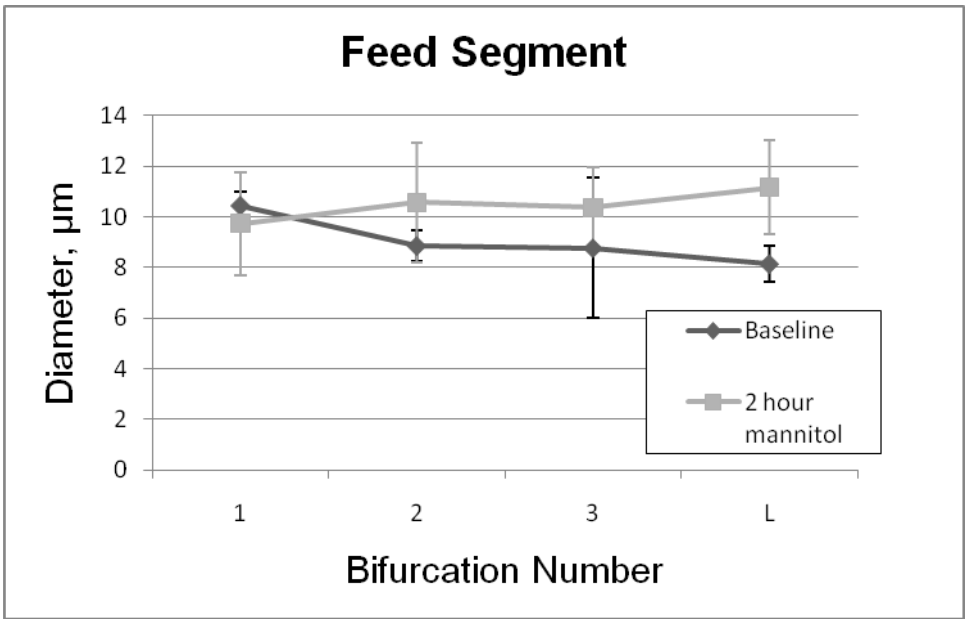

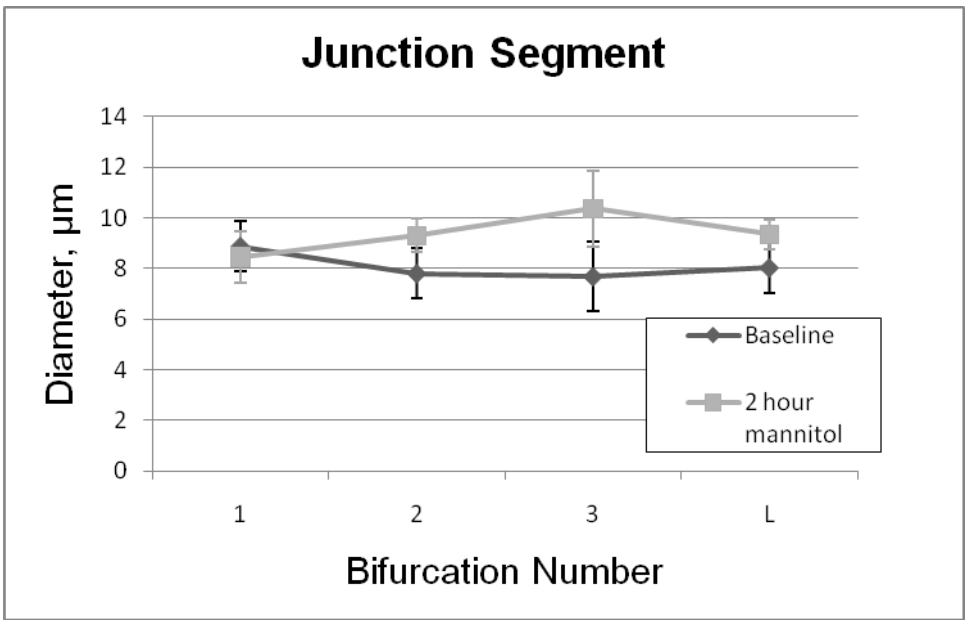

Figure 6.8 (page 2 of 2)

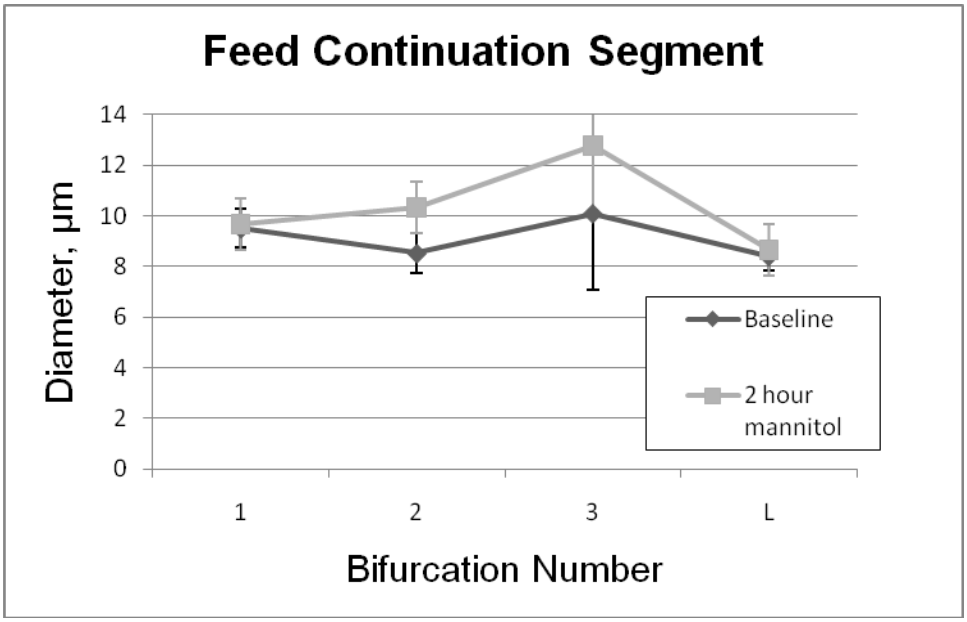

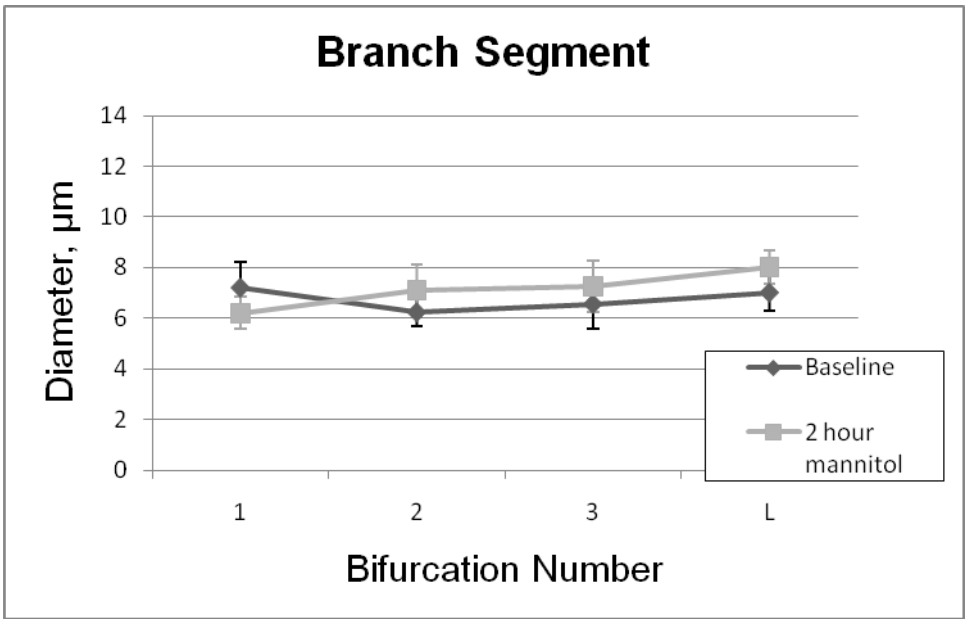

Patterns of dilation in acute experiments. C57/bl6 mice at baseline and at 2 hours of mannitol suffusate exposure. With two hours of mannitol treatment there is a slight increase in diameter at the second and third bifurcation in all four regions. The only other location with a change is the last bifurcation of the feed segment. These changes are not statistically significant at p=0.05, but serve to illustrate that the is a behavior that is localized to the second bifurcation for glucose and control is not restricted to the second bifurcation when the networks are treated with mannitol. Data are presented as mean ± SE

Figure 6.9: Patterns of dilation in acute induced endothelial dysfunction (LNNA) experiments.(page 1 of 2)

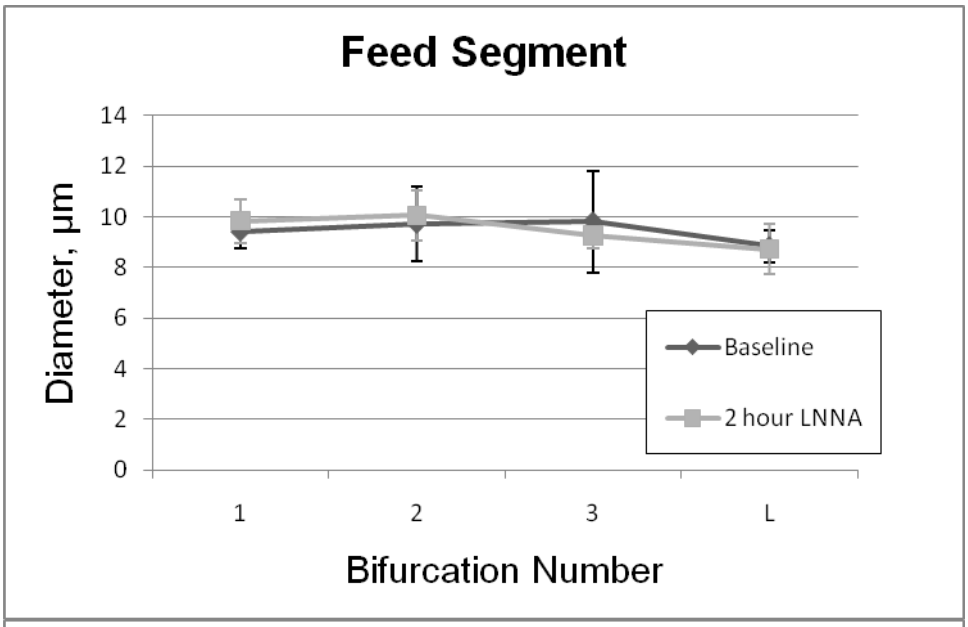

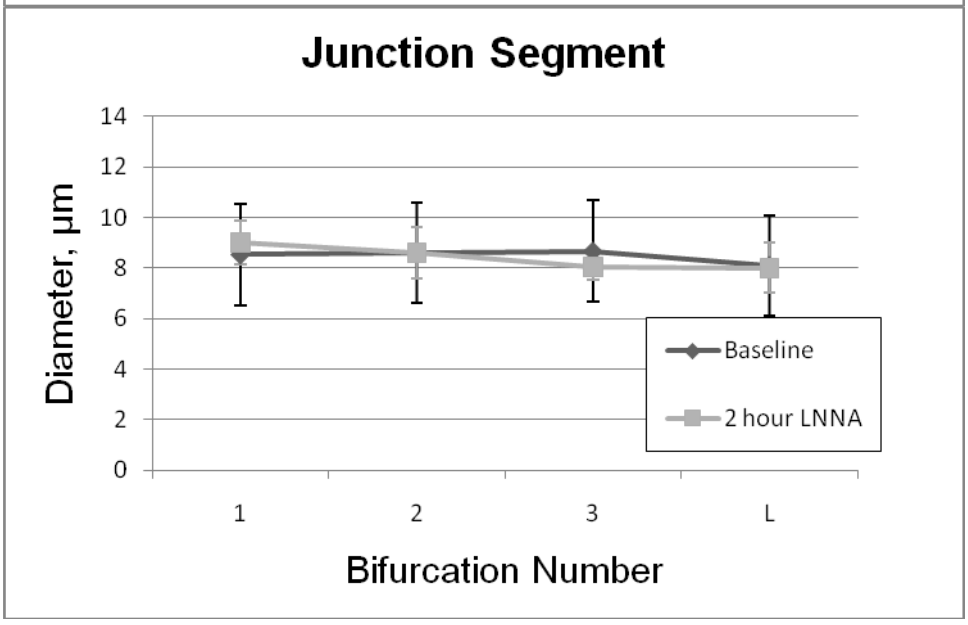

Figure 6.9 (page 2 of 2)

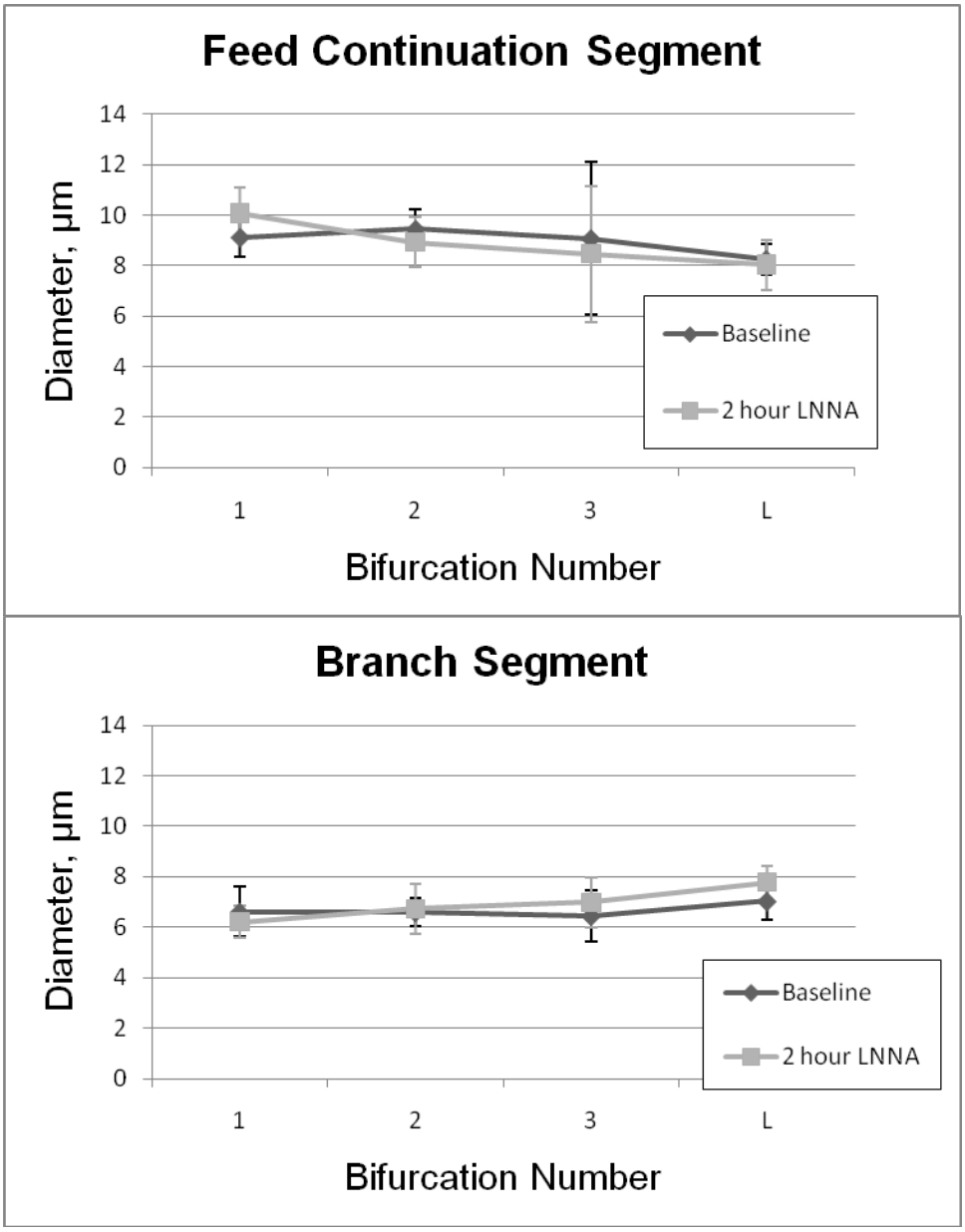

Patterns of dilation in acute experiments. C57/bl6 mice at baseline and at 2 hours of LNNA suffusate exposure. With two hours of LNNA treatment there are not even slight changes in diameter at any location. Data are presented as mean ± SE.

Table 6.4

Feed Diameter			
C57/bl6	10.61	±	0.48
db/db	7.65	±	0.81*
ob/ob	9.80	±	1.48

Branch Diameter			
C57/bl6	7.01	±	0.24
db/db	6.23	±	1.04
ob/ob	7.96	±	1.30

Network diameter across strains with all bifurcations pooled. Diabetic mice had smaller feed and branch diameters as compared to the C57/bl6 mice ($p<0.05$). All data is presented as mean ± SE.

Figure 6.10

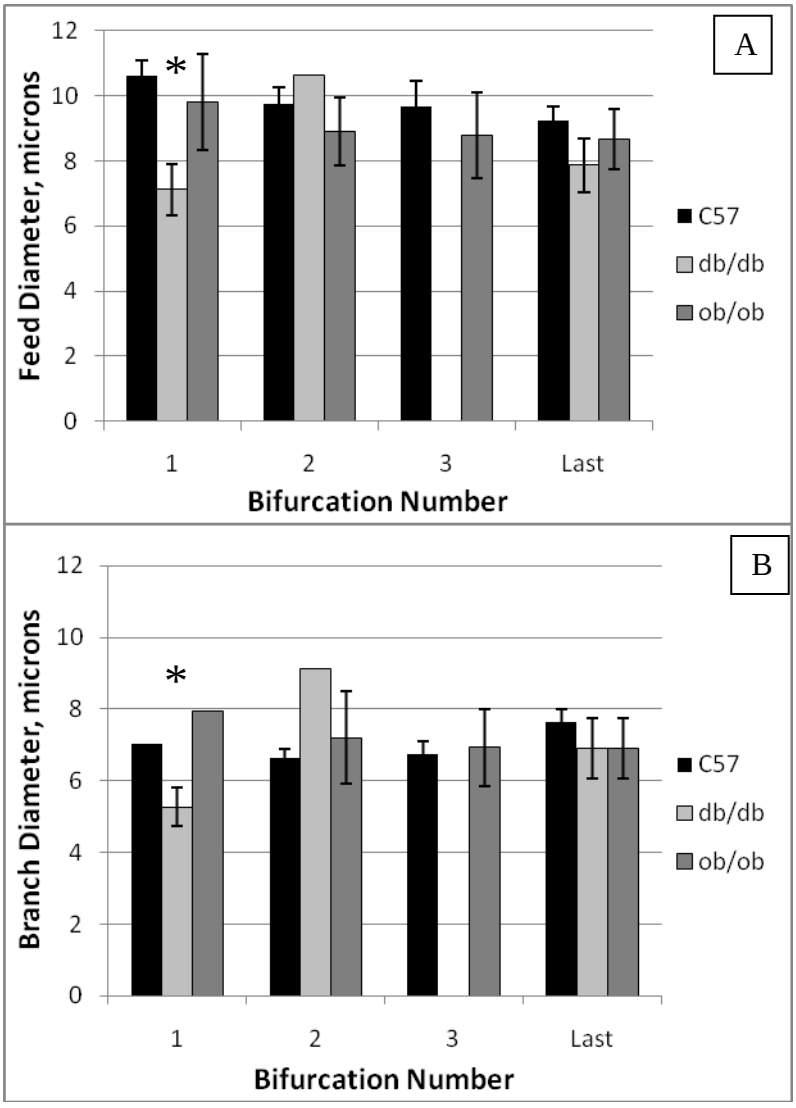

Network diameter across strains by bifurcation. Diabetic mice had smaller feed and branch diameters as compared to the C57/bl6 mice only at the first branch ($p<0.05$). All data is presented as mean ± SE.

Table 6.5

	Feed Segment	Junction Segment	Feed Continuation Segment	Branch Segment
Branch 1				
C57/bl6	11 ± 1	9 ± 1	10 ± 1	7 ± 1
db/db	7 ± 1 *	6 ± 1 *	7 ± 1 *	5 ± 1 *
ob/ob	10 ± 2	9 ± 1	10 ± 1	8 ± 1
Branch 2				
C57/bl6	10 ± 1	9 ± 1	10 ± 1	7 ± 1
db/db	10	10	11	9
ob/ob	9 ± 1	9 ± 1	9 ± 1	7 ± 1
Branch 3				
C57/bl6	10 ± 1	9 ± 1	9 ± 1	9 ± 1
db/db				
ob/ob	9 ± 1	10 ± 1	7 ± 1	8 ± 1
Branch Last				
C57/bl6	9 ± 1	9 ± 1	9 ± 1	8 ± 1
db/db	8 ± 1	8 ± 1	8 ± 1	7 ± 1
ob/ob	9 ± 1	8 ± 1	9 ± 1	7 ± 1

Network segment diameters by strain. The junction diameter at branch 1 is significantly smaller in the diabetic animals ($p<0.05$) as compared to C57/bl6 at the same location. There was only one diabetic animal with a second branch and there were no diabetic animals with a third bifurcation. All data is presented as mean ± SE.

Figure 6.11 (page 1 of 2)

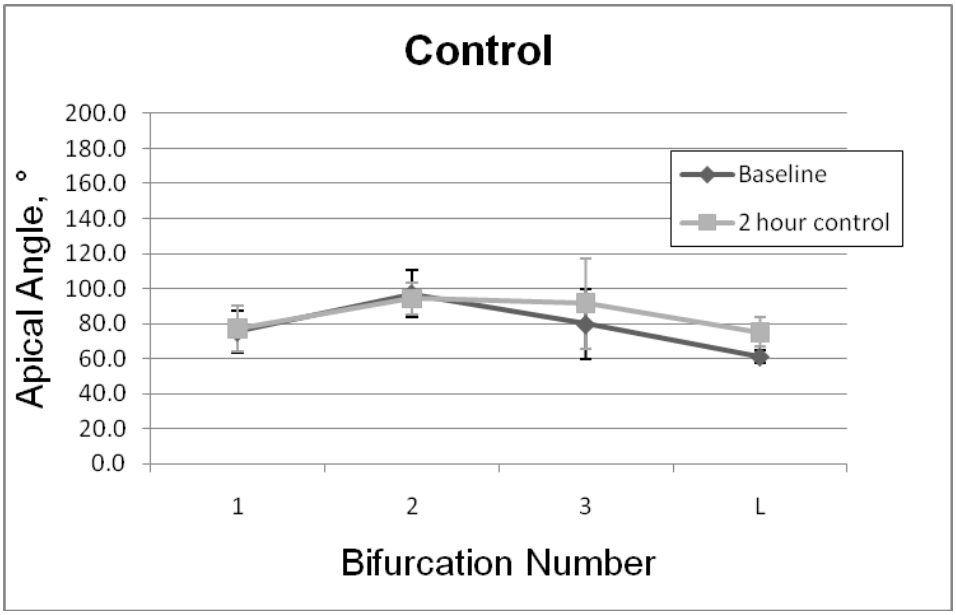

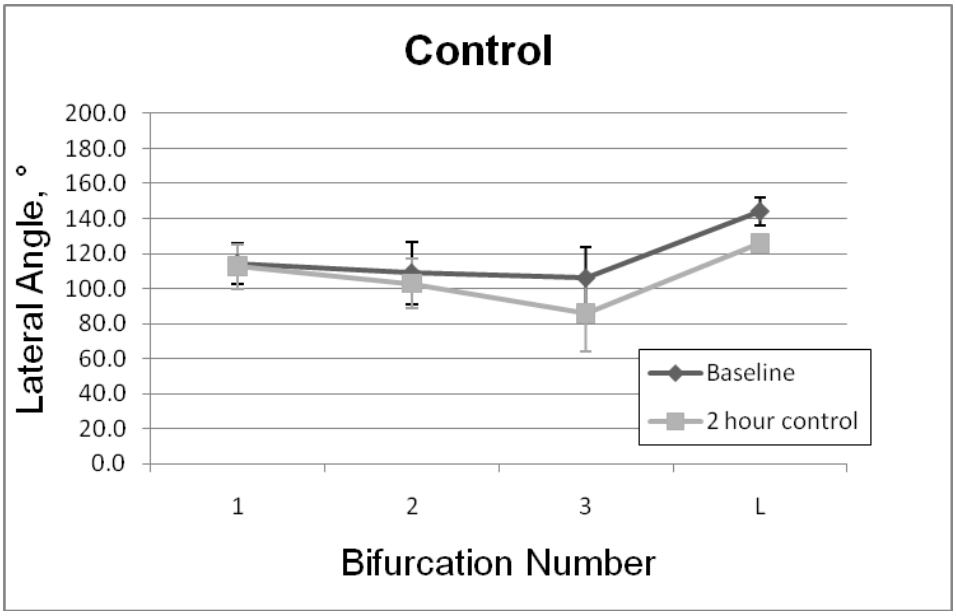

Figure 6.11 (page 2 of 2)

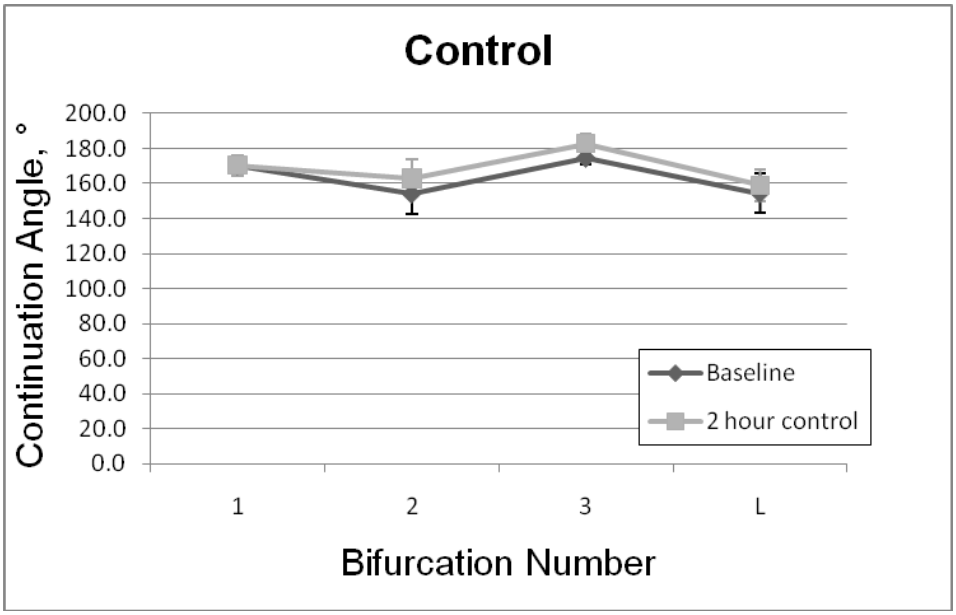

Patterns of bifurcation angle change in acute experiments. C57/bl6 mice at baseline and at 2 hours of control suffusate exposure. With two hours of experimental protocol there are not even slight changes in the apical or continuation angles at any location. There is a slight decrease in angle seen in the lateral angle. This change is not statistically significant ($p < 0.05$) but is shown to demonstrate patterns in angle changes. Data are presented as mean ± SE.

Figure 6.12 (page 1 of 2)

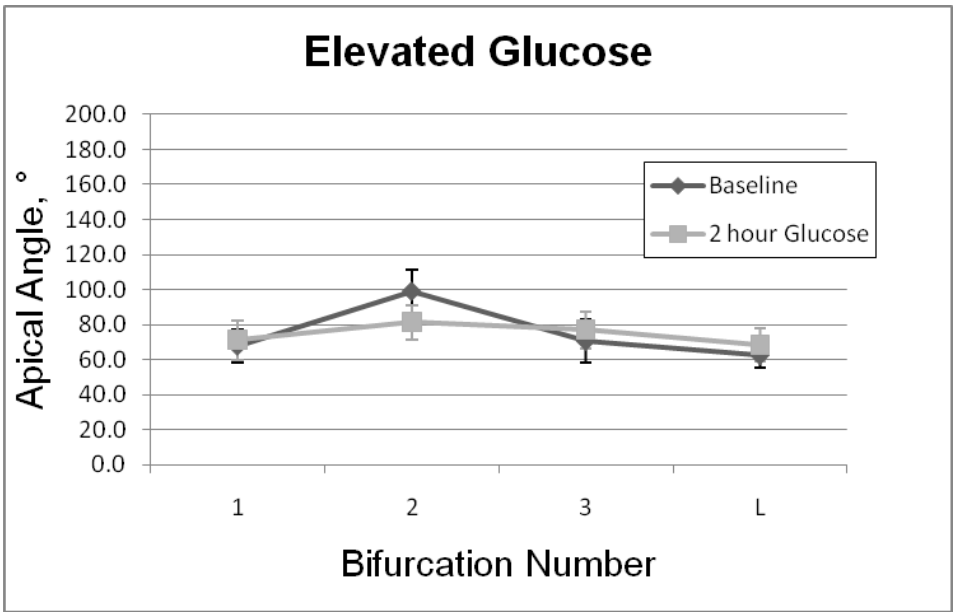

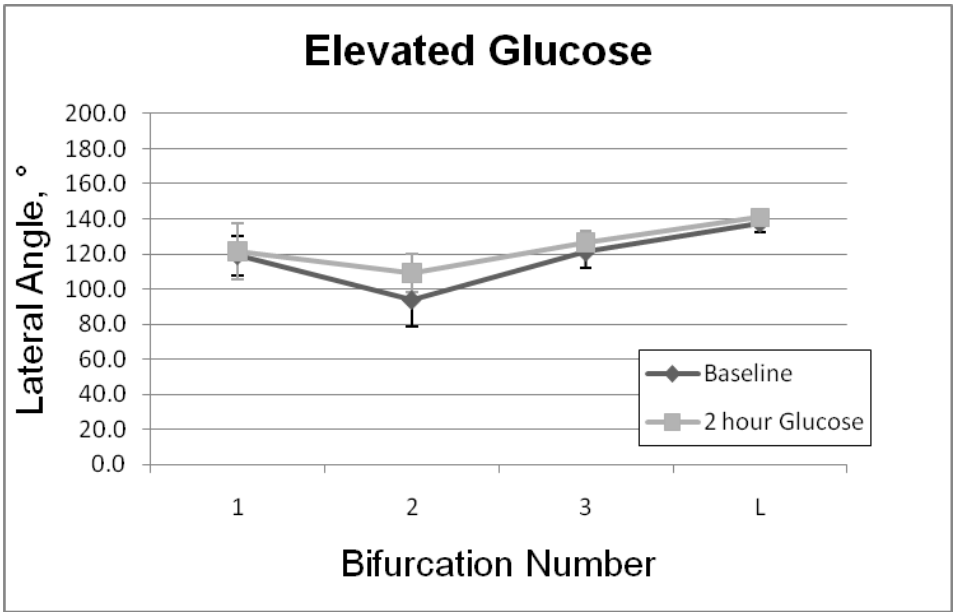

Figure 6.12 (page 2 of 2)

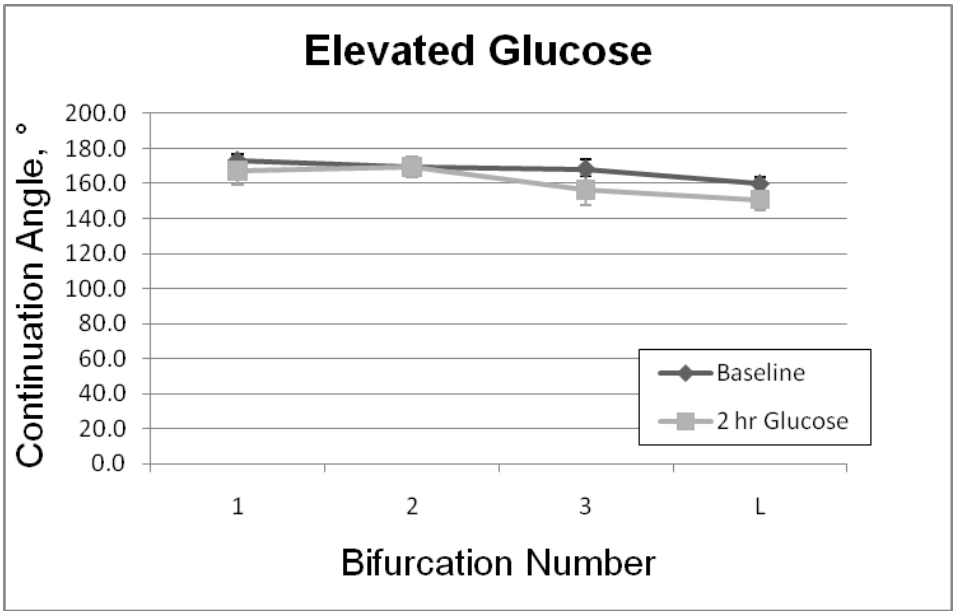

Patterns of bifurcation angle change in acute glucose experiments. C57/bl6 mice at baseline and at 2 hours of elevated glucose suffusate exposure. With two hours of elevated glucose there are not even slight changes in the continuation angles at any bifurcation. There is a slight decrease in apical angle at the second bifurcation and a slight increase in lateral angle also at the second bifurcation. These changes are not statistically significant ($p < 0.05$) but are shown to demonstrate the localization of early glucose affects to the second bifurcation. Data are presented as mean ± SE.

Figure 6.13 (page 1 of 2)

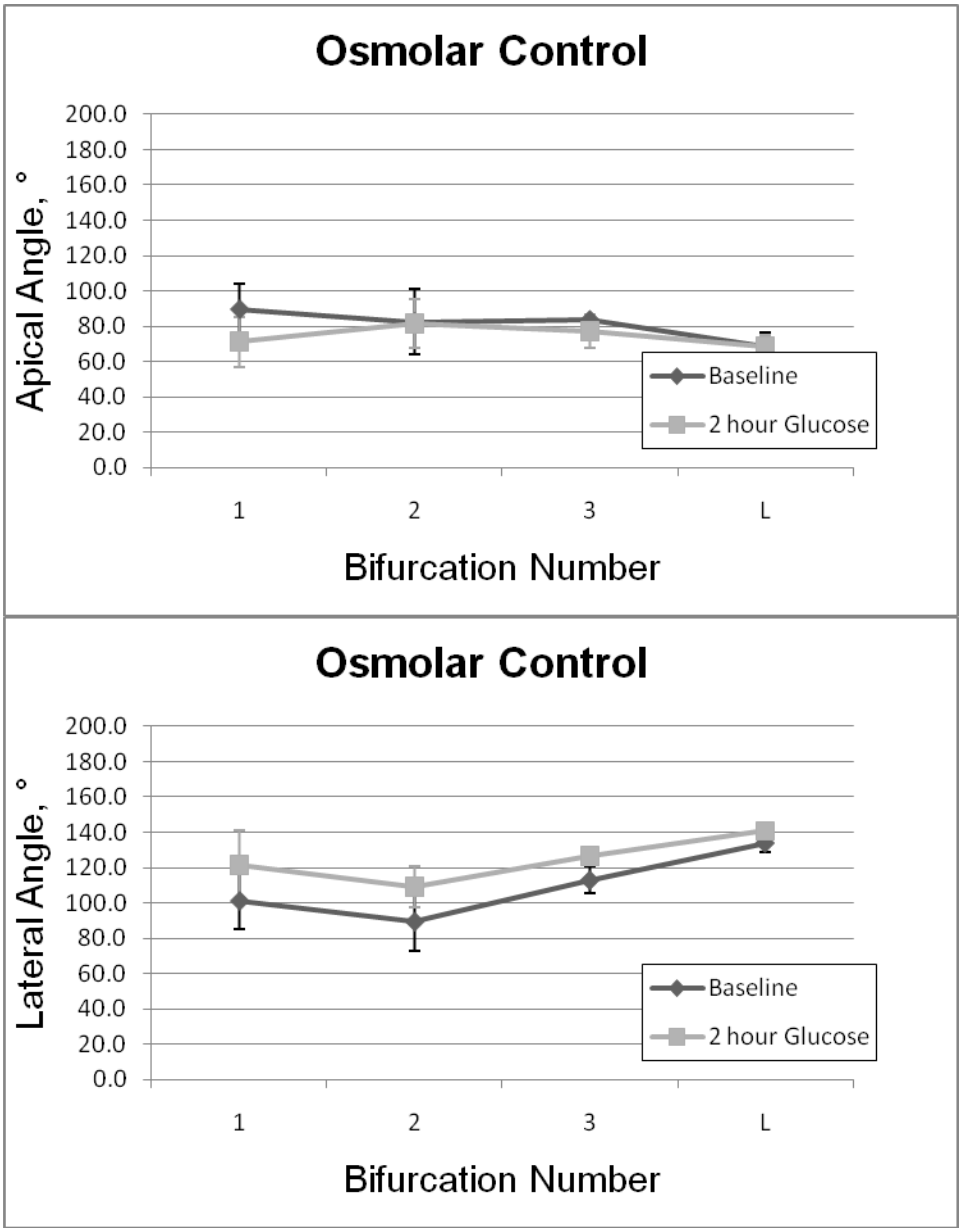

Figure 6.13 (page 2 of 2)

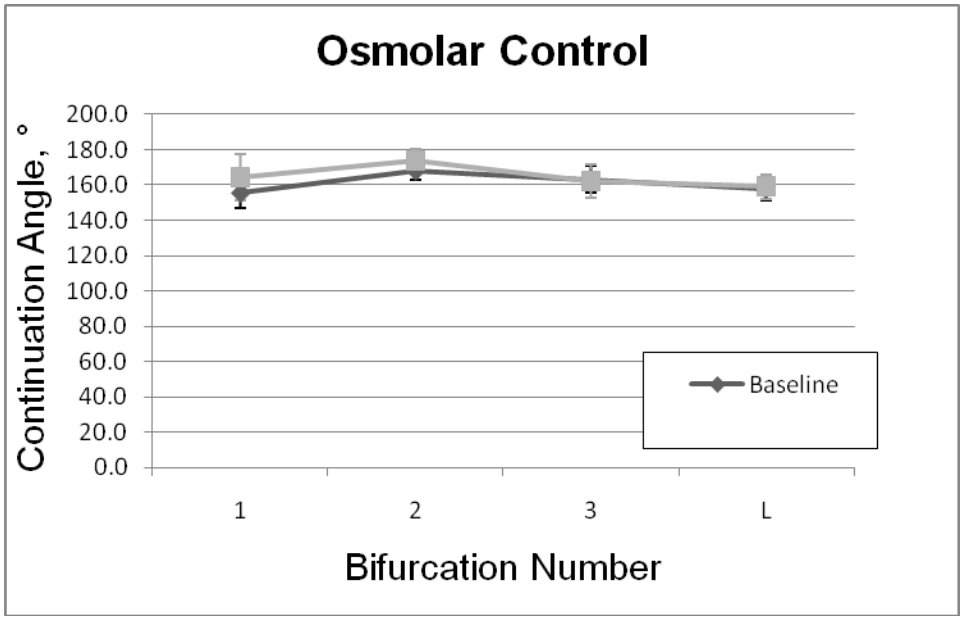

Patterns of bifurcation angle change in acute osmolar control experiments. C57/bl6 mice at baseline and at 2 hours of osmolar control suffusate exposure. With two hours of mannitol suffusate there are not even slight changes in the continuation angles at any bifurcation. There is a slight decrease in apical angle at the first bifurcation and a slight increase in lateral angles at all but the last bifurcation. These changes are not statistically significant ($p < 0.05$) but are shown to demonstrate the exposure to a high osmolar environment affects all but the last bifurcation. Data are presented as mean ± SE.

Figure 6.14 (page 1 of 2)

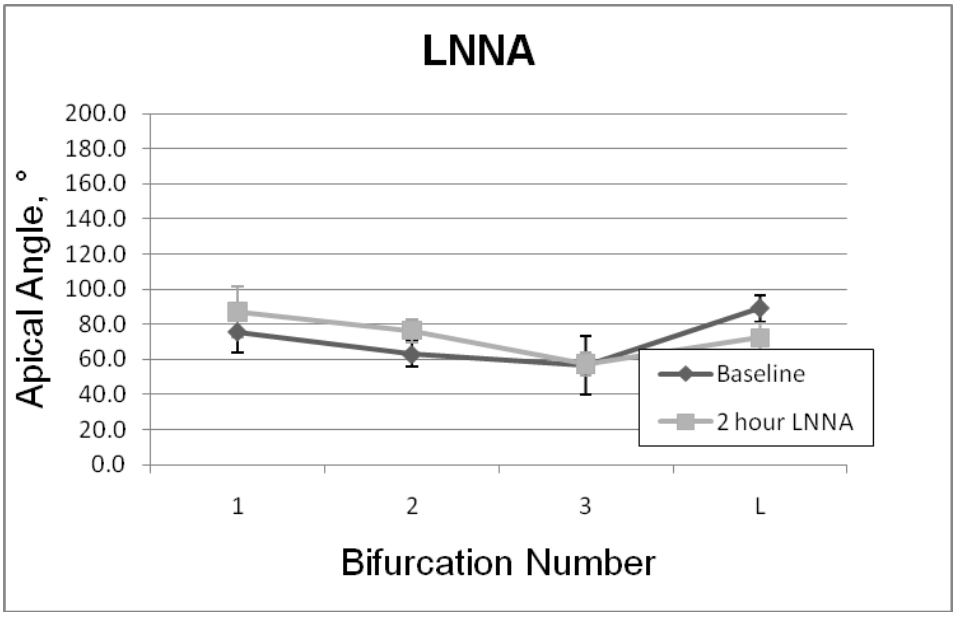

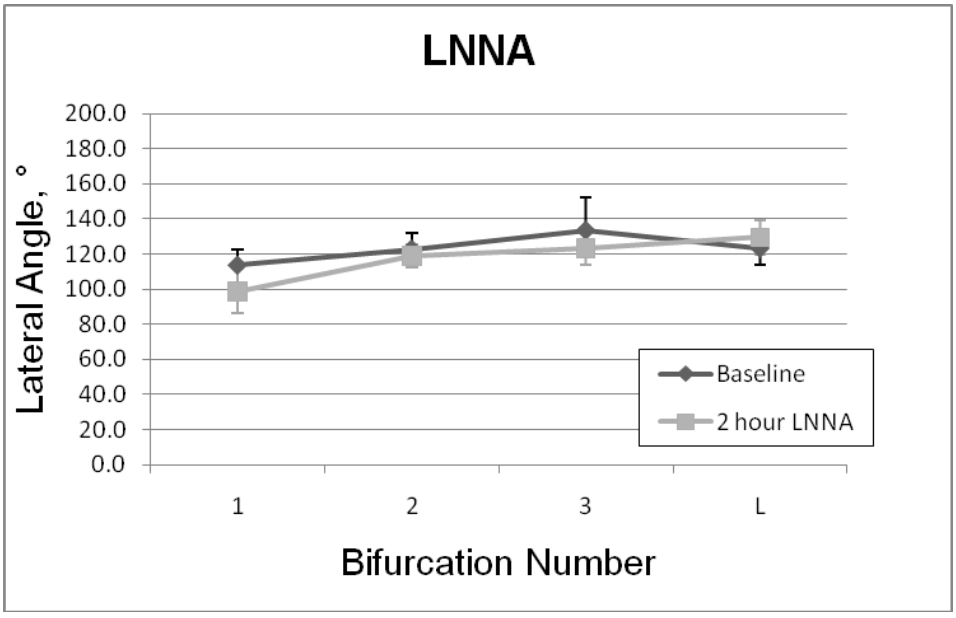

Figure 6.14 (page 2 of 2)

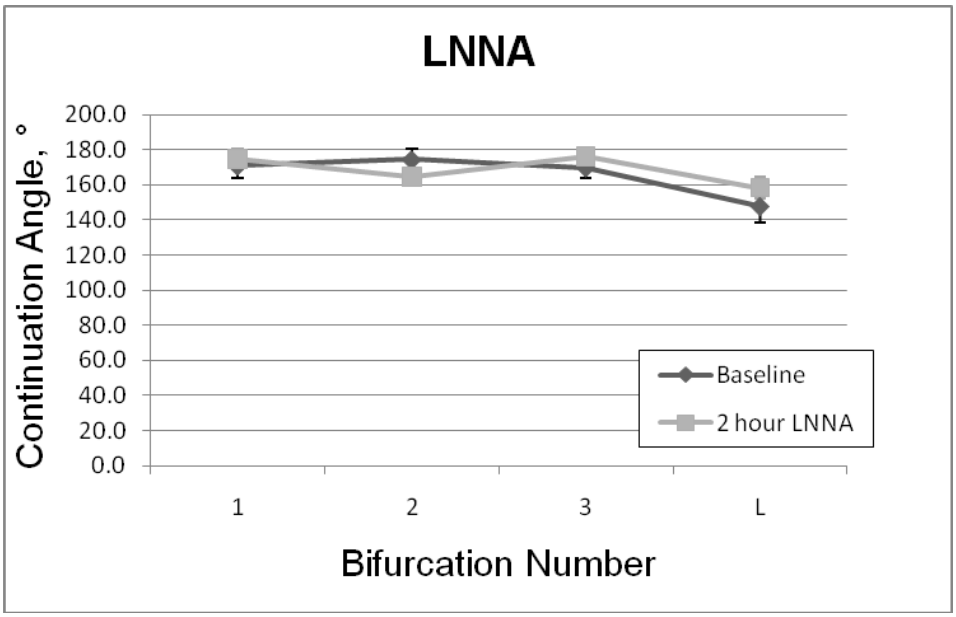

Patterns of bifurcation angle change in acute induced endothelial dysfunction experiments. C57/bl6 mice at baseline and at 2 hours of LNNA suffusate exposure. With two hours of induced endothelial dysfunction there are not even slight changes in the continuation angles at any bifurcation. There is a slight increase in apical angle at the second bifurcation and a slight Decrease in lateral angles at the first bifurcation. These changes are not statistically significant ($p < 0.05$) but are shown to demonstrate the exposure to LNNA does not show a patterned response at any bifurcation. Data are presented as mean ± SE.

Table 6.6

Branch	N	Apical Angle	Lateral Angle	Continuation Angle
C57/bl6				
first	31	77.0 ± 5.9	112.4 ± 5.8	167.6 ± 3.4
second	24	83.1 ± 6.6	105.2 ± 7.1	167.6 ± 3.7
Third	17	68.9 ± 7.9	121.9 ± 7.9	169.3 ± 3.0
Last	30	69.9 ± 3.7	135.3 ± 3.8	154.9 ± 4.1
db/db				
First	4	73.5 ± 12.4	117.5 ± 15.7	169.0 ± 10.2
second	1	102.5 ±	89.6 ±	167.9 ±
last	5	85.4 ± 11.9 *	136.6 ± 16.4	138.0 ± 8.5
ob/ob				
first	6	93.5 ± 12.8	106.3 ± 13.4	160.2 ± 5.2
second	6	99.4 ± 6.8	107.5 ± 8.4	153.1 ± 10.1
third	3	95.1 ± 19.9	106.4 ± 22.6	158.6 ± 21.1
last	6	61.6 ± 16.1	141.6 ± 9.1	156.8 ± 16.7

Branch angles by strain and bifurcation number. The apical angle at the last bifurcation was significantly different between diabetic and C57/bl6 animals. All other angles showed no statistical difference. All data is presented as mean ± SE.

Table 6.7

Branch	N	Resting ROC	2 Hour Exposure
Control			
first	9	2.9 ± 0.7	3.1 ± 0.5
second	5	2.8 ± 0.5	3.3 ± 0.6
third	3	3.5 ± 0.5	6.1 ± 1.7
last	9	2.4 ± 0.5	5.0 ± 2.1
Glucose			
first	7	7.2 ± 3.2	3.1 ± 0.7
second	6	5.1 ± 1.6	4.0 ± 0.9
third	6	3.7 ± 1.2	3.6 ± 0.7
last	8	2.2 ± 0.3	2.4 ± 0.4
Mannitol			
first	7	3.8 ± 1.6	5.8 ± 3.3
second	5	2.6 ± 0.5	2.5 ± 0.4
third	2	2.4 ± 0.4	3.1 ± 0.5
last	6	6.9 ± 2.9	2.9 ± 0.8
LNNA			
first	8	3.2 ± 0.9	4.2 ± 1.4
second	8	4.3 ± 1.1	5.0 ± 2.1
third	6	3.0 ± 0.7	4.2 ± 1.1
last	7	4.5 ± 1.0	2.9 ± 0.7

Radius of curvature estimations for 2 hour exposure experiments. After two hours of all treatments there were no significant changes to ROC values at any bifurcation. For location of measurement, refer to Figure 6.1. All data is presented as mean ± SE.

Table 6.8

	N	ROC			
C57/bl6					
first	31	2.9	±	0.3	
second	24	4.3	±	0.9	
third	17	4.3	±	1.1	
last	29	3.8	±	0.5	
db/db					
first	4	1.2	±	0.3	*
second	1	7.0	±		
last	5	2.2	±	0.4	
ob/ob					
first	6	2.3	±	0.2	
second	6	2.7	±	0.6	
third	3	6.6	±	4.7	
last	6	3.9	±	1.4	

Radius of curvature estimations across strains. There were no significant differences between ROC values at any bifurcation across strains. For location of measurement, refer to Figure 6.1. All data is presented as mean ± SE.

Table 6.9

Branch	N	Resting Bifurcation Volume			2 Hour Exposure		
Control							
first	9	2.311	±	0.616	2.007	±	0.438
second	5	4.522	±	1.050	4.729	±	2.335
third	3	1.878	±	0.263	1.766	±	0.291
last	9	1.666	±	0.298	2.028	±	0.422
Glucose							
first	7	2.400	±	0.557	1.378	±	0.254
second	6	2.150	±	0.519	4.551	±	2.233
third	6	1.266	±	0.201	2.345	±	0.505
last	8	2.244	±	1.077	1.670	±	0.190
Mannitol							
first	7	1.695	±	0.500	1.974	±	0.517
second	5	2.302	±	0.833	2.063	±	1.019
third	2	1.598	±	0.955	3.324	±	1.340
last	6	2.653	±	1.705	1.462	±	0.203
LNNA							
first	8	2.263	±	0.960	2.083	±	0.665
second	8	2.398	±	0.538	3.385	±	1.789
third	6	1.275	±	0.190	2.155	±	0.399
last	7	1.341	±	0.191	1.284	±	0.090

Bifurcation volume estimates for acute treatments. Values are expressed in picoliters. After two hours of all treatments there were no significant changes to bifurcation volumes at any bifurcation. All data is presented as mean ± SE.

Table 6.10

	N	Bifurcation Volume Estimate		
C57/bl6				
first	31	2.546	±	0.357
second	24	2.049	±	0.390
third	17	2.236	±	0.648
last	29	1.873	±	0.310
db/db				
first	4	0.752	±	0.208
second	1	2.473	±	
last	5	1.172	±	0.349
ob/ob				
first	6	2.554	±	0.977
second	6	1.719	±	0.493
third	3	1.493	±	0.562
last	6	1.482	±	0.363

Bifurcation volume estimates across strains. Values are expressed in picoliters. There were no significant differences between bifurcation volumes at any bifurcation for all strains. All data is presented as mean ± SE.

Figure 6.15

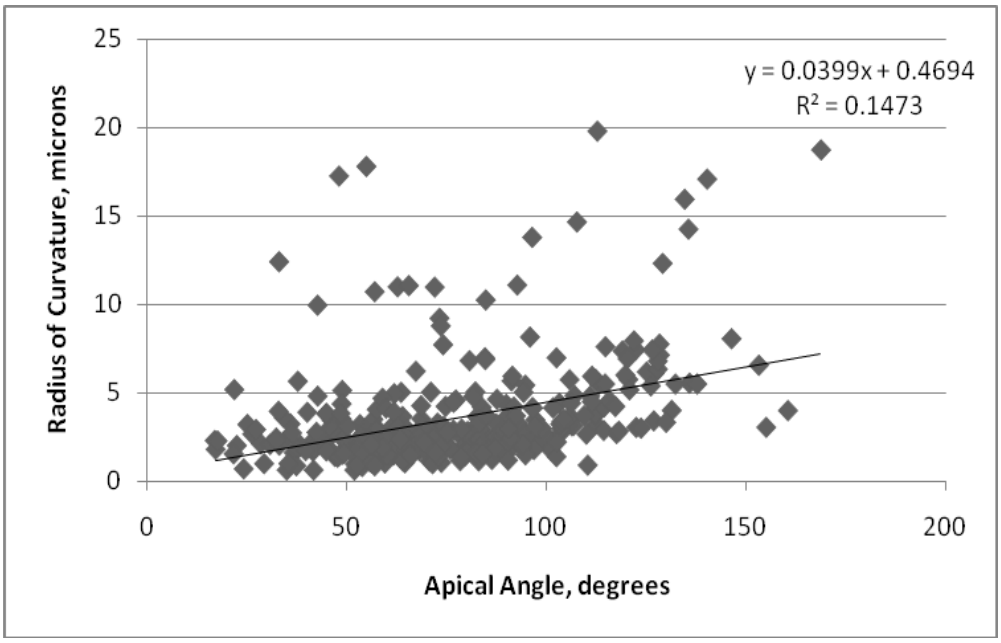

Radius of curvature for all strains and treatments as a function of apical angle. There is no significant correlation between the values estimated for the radius of curvature and the apical angle of the bifurcation. (n = 360, critical value = 0.129)

Figure 6.16

Schematic representation of the locations of the apical angle at the midline (A) , the inner wall angle (B) and the outer wall angle (C).

A) The midline angle is measured at the midline of each branch according to the methods presented in Appendix II.
B) The inner angle is measured as the angle from a point half a feed tube diameter down the feed from the center of mass (A_1) to the apex (A_p) to a point half a branch tube diameter down the branch from the branching wall (E_1). And represents the slope of the wall within one half tube diameter of the apex.
C) The outer angle is measured as the angle from a point a full feed tube diameter down the feed from the center of mass (B_1) to the apex (A_p) to a point a full branch tube diameter down the branch from the branching wall (F_1). And represents the slope of the wall between one half and one full tube diameter of the apex.

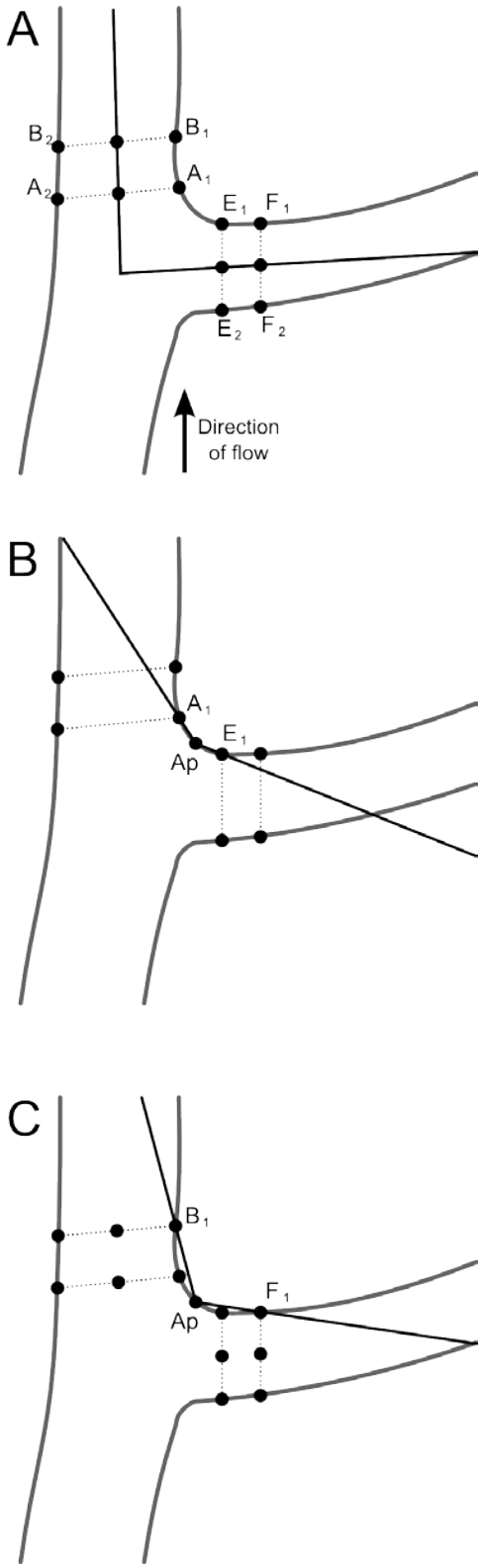

Figure 6.16

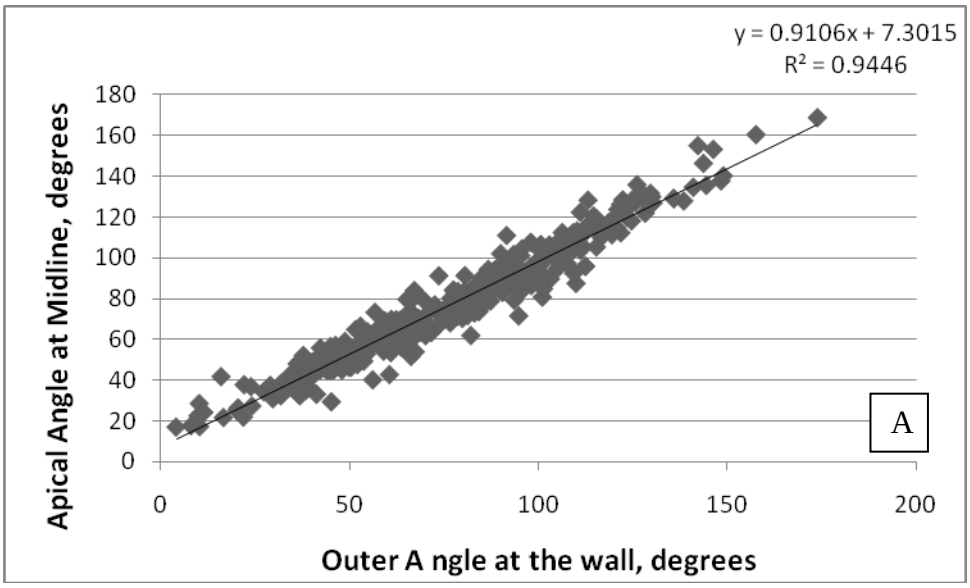

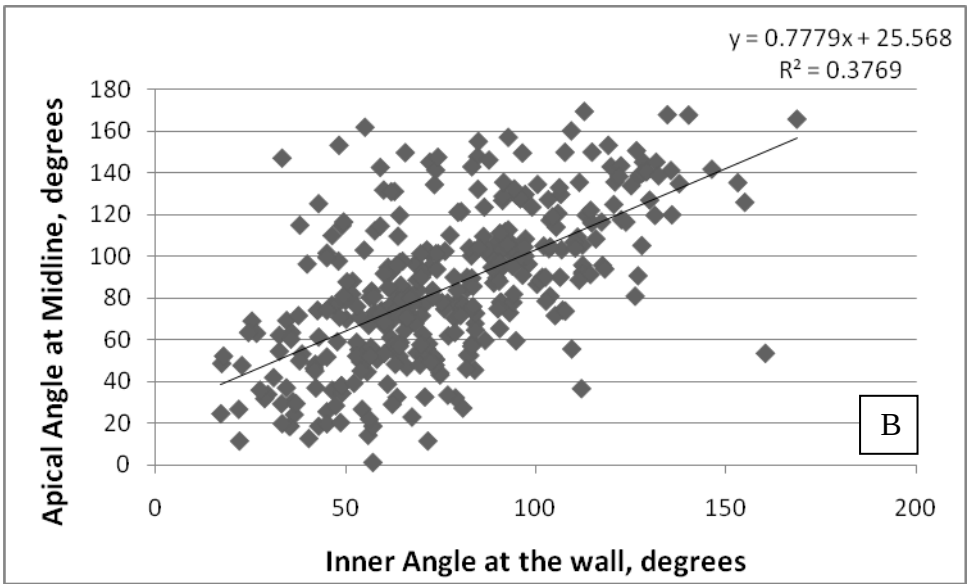

Comparisons of locations for angle measurement. The outer apical wall (A) correlates strongly with the apical angle at the midline (n = 364, critical value = 0.129) and has a slope near 1, indicating that the two values measure the same characteristic. On the other hand the inner apical wall (B) still correlates with the apical angle at the midline (n = 364, critical value = 0.129) but not as strongly, and the slope is lower than 1, indicating that these values may behave similarly, but do not measure the same characteristic. Refer to Figure 6.15 for schematic representation of the three angle locations.

References Cited

1) Marin, P., B. Andersson, et al. (1994). "Muscle fiber composition and capillary density in women and men with NIDDM." Diabetes Care **17**(5): 382-386.

2) Mathieu-Costello, O., A. Kong, et al. (2003). "Regulation of skeletal muscle morphology in type 2 diabetic subjects by troglitazone and metformin: Relationship to glucose disposal." Metabolism **52**(5): 540.

3) Pries, A.R., B. Reglin, et al. (2001). "Structural adaptation of microvascular networks: functional roles of adaptive responses." Am J Physiol Heart Circ Physiol **281**: H1015-H1025.

4) Roudier, E., N. Chapados, et al. (2009). "Angiomotin p80/p130 ratio: a new indicator of exercise-induced angiogenic activity in skeletal muscles from obese and non-obese rats?" J Physiol **587**(16): 4105-4119.

5) Hudlicka, O., M. Brown, et al. (1992). "Angiogenesis in Skeletal and Cardiac Muscle." Physiological Reviews **72(**2): 369-417.

6) Prior, B.M., H.T. Yang, et al. (2004). "What makes vessels grow with exercise training?" J Appl Physiol **97**: 1119-1128.

7) Ferrara, N. (2001). "Role of vascular endothelial growth factor in regulation of physiological angiogenesis." Am J Physiol Cell Physiol **280**: C1358-C1366.

8) Ferrara, N., T. Davis-Smyth. (1997). "The Biology of Vascular Endothelial Growth Factor." Endocrine Reviews **18**(1): 4-25.

9) Martin, A., M.R. Komada, et al. (2003). "Abnormal angiogenesis in Diabetes Mellitus." Medicinal Research Reviews **23**(2): 117-145.

10) Tran, E.D., G.W. Schmid-Schönbein. (2007). "An in-vivo analysis of capillary stasis and endothelial apoptosis in a model of hypertension." Microcirculation **14**(8): 793-804.

11) Geraldes, P., and King, G., (2010) "Activation of Protein Kinase C Isoforms and Its Impact on Diabetic Complications." Circulation Research **106**:1319-1331.

12) Frisbee, J.C. (2005). “Hypertension-independent microvascular rarefaction in the obese Zucker rat model of the metabolic syndrome.” Microcirculation **12**(5): 383-392.

13) Krogh, A. (1919). “The number and distribution of capillaries in muscles with calculations of the oxygen pressure head necessary for supplying the tissue.” J Physiol **52**(6): 409-415.

14) Frisbee, J.C. (2003). “Remodeling of the skeletal muscle microcirculation increases resistance to perfusion in obese Zucker rats.” Am J Physiol Heart Circ Physiol **285**:104-111.

15) Hinghofer-Szalkay, H., J.E. Greenleaf. (1987). “Continuous monitoring of blood volume changes in humans.” J App Phys **63**(3): 1003-1007.

16) Késmárky, G., P. Kenyeres, et. al. (2008). “Plasma viscosity: A forgotten variable” Clinical Hemorheology and Microcirculation **39**(1-4): 243-246.

17) Noren, D., H.J. Palmer, et al. (2000). "Predicted wall shear rate gradients in T-type arteriolar bifurcations." Biorheology **37**(5-6): 325-40.

18) Frame, M.D., I.H. Sarelius. (1993). “Arteriolar bifurcation angles vary with position and when flow is changed.” Microvasc Res **46**(2): 190-205.

19) Bugliarello, G., G.C.C. Hsiao (1964). “Phase separation in suspensions flowing through bifurcations: A simplified hemodynamic model.” Science **143**(3605): 469-471.

20) Noren, D., H.J. Palmer, et al. (2000). "Predicted wall shear rate gradients in T-type arteriolar bifurcations." Biorheology **37**(5-6): 325-40.

21) Pries, A.R., K. Ley, et al. (1989). “Red Cell Distribution at Microvascular Bifurcations.” Microvascular Research **38**:81-101.

22) Boutati, E., and Raptis, S., (2009) “Self-Monitoring of Blood Glucose as Part of the Integral Care of Type 2 Diabetes” Diabetes Care **32**(Supp 1):S205-S210

23) Frame, M.D., I.H. Sarelius. (1993). “Regulation of capillary perfusion by small arterioles is spatially organized.” Circ Res **73**(1): 155-63.

Chapter VII

Effects of Elevated Blood Glucose on Blood Flow and RBC Flux in the Microvasculature

Introduction

It is well established that blood flow in the peripheral microcirculation is reduced in diabetes and related metabolic disorders. Teleologically speaking, this makes sense, since the control of blood flow is designed to be controlled by metabolic demand, and widespread increases in glucose availability should reduce the need for the delivery of additional nutrients, resulting in a reduced circulation. Clinically, this phenomenon is usually measured by the response to induced hyperemia or to applied pharmacological agents that induce nitric oxide (NO) production such as acetylcholine. (The alterations in NO metabolism seen in response to acute elevation in suffusate glucose were shown in chapter IV.) Clinical measurements however, are taken over a large tissue area and as such fail to describe the local distribution changes in blood flow that happen at the level of the terminal arteriolar networks.

When taken as a whole, normal peripheral vascular flow is homogeneous with respect to solute delivery to the tissues. However, at individual microvascular locations, a time and metabolism dependent heterogeneity of flow is observed[1,2]. In fact, at any one time, a substantial number of blood vessels in a peripheral tissue bed may be unperfused under normal conditions creating a flow reserve that can be called upon in times of increased metabolic need [3]. When the number of unperfused but anatomically patent vessels increases due to a pathological cause, it is referred to as functional rarefaction [3]. This is separate from anatomic rarefaction, where patent vessel density is reduced, as described in chapter VI. The heterogeneity of flow under both normal and

pathological conditions is regulated by nerves, myogenic responses and local factors including flow and metabolic state.

Local regulation of the blood flow in the microcirculation relies heavily on the mechanotransduction of shear stress generated by the flow along the endothelial cells that line the blood vessels. Shear stress is the force exerted tangentially to the surface along which a fluid flows. In the case of the blood vessels, it is the force exerted tangentially to the endothelial cell lining of the vessel. One response to shear stress in the microvasculature is a phenomenon known as flow dependent vasodilation. In response to shear stress, the endothelium releases NO, which causes the production of cyclic guanylyl monophosphate (cGMP) within the vascular smooth muscle cells[4]. cGMP then actuates the dilation of the blood vessels, through a mechanism that is largely unknown; it is suspected that cGMP blocks the influx of extracellular calcium into the vascular smooth muscle cells[4]. Through this mechanism, the shearing forces generated by the blood flow through the vessels are a key factor in the regulation of vascular tone. This phenomenon is completely endothelium dependent.

For a Newtonian fluid flowing through a tube, shear stress, T, is calculated by equation 2.3 where η is the viscosity of the fluid, and v is the velocity of the fluid at a radial distance r from the wall of the vessel.

When calculating shear stress in the microcirculation however, this equation is no longer precisely correct as it applies only to Newtonian fluids, fluids in which the viscosity is independent of the applied shear force, and in which the flowing material is itself is a continuum fluid. Blood is a non-Newtonian fluid, properly characterized as having 2-phases due to the suspension of particles (cellular matter, which includes red blood cells (RBCs), white blood cells and platelets) within a Newtonian fluid (plasma)[5]. If the particles are small enough with regard to the diameter of the vessels in question, as in the macrocirculation, then the blood can often be approximated as a Newtonian fluid with Newtonian flow characteristics. In the microcirculation the particle to tube diameter ratio is below the 1:20, which is the threshold where Newtonian approximations become inaccurate.

In addition to the non-Newtonian characteristics of the blood itself, the effects of the large particle to tube diameter ratio in the microcirculation also affect the applicability of the equation above. The Fahraeus effect describes one such effect. The RBC diameter to vessel diameter ratio approaches 1 and therefore the RBCs are carried along the midline of flow, leaving the areas immediately adjacent to the walls nearly particulate free, and causing the particles to move at a faster rate than the bulk fluid A consequence is the F-L effect in which the apparent viscosity of the fluid is decreased due to the decreased tube hematocrit, and the decreased particle concentration at the point of contact against the walls [6]. A reduction in apparent viscosity along the walls makes the application of the above calculation of shear stress inappropriate. To avoid the errors associated with the resultant imprecise viscosity, one can examine shear rate alone, instead of wall shear stress. Shear rate, $\dot{\gamma}$, can be calculated by equation 7.2, which is the slope of the velocity profile. To determine the shear rate being exerted on the walls of the vessel by the flowing fluid requires that the velocity of the fluid at known radial positions near the wall is well described. For our purposes, we calculate the slope of the velocity profile within one RBC diameter, or 5 µm of the wall.

$$\dot{\gamma} = \frac{dv}{dr} \qquad \text{(equation 7.2)}$$

A second equation is available for the approximation of shear rate, shown as equation 7.3. where D is the diameter of the vessel, and $\bar{u}$ is the average velocity of the fluid across the tube. This equation also avoids the errors associated with viscosity measurements. Unlike equation 7.2, this equation assumes a parabolic velocity flow profile, a characteristic of a single phase Newtonian fluid flowing through a tube.

$$\gamma = \frac{8\bar{u}}{D} \qquad \text{(equation 7.3)}$$

This equation too, is not entirely accurate for applications involving blood flow, since blood is not a single phase, and therefore not Newtonian. Additionally, the RBC diameter to tube diameter ratio results in a non-parabolic

velocity profile. A result of the biphasic nature of blood flow is a non-parabolic velocity flow profile. This equation however, represents a good approximation, and will still demonstrate trends. We use both approximations of shear rate in this study, to allow us to not only describe behavior the shear rate at the wall with elevations in glucose, but to also allow us to compare the two means for calculating shear.

Shear stress affects the endothelial cells. How the endothelial cells sense and transduce shear stress has been a topic of intense research over the last two decades. (For review: see Ando *et. al.*[7]). In fact, eight different candidates have been put forward as the sensor for shear stress alone. What is known is that shear stress triggers several different functions of endothelial cells, ranging from production of NO which controls dilatory tone, to expression of cytokines and reactive oxygen species, to gene expression[7]. A change in the shear stress due to diabetes and metabolic disorders therefore causes a change in several different pathways that are all associated in some way or another with diabetic complications and co-morbidities.

Volume flow of the blood (determined by the velocity) and is not the only factors in determining oxygen delivery to the tissues. The number of RBCs that are delivered to each capillary bed plays a strong role as well. This measure is referred to as RBC flux. RBC flux is easily approximated by volumetric flow rate in the larger vessels in the circulatory system. However, in the microcirculation, the high particle diameter to tube diameter ratio has a significant effect on RBC distribution.

One rheological mechanism that may be responsible for local heterogeneity of flux is plasma skimming, a phenomenon in which there is a differential distribution of red blood cells at a branch point[8]. Differential flux may also lead to variations in local tube hematocrit which affects apparent viscosity and therefore flow. In addition, red blood cell distribution affects the distribution of oxygen to the capillary beds[9]. The impact of elevated glucose levels on the distribution of red blood cells has not previously been investigated and may be a

key factor in the dysregulation of blood flow seen in the microcirculation of diabetics.

In this study we examine the effects of elevated glucose on bulk blood viscosity and flux within the terminal arteriolar networks and how changes in the metabolic state change local flow regulation within the networks.

Research Design

Using the methods presented in chapter III, the velocity and location of each fluorescently labeled red blood cell was measured for each bifurcation over 30 seconds. These data were then fed into a custom Matlab program used to calculate the average velocity and shear for each defined geometric portion of the vessel. Matlab code can be found in Appendix V. Geometric portions of the vessels are referred to as segments, regions and zones respectively, full definitions are given in Appendix I. In brief, each bifurcation was sub-divided into 18 zones representing 1-tube diameter sections along the walls of the bifurcation. Two zones on opposing sides of the same axial portion of the vessel together made one region, e.g., zone 13 and 16 were assigned to the entrance of the branch, and together form region 1316. Combinations of regions constituted a segment, e.g., feed or branch. Velocity and flux of fluorescently labeled red blood cells were measured at the entrance to the network as it arose from the arcade, the entrance to each bifurcation (two feed diameters upstream of the center of mass) and the entrance to each branch vessel, thus determining RBC flux distribution directly, and obtaining the velocity to estimate shear rate.

A power analysis was done prior to the start of the experiments to determine the number of animals needed, with a β value of 0.40. It was determined that a sample size of six would be required for each condition. Comparisons were made across treatment types and time of treatment for all wild type animals. Additional comparisons were made across strains and glucose states. All data are expressed as the mean and standard error. All comparisons were done using ANOVA analysis for repeated measures with an α value of 0.05.

Results

Normal terminal arteriolar network: From the baseline data of all C57/bl6 mice we determined that the mean axial fluid velocity in a terminal arteriolar network was 190.2 ± 7.5 μm/s. for all feed and branch locations combined. Segment velocities trend downward by bifurcation (Figure 7.1) with no statistical significance, and there are no differences between segments within each bifurcation (Figure 7.2). An analysis of velocities by bifurcation region shows no significant difference between regions, but a peak velocity at region 1316, the first region in the branch adjacent to the feed, particularly in the first and last branches (Figure 7.3). Normalizing the velocities to the network inflow at baseline of each experimental day removes variability due individual animal differences in baseline flow. When normalized in this way, we see that that first region in the branch (region 1316) is a point of higher velocity, though not significantly (Figure 7.4).

We calculated two different estimations of shear rate. For the metabolically normal C57/bl6 mice, bulk shear rate ($8\overline{u}/d$) is constant throughout the networks, demonstrating no trends by bifurcation sequence or by segments (Figure 7.5). The wall shear rate (dv/dr) is calculated by zones; the peak wall shear rate gradient occurs within the bifurcation junction on the branching feed wall, zones 9 and 10 (Figure 7.6). Additionally, there was a tendency of the wall shear rate to increase at the second bifurcation just prior to the bifurcation on the non-branching wall (zone 4). There are no gradients in the wall shear rate along either branch wall. All wall shear rate values are normalized to the wall shear rate at the network inflow during baseline conditions, in order to compare axial gradients in shear rate throughout the network across treatments. There are no significant differences between zones or bifurcations.

Finally, in the C57/bl6 animals the percentage of red blood cells entering a network passing to each branch was calculated (Figure 7.7). Flux to each branch decreased along the network, with the second, third and last bifurcations

all receive significantly smaller fractions of the network influx than the first bifurcation, with no significant differences between them. Shunting through the network is prevalent, with 55% of cells that come into the network passing through the feed to the last bifurcation, bypassing all branches. The fraction of influx to the last branch is significantly larger than any of the branch fluxes.

Acute Study: In the acute study, there was no difference in velocity at the network entrance with glucose as compared with baseline or two hours of control. However, the entrance velocity with two hours of induced endothelial dysfunction (LNNA treatment) was significantly lower than with two hours of control (Figure 7.8). After normalization to the velocity at the network entrance (region 612), we see that there are no significant changes in velocity gradients in the network with 2 hours of glucose treatment. Both glucose and mannitol however exhibited increased variance with two hours of treatment (Figure 7.9).

The bulk shear rate (8v/d) estimation shows that there are no changes from baseline conditions for any treatment, and remains constant along the network demonstrating no trends by bifurcation sequence or by segments within or across bifurcations (Figures 7.10). However, the wall shear rate (dv/dr) by zones shows distinctly different patterns by treatment (2 hours of control is shown in Figure 7.7, 2 hours of glucose in figure 7.12, 2 hours of mannitol in Figure 7.13 and 2 hours of LNNA treatment is shown in Figure 7.14, all treatments normalized to baseline velocity at the entrance to the network). Two hours of glucose treatment reduces wall shear rate gradients within the network below control levels, a pattern not seen in any other treatment. Mannitol treatment on the other hand causes significant wall shear rate gradients in the first bifurcation (Figure 7.13), whereas 2 hours of LNNA exposure causes significant gradient increases in the branch, where all other treatments see constant wall shear rates (Figure 7.14).

Finally the percentage of network influx to each branch was calculated for each treatment (Figure 7.15). For all treatments, flux to each branch decreases along the network. All treatments have increased variance as compared to

control with two hours of acute glucose treatment (Figure 7.7). Shunting through the network remains prevalent under all four treatments, with the majority of cells that come into the network passing out through the feed and bypassing all branches.

Chronic effects of elevations in glucose as seen in metabolic syndrome models: A comparison across metabolic disease models demonstrates that, when compared to the metabolically normal C57/bl6 animals, the diabetic animals have a significantly smaller network velocity overall whereas the obese animals have a significantly larger network velocity overall (Figure 7.16). When normalized to inflow velocity and broken down by bifurcation, the pattern changes however, and diabetic and C57/bl6 animals are shown to have comparable velocity gradients. The obese animals however, have a lower normalized velocity than C57/bl6 animals at the first bifurcation (Figure 7.17). Like with the acute treatments, further velocity analysis by region does not uncover any new information.

A bulk shear rate analysis performed across strains demonstrates that shear rate gradients remains constant for all segments and bifurcations. The variability however, is increased in the db/db cohort, and further still in the ob/ob cohort as compared to the C57/bl6 animals (Figure 7.18).

An analysis of wall shear rate (Figure 7.19 – C57/bl6, Figure 7.20 – db/db, Figure 7.21 – ob/ob) demonstrates that both metabolic strains have flattened wall shear rate gradients along the network, removing the elevation in overall wall shear rate seen in zones 3 and 4 on the non-branching wall and the slight lower rise in zones 9 and 10 in the branching wall that can be seen in the C57/bl6 (Figure 7.19). Branch wall shear rate gradients are flat for all three strains.

Flux ratio analysis across strains shows that the pattern of shunting and reduced cell flux by bifurcation sequence is maintained in both the db/db and ob/ob mice (Figure 7.22). For the diabetic mice, which have a smaller number of branches, proportionately more of the influx goes out through the last branch.

Our analysis of shear rate uses two different estimates of shear rate, one for the bulk flow, and one that is only estimating the shear within 5μm of the wall. An interesting question that arises is, are the two estimates in agreement with one another. Bulk shear rate and wall shear rate do correlate with each other (Figure 7.23), however the slope is not equal to unity.

Conclusions

This study addresses the short and long term effects of elevated glucose on the flow within the terminal arteriolar networks in the mouse cremaster muscle. Clinically, reduced microvascular blood flow and elevations in blood glucose levels are correlated. In addition, several major complications of diabetes are the result of decreased blood flow including poor wound healing and diabetic ulcer formation. However, few studies have addressed the local regulation that leads to poor perfusion below the tissue level.

This is the first investigation of the effects of short term elevation in glucose on the terminal arteriolar networks that are responsible for providing flow to the capillary beds, and therefore regulating peripheral perfusion. In this study we measured not only the velocity of the red blood cells within the vessels, but also the flux of RBCs to the capillary beds in order to get a more complete picture of blood flow and nutrient delivery. Additionally, we recognize that local regulation of blood flow is linked to the shearing forces generated by the blood and sensed at the wall. In order to begin to understand if the dysregulation of blood flow in diabetes is triggered by a mechanical event, we have measured the shear rate for both the bulk fluid and along to the wall of vessel. The behavior of these two measures of shear may give clues as to the origin of the dysregulation signal under diabetic conditions.

Acute effects of glucose elevation:: As discussed in chapter VI, two hours of elevated glucose marks the earliest time point of pathological impairment of glucose handling. A normo-glycemic individual should have a blood glucose level that returns to under 120mg/dl within two hours of a meal, and as such

would not have blood glucose levels over 120mg/dl for more than that time period. The effects of two hours of glucose on the tissues should indicate the earliest of effects on the tissues. These may represent the beginning of long-term effects that lead to the complications seen in diabetes and other metabolic disorders.

In this study, we have demonstrated that there are no changes in velocitiy or bulk shear rate with two hours of elevated glucose exposure. However, we do at this time point see an increase in the variability of the bulk shear rate that may indicate the earliest stages of dysregulation.

The potential for early dysregulation is seen more clearly in the wall shear rate studies. In metabolically normal animals, the peak wall shear rate occurs along the bifurcating wall of the feed within the region of flow division (in our designation, zone 10). When treated with two hours of glucose however, this point is no longer the point of highest shear gradient. The shear gradients are suppressed throughout the network entirely. While there is no consensus as to the actual structure responsible for mechanotransduction of shear, a reasonable assumption is that the sensor for shear would localized to ensure maximum sensitivity. A suppression of all shear gradients and/or a rearrangement of the locations of peak shear gradients as seen in the db/db and ob/ob animals may disrupt the sensing mechanism responsible for the mechanotransduction of the shear to regulate flow. As such, at two hours of glucose exposure, we are already seeing a redistribution of shear gradients that may adversely affect mechanotransduction. We do not see the same suppression of shear gradients with mannitol or LNNA. In chapter VIII, the relationship between suppression of shear and altered endothelial cell dependent vasoreactivity is addressed.

In a tissue treated with two hours of elevated glucose, we see no change in the flux distribution along the network (Figure 7.15). Like with the baseline animals, percent flux in the branches decreases with bifurcation sequence for all treatments. Again, shunting of flow through the vessel is occurring with the highest percentage of RBC influx going out the feed continuation at the last bifurcation for all treatments.

Chronic effects of elevations in glucose as seen in metabolic syndrome models:

Significant changes in the terminal arteriolar network architecture are discussed in chapter VI. Briefly, diabetic animals have shorter networks with fewer branches and a smaller diameter first branch as compared to C57/bl6, and obese animals have longer networks with a comparable number of branches when compared with the C57/bl6. Thus, the three strains (two metabolic models and the metabolically normal C57/bl6 animals) have three distinct architectural structures.

Despite the significant architectural differences between the three, there are a number of rheological factors that are unchanged between the three models. Most significantly, bulk shear gradients throughout the networks are similar between all three species (Figure 7.18). That is, given the same input velocities, all three strains will have similar patterns of velocity distribution to each of the branches along the network. This suggests that one of the driving forces for the structural changes within the two pathological models may be to maintain homeostasis of velocity and shear within the networks with metabolic changes. Regulation appears to be challenged however, as the variance on the obese population is higher than in the other two strains (Figure 7.18).

Absolute velocities, on the other hand, are significantly different between the three strains. Diabetic animals have a much lower inflow velocity than their C57/bl6 counterparts and obese animals higher (Figure 7.17). Of note, while the averages for the obese mice are higher, the variance on these animals is very large. With these animals there is either no flow at all, or very fast flow. Sudden large changes in velocity suggest a major dysregulation with flow delivered to the terminal arteriolar networks.

Where there is a significant change between the three strains is in the wall shear gradient distribution (Figures 7.19 – 7.21). Similar to the results seen in the two hour exposure to glucose in the acute study, both the diabetic and the obese animals demonstrate a flattening of wall shear rate gradient profiles within the networks. Whereas in the C57/bl6 we see an increase in relative wall shear

rate within zones 3 and 4, there are no similar increases along that wall in the diabetic and obese strains. This flattening of the wall shear gradients within the network may have a significant effect on the regulation of flow as managed by the mechanotransduction of shear forces along the wall.

Finally, with regard to flux, all three strains have similar patterns of flux distribution to the branches of the network. Similar to the bulk shear rate and velocity gradient distributions, this indicates that is another potential driving force for the architectural changes; to maintain flux distribution patterns to the tissue.

Long term reduction of flow through vascular beds (functional rarefaction) has been linked to architectural loss of vessels (structural rarefaction). In this study we see that while velocity and shear gradients in the bulk flow are maintained within networks that experience high levels of glucose (acutely and chronically) the shear signals at the wall are suppressed with glucose exposure. This suppression of wall shear rate signal may be the first step in a mechanism that disrupts regular blood flow regulation.

Shunting in the cremaster muscle of mice: In studies in the rat and hamster, the majority of flux is nutritive, that is to say that the majority of flow is fed to the vessel segments that feed capillary beds and therefore deliver nutrients to the tissues. In these species, shunting flow is seen as a pathological phenomenon, seen in conditions such as sepsis [10]. For the mice in this study however, we see shunting of flow within all of our strains and test conditions, most notably with the control conditions of the metabolically normal animals. This indicates that for these animals, in this tissue bed, shunting is the physiogically normal condition. The reason behind this is unknown.

Assumptions and Limitations of the Study

There are several inherent limitations to the use of fluorescently labeled RBCs as flow markers. First, the labeling process for the RBCs itself may change the mechanical properties of the cells affecting their flow patterns, although these changes have been shown to be minimal in studies of hamster

RBCs [11]. No studies with mouse RBCs are published. Of more impact is the optical methodology used to track the fluorescent particles, in particular the fact that instead of identifying the RBC itself, we are tracking the light given off by the RBC. This light, as collected by the intensified charge coupled device (ICCD) camera varies in intensity based on the motion of the particle, and occasionally results in the blurring of two particles into one, particularly at high velocities. Measures are taken to reduce the occurrence of this phenomenon including the injection of a small enough volume of cells that few labeled cells are traveling through the region of interest simultaneously.

The technology for automated tracking of particles that enter and exit the region of analysis automatically is still in early development stages. In order to minimize technological limitations, the particle tracking program used in these experiments was developed in conjunction with our lab specifically to handle our data. Despite this, there are inherent limitations in the automated tracking of RBCs that remain unsolved. Most notably, the fluorescence given off by a particle as it travels through the vessels is inconstant. Background noise from the bright-field visualization of the vessel walls, the variable depth of a vessel as it runs through the tissue and the variability of the speed of a particle as it travels through the vessel all lead to variations in the intensity of the signal. This, in turn, makes selecting a grayscale value as the threshold value for the tracking of the particle challenging, and results in small variations in the size of the particle. These variations are usually on the order of fewer than a few (2-4) pixels, and as such result in a small measurement error in the location of the cell (<2 microns).

Additional cell tracking errors occur when multiple cells travel together, making only the leading edge of the ‘blob’ able to be tracked. If the cells within the ‘blob’ are moving together at the same velocity, the error inherent is no greater than that caused by fluorescence variability. If, on the other hand, one cell is moving faster than another, the data is discarded. Although, rarely does this occur due to the fact that two cells traveling that closely are usually within the same streamline and are therefore traveling at nearly the same velocity. This

source of error is minimized by controlling the volume of cells injected into the animal to the best of our ability.

In order to remove erroneously identified cellular velocities, any velocity that was calculated beyond the upper limit of the program was discarded. Velocities beyond capable maximum occur when cells are misidentified by the program. The maximum possible distance in the vertical direction that can be traversed by a cell in a single frame is calculated as the distance per pixel times the total number of pixels. At 60x magnification and a region of interest of half the image height, the maximum velocity is calculated as 998 microns/frame, which is equivalent to 59,904 microns/sec. All velocities will be calculated in incremental steps, since minimum movement is 1 pixel per frame. A single pixel movement at 60x magnification results in a calculated velocity of 18 microns/sec. Velocities smaller than 18 microns/sec (but not equal to 0) were set equal to 18 microns/sec.

One other limitation of fluorescently labeled RBC use is highlighted in these results. In both the acute and metabolic model studies, we analyzed the bulk shear rate by bifurcation sequence along the network. In both instances, we also looked at the velocity gradients by region, which provided no further insight into the behavior of the network regulation. One reason for this lies with the methodology we use for measuring the blood velocity. By using fluorescently labeled RBCs as flow markers, we are restricted in our spatial precision. For each frame of video, representing $1/60^{th}$ of a second, the flow marker will move a given distance. As an example, an average RBC under control conditions travels at 290 µm a second, which is equivalent to 4.8 microns in a frame. Our regions are defined by the tube diameter of a vessel, the average of which is 11µm. The cell in our example will be recorded in each region at least once. However, a cell that is traveling faster than that may not be caught in every region.

The final limitation of note is within on our calculation of shear rate. Shear rate is calculated using two different approximations, as both have inherent assumptions that are not completely accurate in this system, as addressed in the background. It is of particular interest to note the differences in results for these

two approximations and to compare both the absolute values of the two approximations, as well as the gradient differences between the two. Neither approximation is going to reflect that absolute functioning of the system, but by using both, we are looking for consistent features reflected regardless of the approximation used.

Summary

This study shows that the shear and velocity gradients in the terminal arteriolar networks of normal mice are spatially organized in a consistent manner, and that the spatial organization of those networks is maintained even in a pathological metabolic state. Additionally, we demonstrate that flux distribution in the terminal arteriolar networks of C57/bl6 mice (and animal models for which C57/bl6 mice are the background) is predominated by shunting behaviors; more than 50% of the flux into the networks bypasses the capillary feeding branches and flows directly to the venous drainage. This flux distribution pattern is maintained under metabolic syndrome conditions. Furthermore, chronic elevations of glucose, as seen in the metabolic strains, induce a suppression of the shear gradients within bifurcations. We postulate that this may lead to the disruption of the mechanosensory signal within the terminal arteriolar networks that may be related to the long term changes seen in the metabolic syndrome mouse models.

Figure 7.1

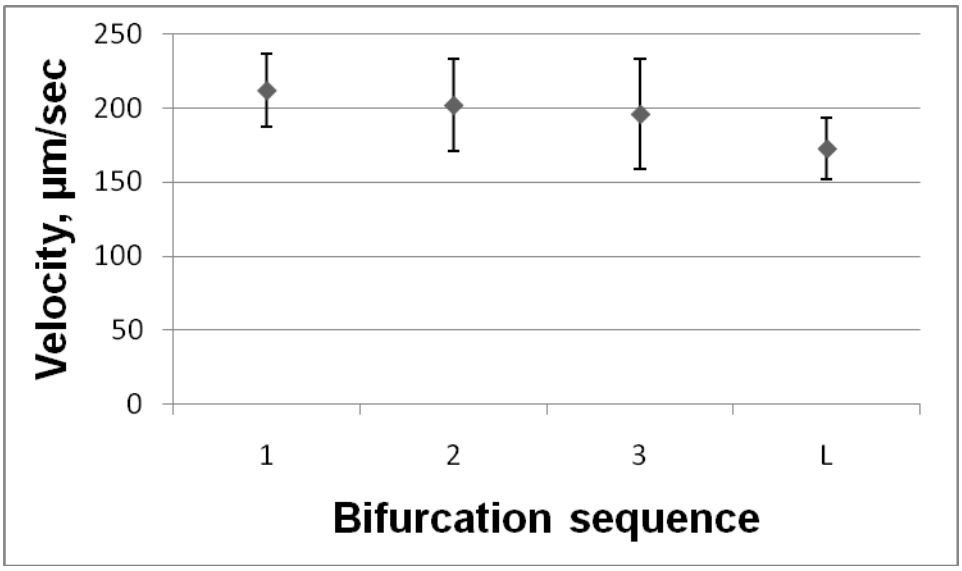

Blood flow velocity in terminal arterioles of metabolically normal C57/bl6 mice. Shown is the mean axial red blood cell velocity (mean+/-SE, µm/s) measured in the terminal branch arterioles arising sequentially from the central feed (1, 1st branch; 2, 2nd branch; 3, 3rd branch; L, last branch) of terminal arteriolar networks (N=34 networks). Branches between the 3rd and Last branches (are not shown) (were not measured). Velocity did not differ between branch arterioles ($p>0.05$).

Figure 7.2

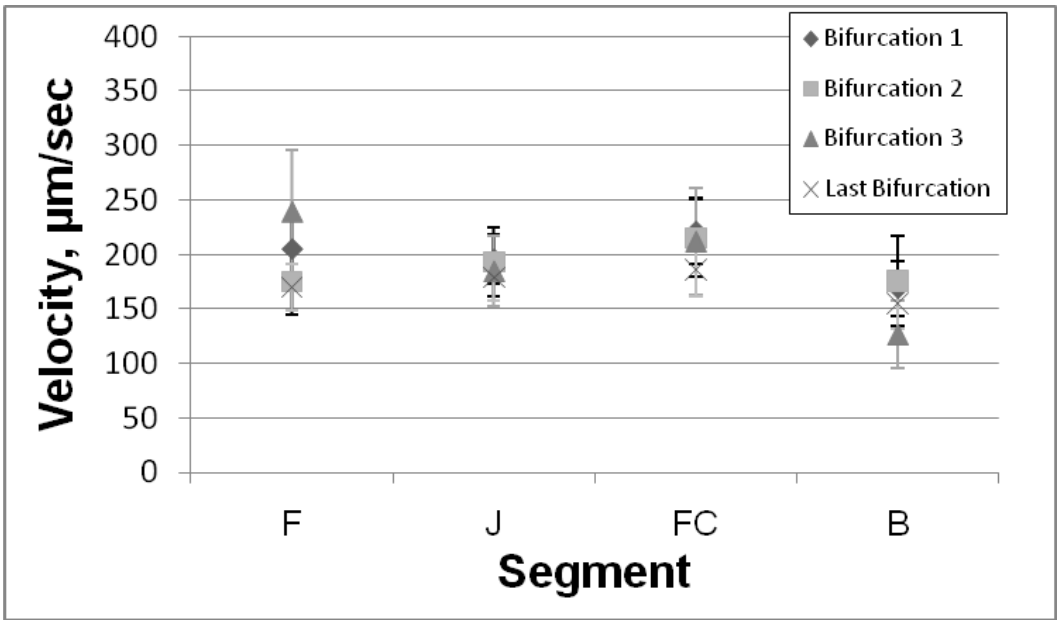

Blood flow velocity in metabolically normal C57/bl6 mice by segment and bifurcation. F = feed segment, J = Junction segment , FC = feed contuation segment, and B = branch segment (N=34 networks). For segment reference see Appendix I. Velocity did not differ between bifurcation segments. ($p<0.05$). All data are presented as mean ± SE.

Figure 7.3

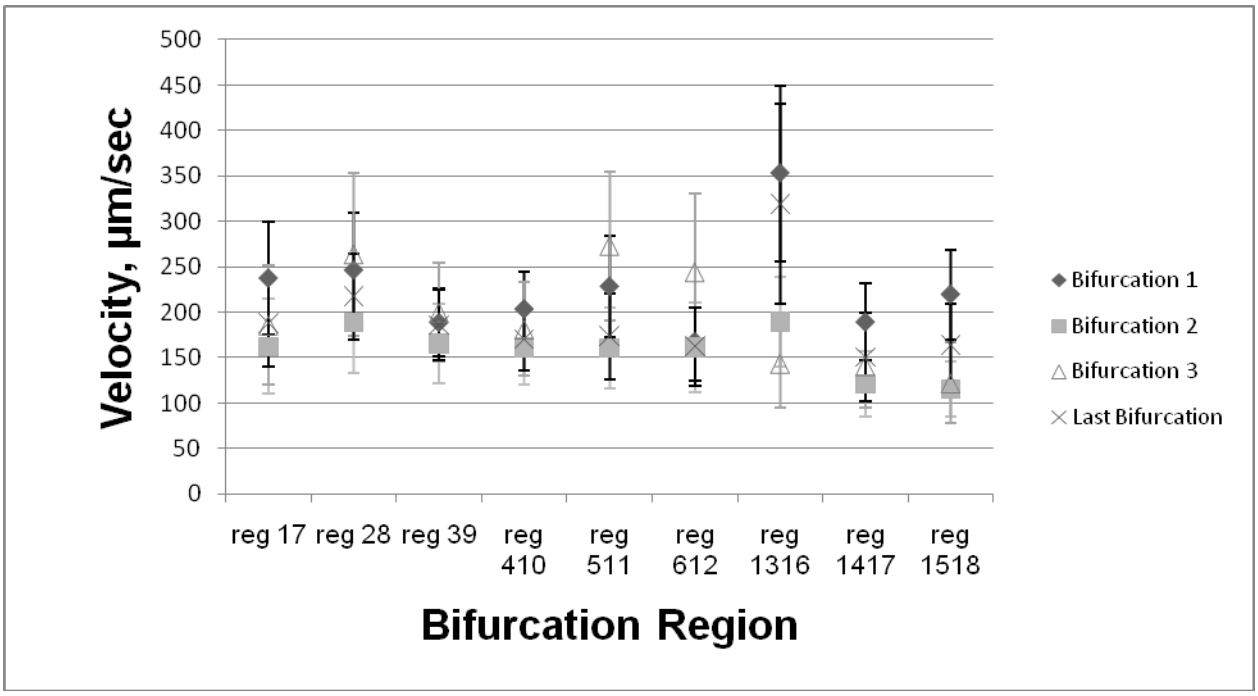

Blood flow velocity in metabolically normal C57/bl6 mice by region and bifurcation (N=34 networks). Region definitions are in Appendix I. There are no significant differences between or among groups ($p<0.05$). All data are presented as mean ± SE.

Figure 7.4

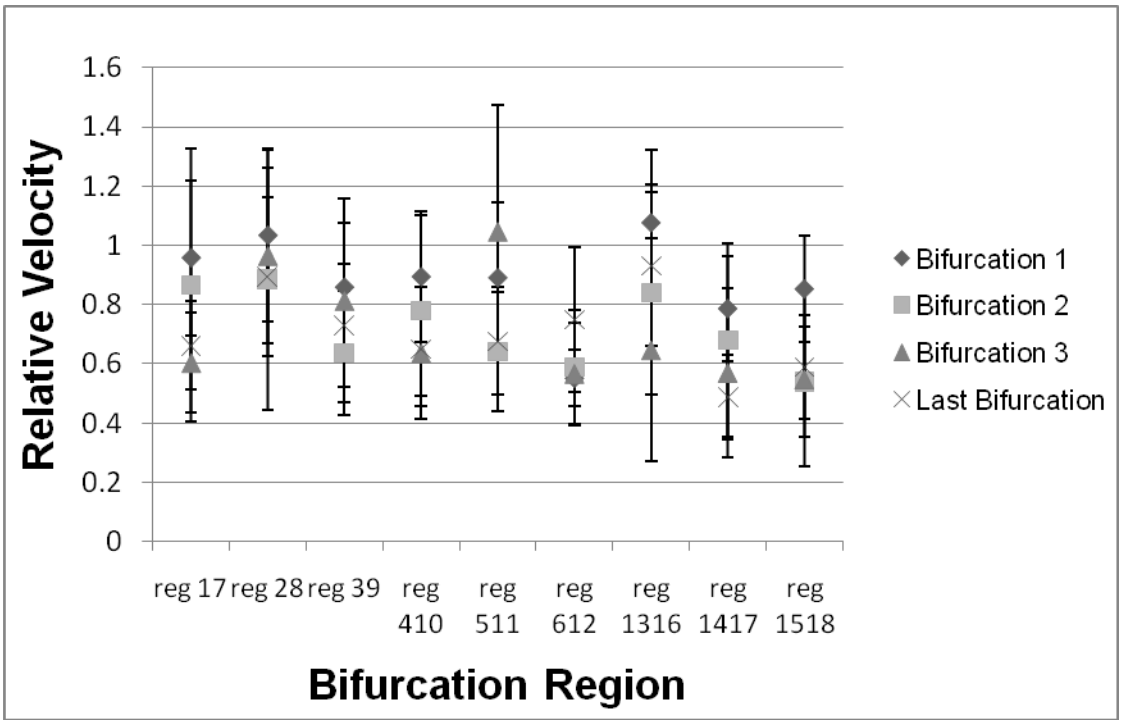

Normalized blood flow velocity in metabolically normal C57/bl6 mice by region and bifurcation (N=34 networks). Blood flow was normalized each day to the inflow velocity at baseline (velocity at region 612). Region definitions are in Appendix I. There are no significant differences between or among groups ($p<0.05$). All data are presented as mean ± SE.

Figure 7.5

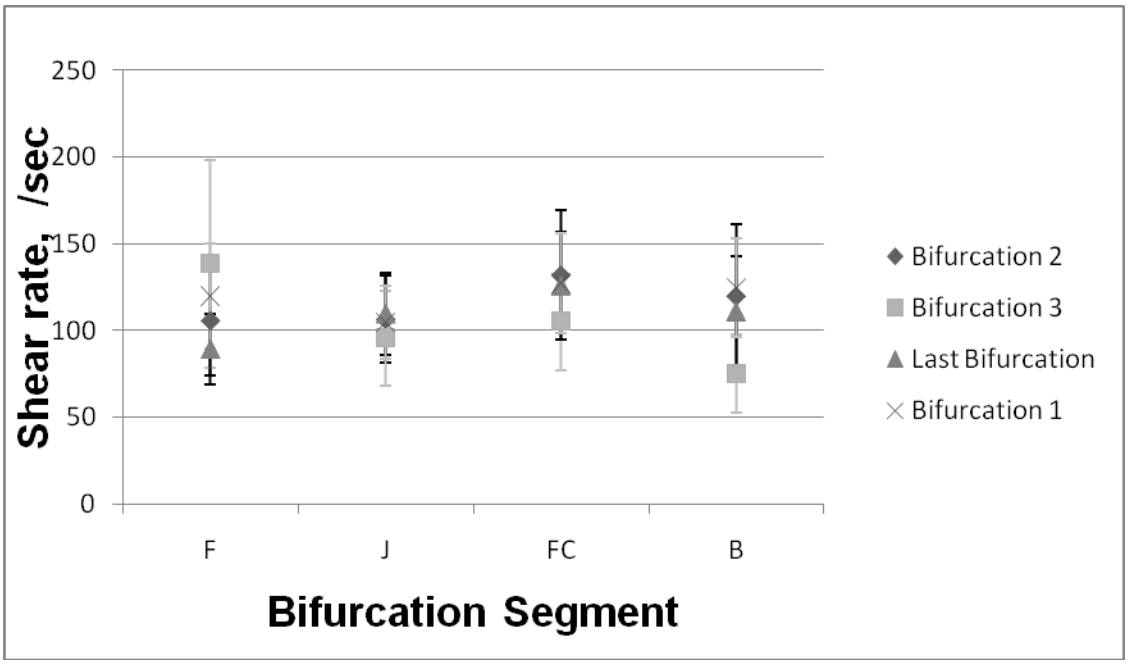

Bulk shear rate in metabolically normal C57/bl6 mice by segment and bifurcation. F = feed segment, J = Junction segment , FC = feed contuation segment, and B = branch segment (N=34 networks). For segment reference see Appendix I. There are no significant differences between or among groups ($p<0.05$). All data are presented as mean ± SE.

Figure 7.6 (page 1 of 2)

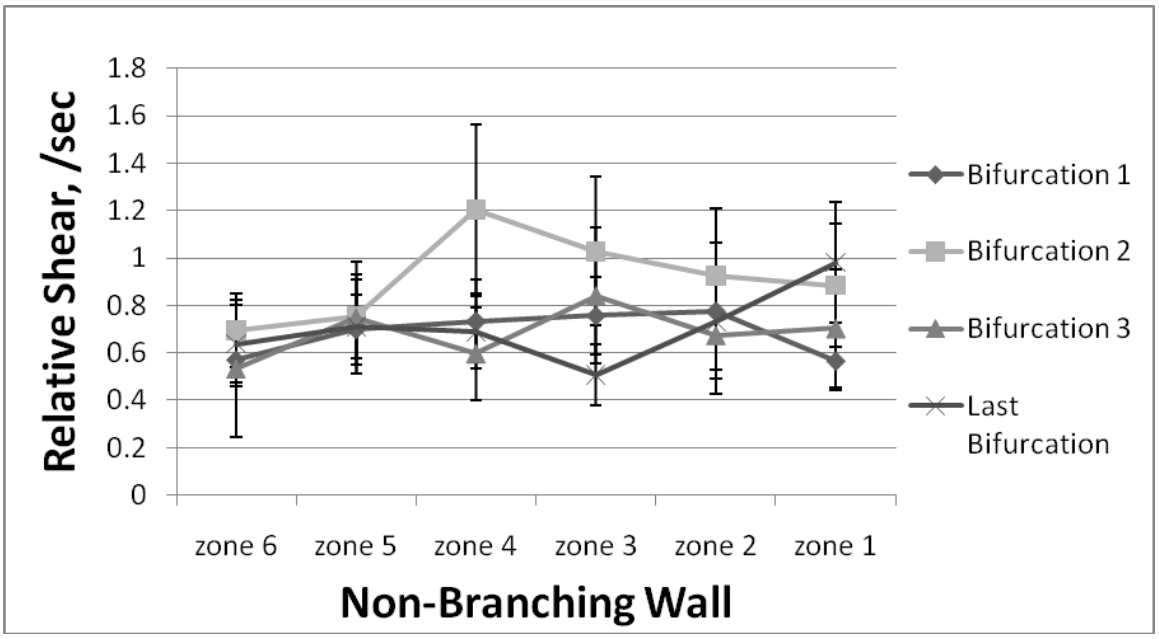

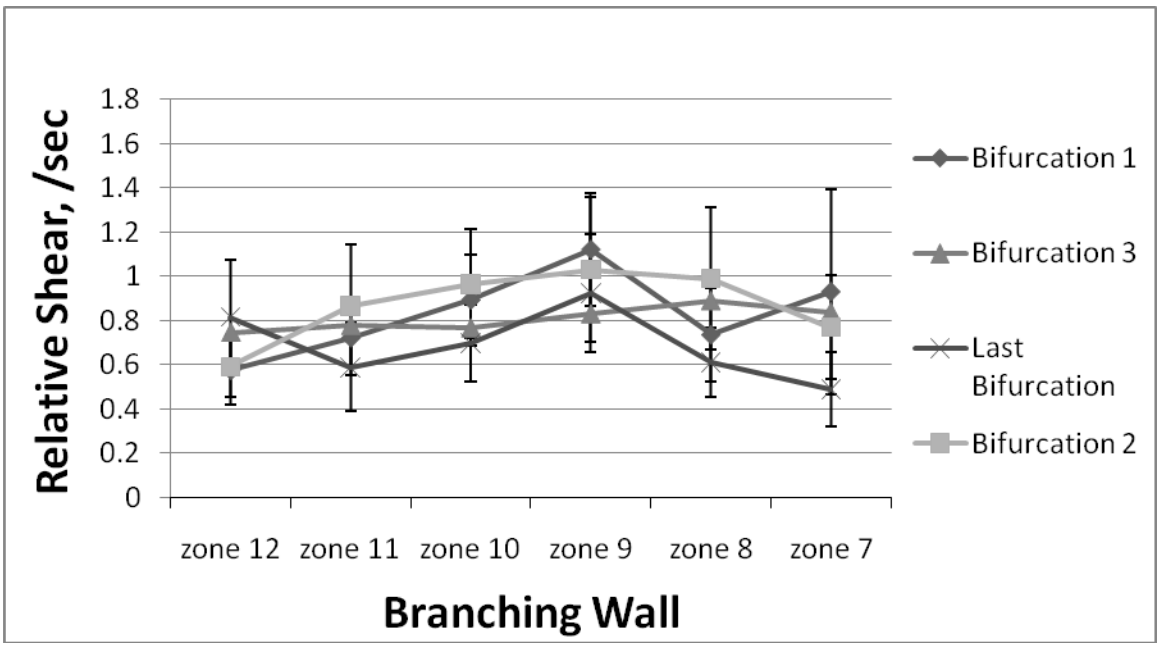

Figure 7.6 (page 2 of 2)

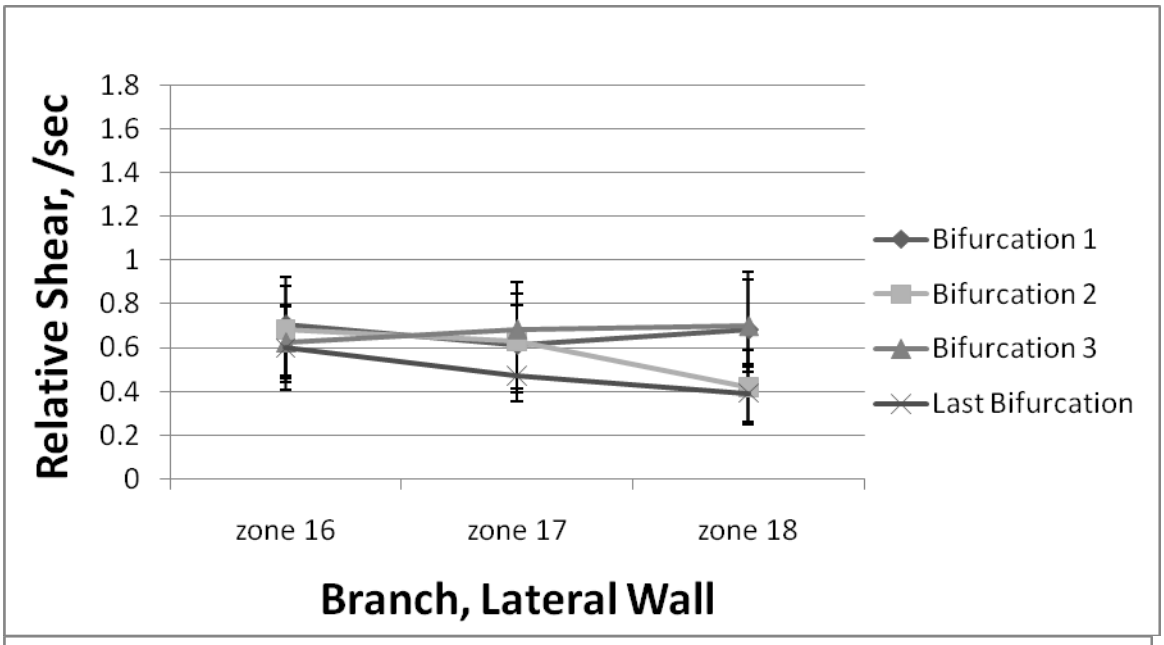

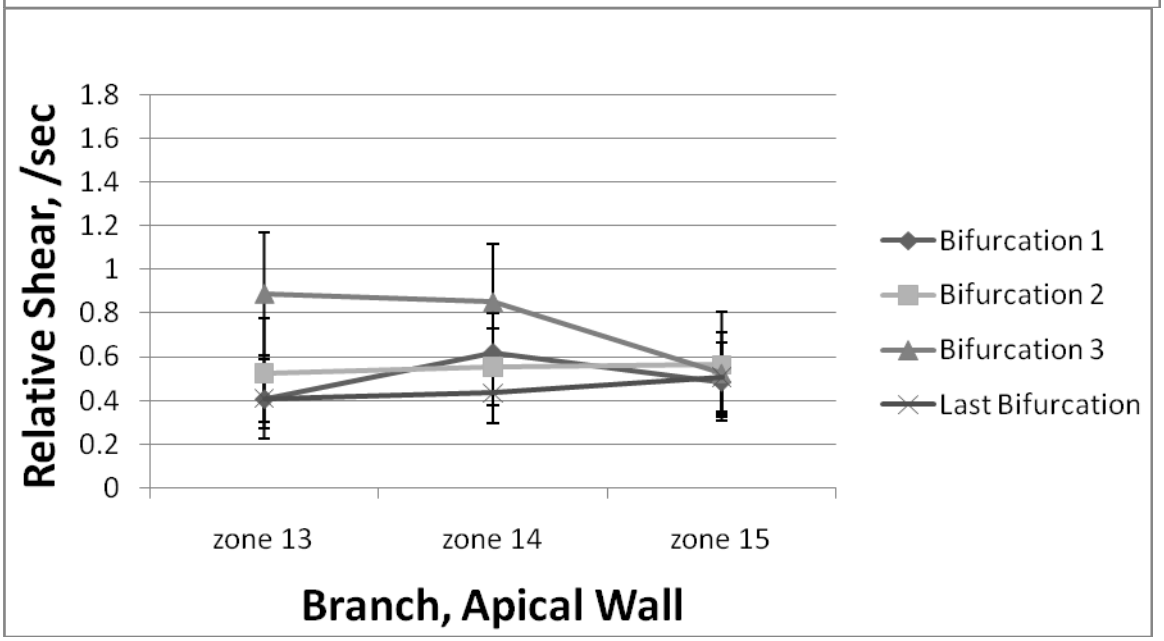

Wall shear rate in metabolically normal C57/bl6 mice by zone and bifurcation (N=34 networks). For zone reference see Appendix I. Shear is normalized to inflow shear at the non-branching wall (zone 6). There are no significant differences between or among zones or bifurcations ($p<0.05$). All data are presented as mean ± SE.

Figure 7.7

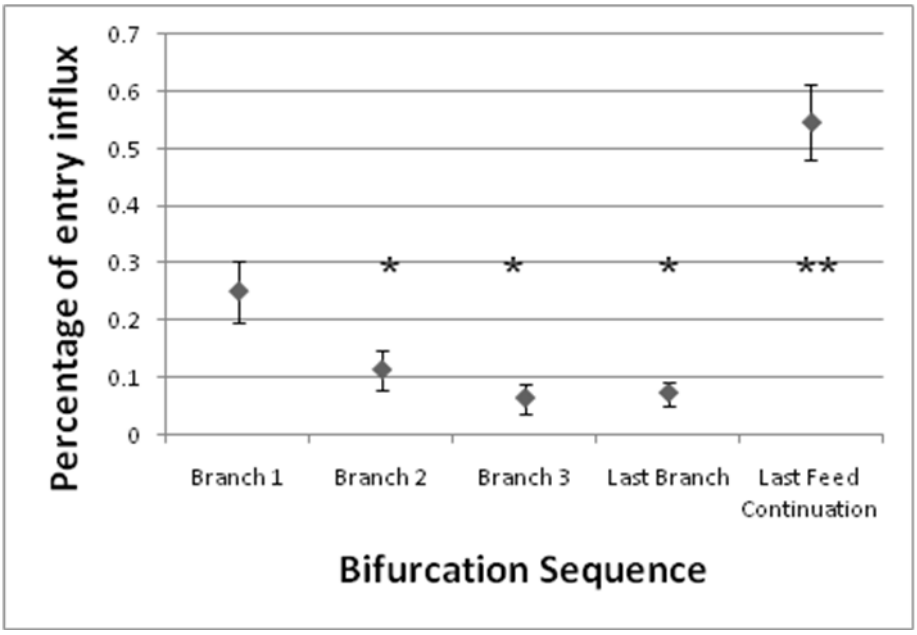

RBC flux distribution in metabolically normal C57/bl6 mice by bifurcation. Data is percent of RBC flux at the entrance to the network (N=34 networks). Flux to the branches decreases along the network. The majority of flow (54 ± 6%) bypasses all branches and flows out the feed continuation. Single asterisk (*) indicates difference from first branch, double asterisk(**) indicates difference from all branches ($p<0.05$). All data are presented as mean ± SE.

Figure 7.8

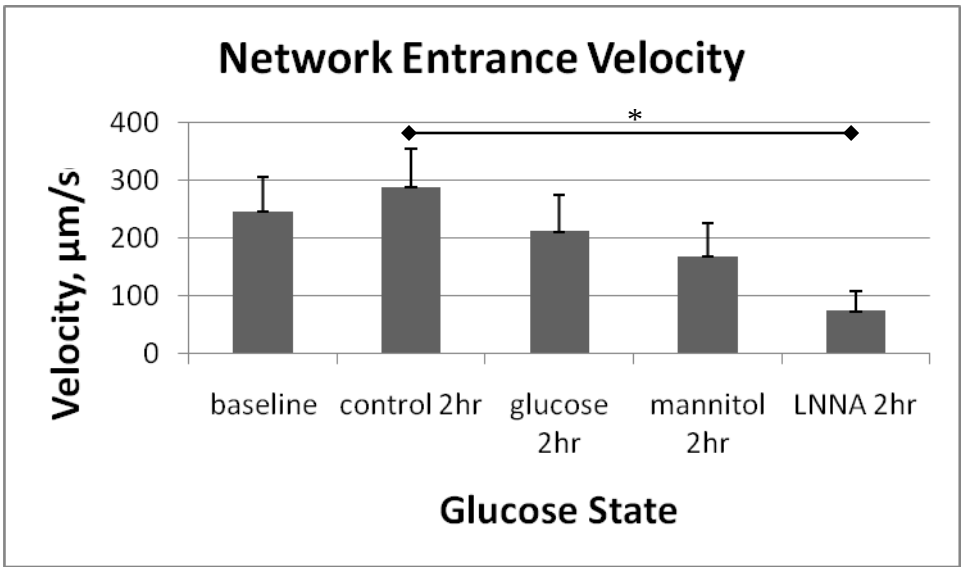

Velocity into the network by treatment (N=8 networks per treatment). LNNA at two hours is significantly smaller than control suffusate at two hours, all other differences are insignificant ($p<0.05$). All data are presented as mean ± SE.

Figure 7.9 (page 1 of 2)

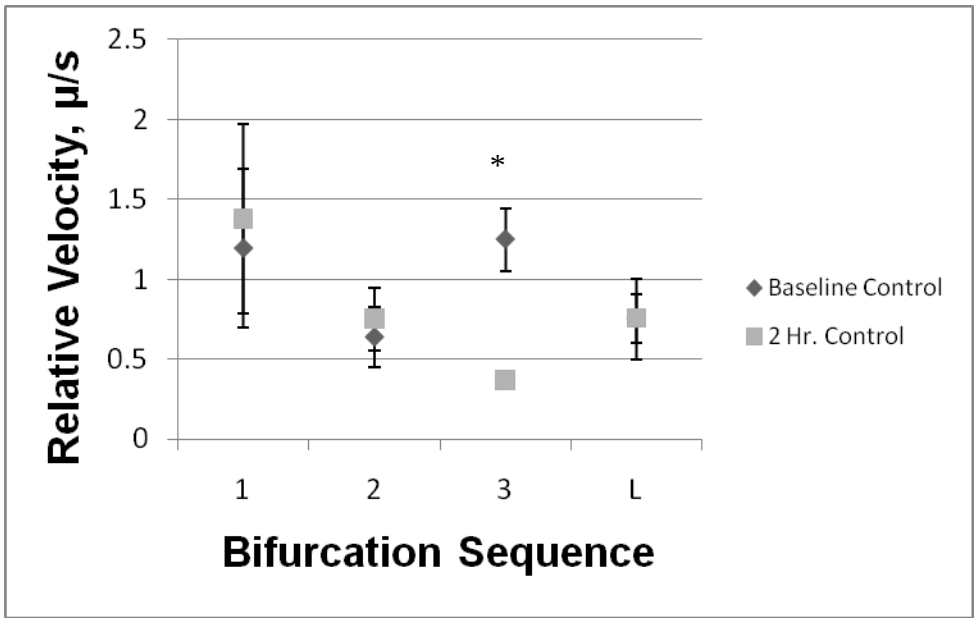

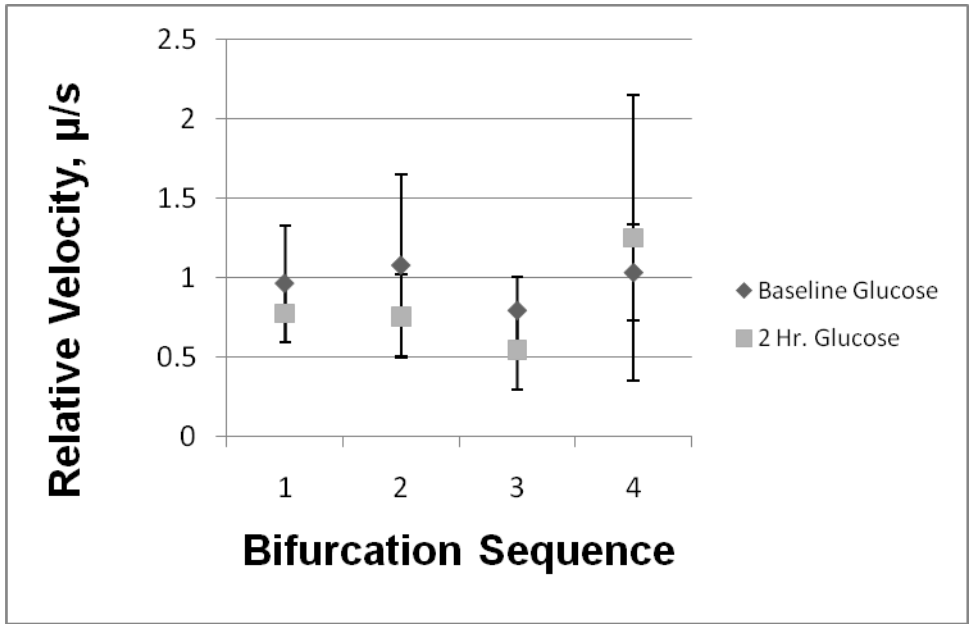

Figure 7.9 (Page 2 of 2)

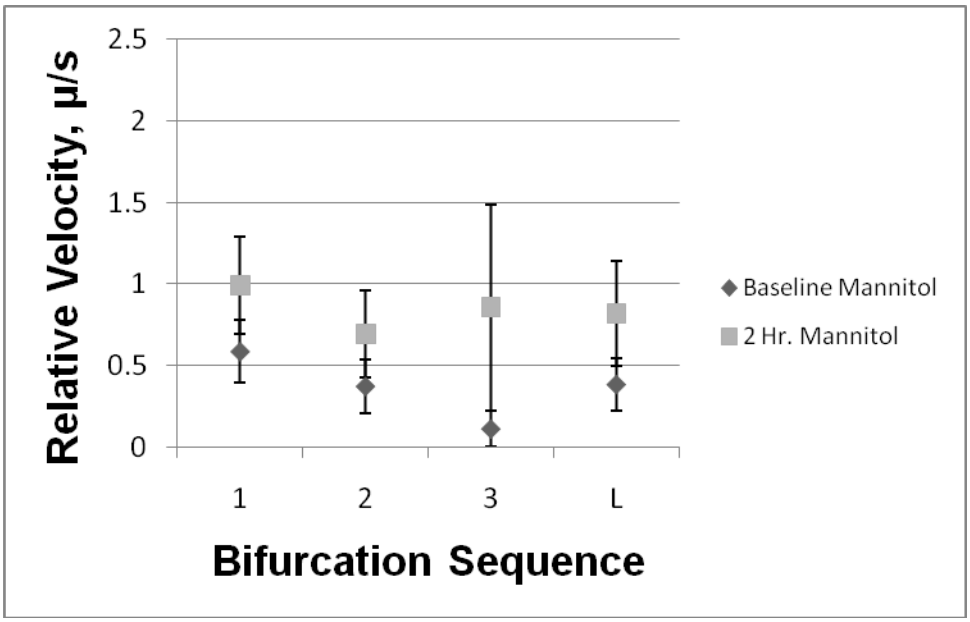

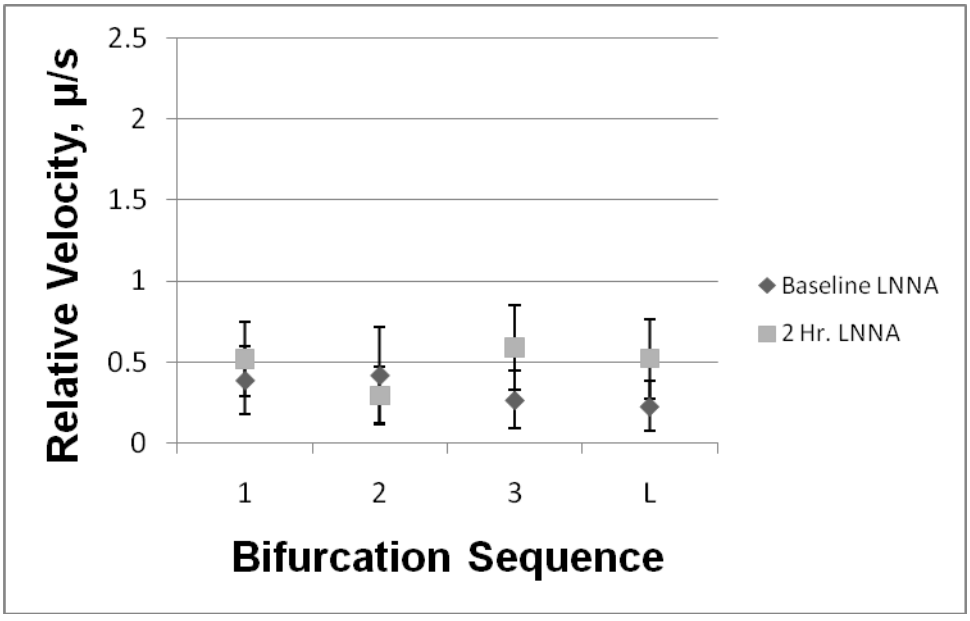

Velocity along the arteriolar network by treatment. All velocities are normalized to the inflow velocity at the first bifurcation (N=8 networks per treatment). Only the third bifurcation under control conditions is significant ($p<0.05$). All data are presented as mean ± SE.

Figure 7.10 (page 1 of 3)

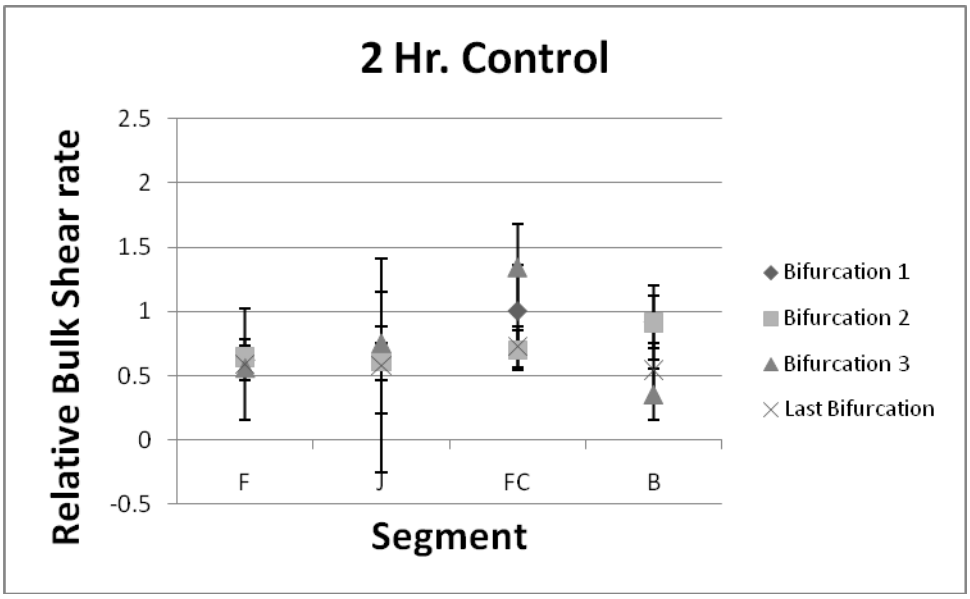

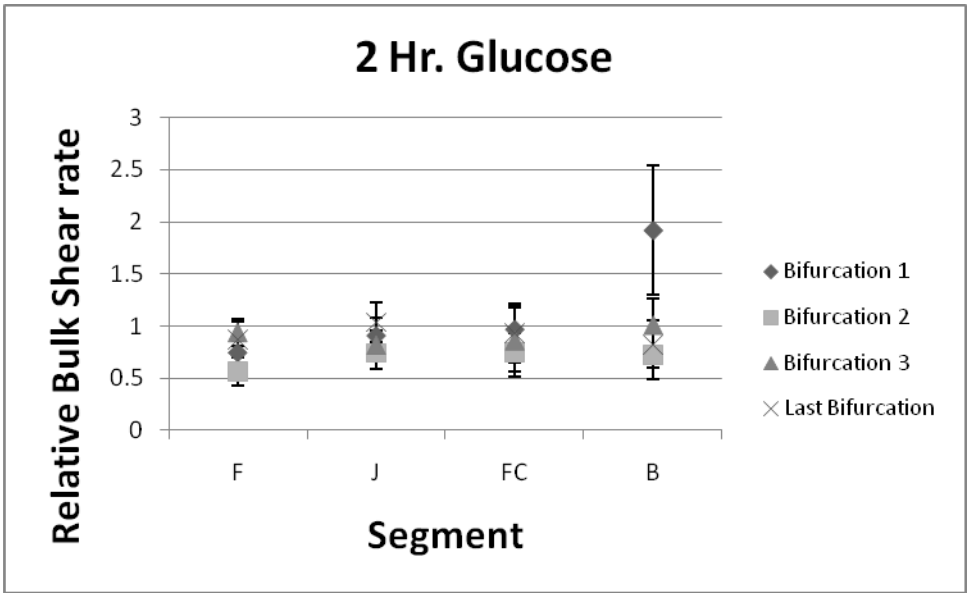

Figure 7.10 (page 2 of 3)

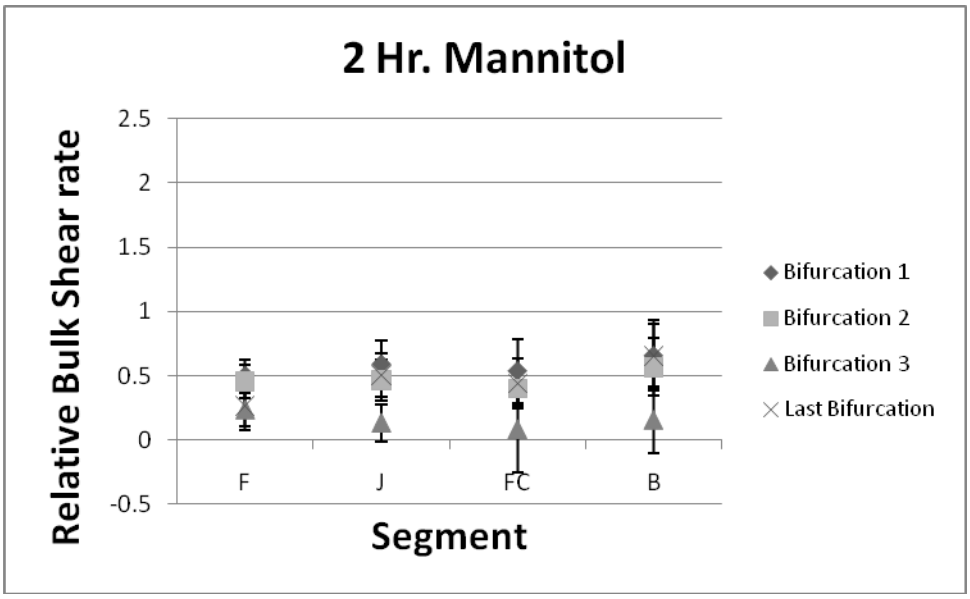

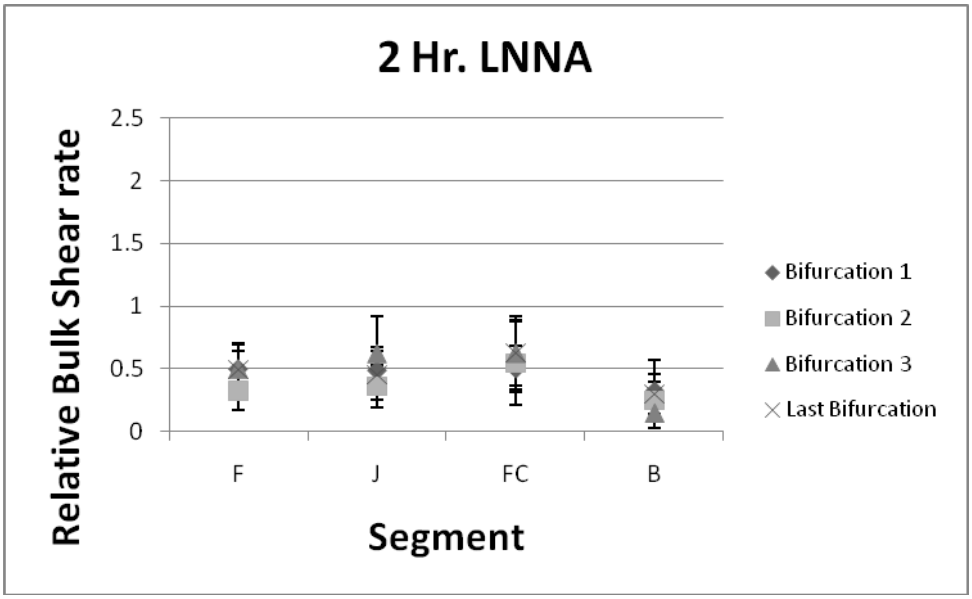

Figure 7.10 (page 3 of 3)

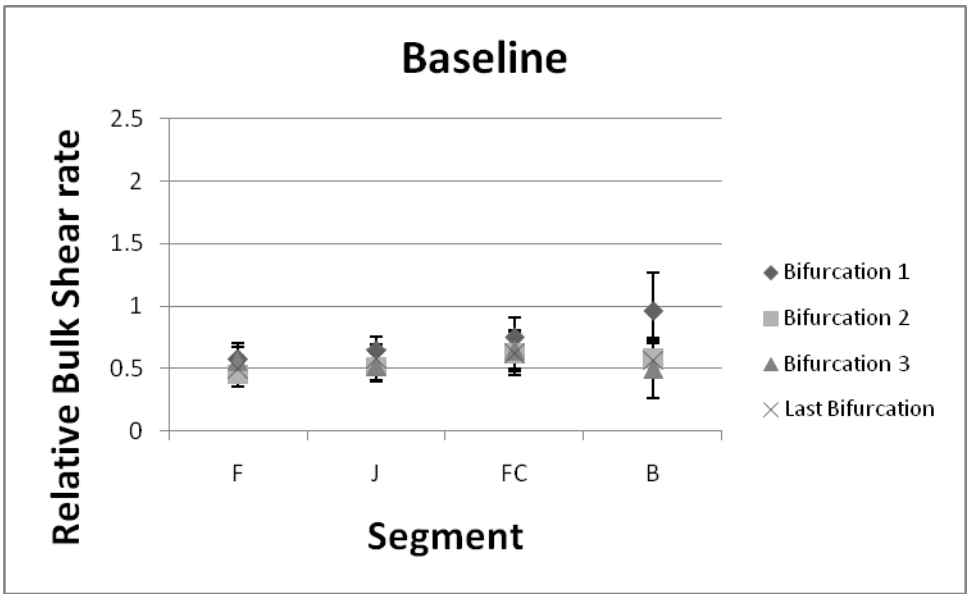

Bulk shear rate along the arteriolar network by treatment by segment and bifurcation. F = feed segment, J = Junction segment , FC = feed contuation segment, and B = branch segment (N=8 networks per treatment). For segment reference see Appendix I. There are no significant differences between or among groups ($p<0.05$). All data are presented as mean ± SE.

Figure 7.11 (page 1 of 2)

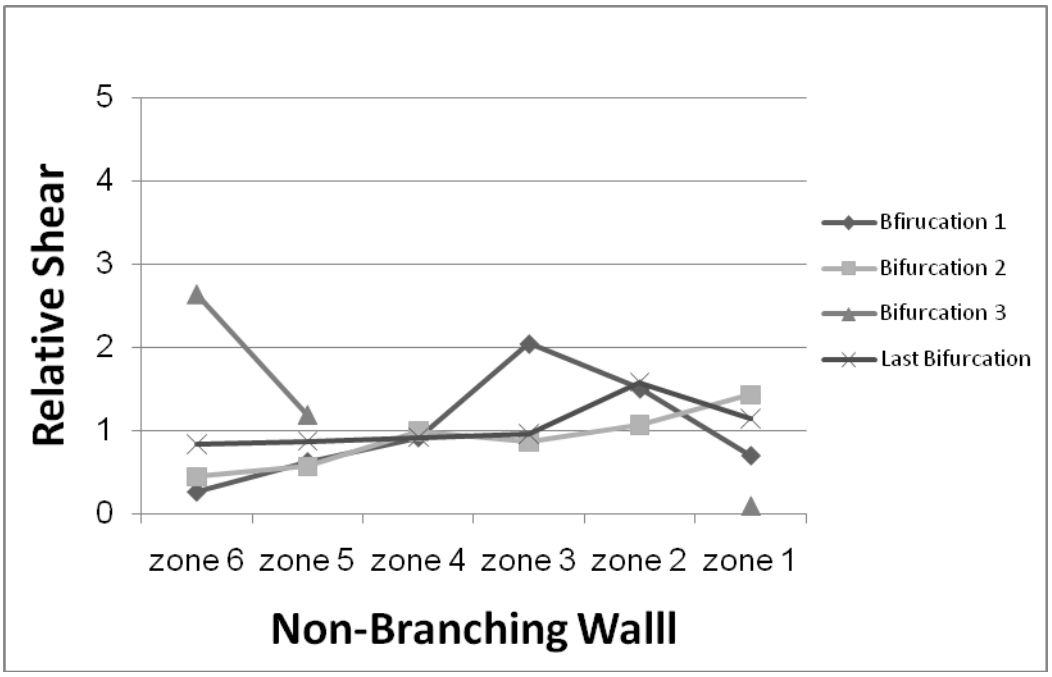

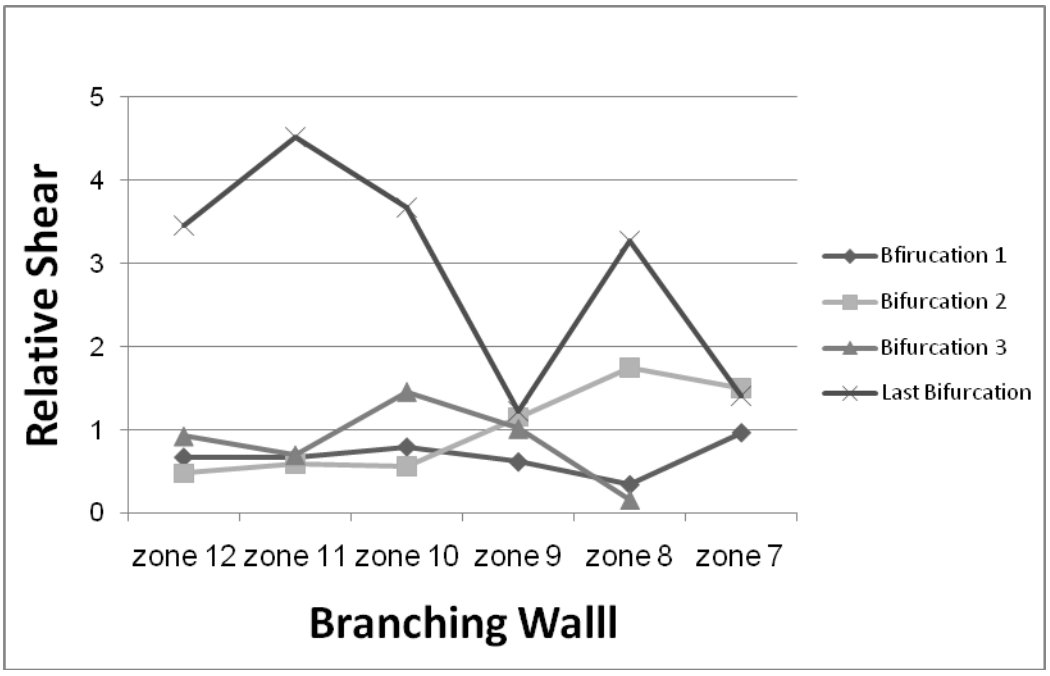

Figure 7.11 (page 2 of 2)

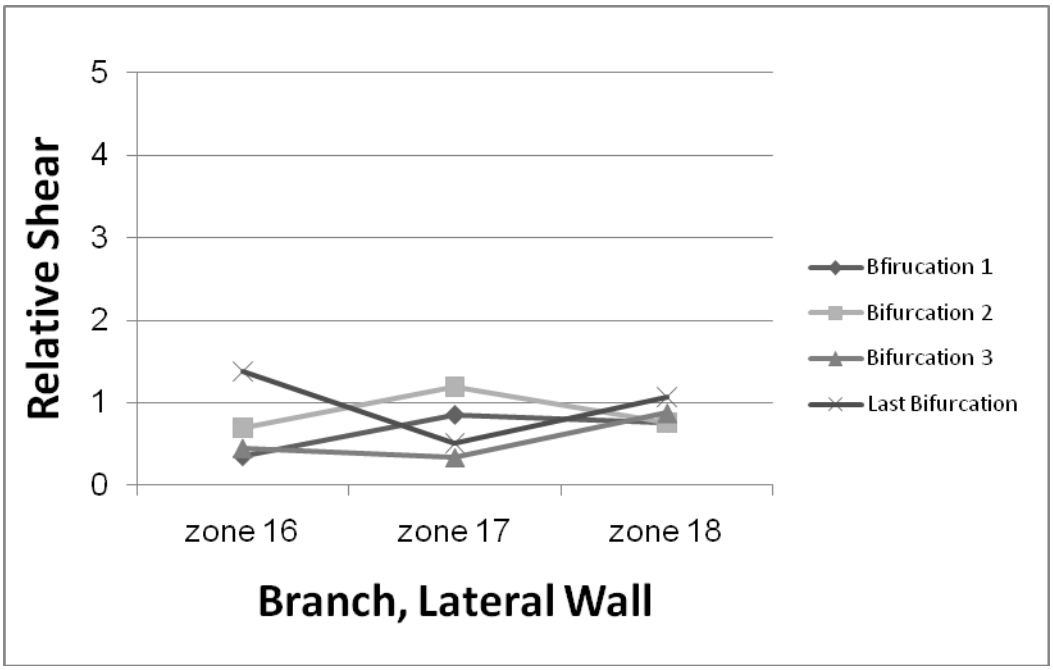

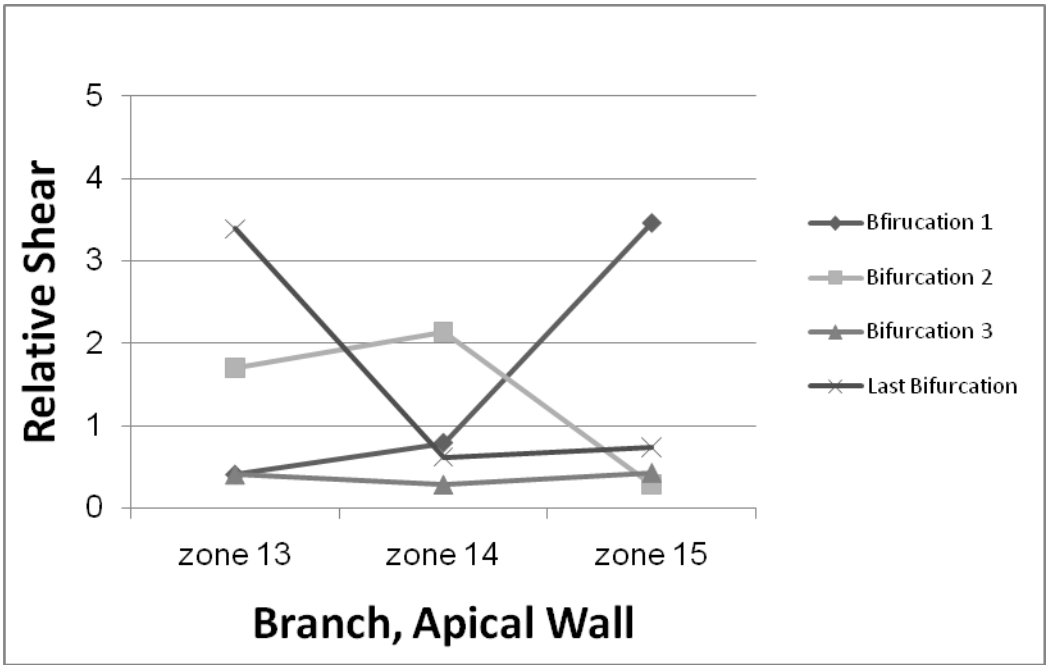

Wall shear rate along the arteriolar network by treatment for 2 hour control suffusate exposure by zone and bifurcation (N=8 networks). For zone reference see Appendix I. Shear is normalized to inflow shear at the non-branching wall (zone 6). There are no significant differences between or among zones or bifurcations ($p<0.05$). All data are presented as mean ± SE.

Figure 7.12 (page 1 of 2)

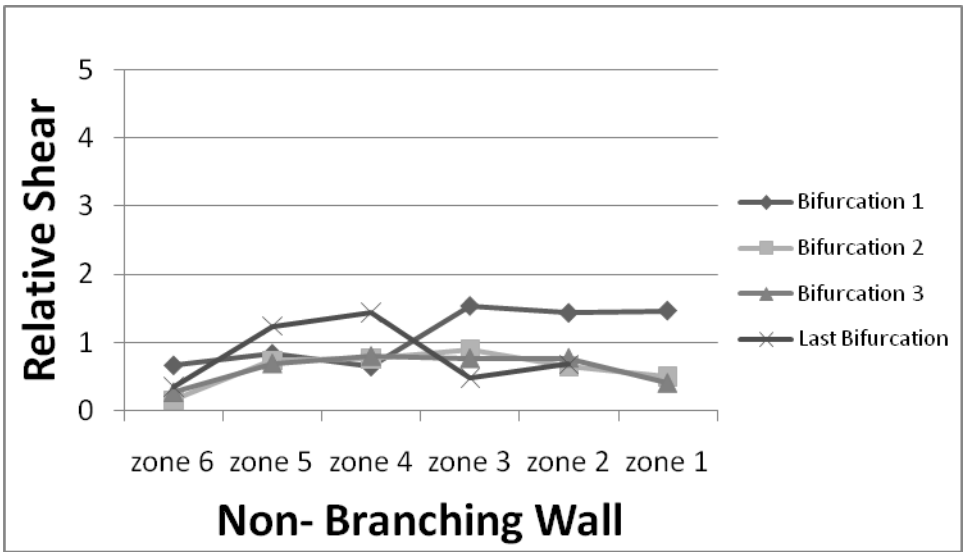

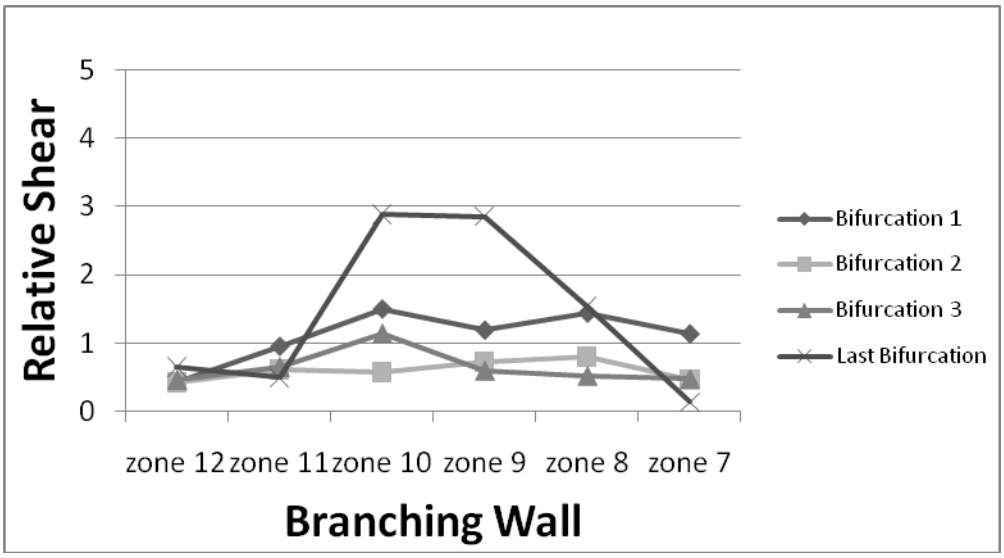

Figure 7.12 (page 2 of 2)

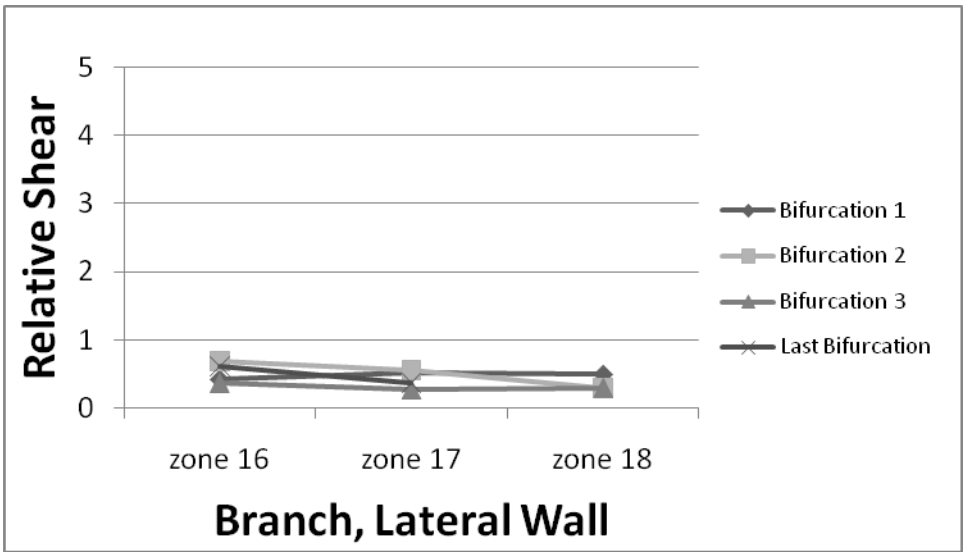

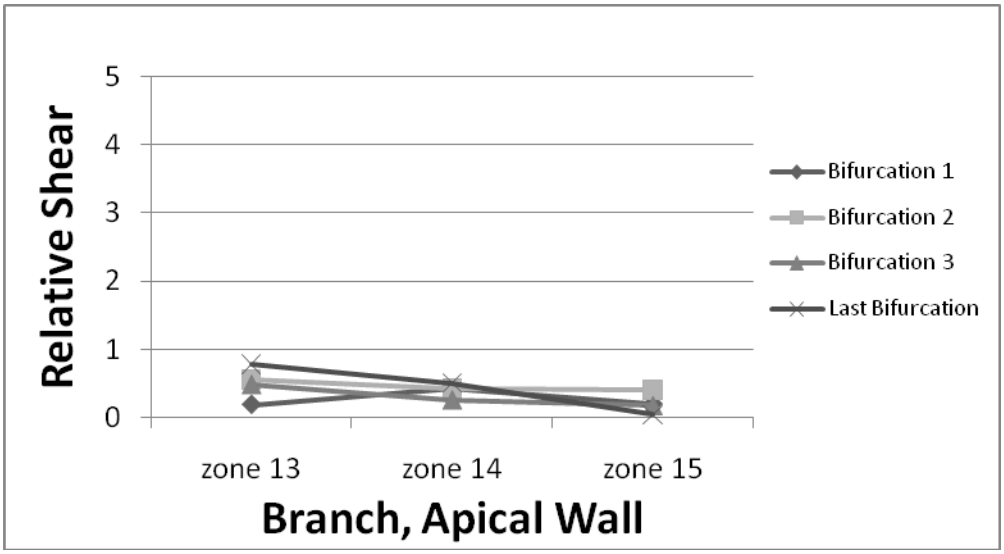

Wall shear rate along the arteriolar network by treatment for 2 hour glucose suffusate exposure by zone and bifurcation (N=8 networks per treatment). For zone reference see Appendix I. Shear is normalized to inflow shear at the non-branching wall (zone 6). Gradient in shear are suppressed along both feed walls as compared to control conditions (Fig 7.11). There are no significant differences between or among zones or bifurcations ($p<0.05$). All data are presented as mean ± SE.

7.13 (page 1 of 2)

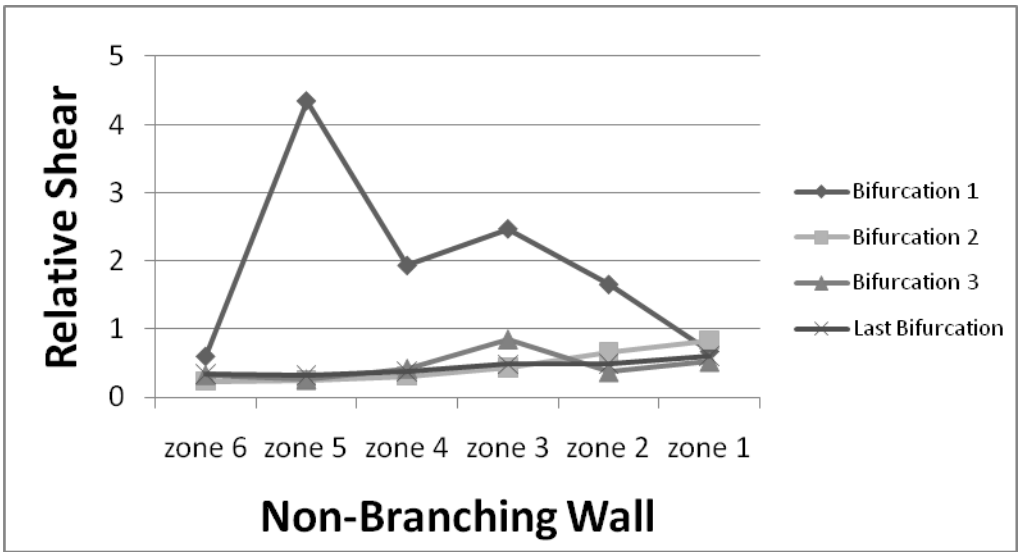

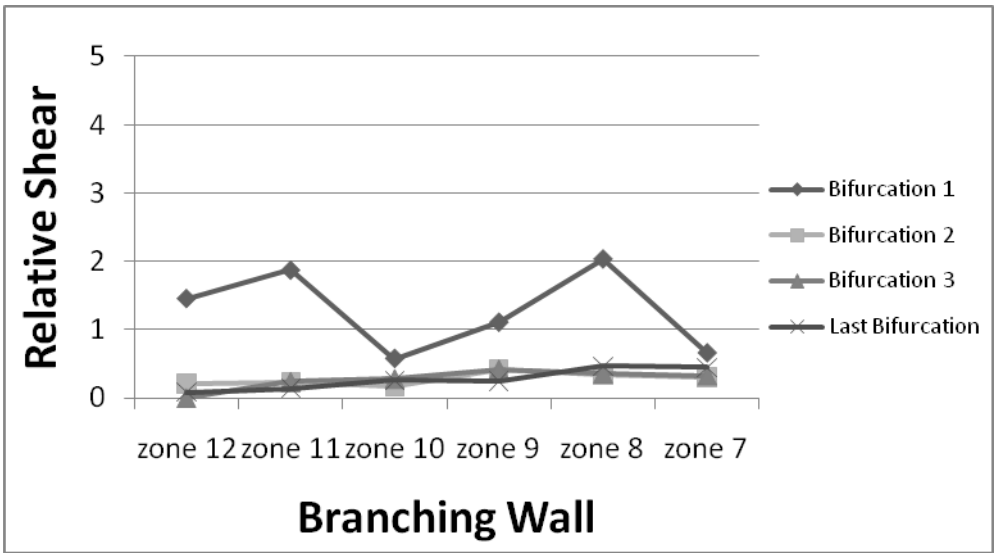

Fig 7.13 (page 2 of 2)

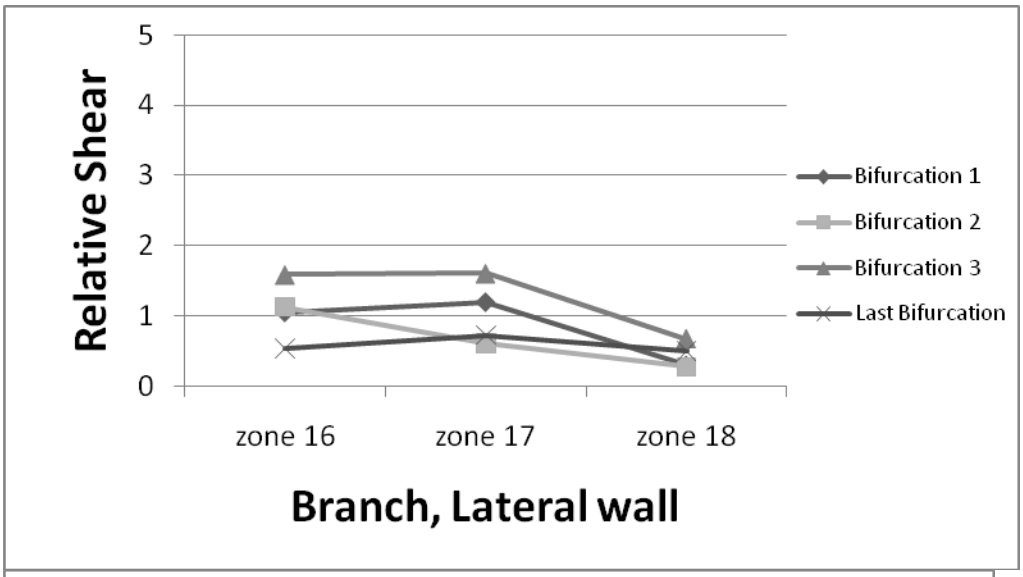

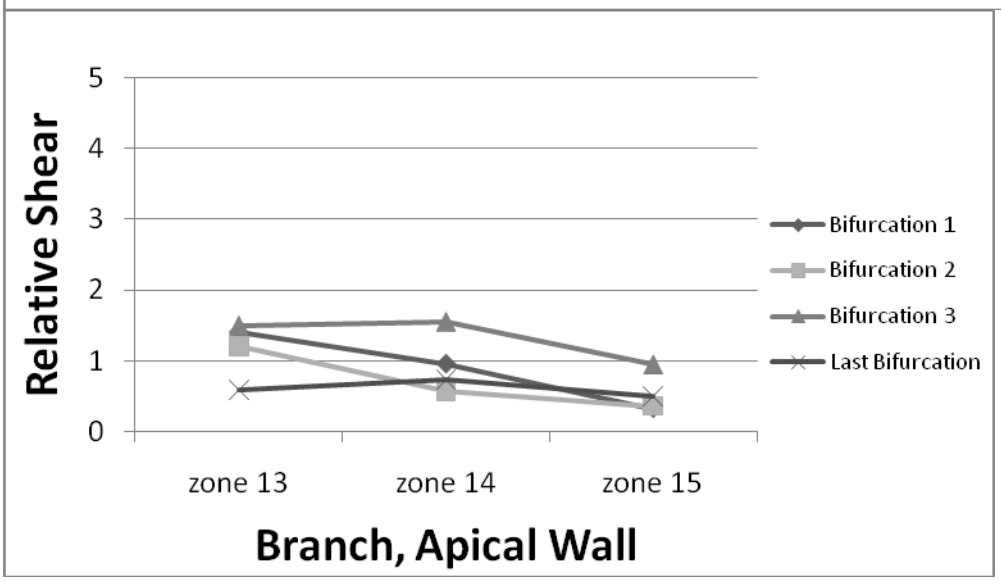

Wall shear rate along the arteriolar network by treatment for 2 hour mannitol suffusate exposure (osmotic control) by zone and bifurcation (N=8 networks). For zone reference see Appendix I. Shear is normalized to inflow shear at the non-branching wall (zone 6). The first bifurcation has increased shear gradients as compared to all other bifurcations along the feed walls. These are not significant.($p<0.05$). All data are presented as mean ± SE.

Figure 7.14 (page 1 of 2)

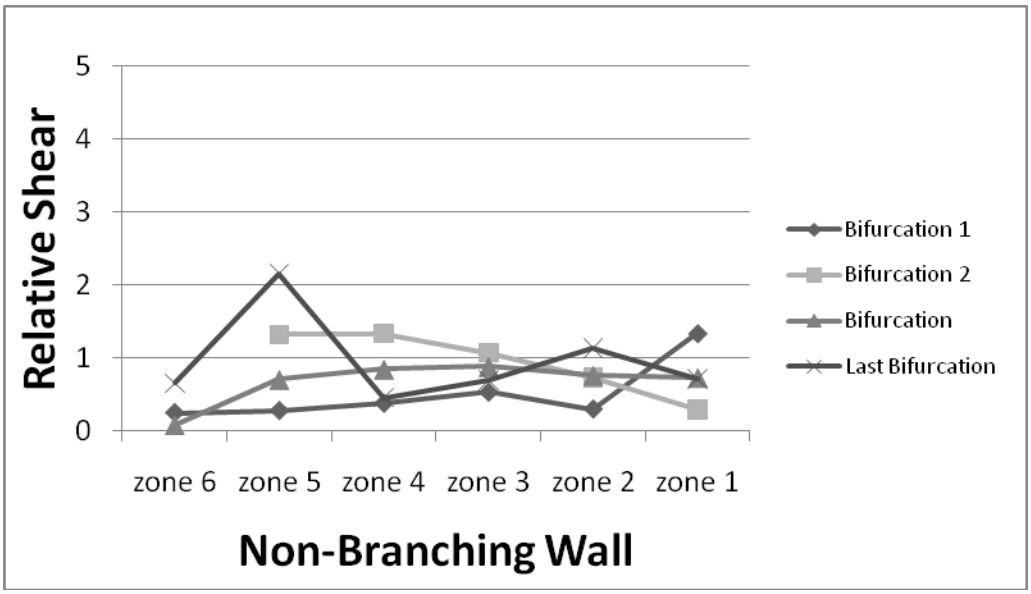

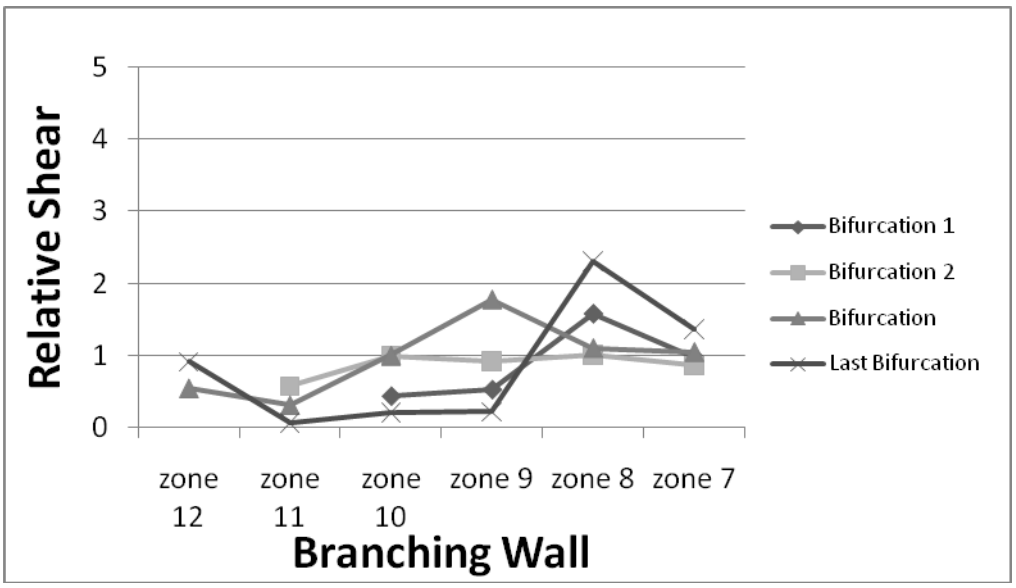

Figure 7.14 (page 2 of 2)

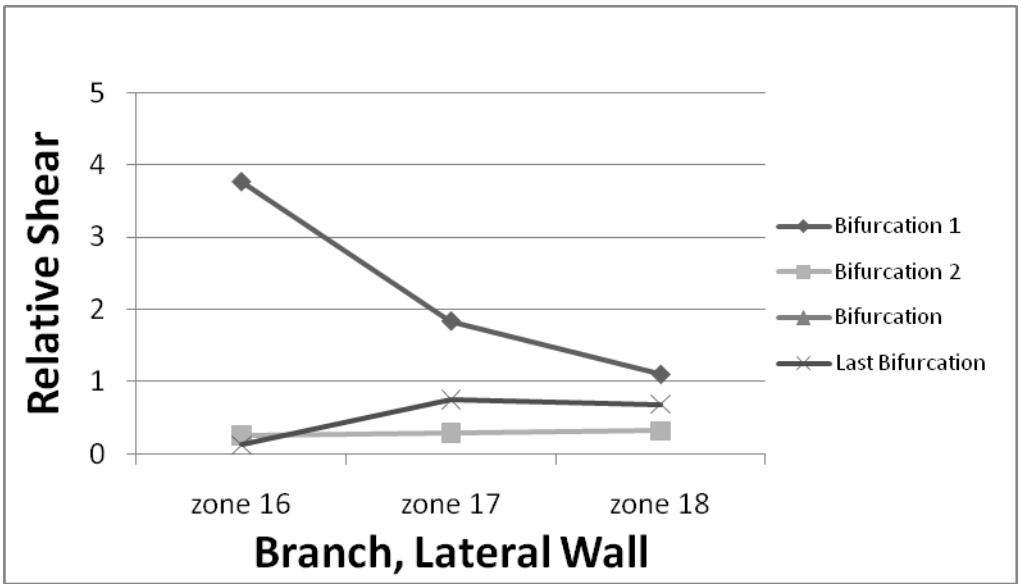

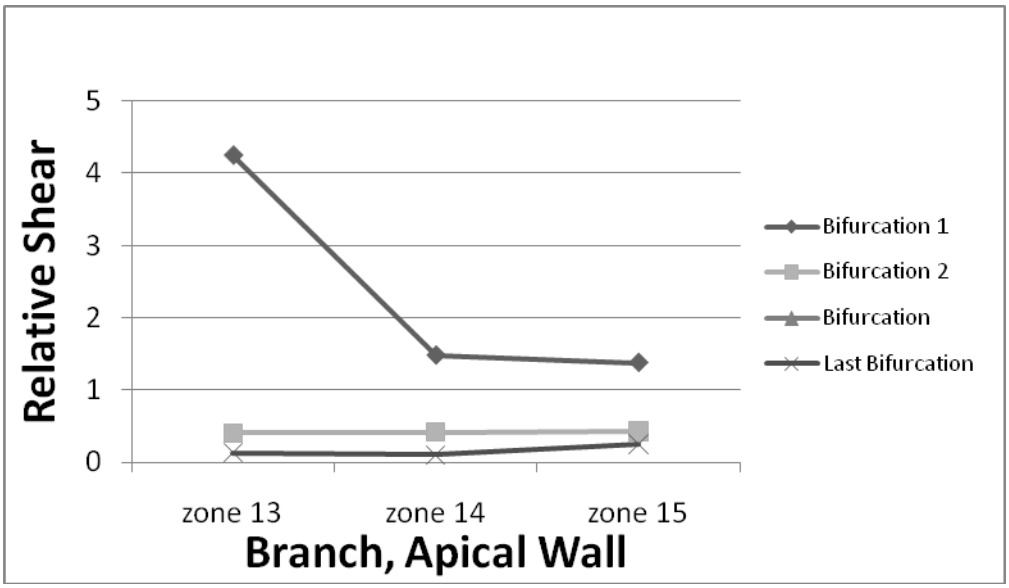

Wall shear rate along the arteriolar network by treatment for 2 hour LNNA exposure by zone and bifurcation. (N=8 networks) For zone reference see Appendix I. Shear is normalized to inflow shear at the non-branching wall (zone 6). Shear gradients along the walls are suppressed as compared to control, whereas the shear gradient at zones 13 and 16 in the first bifurcation are increased. These changes are not significant. ($p<0.05$). All data are presented as mean ± SE.

Figure 7.15

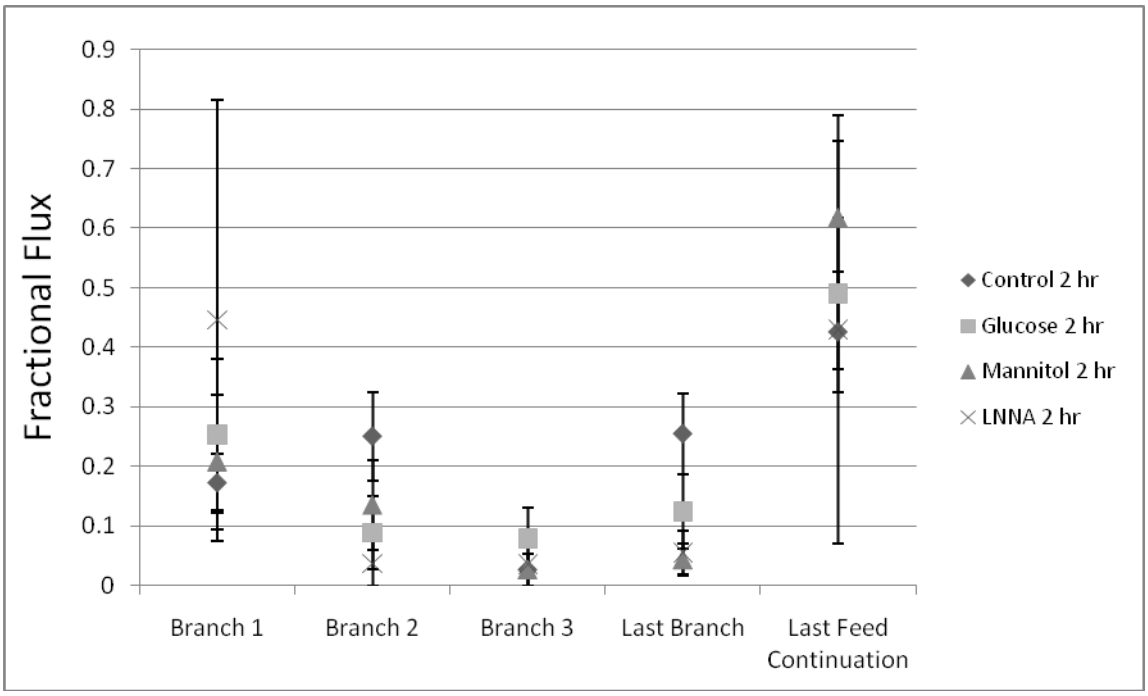

RBC flux distribution for acute treatments by bifurcation (N=8 networks per treatment). Data is percent of RBC flux at the entrance to the network. Flux to the branches decreases along the network for all treatments. The majority of flow bypasses all branches and flows out the feed continuation. Single asterisk (*) indicates difference from first branch, double asterisk(**) indicates difference from all branches ($p<0.05$). All data are presented as mean ± SE.

Figure 7.16

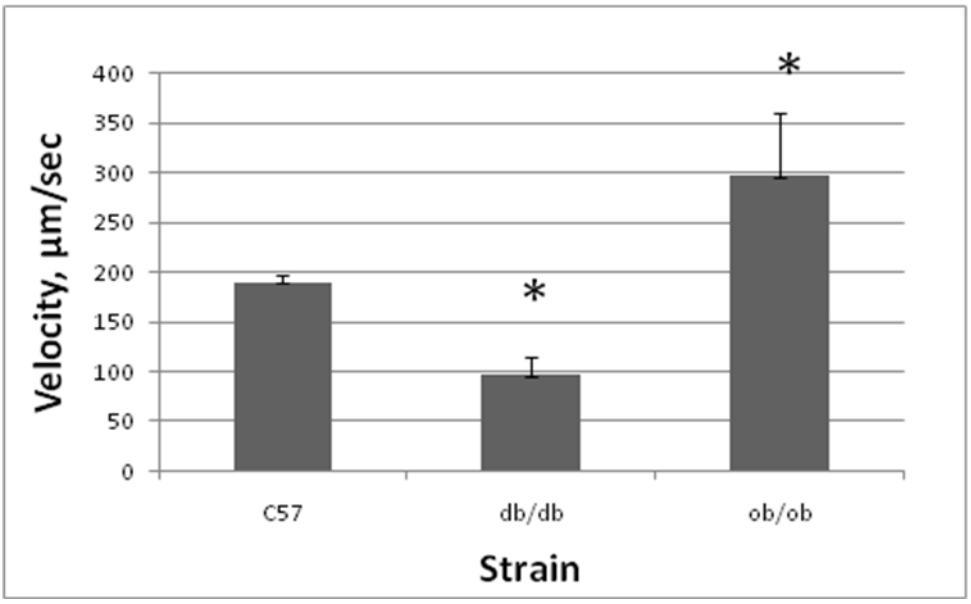

Network inflow velocity by strain, all bifurcations pooled (N=34 networks for C57/bl7, N=5 networks for db/db, N=6 networks for ob/ob). Diabetic animals have a significantly smaller inflow velocity than C57/bl6 animals, whereas obese animals have a significantly larger inflow velocity than C57/bl6 animals ($p<0.05$). All data is presented as mean ± SE.

Figure 7.17

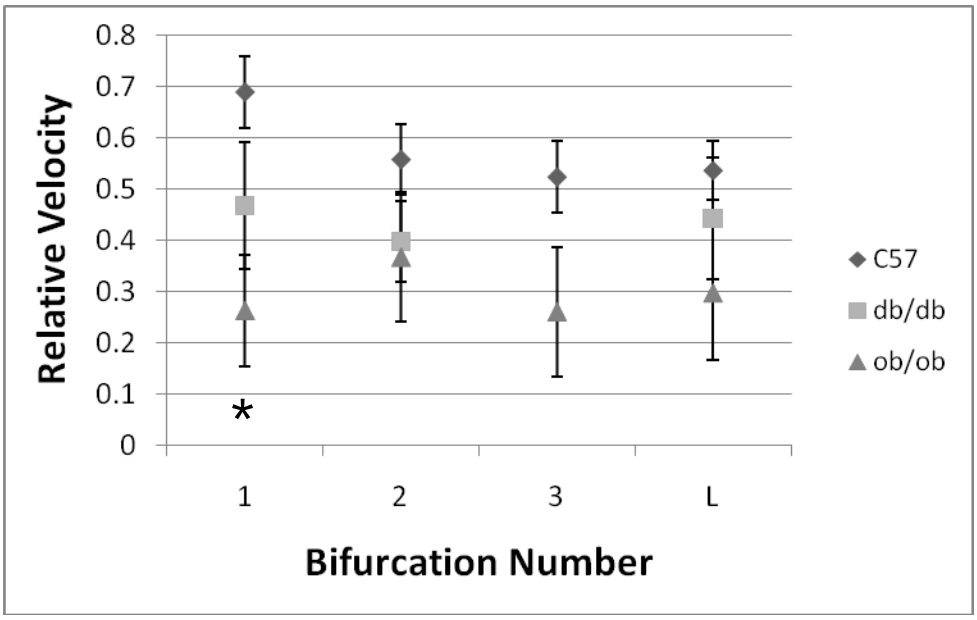

Blood flow velocity across strains by bifurcation(N=34 networks for C57/bl7, N=5 networks for db/db, N=6 networks for ob/ob). The first bifurcation velocity for the obese animals is significantly smaller than the first bifurcation for the C57/bl6 cohort ($p<0.05$). All data is normalized to the inflow velocity of the network. Data is presented as mean ± SE.

Figure 7.18 (page 1 of 2)

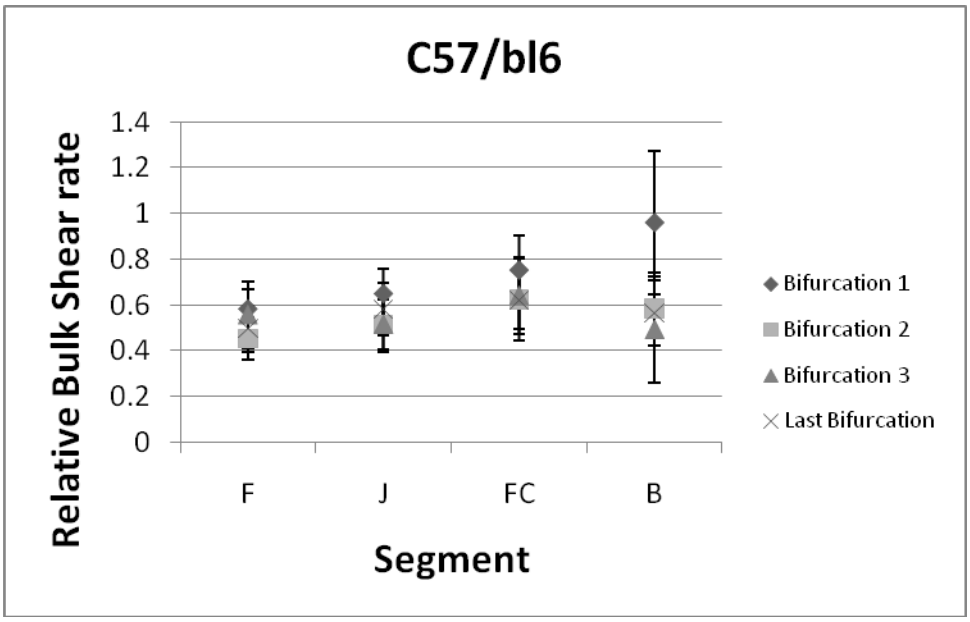

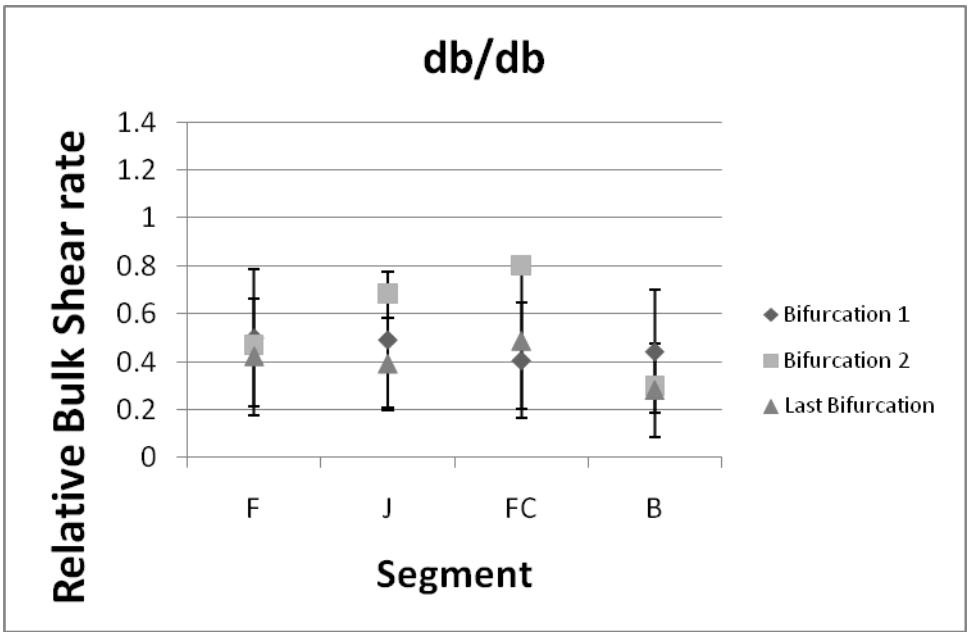

Figure 7.18 (page 2 of 2)

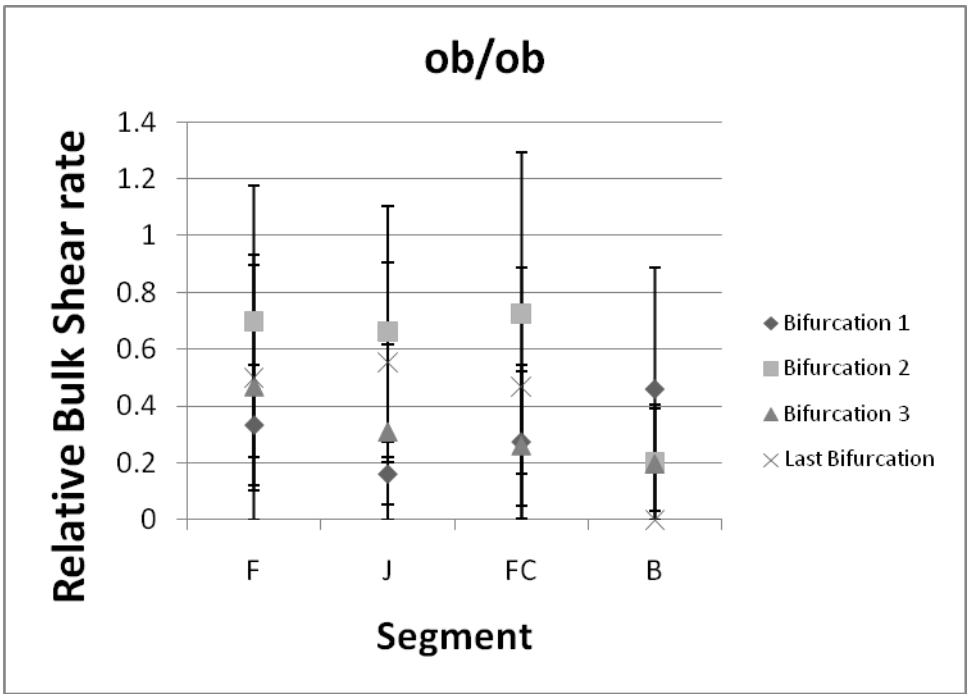

Bulk shear rate by strain by segment and bifurcation (N=34 networks for C57/bl7, N=5 networks for db/db, N=6 networks for ob/ob). F = feed segment, J = Junction segment , FC = feed contuation segment, and B = branch segment. For segment reference see Appendix I. While the means are similar for all three strains, the variability in the db/db animals is increased compared to the C57/bl6 animals. The variability in the obese animals is increased still further. There are no significant differences between or among groups ($p<0.05$). All data are presented as mean ± SE.

Figure 7.19 (page 1 of 2)

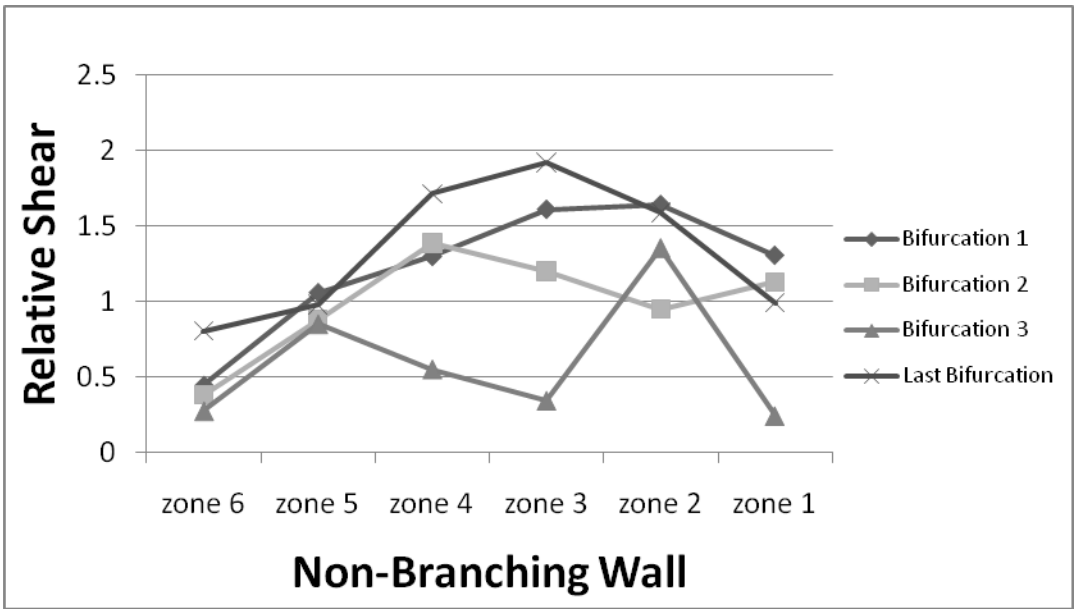

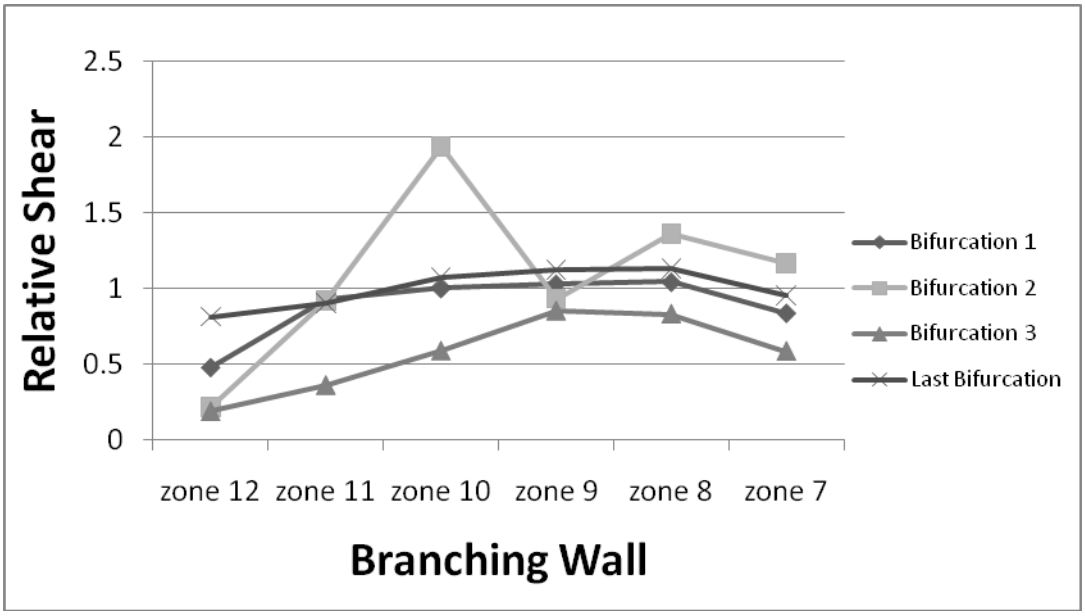

Figure 7.19 page 2 of 2)

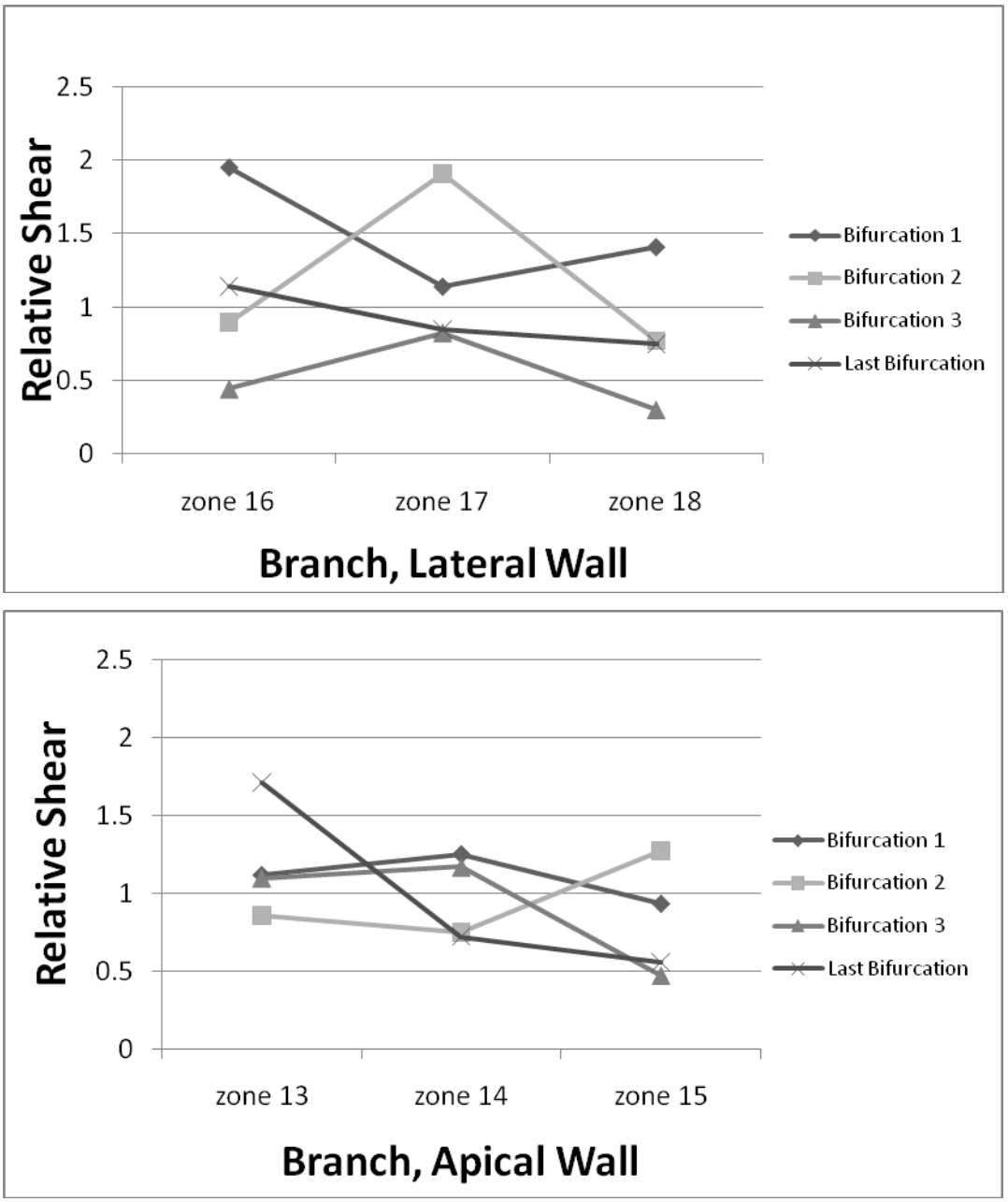

Wall shear rate for C57/bl6 cohort by zone and bifurcation (N=34 networks). For zone reference see Appendix I. Shear is normalized to inflow shear at the non-branching wall (zone 6). There are no significant differences between or among zones or bifurcations ($p<0.05$). All data are presented as mean ± SE.

Figure 7.20

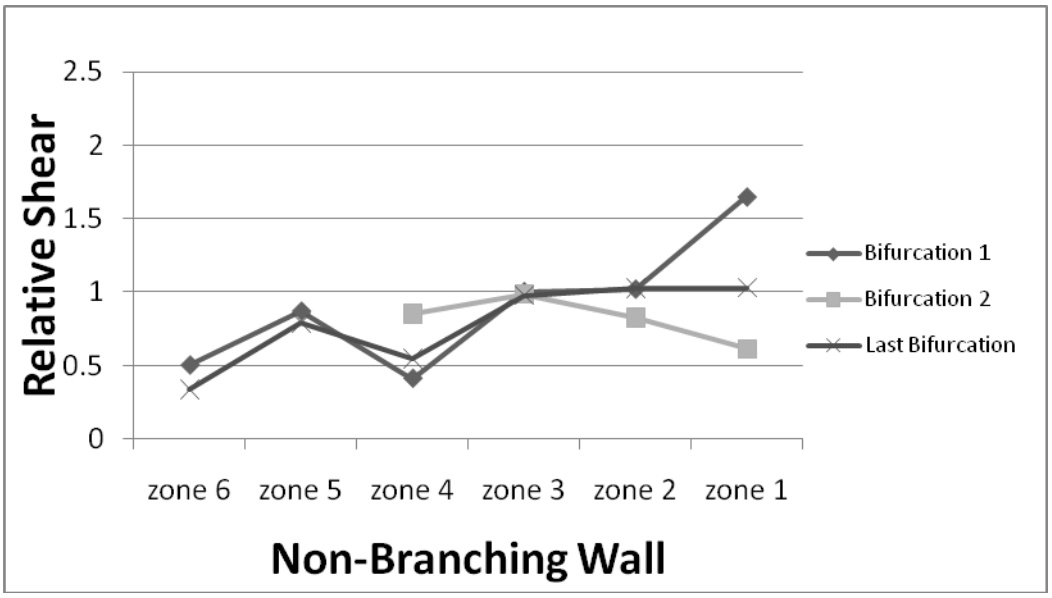
Relative Shear
2.5
2
1.5
1
0.5
0
zone 6
zone 5
zone 4
zone 3
zone 2
zone 1
Bifurcation 1
Bifurcation 2
Last Bifurcation
Non-Branching Wall

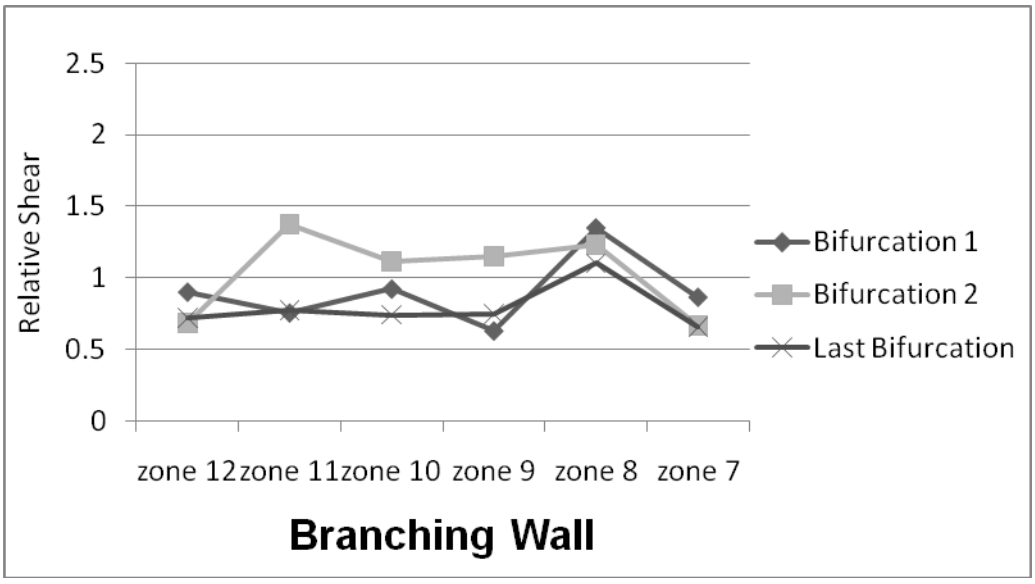
Relative Shear
2.5
2
1.5
1
0.5
0
zone 12
zone 11
zone 10
zone 9
zone 8
zone 7
Bifurcation 1
Bifurcation 2
Last Bifurcation
Branching Wall

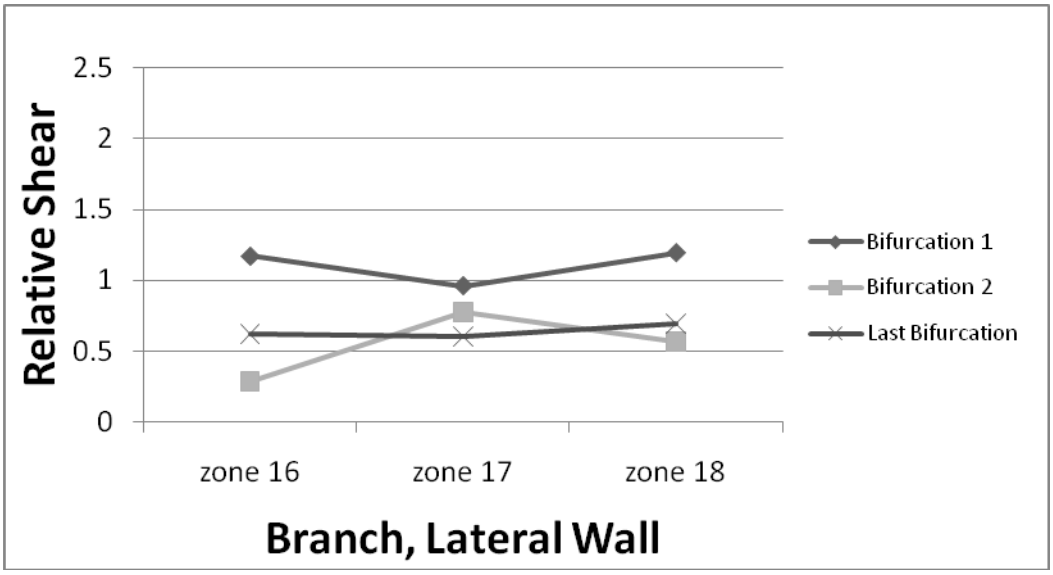

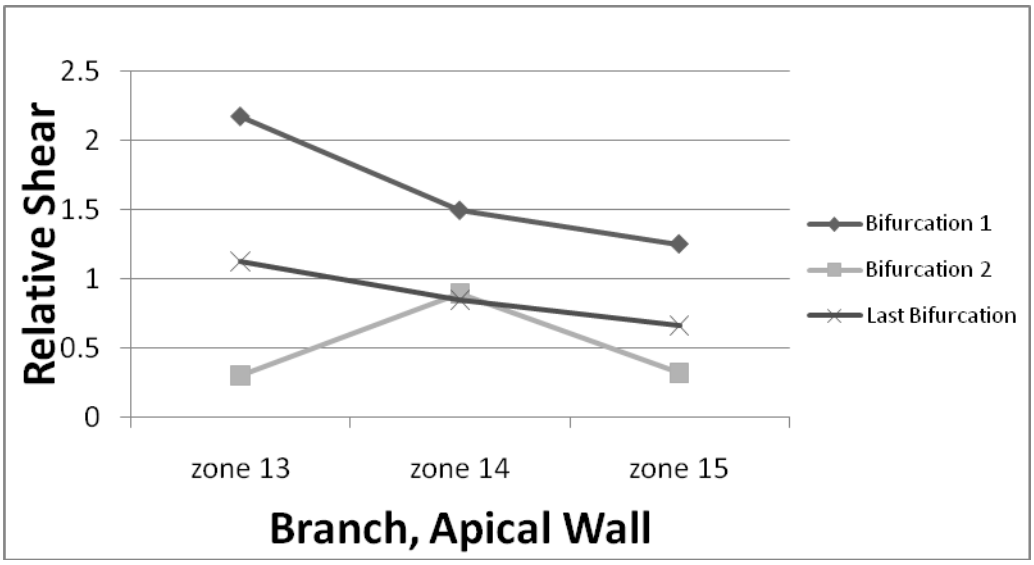

Wall shear rate for db/db cohort by zone and bifurcation (N=5 networks). For zone reference see Appendix I. Shear is normalized to inflow shear at the non-branching wall (zone 6). There are no significant differences between or among zones or bifurcations ($p<0.05$). All data are presented as mean ± SE.

7.21

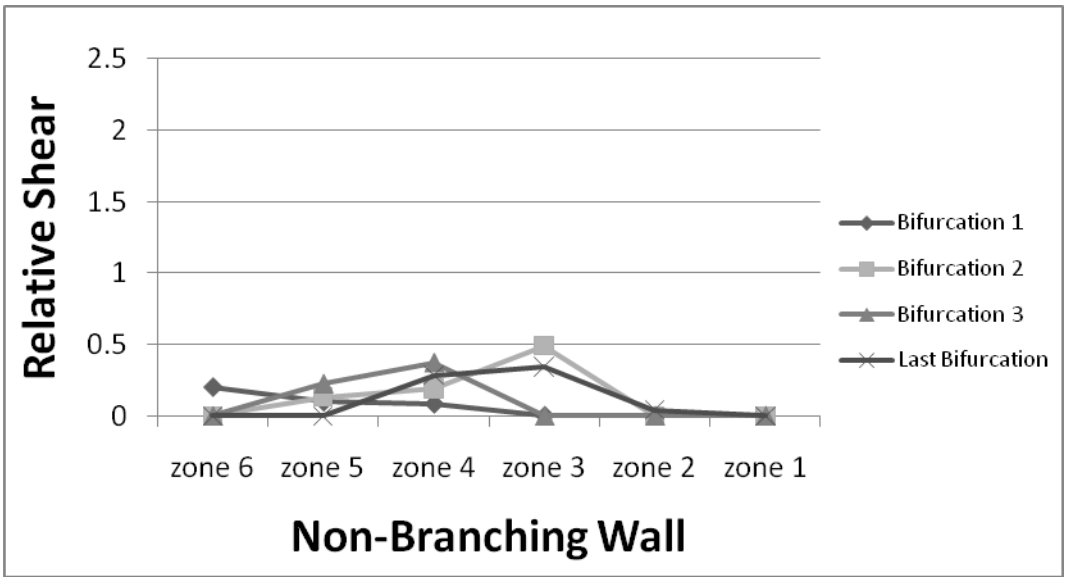
Relative Shear
2.5
2
1.5
1
0.5
0
zone 6
zone 5
zone 4
zone 3
zone 2
zone 1
Non-Branching Wall
Bifurcation 1
Bifurcation 2
Bifurcation 3
Last Bifurcation

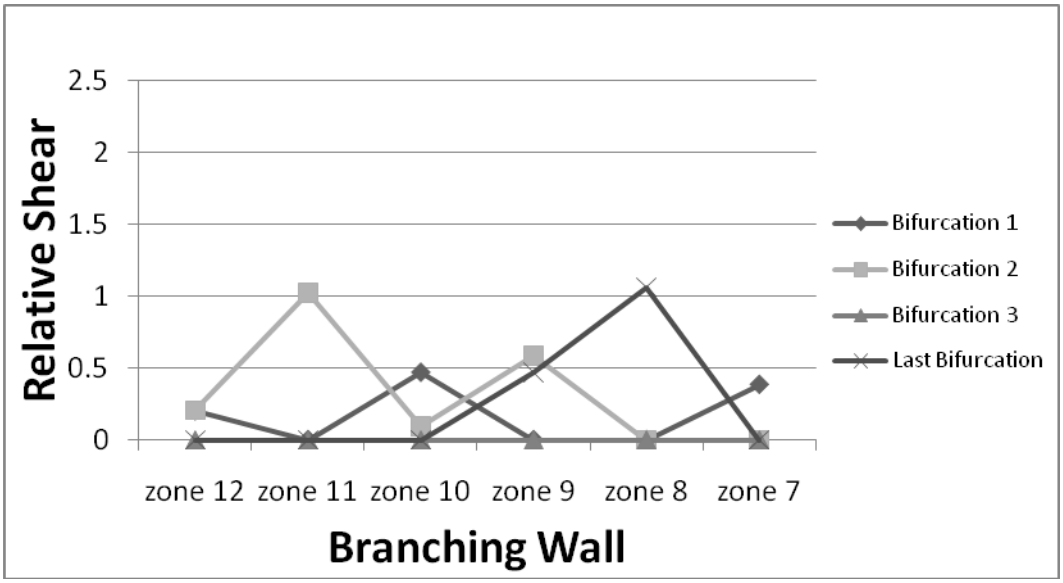
Relative Shear
2.5
2
1.5
1
0.5
0
zone 12
zone 11
zone 10
zone 9
zone 8
zone 7
Branching Wall
Bifurcation 1
Bifurcation 2
Bifurcation 3
Last Bifurcation

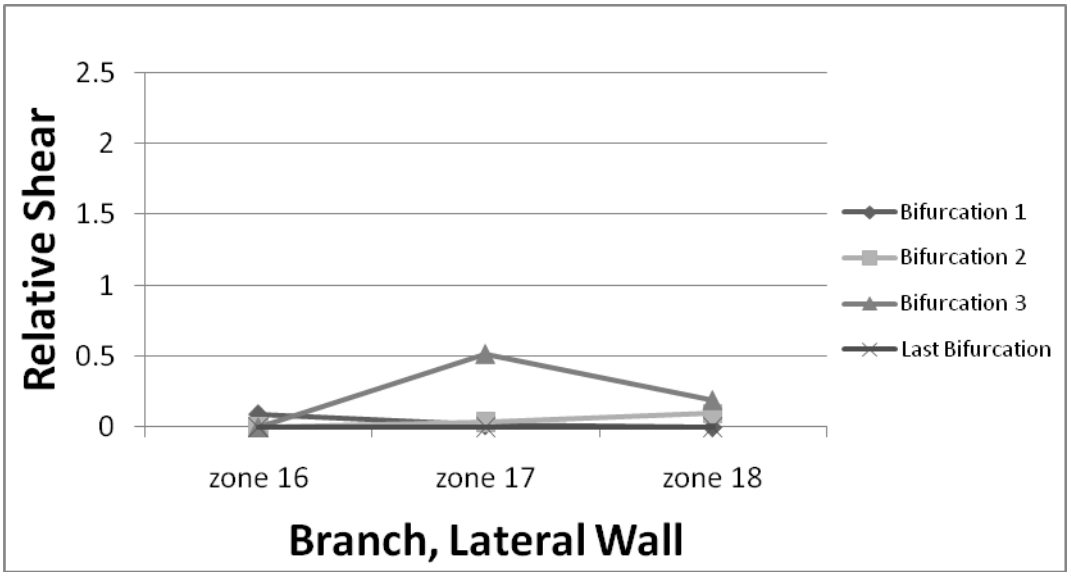

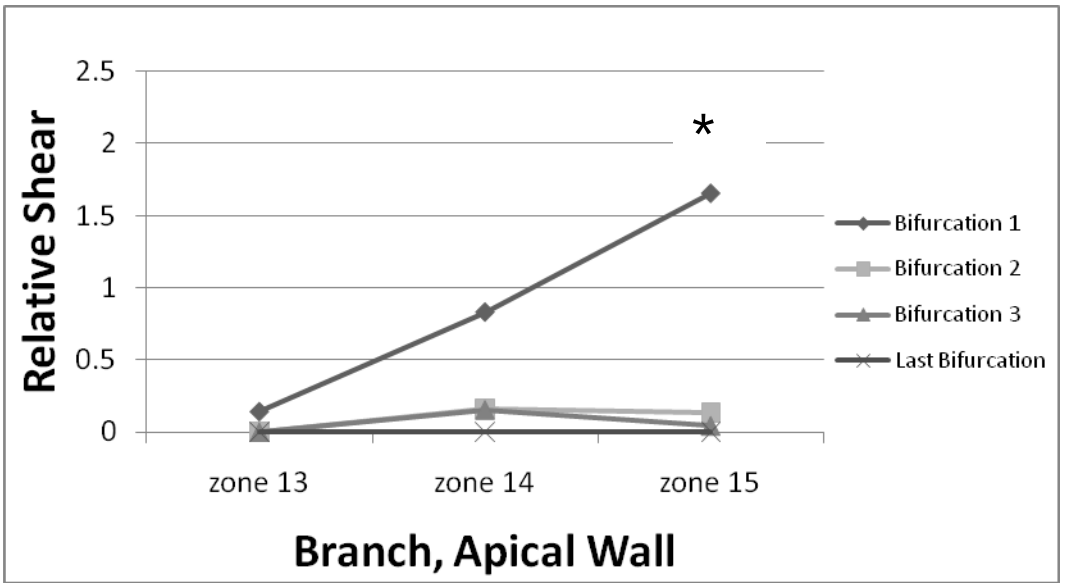

Wall shear rate for ob/ob cohort by zone and bifurcation (N=6 networks). For zone reference see Appendix I. Shear is normalized to inflow shear at the non-branching wall (zone 6). Zone 15 at bifurcation 1 is significantly higher than the other bifurcations. ($p<0.05$). All data are presented as mean ± SE.

7.22

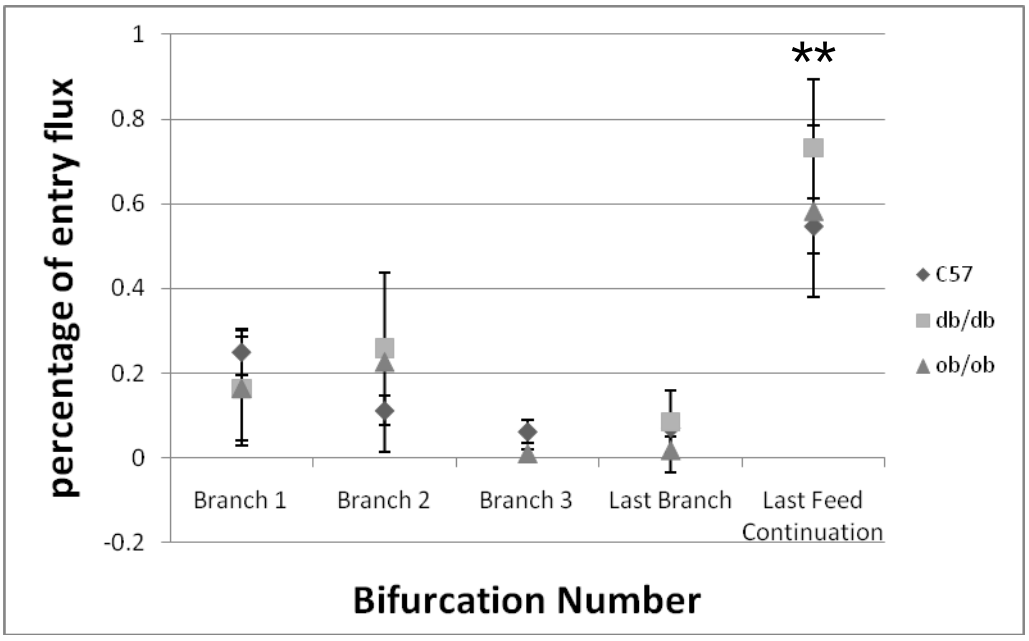

RBC flux distribution across strains by bifurcation (N=34 networks for C57/bl7, N=5 networks for db/db, N=6 networks for ob/ob). Data is percent of RBC flux into the entrance of the network. Flux to the branches decreases along the network for all treatments. The majority of flow bypasses all branches and flows out the feed continuation for all three strains. Single asterisk (*) indicates difference from first branch, double asterisk(**) indicates difference from all branches ($p<0.05$). All data are presented as mean ± SE.

7.23

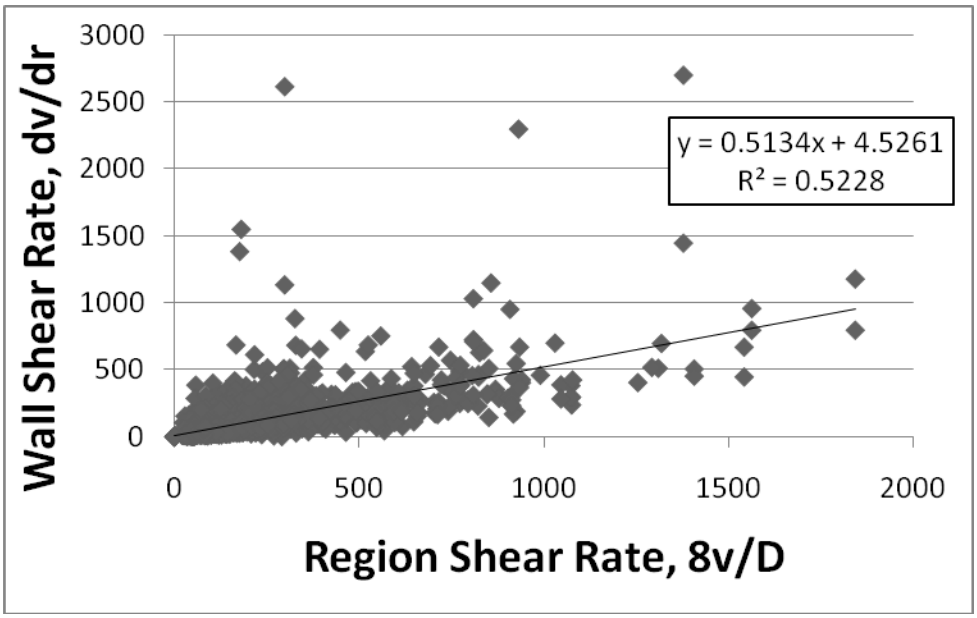

Correlation plot for two approximations of shear rate in this study. (N = 342, critical value = 0.129)

References Cited

1) Laine, H., Knuuti, J., et. al. (1998) “Preserved Relative Dispersion but Blunted Stimulation of Mean Flow, Absolute Dispersion, and Blood Volume by Insulin in Skeletal Muscle of Patients With Essential Hypertension” Circulation **97**:2146-2153

2) De Backer, D., J. Creteur, et al. (2002). "Microvascular Blood Flow Is Altered in Patients with Sepsis." Am. J. Respir. Crit. Care Med. **166**(1): 98-104.

3) Feihl,F., Liaudet, L., et. al. (2006)” Hypertension: A Disease of the Microcirculation?” Hypertension **48**:1012-1017

4) Lee, J. H. and L. Ragolia (2006). "AKT Phosphorylation Is Essential For Insulin-induced Relaxation of Rat Vascular Smooth Muscle Cells." Am J Physiol Cell Physiol: 00125.2006.

5) Graf, C. and J. P. Barras (1979). "Rheological properties of human blood plasma--a comparison of measurements with three different viscometers." Experientia **35**(2): 224-5.

6) Fahraeus, R. and T. Lindqvist (1931). "The viscosity of the blood in narrow capillary tubes." Am J Physiol **96**(3): 562-568

7) Ando, J., Yamamoto, K., (1992) “Vascular Mechanobiology Endothelial Cell Responses to Fluid Shear Stress” Circ J **73**:1983 – 1992

8) Kiani, M. F., A. R. Pries, et al. (1994). "Fluctuations in microvascular blood flow parameters caused by hemodynamic mechanisms." Am J Physiol Heart Circ Physiol **266**(5): H1822-1828.

9) Sarelius, I. H. and J. D. Sinclair (1981). "Effects of small changes of blood volume on oxygen delivery and tissue oxygenation." Am J Physiol Heart Circ Physiol **240**(2): H177-184.

10) Mustafa, S., Rivers, R., et. al. (1999) “Microcirculatory Basis for Nonuniform Flow Delivery with Intravenous Nitroprusside” Anesthesiology **91**:723–31

11) Waugh, R. E. and I. H. Sarelius (1996). "Effects of lost surface area on red blood cells and red blood cell survival in mice." Am J Physiol Cell Physiol **271**(6): C1847-1852.

Chapter VIII

The Effects of Elevated Blood Glucose in the Terminal Arteriolar Networks of the Mouse: Discussion, Conclusions and Directions for Future Research

Clinically, the chronic effects of elevated glucose on the microvasculature present themselves as the symptoms and complications of diabetes. Endothelial dysfunction, microvascular inflammation, and most importantly, vascular rarefaction each is a major contributor to poor perfusion and tissue damage seen in the advanced stages of the diabetic pathophysiology. The origins of these long-term effects are less well understood. In fact, there has been very little research on the earliest stages of elevated glucose and its effects on the microcirculation. Understanding the earliest stages of these complications will give insight as to how to best treat them.

This thesis has produced the most complete description available to date of the effects in the terminal arteriolar networks of acute exposure to elevated glucose. Additionally, it relates the changes at the earliest stages of elevated glucose exposure to the phenotypic changes seen in two leptin compromised models of diabetes, which allows a comparison between the simple case of the acute effect of high glucose, and the more involved/complicated metabolic disorder state, where obesity is examined differently from diabetes in the microcirculation.

In each chapter, we addressed the effects of elevated glucose on a different aspect of the microcirculation in isolation. However, the parts of the microcirculation do not work in isolation, and in fact, the response of each part to elevations in glucose can be affected by the others. Here, we synthesize these pieces to form a whole picture of the responses to elevated glucose within the microcirculation.

Vascular Resistance

Vascular tone, specifically the fourth power of the vascular radius, will dictate vascular resistance and hence is a key regulator of blood flow within the microcirculation. As a result, altered vascular tone regulation not only affects local nutrient delivery in the tissues, but has adverse affects systemically.

In chapter IV, we presented evidence that brief elevations in glucose were sufficient to suppress maximal dilation through both endothelial cell dependent and endothelial cell independent mechanisms. The data suggest that these dilation responses are driven by different mechanisms, and that osmolar effects are not the sole driving force behind suppression of dilation with 2 hours of high glucose exposure. Endothelial cell dependent dilation suppression is demonstrated for both glucose and mannitol over two hours, whereas the endothelial cell independent response is only suppressed with glucose, and not for the osmolar control. Thus, the data suggest that glucose is directly responsible for diminished exogenous NO-mediated dilation via the vascular smooth muscle cells, and indirectly due to excess osmolarity blocking endogenous NO formation via the endothelial cell. The molecular target(s) responsible for these actions were not examined here. This initial project confirmed that endothelial dysfunction, and overall suppressed dilatory capability could be induced by either osmolar increase, or high glucose itself.

The next critical step in understanding glucose induced endothelial cell dysfunction will be to address the mechanisms through which elevations in glucose and elevations of osmolarity act. Key pathway elements to test include: reactive oxygen species effects, calcium metabolism, and myogenic tone. The reactive oxygen pathway is elevated in many inflammatory pathophysiologies, including diabetes and osmotic shock. To test this directly we would examine endothelial cell dependent responses during osmotic shock in the presence of superoxide dismutase plus catalase to block reactive oxygen. There is also some evidence that elevations in osmolarity alone can increase baseline diameters in the skeletal microcirculation through K_{ATP} channels, a response

which is endothelium dependent[1] and may be affected by endothelial dysfunction. Specifically, we could test for a glucose mediated block on guanylyl cyclase or the Ca^{2+} uptake that should be stimulated by cGMP. Finally, an investigation of changes in the myogenic response with elevated glucose would allow us to test the hypothesis that myogenic responsese may be altered in such a way as to compensate for the increase in resistance with hyperglycemia. These experiments would parallel the experiments performed in this study, and would include changes in myogenic responses in normal mice under local acute metabolic changes, and at the myogenic differences between the three strains of animal studied here.

This project demonstrated a likely endothelial dysfunction in the microvasculature of tissues exposed to altered metabolic states. We then turned to an examination of the consequences of this endothelial dysfunction on architecture and rheological parameters. In chapter VI, we examined diameter changes acutely with two hours of glucose treatment and in two murine models of metabolic disease, representing chronic effects of metabolic change. Our data demonstrates that two hours of glucose alone has no effects on total network diameters (Figure 6.2).

In cases where we have full blown metabolic disorders, we see that when compared to metabolically normal C57/bl6 animals, diabetic mice have decreased baseline diameters at all bifurcations except the last branch. Decreased diameters in the diabetic mice will cause an increase in resistance. The decrease in diameter however, is partially offset by the decrease in length of the networks. The end result of which is still an increase in resistance, but the magnitude is not as great as with reduced diameter alone.

Obese mice, on the other hand, have no change in diameter as compared to metabolically normal mice, and longer terminal arteriolar networks, which result in an increase in resistance in the network greater than that of the diabetic animals. For networks with similar viscosity we can use a simplified version of equation 2.2, and the architectural data from chapter VI to get an approximate

idea of the relative resistance in the obese and diabetic networks as compared to the metabolically normal networks.

db/db	ob/ob	C57/bl6
$R = \frac{8\mu L}{\pi r^4}$	$R = \frac{8\mu L}{\pi r^4}$	$R = \frac{8\mu L}{\pi r^4}$
$R_{diabetic} = \frac{206.5}{\left(7.65/2\right)^4} * \frac{8\mu}{\pi}$	$R_{obese} = \frac{761.6}{\left(9.8/2\right)^4} * \frac{8\mu}{\pi}$	$R_{C57/bl6} = \frac{464.9}{\left(10.6/2\right)^4} * \frac{8\mu}{\pi}$
$R_{diabetic} = 0.96 * \frac{8\mu}{\pi}$	$R_{obese} = 1.32 * \frac{8\mu}{\pi}$	$R_{C57/bl6} = 0.82 * \frac{8\mu}{\pi}$

The result is a resistance in the ob/ob animals that is 1.6 times higher in the obese animals and 1.2 times higher in the diabetic animals assuming viscosity is the same in all animals. Higher resistance results in reduced flow through the network.

These two strains therefore, both have increased resistance within the network, by different means, and therefore both strains would likely experience reduced flow and the consequent effects. While these data present the architectural changes that affect resistance in a single network, there may be other compensatory changes that were not measured in this study, including changes to the myogenic response, changes in the number of arteriolar networks present, changes in downstream capillary density, or changes in local blood viscosity.

These results suggest several lines of inquiry that will further our understanding of vascular tone and resistance regulation in metabolic diseases. It is clear that both vascular remodeling and endothelial dysfunction play significant roles, and that both are affected by the presence of an alteration in metabolic conditions.

Flow Heterogeneity and Oxygen supply capacity

The terminal arteriolar networks are designed to distribute blood flow to the capillary networks to provide nutrients to the tissues, especially oxygen. Several modeling studies have postulated that the branching architecture is optimized to achieve that function, therefore a change in delivery of oxygen would be correlated with a change in architecture.

Changes in microvascular form and function are seen clinically in diabetics. We described the effects of elevated levels of glucose on the architecture in chapter VI and flow in chapter VII. The treatment of these two aspects of the microcirculation in isolation however is an artifice as neither works independently. In the section below, we synthesize the results from those two chapters in order to gain further insight into the effects of elevated glucose within this system.

In chapter VI we describe the rarefaction-like architectural changes in that occur in diabetic and obese mice. In both of these animals, increased resistance is a result of architectural changes, but by two different types of remodeling. Diabetic mice have shorter networks, with smaller diameters, and fewer branches, suggesting that they deliver nutrients to a smaller tissue area. Obese mice, on the other hand, have longer networks than the metabolically normal animals with no increase in branch number, indicating that capillary modules fed by those branches may be further spread out. How this affects tissue nutrient delivery is not clear.

In order to better understand how the rarefaction-like architectural changes in the diabetic and obese mice may affect oxygen delivery to the tissues, we did a comparison of theoretical oxygen delivery and a rough estimate of actual oxygen delivery. Using VO_2 max values from the literature, we calculated the ratio of oxygen consumption of metabolically normal to diabetic human patients[2]. We assumed that O_2 delivery was the same in all networks in the body, and scaled each VO_2 max value to the average weight of the respective strain. The result of this calculation estimates that theoretically 2.1 times more oxygen consumption in the metabolically normal animals overall. Using our flux data, we then estimated the oxygen delivery to the network by the

number of red blood cells that enter the network, in order to determine if theoretical oxygen consumption would be mirrored by estimated oxygen delivery in the networks measured. In our studies, each fluorescently labeled cell represents a known fraction of the total number of blood cells as measured by post experiment blood smears. Using this known fraction, we could calculate the number of red cells into each network for each strain. We then calculated the ratio of the total number of red blood cells flowing into the average network for the metabolically normal to diabetic animals. This ratio is 2.51, which indicates that there is 2.51 times more oxygen delivery to the networks of metabolically normal animals than in the diabetic animals. Both the theoretical and experimental ratios indicate that there should be more than twice as much oxygen being handled in each network of the metabolically normal animals as compared to the diabetic animals. Or, restated, that the oxygen usage and delivery by diabetic animals is reduced by half.

A consequence of the results of this rough calculation is the expectation that a compensatory increase in the number or size of networks in the diabetic animals would be observed. Such an increase would increase the total oxygen delivery to the tissue, closer to normal levels. Using additional data, we could then check to see if this supposition was true. Assuming that network length is a viable proxy for network size, we calculated the ratio of network lengths between the metabolically normal and diabetic mice. This would determine if the size of the networks is the compensatory factor. We would expect to see a ratio of network lengths in the metabolically normal animals to the diabetic animals to be equal to 0.4 (e.g. the inverse of 2.5) if the compensating factor is the size of the networks. However, when we calculate that ratio, we find that it is equal to 2.25. It would therefore be expected that there would be an increase in the number of networks in the tissue of the diabetics to compensate for the lower oxygen delivery per network. Rarefaction and diabetics are discussed below.

Flow heterogeneity:

The most critical function of the circulation is to deliver oxygen to the tissues. Oxygen is carried by the red blood cells. Since, the distribution of red blood cells is not equivalent to the distribution of volumetric blood flow, we also measured red blood cell flux in these studies.

We show in chapter VII that the flux distribution in metabolically normal C57/bl6 mice is consistent, and is predominated by a shunting phenomenon where over 50% of the flux into the network is passed out through the last feed continuation bypassing all of the branches. Further, the data shows evidence that the pattern of flux distribution within the network is maintained regardless of the architectural differences between strains. In fact, the only significant change was in the distribution to the feed continuation in the last branch of the diabetic networks, which was higher than the feed continuation in the other two strains. The additional flux however, could be attributed to the db/db animals having fewer branches along the network in those animals.

These results suggest that architectural changes within the terminal arteriolar networks of the obese and diabetic mice may be to maintain flux distribution within the network under changing rheologic conditions. Further evidence of flux maintenance under changing conditions can be seen in the two hour glucose exposure study, where flux distribution was maintained for all treatments, despite an increased variability in both entrance velocity to the network and increased variability in diameters.

These results suggest that flux distribution may be the foremost target of regulation within the terminal arteriolar networks. Since the primary purpose of the circulation is the delivery of oxygen to the capillary networks, this conclusion is a logical one. All of the characteristics of the network are plastic, and are altered as needed to maintain oxygen to the tissue beds as needed.

We have shown that flux distribution is maintained under several different rheological (varied entry velocities) and geometric conditions (varied network lengths and number of branches). What we haven't fully explained yet is how

flux is regulated, ie what determines which cells go down the feed and which cells go down the branch.

Despite our expectations based on a review of the literature, we saw no evidence of a relationship between the curvature at the apical wall and flux distribution. However, it is possible that the ROC measurement used in this study was not a sufficient quantifier of actual wall curvature. Our next step will be to utilize a new method of shape analysis on this data, which will allow us to better characterize and compare the shape of the apical wall at the point of bifurcations. To that end, the video images from this study will be reanalyzed using discriminant analysis techniques to identify significant characters within the wall shape. This data will allow us to compare the curvature at the vessel wall by treatment or strain, but also by flux distribution and shear state furthering our understanding of the fluid dynamics at the point of flow division under normal and pathological conditions. In order to understand this further, we need a systemic approach that isolates factors. To this end both large scale modeling and computer modeling will allow us to alter variables within the network and see which variables are key for flux distribution.

Architectural remodeling and cytokine levels.

Structural (capillary) rarefaction is seen clinically in diabetic patients. Our results also show rarefaction-like architectural changes in diabetic models as compared to the C57/bl6 background genotype. In addition, we show evidence of two distinct phenotypes of rarefaction-like architectural changes in the diabetic and obese mice respectively as discussed above. It is important however, that we make a distinction between actual structural rarefaction, a reduction of the number of capillaries per tissue area, and the rarefaction-like architectural changes we are reporting. Diabetic networks are shorter with fewer branches and obese networks are longer with comparable branch numbers to the metabolically normal mice. These architectural changes are not equivalent to structural rarefaction, but are not unrelated. These measures are taken in the terminal arteriolar networks, which are defined as networks in which each branch

feeds a distinct capillary module. If we assume that in any given tissue bed there are a set number of these networks per tissue area and that there are a set number of capillaries per capillary module, then the length of these networks and the number of branches per network length will be directly proportional to capillary density. As an example, a diabetic network, which is shorter and has fewer branches will deliver oxygen to a smaller number of capillary modules than a normal network that has more branches over a longer network length. (This is in addition to having a smaller RBC flux discussed above.) Similarly, an obese network with a significantly longer length, but the same number of branches as a metabolically normal mouse will have a reduced number of capillary beds over total tissue area than a normal mouse. It follows then, that while we cannot prove or disprove the validity of the two necessary assumptions, the rarefaction-like architectural changes in the diabetic and the obese animals will have a direct effect on the tissue beds that they serve, and with two different phenotypes. These distinct phenotypes indicate that rarefaction is not caused by a single pathology, and may have several mechanisms leading to reduced vascularization per tissue area.

Cytokine expression data presented in chapter V supports the idea that more than one mechanism of action is leading to the rarefaction-like changes seen. Most importantly, the diabetic and obese animals have differential systemic plasma levels of VEGF, with lower levels in diabetic animals and increased levels in obese animals. VEGF is a key mediator of angiogensis, without it, angiogenesis cannot occur. The same pattern of expression is seen with IL-6, which enhances VEGF production. This indicates that angiogenesis may be impaired in the diabetic animal population especially as compared with the obese.

If we focus on the diabetic animals, we have an animal model with attenuated plasma levels of other angiogenic cytokines as well (IL-1β, GM-CSF). These cytokines support migration and proliferation of both endothelial cells and smooth muscle cells. Angiogenesis is critical for both the growth of new blood vessels and the maintenance of vascular networks. If a key angiogenic cytokine

(VEGF) is limited, and many of the supporting cytokines are also reduced, then vascular maintenance, in specific, capillary sprouting, would be severely handicapped, and loss of vessels over time may be a result. Insufficient angiogenic cytokines suggest that impaired angiogenesis may be the cause for the rarefaction-like architectural changes seen in the diabetic animals.

Additionally, the attenuated expression of angiogenic cytokines suggests a possible trigger for the rarefaction-like architectural changes as well. Brown and Hudlicka[1] have shown that VEGF expression is mediated at least in part by shear stress within the network. We show in chapter V that shear rate gradients are suppressed in the diabetic animal model, which would indicate an initial stimulus that could lead to decreased VEGF levels. In fact, lack of shear signal has been shown to be an early signal for apoptosis as well, which may amplify the loss of VEGF signal.

The mechanism behind the distinct phenotype of rarefaction-like architectural changes seen in the obese animal is not as clear. Plasma levels of pro-angiogenic cytokine levels overall are enhanced in the obese animals. Enhanced VEGF expression would support the hypothesis of enhanced angiogenesis and support for vascular remodeling, which may be in effect, resulting in the extremely long network lengths within the tissue as compared to the C57 animals. Despite the added length to the network however, obese animals have no additional branches. The phenotype is distinct from the diabetic animals, which may be attributable to blood glucose levels, which are distinctly higher in the diabetic mouse than in the obese mouse.

Further work into the mechanism behind diabetic rarefaction is suggested by these results. One of the key studies indicated both by these results and by the oxygen supply capacity discussion above, is a true study of capillary rarefaction, wherein the capillary density per tissue area is measured for all three strains. Additionally, relating capillary density to terminal arteriolar network density is a key step in fully understanding the results presented here. Measures of terminal arteriolar networks per tissue area, as well as capillaries per terminal

arteriolar branch will allow the impact of the rarefaction-like architectural changes reported here on tissue nutrient delivery to be better understood.

In order to determine the temporal development of the rarefaction pathology better a comparison over the development of the disease would also be informative. In these studies, the comparison of the normo-glycemic C57/bl6 mouse to the diabetic and obese models, while informative, does not allow a direct comparison of a single network before and after diabetic levels of hyperglycemia. Though we are seeing a smaller number of branches within the diabetic animals as compared to the C57/bl6, we cannot definitively say whether the branches are lost in the diabetic or are never formed. Since our results implicate a loss of angiogenic function, it is more likely to be a lack of de novo formation. Using a diabetic mouse model, a measurement of network density and complexity (ie number of branches, length, etc.) at several age points would allow the development of rarefaction to be quantified. Additionally, blood glucose values at age point would further the understanding of how glucose plays a role. Since the diabetic mouse model does not develop the diabetic phenotype until 4 or 5 weeks of age, the change in vascularization as the disease develops could be addressed. Simultaneously, assays of angiogenesis and apoptosis could be performed to further distinguish between angiogenic changes and apoptotic changes within the tissues.

Shear Stress regulation

Shear stress is important for cell survival, as discussed in chapter VII. In addition to a lack of shear signal inducing apoptosis, mechanotransduction of shear stress is one of the primary regulatory mechanisms of blood flow within the microcirculation. How the shear signal is tranduced is still a subject of intense debate, but there is a general consensus that the sensor is along the walls of the vessels somewhere in the arteriolar networks. Both of these factors make an understanding of shear stress in the terminal arteriolar networks important.

Our results demonstrate that in metabolically normal mice, the wall shear rate within the networks has a regular pattern of gradients independent of branch

angle or diameters. Additionally, our results suggest that with as little as two hours of hyperglycemia, maintenance of normal patterns of shear rate gradients is altered. Additionally, in both metabolic models of diabetes, we demonstrate that shear gradients within the terminal arteriolar networks are suppressed. Changes to the locations or magnitude of the shear signal at the sensor such as these, may adversely affect the ability of the network to sense the shear and therefore regulate blood flow as a result.

The nature of the mechanotransducer is unknown, however, we have shown in chapter IV that as little as two hours of elevated glucose (and/or osmolarity) exposure can induce endothelial dysfunction, potentially disrupting the sensor along the walls. However, these responses were tested at only one location within the networks. Testing these responses at each bifurcation along the network may elucidate a location of highest sensitivity of the endothelium to metabolic changes within the network.

The development of the shear gradient within the network merits further ex vivo investigation. Many studies have shown, both in vivo and ex vivo, that shear stress is essential for vascular responses such as angiogenesis. But it's always been a constant or a pulsatile stress, there have been no studies that investigate shear gradients along the walls on the cellular length-scale. If indeed the dysregulation in shear gradients we are seeing here are causing a mechanosensory failure, then we need to see if we can recreate that in a system where we have control, such as an explanted vessel, a computer model, or in a large scale model.

Global hypothesis for future work

From these results we can postulate a theory that ties together loss of arteriolar network function. First, glucose causes a suppression of shear signal to the intermediate branches in the terminal arteriolar networks. Loss of the shear signal causes a failure of the mechanotransduction mechanism that

regulates flow. A reduction of perfusion, leads to diminished angiogenesis and increased apoptosis. The diameters of affected branches are first reduced, and then lost completely. The complete loss of any branch will reduce total branch number. A combination of increased resistance and altered shearing forces together promotes rarefaction. There are several aspects of this theory that remain to be directly demonstrated, but this is a theoretical framework for the mechanisms by which the microvascular networks are adversely affected in the skeletal muscle tissues of diabetics which will allow us to formulate future hypotheses. We have, for the first time put together all of the elements of the arteriolar network structure and function to describe the early effects of elevated blood glucose on the pathophysiology of diabetes within this system.

References Cited

1. Massett, M., Koller, A., et. al. (2000) “Hyperosmolality dilates rat skeletal muscle arterioles: role of endothelial K(ATP) channels and daily exercise.” Journal of Applied Physiology **89**(6):2227-2234.
2. Rabøl, R., Larsen, S., et. al. (2010) “Regional Anatomic Differences in Skeletal Muscle Mitochondrial Respiration in Type 2 Diabetes and Obesity.” Journal of Endocrinology and Metabolism **95**(2):857-863.

Bibliography

Abularrage, C. J., A. N. Sidawy, et al. (2005). "Evaluation of the microcirculation in vascular disease." Journal of Vascular Surgery **42**(3): 574-581.

Ahmed, N. (2005). "Advanced glycation endproducts-role in pathology of diabetic complications." Diabetes Research and Clinical Practice **67**: 3-21.

Ahmed, N. and P. J. Thornalley (2003). "Quantitative screening of protein biomarkers of early glycation, advanced glycation, oxidation and nitrosation in cellular and extracellular proteins by tandem mass spectrometry multiple reaction monitoring." Biochemical Society Transactions **31**(6): 1417-1422.

American Diabetes Assn. (2006). "Diagnosis and Classification of Diabetes Mellitus." Diabetes Care **29**(suppl_1): S43-48

Ando, J., Yamamoto, K., (1992) “Vascular Mechanobiology Endothelial Cell Responses to Fluid Shear Stress” Circ J **73**:1983 – 1992

Angelini, D., Hyun, S-W., et. al. (2006) “TNF-α increases tyrosine phosphorylation of vascular endothelial cadherin and opens the paracellular pathway through fyn activation in human lung endothelia.” Am J Physiol Lung Cell Mol Physiol **291**:1232-1245

Anis, Y., Leshem, O., et al. (2004). “Antidiabetic effect of novel modulating peptides of G-protein-coupled kinase in experimental models of diabetes.” Diabetologia, **47**:1232-1244

Aussedat, B., M. Dupire-Angel, et al. (2000). "Interstitial glucose concentration and glycemia: implications for continuous subcutaneous glucose monitoring." Am J Physiol Endocrinol Metab **278**(4): E716-728.

Avendano, G. F., R. K. Agarwal, et al. (1999). "Effects of glucose intolerance on myocardial function and collagen-linked glycation." Diabetes **48**(7): 1443-1447.

Baez, S. (1973). "An open cremaster muscle preparation for the study of blood vessels by in vivo microscopy." Microvascular Research **5**(3): 384-94.

Bagi, Z., Koller, A., et. al. (2003) “Superoxide-NO interaction decreases flow- and agonist-induced dilations of coronary arterioles in Type 2 diabetes mellitus.” Am JPhysiol Heart Circ Physiol **285**: H1404–H1410

Bandsma, R., Grefhorst, A., et. al. (2004). “Enhanced glucose cycling and suppressed de novo synthesis of glucose-6-phosphate result in a net unchanged hepatic glucose output in ob/ob mice.” Diabetologia, **47**:2022-2031.

Banks, A., Davis, S., et. al. “Activation of Downstream Signals by the Long Form of the Leptin Receptor.” (2000) **275**(19):14563-14572.

Beisswenger, P. J., B. S. Szwergold, et al. (2001). "Glycated Proteins in Diabetes." Clinics in Laboratory Medicine **21**(1): 53 - 78.

Belcaro, G., S. Vasdekis, et al. (1989). "Evaluation of skin blood flow and venoarteriolar response in patients with diabetes and peripheral vascular disease by laser Doppler flowmetry." Angiology **40**(11): 953-7.

Berne, Robert M., Matthew N. Levy, Bruce M. Koeppen, and Bruce A. Stanton. Berne & Levy Physiology. Philadelphia, PA: Mosby/Elsevier, 2008. Print.

Bjursell, M., Gerdin, A-K., et al. (2006). “Melanin-Concentrating Hormone Receptor 1 deficiency increases insulin sensitivity in obese leptin-deficient mice without affecting body weight.” Diabetes **55**:725-733.

Bohlen, H., Niggl, B., (1979) “Adult microvascular disturbances as a result of juvenile onset diabetes in Db/Db mice.” Blood Vessels.**16**(5):269-76.

Boutati, E., and Raptis, S., (2009) “Self-Monitoring of Blood Glucose as Part of the Integral Care of Type 2 Diabetes” Diabetes Care **32**(Supp 1):S205-S210

Brun, P., Castagliuolo, I., et al. (2007). “Increased intestinal permeability in obese mice: New evidence in the pathogenesis of nonalcoholic steatohepatitis.” Am J Physiol Gastrointest Liver Physiol, **292**:G518-G525.

Bugliarello, G., G.C.C. Hsiao (1964). “Phase separation in suspensions flowing through bifurcations: A simplified hemodynamic model.” Science **143**(3605): 469-471.

Buus, C. L., F. Pourageaud, et al. (2001). "Smooth Muscle Cell Changes During Flow-Related Remodeling of Rat Mesenteric Resistance Arteries." Circ Res **89**(2): 180-186.

Calderan, L., Marzola, P., et al. (2006). “In vivo phenotyping of the ob/ob mouse by magnetic resonance imaging and 1H-magnetic resonance spectroscopy.” Obesity **14**:405-414.

Carley, A., Semeniuk, L., et al. (2004). “Treatment of type 2 diabetic db/db mice with a novel PPARγ agonist improves cardiac metabolism but not contractile function.” Am J Physiol Endocrinol Metab, **286**:E449-E455.

Carmeliet, P., (2003) “Angiogenesis in health and disease.” Nature Medicine **9**(6):653-660.

Carmeliet, P., Collen, D., (1997) “Molecular analysis of blood vessel formation and disease.” Am. J. Physio. Heart Circ. Physiol. **273**:2091-2104.

Centers for Disease Control and Prevention. (2007) “National diabetes fact sheet: general information and national estimates on diabetes in the United States.” Atlanta, GA: U.S. Department of Health and Human Services, Centers for Disease Control and Prevention.

Chia, S., Qadan, M., et. al. (2003) “Intra-Arterial Tumor Necrosis Factor- Impairs Endothelium-Dependent Vasodilatation and Stimulates Local Tissue Plasminogen Activator Release in Humans.” Arterioscler Thromb Vasc Biol. **23**:695-701.

Cohen, K., and Berg, B. et. al. (2000). “Remote arteriolar dilations in response to muscle contraction under capillaries.” Am J Physiol Heart Circ Physiol **278**(6): H1916-1923.

Cohen, K., and Sarelius, I. (2002). “Muscle contraction under capillaries in hamster muscle induces arteriolar dilatation via K(ATP) channels and nitric oxide.” J. Physiol. **539**(Pt. 2): 547-555.

Conway, E., Collen, D., et. al. (2001) “Molecular mechanisms of blood vessel growth.” Cardiovascular Research **49**:507-521.

Courtice, F. C. (1943). "The blood volume of normal animals." J Physiol **102**: 290-3-5.

Cszizar, A., and Ungvari, Z. (2008) “Endothelial dysfunction and vascular inflammation in Type 2 diabetes: interaction of AGE/RAGE and TNF- signaling.” Am J Physiol Heart Circ. Physiol. **295**: 475-476.

Curfs, J., Meis, J., (1997) “A Primer on Cytokines: Sources, Receptors, Effects and Inducers.” Clinical Microbiology Reviews **10**(4):742-780.

Dandona, P., (2002) “Endothelium, Inflammation and Disease” Current Diabetes Reports. **2**:311-315.

Davies, M., Lund, R., (2005) “Low Turnover Osteodystrophy and Vascular Calcification are Amenable to Skeletal Anabolism in an Animal Model of Chronic Kidney Disease and the Metabolic Syndrome” Journal of the American Society of Nephrology **16**(4):917-928

Davies, P., Tripathi, S., (1993) “Mechanical Stress Mechanisms and the Cell: An Endothelial Paradigm” Circulation Research **72**:239-245.

Davis, J., Wu, X., et. al. (2001) “Integrins and mechanotransduction of the vascular myogenic response.” Am J Physiol Heart Circ Physiol **280**: H1427–H1433

De Backer, D., J. Creteur, et al. (2002). "Microvascular Blood Flow Is Altered in Patients with Sepsis." Am. J. Respir. Crit. Care Med. **166**(1): 98-104.

del Carmen Garcia, M., Casanueava, F., et. al. (2000) “Gestational Profile of Leptin Messenger Ribonucleic Acid (mRNA) Content in the Placenta and Adipose Tissue in the Rat, and Regulation of the mRNA Levels of the Leptin Receptor Subtypes in the Hypothalamus During Pregnancy and Lactation.” Biology of Reproduction **62**: 698-703.

del Rey, A., Besedovsky, H. (1989). “Antidiabetic effects of interleukin 1.” PNAS **86**:5943-5947.

Esposito, K., Nappo, F., et. al. (2002) “Inflammatory Cytokine Concentrations Are Acutely Increased by Hyperglycemia in Humans.” Circulation **106**: 2067-2072.

Fahraeus, R. and T. Lindqvist (1931). "The viscosity of the blood in narrow capillary tubes." Am J Physiol **96**(3): 562-568

Fang, Y., Shen, J., (2009) “Granulocyte-macrophage colony-stimulating factor enhances wound healing in diabetes via upregulation of proinflammatory cytokines.” British Journal of Dermatology Epub ahead of print

Feihl,F., Liaudet, L., et. al. (2006)” Hypertension: A Disease of the Microcirculation?” Hypertension **48**:1012-1017

Feng, X., Clark, R., et. al. (1999) “Fibrin and collagen differentially regulate human dermal microvascular endothelial cell integrins: Stabilization of αv/β3 mRNA by Fibrin.” J. Invest. Derm. **113**: 913-919.

Ferrara, N. (2001). “Role of vascular endothelial growth factor in regulation of physiological angiogenesis.” Am J Physiol Cell Physiol **280**: C1358-C1366.

Ferrara, N., T. Davis-Smyth. (1997). “The Biology of Vascular Endothelial Growth Factor.” Endocrine Reviews **18**(1): 4-25.

Ferrera. N., Gerber, H., et. al. (2003) “The biology of VEGF and its receptors.” Nature Medicine **9**(6):669-676.

Fisman, E., Motro, M., et. al. (2003) “Cardiovascular diabetology in the core of a novel interleukins classification: the bad, the good and the aloof.” Cardiovascular Diabetology **12**:2-11.

Fox, R., McDonald, A., et. al. (2004) Introduction to Fluid Mechanics John Wiley and Sons Inc. USA

Frame, M., and Sarelius, I. (1995). “L-arginine-induced conducted signals alter upstream arteriolar responsivity to L-arginine.” Circ. Res. **77**(4): 695-701

Frame, M., Rivers R., et. al. (2007) “Mechanisms initiating integrin-stimulated flow recruitment in arteriolar networks.” J Appl Physiol. **102**(6):2279-87.

Frame, M., and Sarelius, I., (1993) “Regulation of capillary perfusion by small arterioles is spatially organized.” Circulation Research **73**(1):155-163

Frame, M., and Sarelius, I, (1993). “Arteriolar bifurcation angles vary with position and when flow is changed.” Microvasc Res **46**(2): 190-205.

Frisbee, J.C. (2003). “Remodeling of the skeletal muscle microcirculation increases resistance to perfusion in obese Zucker rats.” Am J Physiol Heart Circ Physiol **285**:104-111.

Frisbee, J.C. (2005). “Hypertension-independent microvascular rarefaction in the obese Zucker rat model of the metabolic syndrome.” Microcirculation **12**(5): 383-392.

Furchgott, R., (1983) “Role of endothelium in responses of vascular smooth muscle.” Circulation Research **53**(5):557-573.

Gao X., Zhang, H., et. al. (2008) “AGE/RAGE produces endothelial dysfunction in coronary arterioles in Type 2 diabetic mice.” Am J Physiol Heart Circ Physiol **295:** H491–H498.

Georgi, M., Dewar, A., et. al. (2010) “Downstream Exposure to Growth Factors Causes Elevated Velocity and Dilation in Arteriolar Networks.” Journal of Vascular Research In Press

Geraldes, P., and King, G., (2010) “Activation of Protein Kinase C Isoforms and Its Impact on Diabetic Complications.” Circulation Research **106**:1319-1331.

Giardino, I., D. Edelstein, et al. (1996). "BCL-2 Expression or Antioxidants Prevent Hyperglycemia-induced Formation of Intracellular Advanced Glycation Endproducts in Bovine Endothelial Cells." J. Clin. Invest. **97**(6): 1422-1428.

Goldin, A., Beckman, J., et. al. (2006). “Advanced Glycation End Products Sparking the Development of Diabetic Vascular Injury.” Circulation **114**: 597-605.

Gomes, M., Affonso, F., et. al.(2004) “Glucose levels observed in daily clinical practice induce endothelial dysfunction in the rabbit macro- and microcirculation.” Fundamental and Clinical Pharmacology **18**(3): 339-346

Graf, C. and J. P. Barras (1979). "Rheological properties of human blood plasma--a comparison of measurements with three different viscometers." Experientia **35**(2): 224-5.

Grefhorst, A., van Dijk, T., et al. (2005). “Differential effects of pharmacological liver X receptor activation on hepatic and peripheral insulin sensitivity in lean and ob/ob mice.” Am J Physiol Endocrinol Metab **289**:829-838.

Guo, X., Lin, W., et. al. (2000) “High glucose impairs endothelium-dependent relaxation in rabbit aorta.” Acta Pharmacol Sin **21**(2):169-73

Hafstad, A. D., Solevåg, G. H., et. al.(2006) “Perfused hearts from 2 Type1 diabetic (db/db) mice show metabolic responsiveness.to insulin.” Am J Physiol Heart Circ Physiol, **290:** H1763-H1769.

Hinghofer-Szalkay, H., J.E. Greenleaf. (1987). “Continuous monitoring of blood volume changes in humans.” J App Phys **63**(3): 1003-1007.

Hoffman, S., Dong, H., et. al. (2002) “Improved Insulin Sensitivity Is Associated With Restricted Intake of Dietary Glycoxidation Products in the db/db Mouse.” Diabetes **51**: 2082-2089.

Höppener, J., Oosterwijk, C., et al. (1999) “Extensive islet amyloid formation is induced by development of Type II diabetes mellitus and contributes to its progression: Pathogenesis of diabetes in a mouse model.” Diabetologia **42**:427-434.

Howarth, A., Wiehler, W., (2006) “A Nonthiazolidinedione Peroxisome Proliferator-Activated Receptor γ Agonist Reverses Endothelial Dysfunction in Diabetic (db/db-/-) Mice” The Journal of Pharmacology and Experimental Therapeutics **316**(1):364-370.

Hruz, P., and Mueckler, M., (2001) "Structural Analysis of the Glut1 facilitative glucose transporter." Mol. Membr. Biol. **18**(3) :183-193.

Hudlicka, O., M. Brown, et al. (1992). “Angiogenesis in Skeletal and Cardiac Muscle.” Physiological Reviews **72(**2): 369-417.

Igel, M., Becker, W., et. al. (1997) “Hyperleptinemia, leptin resistance, and polymorphic leptin receptor in the New Zealand obese mouse.” Endocrinology **138:**4234-4239.

Igel, M., Lindenthal, B., et. al. (2002). “Evidence that leptin contributes to intestinal cholesterol absorption in obese (ob/ob) mice and wild-type mice.” Lipids **37:**153-157.

Jakus, V. and N. Rietbrock (2004). "Advanced Glycation End-Products and the Progress of Diabetic Vascular Complications." Physiological Research **53**(2): 131-142.

Jalili, S., Pozo, M., et. al. (2001) Integrin-mediated mechanotransduction requires its dynamic interaction with specific extracellular matrix (ECM) ligands.” PNAS **98**(3):1042-1046.

Jin ZG, Ueba H, Tanimoto T, Lungu AO, Frame MD, Berk BC. Ligand-independent activation of vascular endothelial growth factor receptor 2 by fluid shear stress regulates activation of endothelial nitric oxide synthase. Circ.Res. 2003; **93:** 354-63.

Jin, Z., Ueba, H, et. al. (2003) “Ligand-independent activation of vascular endothelial growth factor receptor 2 by fluid shear stress regulates activation of endothelial nitric oxide synthase.” Circ Res. **93**(4):354-63

Jones, S., Girod, W., et. al. (1999). “Reperfusion injury is not affected by blockade of P-selectin in the diabetic mouse heart.” Am J Physiol Heart Circ Physiol **277**:763-769.

Junger, M., Steins, A., et. al. “Microcirculatory Dysfunction in Chronic Venous Insufficiency (CVI)” Microcirculation 76(6)S3-S12 2000.

Kaiser, D., Freyberg., M., et. al. (1997) “Integrin-mediated mechanotransduction requires its dynamic interaction with specific extracellular matrix (ECM) ligands.” Biochemical And Biophysical Research Communications. **231**: 586–590

Késmárky, G., P. Kenyeres, et. al. (2008). “Plasma viscosity: A forgotten variable” Clinical Hemorheology and Microcirculation **39**(1-4): 243-246.

Kharitonenkov, A., Shiyanona, T., et al. (2005). “FGF-21 as a novel metabolic regulator.” The Journal of Clinical Investigation **115:**1627-1635.

Kiani, M. F., A. R. Pries, et al. (1994). "Fluctuations in microvascular blood flow parameters caused by hemodynamic mechanisms." Am J Physiol Heart Circ Physiol **266**(5): H1822-1828

Kocis, E., Pacher, P., (2000) “Hyperglycaemia alters the endothelium-dependent relaxation of canine coronary arteries.” Acta Physiol Scand. **169**(3): 183-7.

Koller, A. and G. Kaley (1991). "Endothelial regulation of wall shear stress and blood flow in skeletal muscle microcirculation." Am J Physiol Heart Circ Physiol **260**(3): H862-868.

Koya, D., Haneda, M., et. al. (2000) “Amelioration of accelerated diabetic mesangial expansion by treatment with a PKCβ inhibitor in diabetic db/db mice, a rodent model for type 2 diabetes.” FASEB J. **14**:439-447.

Krogh, A. (1919). “The number and distribution of capillaries in muscles with calculations of the oxygen pressure head necessary for supplying the tissue.” J Physiol **52**(6): 409-415.

Kulcu, E., J. A. Tamada, et al. (2003). "Physiological Differences Between Interstitial Glucose and Blood Glucose Measured in Human Subjects." Diabetes Care **26**(8): 2405-2409.

Laine, H., Knuuti, J., et. al. (1998) “Preserved Relative Dispersion but Blunted Stimulation of Mean Flow, Absolute Dispersion, and Blood Volume by Insulin in Skeletal Muscle of Patients With Essential Hypertension” Circulation **97**:2146-2153

Lash, J., Bohlen, G., (1991) “Structural and functional origins of suppressed acetylcholine vasodilation in diabetic rat intestinal arterioles.” Circulation Research 69:1259-1268

Lee, J. H. and L. Ragolia (2006). "AKT Phosphorylation Is Essential For Insulin-induced Relaxation of Rat Vascular Smooth Muscle Cells." Am J Physiol Cell Physiol:

Liu, Y., Connoley, I., et. al. (2005). “Effects of the cannabinoid CB1 receptor antagonist SR141716 on oxygen consumption and soleus muscle glucose uptake in Lepob/Lepob mice.” International Journal of Obesity **29**:183-187.

Marfella, R., Quagliaro, L., et. al. (2001) “Acute Hyperglycemia induces an oxidative stress in healthy subjects.” The Journal of Clinical Investigation **108**(4):635-636.

Marin, P., B. Andersson, et al. (1994). "Muscle fiber composition and capillary density in women and men with NIDDM." Diabetes Care **17**(5): 382-386.

Mark, A., Shaffer, R., et. al. (1999) “Contrasting blood pressure effects of obesity in leptin-deficient ob/ob mice and agouti yellow obese mice” J. Hypertension **17**:1949-1953.

Martin, A., M.R. Komada, et al. (2003). “Abnormal angiogenesis in Diabetes Mellitus.” Medicinal Research Reviews **23**(2): 117-145.

Massett, M., Michael, P., et. al. (2000) “Hyperosmolality dilates rat skeletal muscle arterioles: role of endothelial KATP channels and daily exercise.” J Appl Physiol **89**: 2227–2234

Matarese, G., Di Giacomo, A., et al. (2001). “Requirement for leptin in the induction and progression of autoimmune encephalomyelitis.” The Journal of Immunology **166**: 5909-5916.

Mathieu-Costello, O., A. Kong, et al. (2003). "Regulation of skeletal muscle morphology in type 2 diabetic subjects by troglitazone and metformin: Relationship to glucose disposal." Metabolism **52**(5): 540.

McDonald, D., Coleman, G. et. al. (2009). Advanced glycation of the Arg-Gly-Asp (RGD) tripeptide motif modulates retinal microvascular endothelial cell dysfunction.” Molecular Vision **15**:1509-1520.

Meredith, J., Fazeli, B., et. al. “The Extracellular Matrix as a Cell Survival Factor.” Molecular Biology of the Cell **4**: 953-961.

Michiels, C., (2003) “Endothelial Cell Functions.” Journal of Cellular Physiology **196**:430–443

Miller, B., Gattone, V., et. al. (1986) “Morphological Evaluation of Vascular Smooth Muscle Cell: Length and Width From a Single Scanning Electron Micrograph of Microvessels.” The Anatomical record **216**: 95-103.

Moberg, E., E. Hagström-Toft, et al. (1997). "Protracted glucose fall in subcutaneous adipose tissue and skeletal muscle compared with blood during insulin-induced hypoglycaemia." Diabetologia **40**(11): 1320.

Mustafa, S., Rivers, R., et. al. (1999) “Microcirculatory Basis for Nonuniform Flow Delivery with Intravenous Nitroprusside” Anesthesiology **91**:723–31

Noren, D., H. J. Palmer, et al. (2000). "Predicted wall shear rate gradients in T-type arteriolar bifurcations." Biorheology **37**(5-6): 325-40.

Oakes, N. D., Thalén, P., et. al.(2006).”Cardiac metabolism in mice: Tracer method developments and in vivo application revealing profound metabolic inflexibility in diabetes.” Am J Physiol Endocrinol Metab, **290**: 870-881.

Park, Y., Capobianco, S, et. al. (2008) “Role of EDHF in type 2 diabetes-induced endothelial dysfunction.” Am J Physiol Heart Circ Physiol **295**: H1982–H1988

Patel, S., Garry, M., et. al. “Leptin: Linking Obesity, the Metabolic Syndrome, and Cardiovascular Disease.” Current Hypertension Reports. **10**:131-137.

Picchi A., Gao, X., et. al. (2006) “Tumor necrosis factor-alpha induces endothelial dysfunction in the prediabetic metabolic syndrome.” Circulation Research **99**:69-77

Pohl, U., DeWit, C., et. al. (2000) “Large arterioles in the control of blood flow: role of endothelium-dependent dilation.” Acta Physiol Scand, **168**: 505-510

Pries, A., Secomb., et. al. (1994) “Resistance to blood flow in microvessels in vivo” Circ. Res.**75**;904-915

Pries, A., B. Reglin, et al. (2001). “Structural adaptation of microvascular networks: functional roles of adaptive responses.” Am J Physiol Heart Circ Physiol **281**: H1015-H1025.

Pries, A., K. Ley, et al. (1989). “Red Cell Distribution at Microvascular Bifurcations.” Microvascular Research **38**:81-101.

Priestman, D., van der Spoel, A., et. al. (2008). “N-butyldeoxynojirimycin causes weight loss as a results of appetite suppression in lean and obese mice.” Diabetes, Obesity and Metabolism **10:**159-166.

Prior, B.M., H.T. Yang, et al. (2004). “What makes vessels grow with exercise training?” J Appl Physiol **97**: 1119-1128.

Pugh, C., Ratcliffe, P., (2003) “Regulation of angiogenesis by hypoxia: Role of the HIF system.” Nature Medicine **9**(6):677-684.

Qian, L., Wang, H., et. al. (2006) ” Interleukin-2 protects against endothelial dysfunction induced by high glucose levels in rats.” Vascular Pharmacology **45**: 374-382.

Rabøl, R., Larsen, S., et. al. (2010) “Regional Anatomic Differences in Skeletal Muscle Mitochondrial Respiration in Type 2 Diabetes and Obesity.” Journal of Endocrinology and Metabolism 95(2):857-863.

Rafael, J., Herling, A. (2000). “Leptin effect in ob/ob mice under thermoneutral conditions depends not necessarily on central satiation.” Am J Physiol Regulatory Integrative Comp Physiol, **278**:R790-R795.

Rajavashisth, T., Andalibi, A., et. al. (1990) “Induction of endothelial cell expression of granulocyte and macrophage colony-stimulating factors by modified low-density lipoproteins.” Nature **344**:254-257

Rana, S. (2007). Short Term Exposure to High Glucose Has Multiple Adverse Effects on Wound Provisional Matrix Molecules and a Bioengineered Matrix. Biomedical Engineering. Stony Brook, NY, University of Stony Brook. **Doctor of Philosophy:** 138.

Rapoport, S. (1998) “Osmotic Opening of the Blood–Brain Barrier: Principles, Mechanism, and Therapeutic Applications.” Cellular and Molecular Neurobiology **20**(2): 217-230.

Rask-Madsen, C. and G. L. King (2007). "Mechanisms of Disease: endothelial dysfunction in insulin resistance and diabetes." Nature Clinical Practice Endocrinology and Metabolism **3**(1): 46-56.

Re, F., Zanetti, A., (1994) “Inhibition of Anchorage-dependent Cell Spreading Triggers Apoptosis in Cultured Human Endothelial Cells.” The Journal of Cell Biology **127**(2):537-546

Renard, E. (2005). "Monitoring glycemic control: the importance of self-monitoring of blood glucose." The American Journal of Medicine **118**(9, Supplement 1): 12-19.

Roche, H., Noone, E., et al. (2002). “Isomer-dependent metabolic effects of conjugated linoleic acid.” Diabetes **51:**2037-2044.

Rodgers, K., Ellefson, D., et. al. (2006). “Expression of intracellular filament, collagen, and collagenase genes in diabetic and normal skin after injury.” Wound Rep Reg, **14**(298-305).

Rodriguez, C., Miyake, Y., et al. (2005). “Relation of plasma glucose and endothelial function in a population-based multiethnic sample of subjects without diabetes mellitus.” Am J. Cardiol. **96**(9): 1273-1277

Rodriguez, C., Miyake, Y., et al. (2005). “Relation of plasma glucose and endothelial function in a population-based multiethnic sample of subjects without diabetes mellitus.” Am J. Cardiol. **96**(9): 1273-1277

Rossitti, S. and J. Lofgren (1993). "Vascular dimensions of the cerebral arteries follow the principle of minimum work." Stroke **24**(3): 371-377.

Roudier, E., N. Chapados, et al. (2009). “Angiomotin p80/p130 ratio: a new indicator of exercise-induced angiogenic activity in skeletal muscles from obese and non-obese rats?” J Physiol **587**(16): 4105-4119.

Rubanyi, G., Romero, J.C., et. al. (1986) “Flow induced release of endothelium-derived relaxing factor” Am. J. Physiol. Heart Circ. Physiol. **250**(6):H1145-H1149

Sarelius, I., and Duling, B., (1982). "Direct measurement of microvessel hematocrit, red cell flux, velocity, and transit time." Am J Physiol Heart Circ Physiol **243**(6): H1018-1026.

Sarelius, I., and Sinclair, J., (1981). "Effects of small changes of blood volume on oxygen delivery and tissue oxygenation." Am J Physiol Heart Circ Physiol **240**(2): H177-184.

Schaefer, C., Biermann, T., et. al. (2009). “Early Microvascular Complications of prediabetes in mice with impaired glucose tolerance and dyslipidemia.” Acta Diabetol. (Epub ahead of print)

Schafer A, and Bauersachs J.(2008) “Endothelial dysfunction, impaired endogenous platelet inhibition and platelet activation in diabetes and atherosclerosis.” Curr. Vasc. Pharm. **6**:52-60.

Schneider, J. G., Finck, B. N., et. al. (2006). “ATM-dependent suppression of stress signaling reduces vascular disease in metabolic syndrome.” Cell Metabolism **4**: 377-389.

Secomb, T. W., R. Hsu, et al. (2001). "Effect of the endothelial surface layer on transmission of fluid shear stress to endothelial cells." Biorheology **38**: 143 - 150.

Segal, S. S. (2005). "Regulation of Blood Flow in the Microcirculation." Microcirculation **12**: 33-45.

Shyy, J., Chien, S., (2002) “Role of Integrins in Endothelial Mechanosensing of Shear Stress.” Circ. Res. **91**:769-775

Sokol, R. and Rohlf, J. (1994) Biometry: The Principles and Practices of Statistics in Biological Research Third Edition. W.H.Freeman pub.

Stenina, O., (2005) “Regulation of Vascular Genes by Glucose”, Current Pharmaceutical Design. **11**:2367-2381

Su, J., Lucchesi, P., et. al. (2008) “Role of advanced glycation end products with oxidative stress in resistance artery dysfunction in type 2 diabetic mice.” Arterioscler Thromb Vasc Biol. **28**(8):1432-8

Su, Y., Liu, X., et. al. (2008). “The relationship between endothelial dysfunction and oxidative stress in diabetes and prediabetes.” Int. J. Clin. Pract. **62**(6): 877-882.

Sweeney, T., and Sarelius, I. (1989). “Arteriolar control of capillary cell flow in striated muscle.” Circ. Res. **64**(1): 112-120.

Takahashi, M., Berk, B., (1996) “Mitogen-activated Protein Kinase (ERK1/2) Activation by Shear Stress and Adhesion in Endothelial Cells Essential Role for a Herbimycin-sensitive Kinase” J. Clin. Invest. **98**:2623–2631

Takahashi, N., Waelput, W., et. al. (1999). ”Leptin is an endogenous protective protein against the toxicity exerted by Tumor Necrosis Factor.” J Exp Med, **189**:207-212.

Tanaka, K., Kawano, T., et al (2009) “Mechanisms of Impaired Glucose Tolerance and Insulin Secretion during Isoflurane Anesthesia” Anesthesiology **111**:1044-1051

Tang, M., W. Zhang, et al. (2007). " Molecular and Cellular Biochemistry High glucose promotes the production of collagen types I and III by cardiac fibroblasts through a pathway dependent on extracellular-signal-regulated kinase 1/2." Molecular and Cellular Biochemistry **301**(1-2): 109-114.

Tarzi, R., Cook, H, et. al. (2004). “Leptin-deficient mice are protected from accelerated nephrotoxic nephritis.” Am J Pathology **164**:385-390.

Tesfamariam, B., Cohen, R., (1992) “Free radicals mediate endothelial cell dysfunction caused by elevated glucose.” Am J Physiol Heart Circ Physiol **263**: H321–H326.

Tkachuk, V., Plekhanova, O., et. al. (2009) “Regulation of arterial remodeling and angiogenesis by urokinase-type plasminogen activator.” Can. J. Physiol. Pharmacol. **87**: 231–251

Toma, L., Stancu, C. et. al. (2009). “Irreversibly glycated LDL induce oxidative and inflammatory state in human endothelial cells; added effect of high glucose.” Biochemical and Biophysical Research Communications **390:** 877-882.

Tran, E.D., G.W. Schmid-Schönbein. (2007). “An in-vivo analysis of capillary stasis and endothelial apoptosis in a model of hypertension.” Microcirculation **14**(8): 793-804.

Utriainen, T., Nuutila, P., et al. (1997). “Intact insulin stimulation of skeletal muscle blood flow, its heterogeneity and redistribution, but not of glucose uptake in non-insulin-dependent diabetes mellitus.” J. Clin. Invest. **100**(4): 777-785

Valerio, A., Cardile, A., et al. (2006). “TNF-α downregulates eNOS expression and mitochondrial biogenesis in fat and muscle of obese rodents.” The Journal of Clinical Investigation **116**:2791-2798

Vanhoutte, P., (2009) “Endothelial dysfunction and vascular disease,” Acta Physiologica **196**(2):193-222.

Vettor, R., Milan, G., et. al. “Review article: adipocytokines and insulin resistance.” Aliment Pharmacol Ther **22**(Suppl. 2): 3–10.

Wang, D. H. and R. L. Prewitt (1993). "Alterations of mature arterioles associated with chronically reduced blood flow." Am J Physiol Heart Circ Physiol **264**(1): H40-44.

Wang, S., Xiong, X, et. al. (2005) “Protective effects of cariporide on endothelial dysfunction induced by high glucose.” Acta Pharmicological Sinica **26**(3): 329-333.

Waterman, I., Zammit, V. (2002). “Activities of overt and latent diacylglycerol acyltransferases (DGATs I and II) in liver microsomes of ob/ob mice.” International Journal of Obesity **26**:742-743.

Waugh, R. E. and I. H. Sarelius (1996). "Effects of lost surface area on red blood cells and red blood cell survival in mice." Am J Physiol Cell Physiol **271**(6): C1847-1852.

Weinbaum, S., X. Zhang, et al. (2003). "Mechanotransduction and flow across the endothelial glycocalyx." PNAS **100**(13): 7988-7995.

Wiegman, C., Bandsma, R., et al. (2003). “Hepatic VLDL production in ob/ob mice is not stimulated by massive de novo lipogenesis but is less sensitive to the suppressive effects of insulin.” Diabetes **52**:1081-1089.

Williams, T., and Moreley, J., (1973) “Prostaglandins as Potentiators of Increased Vascular Permeability in Inflammation”, Nature **246**:215-217.

Wu, W., Peng, H., et. al. (2003) “Disintegrin causes proteolysis of β-catenin and apoptosis of endothelial cells Involvement of cell—cell and cell—ECM interactions in regulating cell viability “ Experimental Cell Research **286**:115–127

Yakubu, M., Sofola, O., et. al. (2004) “Link between free radicals and protein kinase C in glucose-induced alteration of vascular dilation” Life Sciences **75**: 2921–2932

Appendix I

Branch Geometry and Definitions of Terms
Definition of Zones 1-18 and Regions:

A schematic of all terms and their definitions can be found on the pages that follow.

Terms:

Bifurcation:
The bifurcation is the section of blood vessel within two tube diameters of each bifurcation point.

Each bifurcation is broken up into a series of sections depending on the data type. The section definitions are as follows.

Zones:
There are 18 zones. Zones are indicated by a single numbered bracket, and are defined as the section of the vessel interior within 5 microns of the wall.

Regions
There are 9 regions, regions are defined by a pair of brackets and are designated as the numbers on either side (ie region 17 is between zone 1 and zone 7) they are defined as the entire vessel section within the desgingated length of vessel.

Segments:
There are 4 segments. Segments represent the functional fluid section of the vessel. Each is made up of a group of regions.

The Feed segment contains the inflow into the bifurcation. It is made up of regions 511 and 612.

The junction segment contains the point of bifurcation and flow division. It is made up of regions 39, 410, and 1316

The Feed Continuation segment (often designated FC) is the segment of outflow which is past the entry length. Therefore the velocity profile should be reestablished in the feed continuation. It is made up of regions 17 and 28.

The branch region is the section of the branch after the bifurcation entry length. The velocity profile should also be established here. It is made up of regions 1417 and 1518.

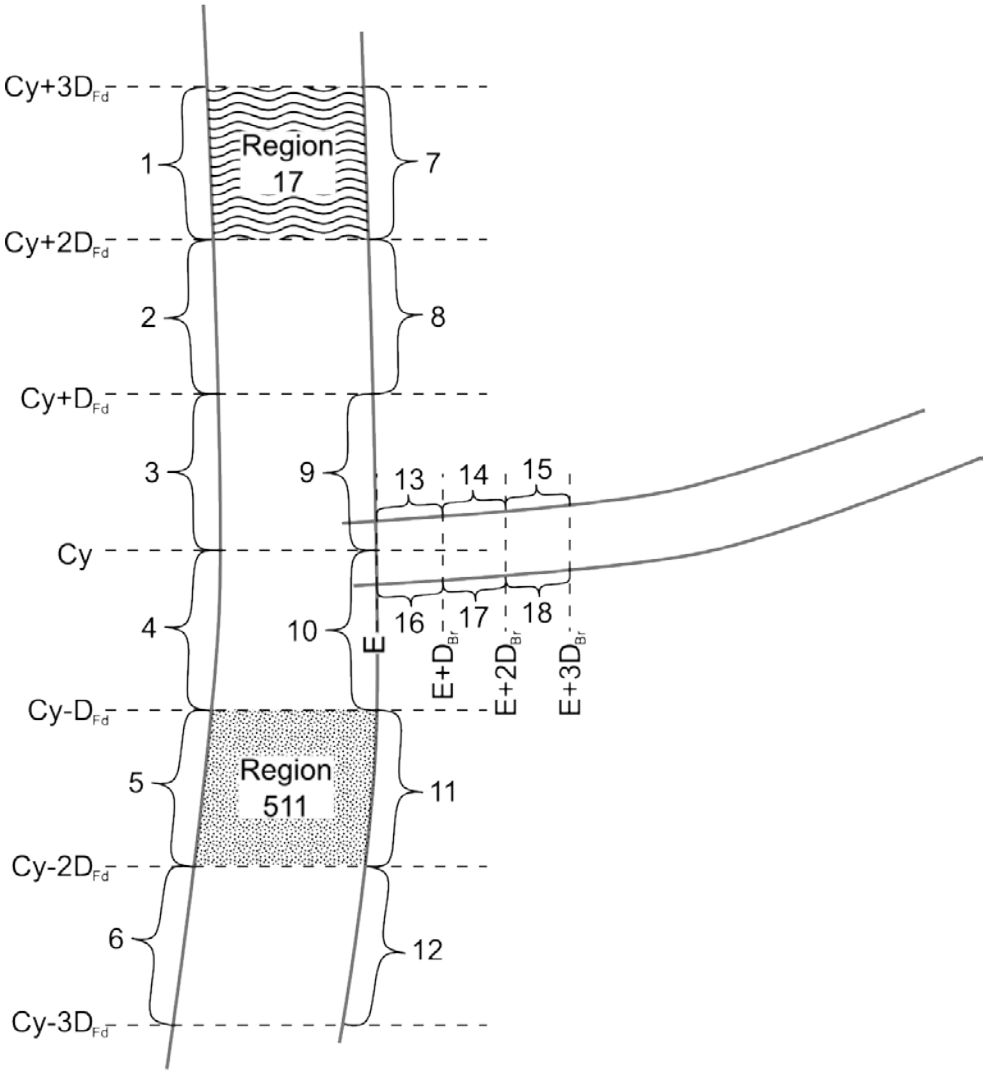

$$E = Cx + \frac{D_{Fd}}{2}$$

For definitions of *Cx*, *Cy*, D_{Fd}, and D_{Br}, see center of mass method on the following page.

Method for finding bifurcation center of mass:

$D_{Fd} = \overline{(X_{B2} - X_{B1})}$ and $D_{Br} = \overline{(Y_{B3} - Y_{B4})}$

$c = \min(a, b)$ and $k = \frac{i + j}{2}$

$l = \overline{X}_{B1}$ where $k - 2D_{Fd} \le Y_{B1} \le k + 2D_{Fd}$

$m = \overline{X}_{B2}$ where $k - 2D_{Fd} \le Y_{B2} \le k + 2D_{Fd}$

$n = \overline{Y}_{B3}$ where $c \le X_{B3} \le c + 2D_{Br}$

$o = \overline{Y}_{B4}$ where $c \le X_{B4} \le c + 2D_{Br}$

$Cx = \frac{l + m}{2}$ and $Cy = \frac{n + o}{2}$

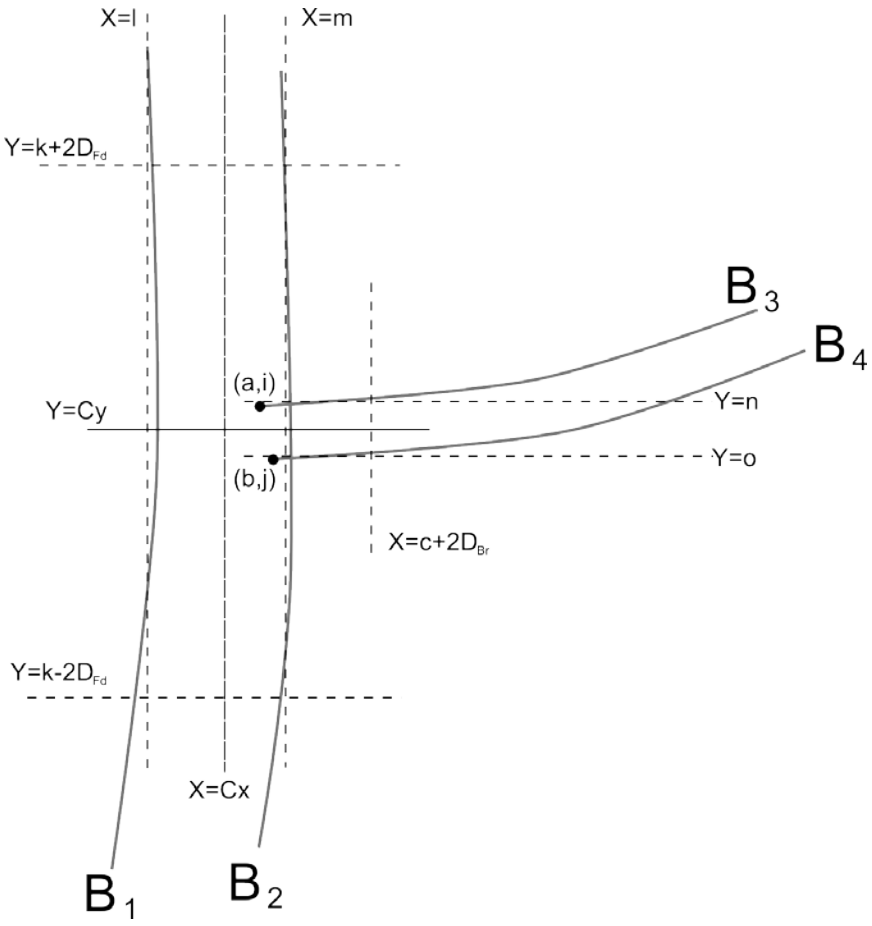

Appendix II

Angle of bifurcation measurement and rationale

The following is a description of the complete calculations of bifurcation angles along the midline of the vessel as they were used for this thesis. These calculations measure angles using lines defined one tube diameter from the bifurcation in all directions. According to fluid dynamics theory, a disturbance in flow will occur at a bifurcation, eliminating laminarity. The distance required to reestablish the velocity profile and therefore laminar flow, is called the entry length L_e. Using the approximated Reynold's number for this system ($Re \approx 0.1$) we can calculate the entry length to be approximately one tube diameter. We chose to measure our angles one tube diameter in all directions from the center of mass of the bifurcation in order to define the angle in areas of laminar flow. The following methods were originally developed by M. Zamir.

This process starts with a properly scaled image of the vascular bifurcation. For the purposes of this process, the left feed wall is defined as wall 1, the right feed wall is defined as wall 2, the top branch wall is defined as wall 3 and the bottom branch wall is defined as wall 4. Flow is assumed to be from the bottom of the image to the top.

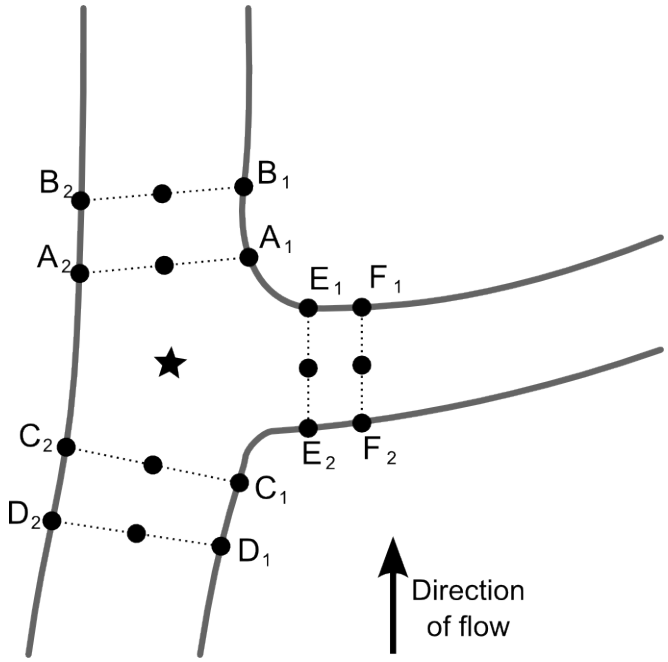

1) Measure the diameters of the feed(D_f) and the branch(D_b)

2) From the center of mass (indicated on the figure by a star) measure up the centerline of the vessel along the feed the distance of $0.5D_f$, and draw a line perpendicular to the vessel at this point, this is line A. Measure and

mark the points at either end of this line. Label the point on wall 1, A_1 and the point on wall 2, A_2. (see figure).

3) From line A, measure upstream another length $0.5D_f$, at this point, draw a second line perpendicular to the vessel wall, this is line B. Mark the ends as B_1 and B_2.

4) Repeat this process from the COM down one $0.5D_f$ for line C and from line C one additional $0.5D_f$ for line D.

5) Starting at the boundary of the branching wall, measure one $0.5D_b$ up the branch and draw a line perpendicular to the branch vessel, this is line E. Label the ends appropriately, according to the figure. Repeat for line F.

6) For each line, using the coordinates of the endpoints, calculate the midpoint coordinates of the line by equation A2.1 using the 1 and 2 points for each line..

$$mid_x = \frac{(1_x + 2_x)}{2}$$
$$mid_y = \frac{(1_y + 2_y)}{2} \qquad \text{(equation A2.1)}$$

7) Calculate angles.

   a. The apical angle is the angle described by the centerlines of the feed continuation and the branch and is calculated by equation A2.2.

$$\angle_A = \frac{(Bmid_x - Amid_x)(Fmid_x - Emid_x) + (Bmid_y - Amid_y)(Fmid_y - Emid_y)}{\sqrt{(Bmid_x - Amid_x)^2 + (Bmid_y - Amid_y)^2}\sqrt{(Fmid_x - Emid_x)^2 + (Fmid_y - Emid_y)^2}} ($$

equation A2.2)

   b. The lateral angle is the angle described by the centerlines of the branch and the feed and is calculated by equation A2.3.

$$\angle_A = \frac{(Dmid_x - Cmid_x)(Fmid_x - Emid_x) + (Dmid_y - Cmid_y)(Fmid_y - Emid_y)}{\sqrt{(Dmid_x - Cmid_x)^2 + (Dmid_y - Cmid_y)^2}\sqrt{(Fmid_x - Emid_x)^2 + (Fmid_y - Emid_y)^2}}$$

(equation A2.3*)

   c. The continuation angle is the angle described by the centerlines of the feed and the feed continuation and is calculated by equation A2.4

$$\angle_A = \frac{(Dmid_x - Cmid_x)(Bmid_x - Amid_x) + (Dmid_y - Cmid_y)(Bmid_y - Amid_y)}{\sqrt{(Dmid_x - Cmid_x)^2 + (Dmid_y - Cmid_y)^2}\sqrt{(Bmid_x - Amid_x)^2 + (Bmid_y - Amid_y)^2}}$$

(equation A2.4*)

* Note: equations A2.2, A2.3, and A2.4 are the same basic equation with the variables substituted for the proper angles to avoid any ambiguity of terms.

Appendix III

Radius of Curvature Calculations and Theory

The following is a description of the approximation of the radius of curvature of the apical wall within a bifurcation. This approximation estimates the curvature by fitting circle to three functionally defined points as seen in the figure below.

This process starts with a properly scaled image of the vascular bifurcation. For the purposes of this process, the left feed wall is defined as wall 1, the right feed wall is defined as wall 2, the top branch wall is defined as wall 3 and the bottom branch wall is defined as wall 4. Flow is assumed to be from the bottom of the image to the top.

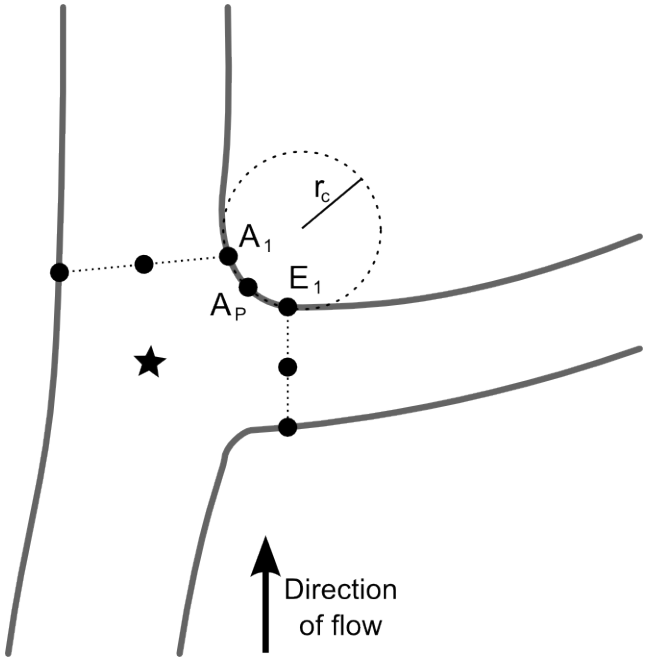

8) Measure the diameters of the feed(D_f) and the branch(D_b)

9) From the center of mass (indicated on the figure by a star) measure up the centerline of the vessel along the feed the distance of $0.5D_f$, and draw a line perpendicular to the vessel at this point, this is line A. Measure and mark the points at either end of this line. Label the point on wall one, A_1 and the point on wall two, A_2. (see figure).

10) Starting at the boundary of the branching wall, measure one $0.5D_b$ up the branch and draw a line perpendicular to the branch vessel, this is line E. Label the ends appropriately, according to the figure.

11) Identify the apex (Ap) as the point of the inflection of curvature between the feed and the branch.

12) From the points A_1, E_1, and Ap, calculate the radius of curvature by the following steps (equations for the fit of a circumcircle from Weissman[1])

    a. Calculate the length of line segment defined by point A_2 and the apex.

$$L_{A-Ap} = \sqrt{\left(Ap_x - A_{1x}\right)^2 + \left(Ap_y - A_{1y}\right)^2}$$

    b. Repeat the calculation for the other two defined line segments

$$L_{A-E} = \sqrt{\left(A_{1x} - E_{1x}\right)^2 + \left(A_{1y} - E_{1y}\right)^2}$$

$$L_{E-Ap} = \sqrt{\left(Ap_x - E_{1x}\right)^2 + \left(Ap_y - E_{1y}\right)^2}$$

    c. Calculate the length of the semiperimeter, defined as one half of the perimeter of the triangle described by those three points

$$SP = \frac{\left(L_{A-Ap} + L_{E-Ap} + L_{A-E}\right)}{2}$$

13) From these four values, calculate the radius of the circumscribed circle.

$$r = \frac{\left(L_{A-Ap} * L_{A-E} * L_{E-Ap}\right)}{4\sqrt{SP\left(L_{A-Ap} + L_{A-E} - SP\right)\left(L_{A-Ap} + L_{E-Ap} - SP\right)\left(L_{A-E} + L_{E-Ap} - SP\right)}}$$

1) Weisstein, Eric W. "Circumcircle." From MathWorld--A Wolfram Web Resource. http://mathworld.wolfram.com/Circumcircle.html

Appendix IV

Bifurcation Volume Estimation Calculations and Theory

In the area of the bifurcation (e.g. where the branch comes off of the feed) there is an expansion of flow. Estimating the volume in that segment allows us to see one aspect of the change in environment that affects the flow.

The following is a description of the approximation of the junction segment within a bifurcation. This segment is described as the section of vessel along the feed within one tube diameter of the center of mass upstream and one tube diameter of the center of mass downstream, and the section of the branch within one branch diameter of the bifurcating wall. (see figure A4.1)

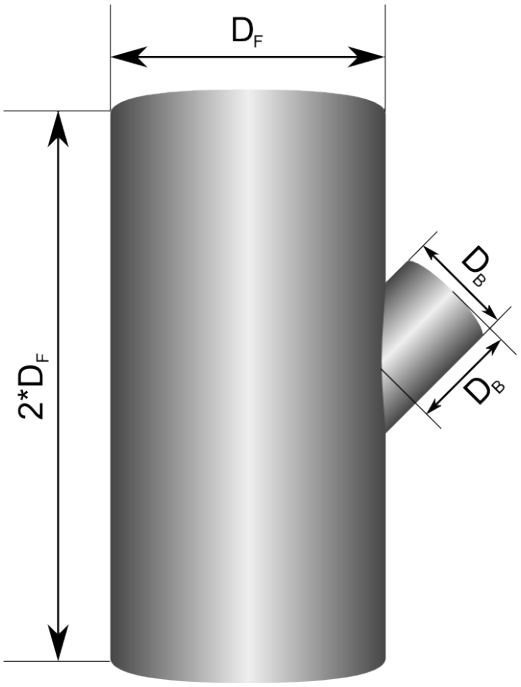

Figure A4.1 The volume being estimated

The geometry of the bifurcation volume can be approximated by two cylinders intersecting at an angle, where one of the two cylinders is sliced off at the angle of intersection Θ. (see figure A4.2). Using this approximation results in an error of less than 1%.

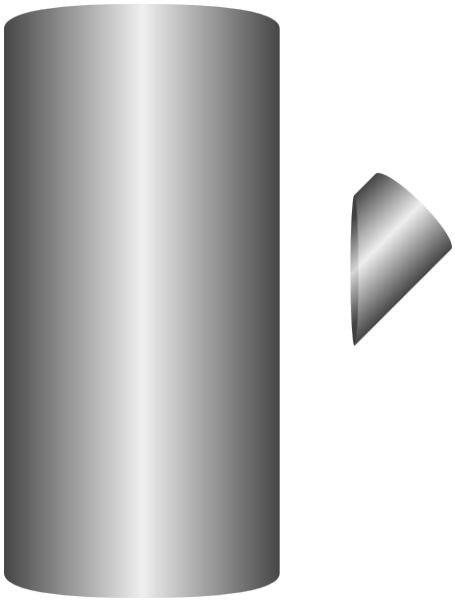

Figure A4.2: Two cylinder model for estimating bifurcation volume

To calculate this approximation we first calculate the feed volume as a right cylinder with a length of two tube diameters. We then calculate the branch volume by dividing it into two cylinders, one right cylinder and one cylinder sliced at an angle Θ. (see figure A4.3) The total length of both of these cylinders will be one branch tube diameter.

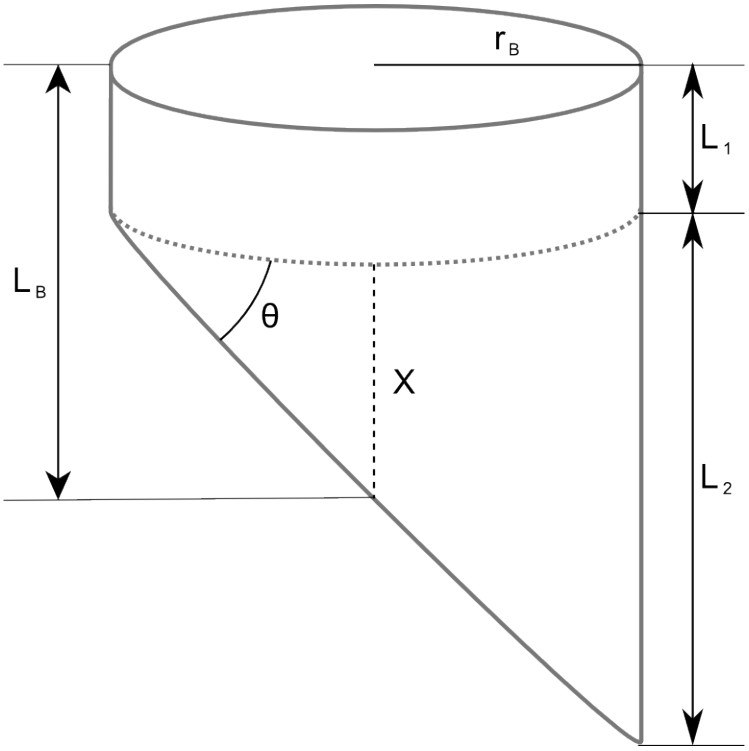

Figure A4.3: Schematic of the variables for the sliced cylinder

Variables:

D_F : feed diameter
D_B : branch diameter

r_F : feed radius = $0.5D_F$
r_B : branch radius = $0.5D_B$
L_F : feed length = $2D_F$
L_B : branch length = D_B

V_F : feed volume
L_1 : length of cylinder 1 (non-sliced)
L_2 : length of cylinder 2 (sliced)
x : distance from bottom midpoint of cylinder 1 to bottom midpoint of cylinder 2
V_1 : cylinder 1 volume
V_2 : cylinder 2 volume
θ : angle of bifurcation at apex

V_{bif} : total bifurcation volume

Calculations

1) Calculate the volume of the feed cylinder
   $V_F = \pi r^2 L_F$
2) Calculate the volume of the branch cylinder
   a. Break the cylinder into two, and calculate the height at the wall of the two cylinders.
      $\tan\theta = \frac{x}{r_B}$ $\qquad$ $\tan\theta = \frac{L_2}{2r_B}$
      $x = r_B \tan\theta$ $\qquad$ $L_2 = 2r_B \tan\theta$
      $L_1 = L_B - x$
   b. Calculate the volume of cylinder 1 (right cylinder)
      $V_1 = \pi r_B^2 L_1$
      $V_1 = \pi r_B^2 (L_B - x)$
   c. Calculate the volume of cylinder 2 (cylinder sliced at angle Θ)
      $V_2 = \frac{\pi r_B^2 L_2}{2}$
      $V_2 = \frac{\pi r_B^2 (2r_B \tan\theta)}{2}$

d. Add the volume of cylinder 1 to the volume of cylinder 2 to get the total branch volume.

$$V_B = V_1 + V_2$$

$$V_B = \pi r_B^2 \left(L_B - x\right) + \frac{\pi r_B^2 \left(2 r_B \tan\theta\right)}{2}$$

3) Calculate total estimation of bifurcation volume

$$V_{bif} = V_F + V_B$$

$$V_{bif} = \pi r^2 L_F + \pi r_B^2 \left(L_B - x\right) + \frac{\pi r_B^2 \left(2 r_B \tan\theta\right)}{2}$$

Appendix V

Matlab code for Analysis of ProAnalyst data

PRIMARY DATA ANALYSIS

```
%Version updates:
%052209L branch starts at proper end for Left branches.
%052209 changed calculations of regions so that it does not take into
%account wall 'wobble' direct distances used.
%051109 fixed B#/B4 sorting so that midpoint was accurately calculated
%043009 changed td5_B1 and B2 to account for short data set
%040109 changed B4 to account for branches so short they don't even get a
%full first region
%032309: changed sorting to handle re-curving boundaries, handles any,
%corrected zone sorting error and duplicate zone 17 error
%single (seconds) dataset
%022509: branchless data handling
%prior problems solved: data outside of regions, empty regions, right or left
branches,
%missing 1st 10 seconds of data

%import routine
'importing text files'
merged=zeros(1,23);
merged=merged-1;
pmax = 0;

reply = input('Do you wish to open a text file? 1 if yes, 2 if no: ');
   while reply==1
      uiimport

      startframe=input('What is the starting frame number? :');
      endframe=input('What is the ending frame number? :');

      'trimming dataset'
      %remove frames before
      L = size(data,1);
      for H=L:-1:1,
         if data(H,1)<startframe
         data(H,:)=[];
         end
      end
```

```
        %remove frames after
        L = size(data,1);
        for H=L:-1:1,
           if data(H,1)>endframe
           data(H,:)=[];
           end
        end

        %create seconds column
        'adding columns'
        sec=input('Which 10 seconds is this, 10, 20, or 30? :');
        L = size(data,1);
        seconds=sec*ones(L,1);

        %concatenate seconds onto data
        data=[data seconds];

        %create partN column and correct frames column assuming 600 frames
        %per 10 seconds import
        partN=[];
        for H=1:L,
           if sec==10
              partN(H,:)=data(H,3);
           else
              partN(H,:)=data(H,3)+pmax;
              data(H,1)=data(H,1)+((sec/10*600)-600);
           end
        end

        %concatenate partN onto data
        data=[data partN];

        %Create merged datafile
        'merging data'
        if size(merged,1)==1
           merged=data;
        else
           merged=[merged;data];
        end
        pmax=max(merged(:,23));
        reply=input('Do you have another text file to import? 1 if yes, 2 if no :');
     end
%clean up data
%Remove non-data lines
'removing empty lines'
```

```
L = size(merged,1);
for H=L:-1:1,
   if merged(H,3)==-1.0000;
      merged(H,:)=[];
   end
end

%convert to microns and convert y axis properly
'converting to microns and scaling'
L = size(merged,2);
convert=merged';
cal=eye(L);
cal=cal*1000; %convert all columns to microns
cal(1,1)=1; %correct frame
cal(2,2)=1; %correct time
cal(3,3)=1; %correct particle
cal(4,4)=cal(4,4)*1000*2.35; %correct size(1) for microns square, & y conversion
cal(6,6)=cal(6,6)*2.35; %y leading edge converted in y direction
cal(8,8)=cal(8,8)*2.35; %y boundary 1 converted in y direction
cal(11,11)=cal(11,11)*2.35; %y boundary 2 converted in y direction
cal(13,13)=cal(13,13)*1000*2.35; %correct size(2) for microns square, & y
conversion
cal(15,15)=cal(15,15)*2.35; %y leading edge converted in y direction
cal(17,17)=cal(17,17)*2.35; %y boundary 3 converted in y direction
cal(20,20)=cal(20,20)*2.35; %y boundary 4 converted in y direction
cal(22,22)=1; %correct seconds
cal(23,23)=1; %correct particleN

main=(cal*convert);
main=main';

%plot graph in figure 1
'plotting data'
%create boundary wall pairs
B1=[main(:,7) main(:,8)];
B1(:,3)=0;
B2=[main(:,10) main(:,11)];
B2(:,3)=0;
B3=[main(:,16) main(:,17)];
B3(:,3)=0;
B4=[main(:,19) main(:,20)];
B4(:,3)=0;

%create cell pairs, column 3 indicates what line in main it came from
L=size(main,1);
```

```
cells=zeros(L,3);
   for H=1:L,
      cells(H,3)=H;
      if main(H,4)>0
         cells(H,1)=main(H,5);
         cells(H,2)=main(H,6);
      else
         cells(H,1)=main(H,14);
         cells(H,2)=main(H,15);
      end
   end

'sorting wall vectors'
%sort pairs for order to clean line
%remove non-wall data lines, col 3 indicates line # from main

%boundary 1
   L=size(B1,1);
   for H=L:-1:1,
      if B1(H,1)==-1000
         B1(H,:)=[];
      else
         B1(H,3)=H;
      end
   end
B1=sortrows(B1,2);  %sort by y first
B1=flipud(B1);

%boundary 2
   L=size(B2,1);
   for H=L:-1:1,
      if B2(H,1)==-1000
         B2(H,:)=[];
      else
         B2(H,3)=H;
      end
   end
B2=sortrows(B2,2);  %sort by y first
B2=flipud(B2);

%determine branch existence, if branchverify=0 there is no branch in the
%dataset
L=size(B4,1);
   for H=L:-1:1,
      if B4(H,1)==-1000
```

```
        B4(H,:)=[];
      else
        B4(H,3)=H;
      end
   end

L=size(B3,1);
   for H=L:-1:1,
      if B3(H,1)==-1000
        B3(H,:)=[];
      else
        B3(H,3)=H;
      end
   end

if size(B3,1)==0;
   branchverify=0;
else
   branchverify=1;
end

if branchverify==1

B3=sortrows(B3,1); %sort boundary 3 by x values, increasing
B4=sortrows(B4,1);

end

%plot data

figure(1)
plot(B1(:,1),B1(:,2))
hold on
plot(B2(:,1),B2(:,2))
plot(B3(:,1),B3(:,2))
plot(B4(:,1),B4(:,2))
plot(cells(:,1),cells(:,2),'.y')

'creating ROI'
%ROI creation
ROI = 1;
ROImain=main;
ROI=input('Do you wish to create an ROI for this dataset? 1 if yes, 2 if no: ' );
   while ROI==1
      where =0;
```

```
        where=input('Does the ROI need to affect the feed or the branch? 1 if feed,
2 if branch.:' );
            if where==1
               m=min(B1(:,2));
               n=min(B2(:,2));
               L=size(B1,1);
               if m<n,
                     for H=L:-1:1,
                        if B1(H,2)==m
                           ROImain(B1(H,3),1)=-1;
                           ROImain(B2(H,3),1)=-1;
                           B1(H,:)=[];
                           B2(H,:)=[];
                        end
                        if B2(H,2)<=m
                           ROImain(B1(H,3),1)=-1;
                           ROImain(B2(H,3),1)=-1;
                           B1(H,:)=[];
                           B2(H,:)=[];
                        end
                     end
               end
               if n<m,
                     for H=L:-1:1,
                        if B1(H,2)==n
                           ROImain(B1(H,3),1)=-1;
                           ROImain(B2(H,3),1)=-1;
                           B1(H,:)=[];
                           B2(H,:)=[];
                        end
                        if B2(H,2)<=n
                           ROImain(B1(H,3),1)=-1;
                           ROImain(B2(H,3),1)=-1;
                           B1(H,:)=[];
                           B2(H,:)=[];
                        end
                     end
               end

            else
               m=min(B3(:,1));
               n=min(B4(:,1));
               L=size(B3,1);
               if m<n,
                     for H=L:-1:1,
```

```
                    if B3(H,1)==m
                       ROImain(B3(H,3),1)=-1;
                       ROImain(B4(H,3),1)=-1;
                       B3(H,:)=[];
                       B4(H,:)=[];
                    end
                    if B4(H,1)<=m
                       ROImain(B3(H,3),1)=-1;
                       ROImain(B4(H,3),1)=-1;
                       B3(H,:)=[];
                       B4(H,:)=[];
                    end
                 end
              end
              if n<m,
                 for H=L:-1:1,
                       ROImain(B3(H,3),1)=-1;
                       ROImain(B4(H,3),1)=-1;
                    if B3(H,1)==n
                       B3(H,:)=[];
                       B4(H,:)=[];
                    end
                    if B4(H,1)<=n
                       ROImain(B3(H,3),1)=-1;
                       ROImain(B4(H,3),1)=-1;
                       B3(H,:)=[];
                       B4(H,:)=[];
                    end
                 end
              end
        end

%plot data

figure(2)
plot(B1(:,1),B1(:,2))
hold on
plot(B2(:,1),B2(:,2))
plot(B3(:,1),B3(:,2))
plot(B4(:,1),B4(:,2))
hold off

ROI = input('Do further corrections need to be made to the ROI? 1 if yes, 2 if no:
');
end
```

```
figure(2)
hold on
plot(B1(:,1),B1(:,2))
plot(B2(:,1),B2(:,2))
plot(B3(:,1),B3(:,2))
plot(B4(:,1),B4(:,2))

%remove empty rows from ROImain file

L=size(ROImain,1);
for H=L:-1:1,
   if ROImain(H,1)==-1
      ROImain(H,:)=[];
   end
end

'moving RBCs outside of walls'
%corrected distance column generation
%Calibrations
%fill distance from boundary X columns
L=size(ROImain,1);
      CB1=zeros(L,1);
      CB2=zeros(L,1);
      CB3=zeros(L,1);
      CB4=zeros(L,1);
for H=L:-1:1,
   if ROImain (H,4)>0
      ROImain(H,9)=sqrt(((ROImain(H,7)-ROImain(H,5))^2)+((ROImain(H,8)-
ROImain(H,6))^2));
      ROImain(H,12)=sqrt(((ROImain(H,10)-ROImain(H,5))^2)+((ROImain(H,11)-
ROImain(H,6))^2));
   end
   if ROImain (H,12)>0
      ROImain(H,18)=sqrt(((ROImain(H,16)-ROImain(H,14))^2)+((ROImain(H,17)-
ROImain(H,15))^2));
      ROImain(H,21)=sqrt(((ROImain(H,19)-ROImain(H,14))^2)+((ROImain(H,20)-
ROImain(H,15))^2));
   end

%create corrected distance vectors

      if ROImain (H,4)>0
         if ROImain(H,9)<0.7
         CB1(H)=0.7;
```

```
        else
        CB1(H)=ROImain(H,9);
        end
        if ROImain(H,12)<0.7
        CB2(H)=0.7;
        else
        CB2(H)=ROImain(H,12);
        end
      end
      if ROImain(H,13)>0
        if ROImain(H,18)<0.7
        CB3(H)=0.7;
        else
        CB3(H)=ROImain(H,18);
        end
        if ROImain(H,21)<0.7
        CB4(H)=0.7;
        else
        CB4(H)=ROImain(H,21);
        end
      end
end
%concatenate CB columns onto main
      ROImain=[ROImain CB1 CB2 CB3 CB4];

'calculating diameters'
%create diameter column
diameter=zeros(L,1);

%fill diameter column
for H=1:L,
   if ROImain(H,4)>0
      diameter(H)=sqrt(((ROImain(H,10)-ROImain(H,7))^2)+((ROImain(H,11)-
ROImain(H,8))^2));
   else
      diameter(H)=sqrt(((ROImain(H,19)-ROImain(H,16))^2)+((ROImain(H,20)-
ROImain(H,17))^2));
   end
end

%concatenate diameter column onto main
      ROImain=[ROImain diameter];

%find average diameters for feed (D) and branch (d)
C=0;
```

```
Total=0;
c=0;
total=0;

for H=1:L,
   if ROImain(H,4)>0
      C=C+1;
      Total=Total+ROImain(H,28);
   else
      c=c+1;
      total=total+ROImain(H,28);
   end
end

D=Total/C;
d=total/c;

%determine branch direction
%find average x value of wall 1 and wall 2
'calculating branch parameters'

avg1=sum(B1(:,1))/size(B1,1);
avg2=sum(B2(:,1))/size(B2,1);

if branchverify==0;
   side=0;
else
if max(B3(:,1))>avg2 %a value of 1 indicates a right branch, a value of 2 indicates
a left branch, a value of 0 indicates no branch
      side=1;
else side=2;
end
end

% find intersection of feed and branch, if no branch data, next relevant
% line is near 595
   if side==1
% locate closest feed point to branch
   L=size(B2,1);
   line3=1;
   line4=1;
   distance3=sqrt(((B2(1,1)-B3(1,1))^2)+((B2(1,2)-B3(1,2))^2));
   distance4=sqrt(((B2(1,1)-B4(1,1))^2)+((B2(1,2)-B4(1,2))^2));
   for H=1:L,
      testdistance3=sqrt(((B2(H,1)-B3(1,1))^2)+((B2(H,2)-B3(1,2))^2));
```

```
      testdistance4=sqrt(((B2(H,1)-B4(1,1))^2)+((B2(H,2)-B4(1,2))^2));

      if testdistance3<=distance3;
         line3=H;
         distance3=testdistance3;
      end
      if testdistance4<=distance4;
         line4=H;
         distance4=testdistance4;
      end
   end
end

   if side==2
% locate closest feed point to branch
   L=size(B1,1);
   W=size(B3,1);
   line3=1;
   line4=1;
   distance3=sqrt(((B1(1,1)-B3(1,1))^2)+(B1(1,2)-B3(1,2))^2);
   distance4=sqrt(((B1(1,1)-B4(1,1))^2)+(B1(1,2)-B4(1,2))^2);
   for H=1:L,
      testdistance3=sqrt(((B1(H,1)-B3(1,1))^2)+(B1(H,2)-B3(1,2))^2);
      testdistance4=sqrt(((B1(H,1)-B4(1,1))^2)+(B1(H,2)-B4(1,2))^2);

      if testdistance3<=distance3;
         line3=H;
         distance3=testdistance3;
      end
      if testdistance4<=distance4;
         line4=H;
         distance4=testdistance4;
      end
   end
end

%find midpoint of branch intersection with feed.
   if side==0
      xmid=input('NO BRANCH DATA please enter the x coordinate for the
bifurcation point:');
      ymid=input('NO BRANCH DATA please enter the y coordinate for the
bifurcation point:');
      xmid=xmid/2.63;
      ymid=ymid/2.63;
      mid=[xmid ymid];
```

```
    end

if side==1
    cept3=[B2(line3,1),B2(line3,2)];
    cept4=[B2(line4,1),B2(line4,2)];

    xmid=(cept3(1,1)+cept4(1,1))/2;
    ymid=(cept3(1,2)+cept4(1,2))/2;

    mid=[xmid ymid];
end

if side==2

    cept3=[B1(line3,1),B1(line3,2)];
    cept4=[B1(line4,1),B1(line4,2)];

    xmid=(cept3(1,1)+cept4(1,1))/2;
    ymid=(cept3(1,2)+cept4(1,2))/2;

    mid=[xmid ymid];
end

%plot midpoint
figure(2)
plot(mid(1,1),mid(1,2),'mo')

%branch region point calculations
W=size(B3,1);
if side==2
    td1_B3=distance3;  %initialize variable to distance between closest point on
feed and first point on branch, when this variable = branch tube diameter, point
will be used
    x=2;       %initialize variable, allows first subtraction
    while td1_B3<d  %will run until distance = branch tube diameter
        td1_B3=(sqrt(((cept3(1,1)-B3(x,1))^2)+((cept3(1,2)-B3(x,2))^2))); %sum of
distances between all branch points to this point
        x=x+1;      %increment step
        if x==W-1    %prevents index from exceeding matrix dimensions
           x=x-1;   % sets x back by 1 so that next loop doesn't exceed matrix
dimensions
            break
        end
    end
    B3A=[B3(x,1) B3(x,2)];       %record value of point
```

```
   td2_B3=0;  %reinitialize variable
   while td2_B3<d  %will run until distance = branch tube diameter
      td2_B3=(sqrt(((B3A(1,1)-B3(x,1))^2)+((B3A(1,2)-B3(x,2))^2)));  %sum of
distances between all branch points to this point
      x=x+1; %increment step
      if x==W-1    %prevents index from exceeding matrix dimensions
        x=x-1;   % sets x back by 1 so that next loop doesn't exceed matrix
dimensions
        break
      end
   end

   B3B=[B3(x,1) B3(x,2)];   %record value of point

   td3_B3=0;  %reinitialize variable
   while td3_B3<d  %will run until distance = branch tube diameter
      td3_B3=(sqrt(((B3B(1,1)-B3(x,1))^2)+((B3B(1,2)-B3(x,2))^2)));  %sum of
distances between all branch points to this point
      x=x+1; %increment step
      if x==W-1    %prevents index from exceeding matrix dimensions
        break
      end
   end

   B3C=[B3(x,1) B3(x,2)];   %record value of point

   %boundary 4
   LL=size(B4,1);
   td1_B4=distance4;  %initialize variable to distance between feed and branch,
when this variable = branch tube diameter, point will be used
   z=2;       %initialize variable, allows first subtraction
   while td1_B4<d  %will run until distance = branch tube diameter
      td1_B4=(sqrt(((cept4(1,1)-B4(z,1))^2)+((cept4(1,2)-B4(z,2))^2))); %sum of
distances between all branch points to this point
      z=z+1;      %increment step
      if z==LL-1    %prevents index from exceeding matrix dimensions
        z=z-1;   % sets z back by 1 so that next loop doesn't exceed matrix
dimensions
        break
      end
   end
   B4A=[B4(z,1) B4(z,2)];       %record value of point

   td2_B4=0;  %reinitialize variable
```

```
   while td2_B4<d  %will run until distance = branch tube diameter
      td2_B4=(sqrt(((B4A(1,1)-B4(z,1))^2)+((B4A(1,2)-B4(z,2))^2)));  %sum of
distances between all branch points to this point
      z=z+1; %increment step
      if z==LL-1    %prevents index from exceeding matrix dimensions
        z=z-1;   % sets z back by 1 so that next loop doesn't exceed matrix
dimensions
        break
      end
   end

   B4B=[B4(z,1) B4(z,2)];   %record value of point

   td3_B4=0;  %reinitialize variable
   while td3_B4<d  %will run until distance = branch tube diameter
      td3_B4=(sqrt(((B4B(1,1)-B4(z,1))^2)+((B4B(1,2)-B4(z,2))^2)));  %sum of
distances between all branch points to this point
      z=z+1; %increment step
      if z==LL-1    %prevents index from exceeding matrix dimensions
        z=z-1;   % sets z back by 1 so that next loop doesn't exceed matrix
dimensions
         break
      end
   end

   B4C=[B4(z,1) B4(z,2)];   %record value of point

elseif side==1

   td1_B3=distance3;  %initialize variable to distance between closest point on
feed and first point on branch, when this variable = branch tube diameter, point
will be used
   L=size(B3,1);
   x=1;       %initialize variable to end, allows for first incrementation
   while td1_B3<d  %will run until distance = branch tube diameter
      td1_B3=(sqrt(((cept3(1,1)-B3(x,1))^2)+((cept3(1,2)-B3(x,2))^2))); %sum of
distances between all branch points to this point
      x=x+1;      %increment step
      if x==L
         x=L-1;
         break
      end
   end
   B3A=[B3(x,1) B3(x,2)];       %record value of point
```

```
   td2_B3=0;  %reinitialize variable
   while td2_B3<d  %will run until distance = branch tube diameter
      td2_B3=(sqrt(((B3A(1,1)-B3(x,1))^2)+((B3A(1,2)-B3(x,2))^2)));  %sum of
distances between all branch points to this point
      x=x+1; %increment step
      if x==L
         x=L-1;
         break
      end
   end

   B3B=[B3(x,1) B3(x,2)];   %record value of point

   td3_B3=0;  %reinitialize variable
   while td3_B3<d  %will run until distance = branch tube diameter
      td3_B3=(sqrt(((B3B(1,1)-B3(x,1))^2)+((B3B(1,2)-B3(x,2))^2)));  %sum of
distances between all branch points to this point
      x=x+1; %increment step
      if x==L
         x=L-1;
         break
      end

   end

   B3C=[B3(x,1) B3(x,2)];   %record value of point

   %boundary 4
   td1_B4=distance4; %initialize variable to distance between feed and branch,
when this variable = branch tube diameter, point will be used
   z=1;       %initialize variable, allows first subtraction
   while td1_B4<d  %will run until distance = branch tube diameter
      td1_B4=(sqrt(((cept4(1,1)-B4(z,1))^2)+((cept4(1,2)-B4(z,2))^2))); %sum of
distances between all branch points to this point
      z=z+1;      %increment step
         if z==L
         z=L-1;
         break
         end
   end
   B4A=[B4(z,1) B4(z,2)];       %record value of point

   td2_B4=0;  %reinitialize variable
   while td2_B4<d  %will run until distance = branch tube diameter
```

```
        td2_B4=(sqrt(((B4A(1,1)-B4(z,1))^2)+((B4A(1,2)-B4(z,2))^2)));  %sum of
distances between all branch points to this point
        z=z+1; %increment step
        if z==L
            z=L-1;
            break
        end

    end

    B4B=[B4(z,1) B4(z,2)];   %record value of point

    td3_B4=0;  %reinitialize variable
    while td3_B4<d  %will run until distance = branch tube diameter
        td3_B4=(sqrt(((B4B(1,1)-B4(z,1))^2)+((B4B(1,2)-B4(z,2))^2)));  %sum of
distances between all branch points to this point
        z=z+1; %increment step
        if z==L
            z=L-1;
            break
        end

    end


    B4C=[B4(z,1) B4(z,2)];   %record value of point

end

if side==0
else
%plot points
figure(2)
hold on
plot(B4A(1,1),B4A(1,2),'gx')
plot(B4B(1,1),B4B(1,2),'rx')
plot(B4C(1,1),B4C(1,2),'bx')
plot(B3A(1,1),B3A(1,2),'gx')
plot(B3B(1,1),B3B(1,2),'rx')
plot(B3C(1,1),B3C(1,2),'bx')
end

%find nearest wall point to midpoint
%on wall 2
    L=size(B2,1);
```

```
   line1=1;
   line2=1;
   dist2=sqrt((B2(1,1)-mid(1,1))^2+(B2(1,2)-mid(1,2))^2);  %distance from
midpoint to B2
   dist1=sqrt((B1(1,1)-mid(1,1))^2+(B1(1,2)-mid(1,2))^2);  %distance from
midpoint to B1
      for H=1:L,
      testdistance2=sqrt((B2(H,1)-mid(1,1))^2+(B2(H,2)-mid(1,2))^2);
      testdistance1=sqrt((B1(H,1)-mid(1,1))^2+(B1(H,2)-mid(1,2))^2);
         if testdistance2<dist2
         line2=H;
         dist2=testdistance2;
         end

%on wall 1
         if testdistance1<dist1
         line1=H;
         dist1=testdistance1;
         end
      end

%plot points
figure(2)
hold on
plot(B1(line1,1),B1(line1,2),'mx')
plot(B2(line2,1),B2(line2,2),'mx')

F1=[B1(line1,1) B1(line1,2)];
F2=[B2(line2,1) B2(line2,2)];

%find feed region points
% boundary 1
   L=size(B1,1);
   td1_B1=0;  %initialize variable to 0, when this variable = branch tube diameter,
point will be used
   x=line1;      %initialize variable, allows first subtraction

   if x==1,
      x=2;
   end

   while td1_B1<D  %will run until distance = feed tube diameter
      td1_B1=(sqrt(((F1(1,1)-B1(x,1))^2)+((F1(1,2)-B1(x,2))^2))); %sum of
distances between all branch points to this point
      x=x+1;      %increment step
```

```
        if x==L
            x=x-1;
            break
        end
    end
    F1C=[B1(x,1) B1(x,2)];      %record value of point

    td2_B1=0;  %initialize variable to 0, when this variable = branch tube diameter,
point will be used
    while td2_B1<D  %will run until distance = feed tube diameter
        td2_B1=(sqrt(((F1C(1,1)-B1(x,1))^2)+((F1C(1,2)-B1(x,2))^2))); %sum of
distances between all branch points to this point
        x=x+1;      %increment step
        if x==L
            x=x-1;
            break
        end
    end
    F1B=[B1(x,1) B1(x,2)];      %record value of point

    td3_B1=0;  %initialize variable to 0, when this variable = branch tube diameter,
point will be used
    while td3_B1<D  %will run until distance = feed tube diameter
        td3_B1=(sqrt(((F1B(1,1)-B1(x,1))^2)+((F1B(1,2)-B1(x,2))^2))); %sum of
distances between all branch points to this point
        x=x+1;      %increment step
        if x==L
            x=x-1;
            break
        end
    end
    F1A=[B1(x,1) B1(x,2)];      %record value of point

    td4_B1=0;  %initialize variable to 0, when this variable = branch tube diameter,
point will be used
    x=line1;       %initialize variable, allows first subtraction

    if x==1
        x=2;
    end

    while td4_B1<D  %will run until distance = feed tube diameter
        td4_B1=(sqrt(((F1(1,1)-B1(x,1))^2)+((F1(1,2)-B1(x,2))^2))); %sum of
distances between all branch points to this point
        x=x-1;      %increment step
```

```
        if x==1
            x=2;
            break
        end
    end
    F1D=[B1(x,1) B1(x,2)];       %record value of point

    td5_B1=0;  %initialize variable to 0, when this variable = branch tube diameter,
point will be used
    while td5_B1<D  %will run until distance = feed tube diameter
        td5_B1=(sqrt(((F1D(1,1)-B1(x,1))^2)+((F1D(1,2)-B1(x,2))^2))); %sum of
distances between all branch points to this point
        x=x-1;      %increment step
        if x<=1
            break
        end
    end
    F1E=[B1(x,1) B1(x,2)];       %record value of point

    td6_B1=0;  %initialize variable to 0, when this variable = branch tube diameter,
point will be used
    while td6_B1<D  %will run until distance = feed tube diameter
        if x==1
            x=2;
            break
        end
        td6_B1=(sqrt(((F1E(1,1)-B1(x,1))^2)+((F1E(1,2)-B1(x,2))^2))); %sum of
distances between all branch points to this point
        x=x-1;      %increment step
    end
    F1F=[B1(x,1) B1(x,2)];       %record value of point

%plot points
figure(2)
hold on
plot(F1A(1,1),F1A(1,2),'rx')
plot(F1B(1,1),F1B(1,2),'gx')
plot(F1C(1,1),F1C(1,2),'bx')
plot(F1D(1,1),F1D(1,2),'cx')
plot(F1E(1,1),F1E(1,2),'yx')
plot(F1F(1,1),F1F(1,2),'mx')

% boundary 2
    td1_B2=0;  %initialize variable to 0, when this variable = branch tube diameter,
point will be used
```

```
   x=line2;       %initialize variable, allows first subtraction

   if x==1
      x=2;
   end

   while td1_B2<D  %will run until distance = feed tube diameter
      td1_B2=(sqrt(((F2(1,1)-B2(x,1))^2)+((F2(1,2)-B2(x,2))^2))); %sum of
distances between all branch points to this point
      x=x+1;      %increment step
      if x==L
         break
      end
   end
   F2C=[B2(x,1) B2(x,2)];       %record value of point

   td2_B2=0;  %initialize variable to 0, when this variable = branch tube diameter,
point will be used
   while td2_B2<D  %will run until distance = feed tube diameter
      td2_B2=(sqrt(((F2C(1,1)-B2(x,1))^2)+((F2C(1,2)-B2(x,2))^2))); %sum of
distances between all branch points to this point
      x=x+1;      %increment step
      if x>=L
         x=L;
         break
      end
   end
   F2B=[B2(x,1) B2(x,2)];       %record value of point

   td3_B2=0;  %initialize variable to 0, when this variable = branch tube diameter,
point will be used
   while td3_B2<D  %will run until distance = feed tube diameter
      td3_B2=(sqrt(((F2B(1,1)-B2(x,1))^2)+((F2B(1,2)-B2(x,2))^2))); %sum of
distances between all branch points to this point
      x=x+1;      %increment step
      if x>=L
         x=L;
         break
      end
   end
   F2A=[B2(x,1) B2(x,2)];       %record value of point

   td4_B2=0;  %initialize variable to 0, when this variable = branch tube diameter,
point will be used
   x = line2       %initialize variable, allows first subtraction
```

```
    if x==1,
        x=2;
    end

    while td4_B2<D  %will run until distance = feed tube diameter
        td4_B2=(sqrt(((F2(1,1)-B2(x,1))^2)+((F2(1,2)-B2(x,2))^2))); %sum of
distances between all branch points to this point
        x=x-1;      %increment step
        if x==1
            x=2;
            break
        end
    end
    F2D=[B2(x,1) B2(x,2)];       %record value of point

    td5_B2=0;  %initialize variable to 0, when this variable = branch tube diameter,
point will be used
    while td5_B2<D  %will run until distance = feed tube diameter
        td5_B2=(sqrt(((F2D(1,1)-B2(x,1))^2)+((F2D(1,2)-B2(x,2))^2))); %sum of
distances between all branch points to this point
        x=x-1;      %increment step
        if x==1
            break
        end
    end
    F2E=[B2(x,1) B2(x,2)] ;      %record value of point

    td6_B2=0;  %initialize variable to 0, when this variable = branch tube diameter,
point will be used
    while td6_B2<D  %will run until distance = feed tube diameter
        if x==1
            x=2;
            break
        end
        td6_B2=(sqrt(((F2E(1,1)-B2(x,1))^2)+(F2E(1,2)-B2(x,2))^2)); %sum of
distances between all branch points to this point
        x=x-1;      %increment step
    end
    F2F=[B2(x,1) B2(x,2)];       %record value of point

%plot points
figure(2)
hold on
plot(F2A(1,1),F2A(1,2),'rx')
```

```
plot(F2B(1,1),F2B(1,2),'gx')
plot(F2C(1,1),F2C(1,2),'bx')
plot(F2D(1,1),F2D(1,2),'cx')
plot(F2E(1,1),F2E(1,2),'yx')
plot(F2F(1,1),F2F(1,2),'mx')

%create region zone and segment columns
L=size(ROImain,1);
region=zeros(L,1);
segment=zeros(L,1); %1=feed, 2=junction, 3=fc 4=branch
zone=zeros(L,1);

'allocating cell steps to regions and segments'
%fill region and segment columns
for H=1:L,
   if ROImain (H,4)>0%if cell is in feed
        %check if cell is in 6_12
        V0=[0,0];
        V1=F2B-F1B;
        V2=F1A-F1B;
        V=[ROImain(H,5)-F1B(1), ROImain(H,6)-F1B(2)];

        %calculate determinates (called terms)
        termVV2=(V(1,1)*V2(1,2))-(V(1,2)*V2(1,1));
        termV0V2=(V0(1,1)*V2(1,2))-(V0(1,2)*V2(1,1));
        termV1V2=(V1(1,1)*V2(1,2))-(V1(1,2)*V2(1,1));
        termVV1=(V(1,1)*V1(1,2))-(V(1,2)*V1(1,1));
        termV0V1=(V0(1,1)*V1(1,2))-(V0(1,2)*V1(1,1));

        a=(termVV2-termV0V2)/termV1V2;
        b=-(termVV1-termV0V1)/termV1V2;

        if a>0
           if b>0
              V1=F1A-F2A;
              V2=F2B-F2A;
              V=[ROImain(H,5)-F2A(1), ROImain(H,6)-F2A(2)];

              %calculate determinates (called terms)
              termVV2=(V(1,1)*V2(1,2))-(V(1,2)*V2(1,1));
              termV0V2=(V0(1,1)*V2(1,2))-(V0(1,2)*V2(1,1));
              termV1V2=(V1(1,1)*V2(1,2))-(V1(1,2)*V2(1,1));
              termVV1=(V(1,1)*V1(1,2))-(V(1,2)*V1(1,1));
              termV0V1=(V0(1,1)*V1(1,2))-(V0(1,2)*V1(1,1));
```

```
        a=(termVV2-termV0V2)/termV1V2;
        b=-(termVV1-termV0V1)/termV1V2;

        if a>0
           if b>0
              region(H)=612;
              segment(H)=1;
            end
         end
      end
 end
%check if cell is in 5_11
V0=[0,0];
V1=F2C-F1C;
V2=F1B-F1C;
V=[ROImain(H,5)-F1C(1), ROImain(H,6)-F1C(2)];

%calculate determinates (called terms)
termVV2=(V(1,1)*V2(1,2))-(V(1,2)*V2(1,1));
termV0V2=(V0(1,1)*V2(1,2))-(V0(1,2)*V2(1,1));
termV1V2=(V1(1,1)*V2(1,2))-(V1(1,2)*V2(1,1));
termVV1=(V(1,1)*V1(1,2))-(V(1,2)*V1(1,1));
termV0V1=(V0(1,1)*V1(1,2))-(V0(1,2)*V1(1,1));

a=(termVV2-termV0V2)/termV1V2;
b=-(termVV1-termV0V1)/termV1V2;

if a>0
   if b>0
      V1=F1B-F2B;
      V2=F2C-F2B;
      V=[ROImain(H,5)-F2B(1), ROImain(H,6)-F2B(2)];

      %calculate determinates (called terms)
      termVV2=(V(1,1)*V2(1,2))-(V(1,2)*V2(1,1));
      termV0V2=(V0(1,1)*V2(1,2))-(V0(1,2)*V2(1,1));
      termV1V2=(V1(1,1)*V2(1,2))-(V1(1,2)*V2(1,1));
      termVV1=(V(1,1)*V1(1,2))-(V(1,2)*V1(1,1));
      termV0V1=(V0(1,1)*V1(1,2))-(V0(1,2)*V1(1,1));

      a=(termVV2-termV0V2)/termV1V2;
      b=-(termVV1-termV0V1)/termV1V2;

      if a>0
         if b>0
```

```
            region(H)=511;
            segment(H)=1;
          end
        end
    end
 end
%check if cell is in 4_10
V0=[0,0];
V1=F2-F1;
V2=F1C-F1;
V=[ROImain(H,5)-F1(1), ROImain(H,6)-F1(2)];

%calculate determinates (called terms)
termVV2=(V(1,1)*V2(1,2))-(V(1,2)*V2(1,1));
termV0V2=(V0(1,1)*V2(1,2))-(V0(1,2)*V2(1,1));
termV1V2=(V1(1,1)*V2(1,2))-(V1(1,2)*V2(1,1));
termVV1=(V(1,1)*V1(1,2))-(V(1,2)*V1(1,1));
termV0V1=(V0(1,1)*V1(1,2))-(V0(1,2)*V1(1,1));

a=(termVV2-termV0V2)/termV1V2;
b=-(termVV1-termV0V1)/termV1V2;

if a>0
   if b>0
      V1=F1C-F2C;
      V2=F2-F2C;
      V=[ROImain(H,5)-F2C(1), ROImain(H,6)-F2C(2)];

      %calculate determinates (called terms)
      termVV2=(V(1,1)*V2(1,2))-(V(1,2)*V2(1,1));
      termV0V2=(V0(1,1)*V2(1,2))-(V0(1,2)*V2(1,1));
      termV1V2=(V1(1,1)*V2(1,2))-(V1(1,2)*V2(1,1));
      termVV1=(V(1,1)*V1(1,2))-(V(1,2)*V1(1,1));
      termV0V1=(V0(1,1)*V1(1,2))-(V0(1,2)*V1(1,1));

      a=(termVV2-termV0V2)/termV1V2;
      b=-(termVV1-termV0V1)/termV1V2;

      if a>0
         if b>0
            region(H)=410;
            segment(H)=2;
         end
      end
   end
```

```
 end
%check if cell is in 3_9
V0=[0,0];
V1=F2D-F1D;
V2=F1-F1D;
V=[ROImain(H,5)-F1D(1), ROImain(H,6)-F1D(2)];

%calculate determinates (called terms)
termVV2=(V(1,1)*V2(1,2))-(V(1,2)*V2(1,1));
termV0V2=(V0(1,1)*V2(1,2))-(V0(1,2)*V2(1,1));
termV1V2=(V1(1,1)*V2(1,2))-(V1(1,2)*V2(1,1));
termVV1=(V(1,1)*V1(1,2))-(V(1,2)*V1(1,1));
termV0V1=(V0(1,1)*V1(1,2))-(V0(1,2)*V1(1,1));

a=(termVV2-termV0V2)/termV1V2;
b=-(termVV1-termV0V1)/termV1V2;

if a>0
   if b>0
      V1=F1-F2;
      V2=F2D-F2;
      V=[ROImain(H,5)-F2(1), ROImain(H,6)-F2(2)];

      %calculate determinates (called terms)
      termVV2=(V(1,1)*V2(1,2))-(V(1,2)*V2(1,1));
      termV0V2=(V0(1,1)*V2(1,2))-(V0(1,2)*V2(1,1));
      termV1V2=(V1(1,1)*V2(1,2))-(V1(1,2)*V2(1,1));
      termVV1=(V(1,1)*V1(1,2))-(V(1,2)*V1(1,1));
      termV0V1=(V0(1,1)*V1(1,2))-(V0(1,2)*V1(1,1));

      a=(termVV2-termV0V2)/termV1V2;
      b=-(termVV1-termV0V1)/termV1V2;

      if a>0
         if b>0
            region(H)=39;
            segment(H)=2;
          end
       end
    end
 end

%check if cell is in 2_8
V0=[0,0];
V1=F2E-F1E;
```

```
V2=F1D-F1E;
V=[ROImain(H,5)-F1E(1), ROImain(H,6)-F1E(2)];

%calculate determinates (called terms)
termVV2=(V(1,1)*V2(1,2))-(V(1,2)*V2(1,1));
termV0V2=(V0(1,1)*V2(1,2))-(V0(1,2)*V2(1,1));
termV1V2=(V1(1,1)*V2(1,2))-(V1(1,2)*V2(1,1));
termVV1=(V(1,1)*V1(1,2))-(V(1,2)*V1(1,1));
termV0V1=(V0(1,1)*V1(1,2))-(V0(1,2)*V1(1,1));

a=(termVV2-termV0V2)/termV1V2;
b=-(termVV1-termV0V1)/termV1V2;

if a>0
   if b>0
      V1=F1D-F2D;
      V2=F2E-F2D;
      V=[ROImain(H,5)-F2D(1), ROImain(H,6)-F2D(2)];

      %calculate determinates (called terms)
      termVV2=(V(1,1)*V2(1,2))-(V(1,2)*V2(1,1));
      termV0V2=(V0(1,1)*V2(1,2))-(V0(1,2)*V2(1,1));
      termV1V2=(V1(1,1)*V2(1,2))-(V1(1,2)*V2(1,1));
      termVV1=(V(1,1)*V1(1,2))-(V(1,2)*V1(1,1));
      termV0V1=(V0(1,1)*V1(1,2))-(V0(1,2)*V1(1,1));

      a=(termVV2-termV0V2)/termV1V2;
      b=-(termVV1-termV0V1)/termV1V2;

      if a>0
         if b>0
            region(H)=28;
            segment(H)=3;
          end
       end
    end
 end

%check if cell is in 1_7
V0=[0,0];
V1=F2F-F1F;
V2=F1E-F1F;
V=[ROImain(H,5)-F1F(1), ROImain(H,6)-F1F(2)];

%calculate determinates (called terms)
```

```
    termVV2=(V(1,1)*V2(1,2))-(V(1,2)*V2(1,1));
    termV0V2=(V0(1,1)*V2(1,2))-(V0(1,2)*V2(1,1));
    termV1V2=(V1(1,1)*V2(1,2))-(V1(1,2)*V2(1,1));
    termVV1=(V(1,1)*V1(1,2))-(V(1,2)*V1(1,1));
    termV0V1=(V0(1,1)*V1(1,2))-(V0(1,2)*V1(1,1));

    a=(termVV2-termV0V2)/termV1V2;
    b=-(termVV1-termV0V1)/termV1V2;

    if a>0
       if b>0
          V1=F1E-F2E;
          V2=F2F-F2E;
          V=[ROImain(H,5)-F2E(1), ROImain(H,6)-F2E(2)];

          %calculate determinates (called terms)
          termVV2=(V(1,1)*V2(1,2))-(V(1,2)*V2(1,1));
          termV0V2=(V0(1,1)*V2(1,2))-(V0(1,2)*V2(1,1));
          termV1V2=(V1(1,1)*V2(1,2))-(V1(1,2)*V2(1,1));
          termVV1=(V(1,1)*V1(1,2))-(V(1,2)*V1(1,1));
          termV0V1=(V0(1,1)*V1(1,2))-(V0(1,2)*V1(1,1));

          a=(termVV2-termV0V2)/termV1V2;
          b=-(termVV1-termV0V1)/termV1V2;

          if a>0
             if b>0
                region(H)=17;
                segment(H)=3;
             end
          end
       end
    end
else          %if cell is in branch

 %check if cell is in 13_16
    V0=[0,0];
    V1=B3A-cept3;
    V2=cept4-cept3;
    V=[ROImain(H,14)-cept3(1), ROImain(H,15)-cept3(2)];

    %calculate determinates (called terms)
    termVV2=(V(1,1)*V2(1,2))-(V(1,2)*V2(1,1));
    termV0V2=(V0(1,1)*V2(1,2))-(V0(1,2)*V2(1,1));
    termV1V2=(V1(1,1)*V2(1,2))-(V1(1,2)*V2(1,1));
```

```
termVV1=(V(1,1)*V1(1,2))-(V(1,2)*V1(1,1));
termV0V1=(V0(1,1)*V1(1,2))-(V0(1,2)*V1(1,1));

a=(termVV2-termV0V2)/termV1V2;
b=-(termVV1-termV0V1)/termV1V2;

if a>0
   if b>0
      V1=cept4-B4A;
      V2=B3A-B4A;
      V=[ROImain(H,14)-B4A(1), ROImain(H,15)-B4A(2)];

      %calculate determinates (called terms)
      termVV2=(V(1,1)*V2(1,2))-(V(1,2)*V2(1,1));
      termV0V2=(V0(1,1)*V2(1,2))-(V0(1,2)*V2(1,1));
      termV1V2=(V1(1,1)*V2(1,2))-(V1(1,2)*V2(1,1));
      termVV1=(V(1,1)*V1(1,2))-(V(1,2)*V1(1,1));
      termV0V1=(V0(1,1)*V1(1,2))-(V0(1,2)*V1(1,1));

      a=(termVV2-termV0V2)/termV1V2;
      b=-(termVV1-termV0V1)/termV1V2;

      if a>0
         if b>0
            region(H)=1316;
            segment(H)=2;
         end
      end
   end
end

%check if cell is in 14_17
   V1=B3B-B3A;
   V2=B4A-B3A;
   V=[ROImain(H,14)-B3A(1), ROImain(H,15)-B3A(2)];

   %calculate determinates (called terms)
   termVV2=(V(1,1)*V2(1,2))-(V(1,2)*V2(1,1));
   termV0V2=(V0(1,1)*V2(1,2))-(V0(1,2)*V2(1,1));
   termV1V2=(V1(1,1)*V2(1,2))-(V1(1,2)*V2(1,1));
   termVV1=(V(1,1)*V1(1,2))-(V(1,2)*V1(1,1));
   termV0V1=(V0(1,1)*V1(1,2))-(V0(1,2)*V1(1,1));

   a=(termVV2-termV0V2)/termV1V2;
   b=-(termVV1-termV0V1)/termV1V2;
```

```
if a>0
   if b>0
      V1=B4A-B4B;
      V2=B3B-B4B;
      V=[ROImain(H,14)-B4B(1), ROImain(H,15)-B4B(2)];

      %calculate determinates (called terms)
      termVV2=(V(1,1)*V2(1,2))-(V(1,2)*V2(1,1));
      termV0V2=(V0(1,1)*V2(1,2))-(V0(1,2)*V2(1,1));
      termV1V2=(V1(1,1)*V2(1,2))-(V1(1,2)*V2(1,1));
      termVV1=(V(1,1)*V1(1,2))-(V(1,2)*V1(1,1));
      termV0V1=(V0(1,1)*V1(1,2))-(V0(1,2)*V1(1,1));

      a=(termVV2-termV0V2)/termV1V2;
      b=-(termVV1-termV0V1)/termV1V2;
      if a>0
         if b>0
            region(H)=1417;
            segment(H)=4;
         end
      end
   end
end
%check if cell is in 15_18
V1=B3C-B3B;
V2=B4B-B3B;
V=[ROImain(H,14)-B3B(1), ROImain(H,15)-B3B(2)];

%calculate determinates (called terms)
termVV2=(V(1,1)*V2(1,2))-(V(1,2)*V2(1,1));
termV0V2=(V0(1,1)*V2(1,2))-(V0(1,2)*V2(1,1));
termV1V2=(V1(1,1)*V2(1,2))-(V1(1,2)*V2(1,1));
termVV1=(V(1,1)*V1(1,2))-(V(1,2)*V1(1,1));
termV0V1=(V0(1,1)*V1(1,2))-(V0(1,2)*V1(1,1));

a=(termVV2-termV0V2)/termV1V2;
b=-(termVV1-termV0V1)/termV1V2;

if a>0
   if b>0
      V1=B4B-B4C;
      V2=B3C-B4C;
      V=[ROImain(H,14)-B4C(1), ROImain(H,15)-B4C(2)];
```

```
                    %calculate determinates (called terms)
                    termVV2=(V(1,1)*V2(1,2))-(V(1,2)*V2(1,1));
                    termV0V2=(V0(1,1)*V2(1,2))-(V0(1,2)*V2(1,1));
                    termV1V2=(V1(1,1)*V2(1,2))-(V1(1,2)*V2(1,1));
                    termVV1=(V(1,1)*V1(1,2))-(V(1,2)*V1(1,1));
                    termV0V1=(V0(1,1)*V1(1,2))-(V0(1,2)*V1(1,1));

                    a=(termVV2-termV0V2)/termV1V2;
                    b=-(termVV1-termV0V1)/termV1V2;
                    if a>0
                       if b>0
                          region(H)=1518;
                          segment(H)=4;
                       end
                    end
                 end
              end
           end
        end

%plot region cells
figure(2)
hold on
L=size(ROImain(:,1));
for H=1:L
   if region(H)==1316
      plot(ROImain(H,14),ROImain(H,15),'gd')
   elseif region(H)==1417
      plot(ROImain(H,14),ROImain(H,15),'rd')
   elseif region(H)==1518
      plot(ROImain(H,14),ROImain(H,15),'bd')
   elseif region(H)==17
      plot(ROImain(H,5),ROImain(H,6),'md')
   elseif region(H)==28
      plot(ROImain(H,5),ROImain(H,6),'yd')
   elseif region(H)==39
      plot(ROImain(H,5),ROImain(H,6),'cd')
   elseif region(H)==410
      plot(ROImain(H,5),ROImain(H,6),'bd')
   elseif region(H)==511
      plot(ROImain(H,5),ROImain(H,6),'gd')
   elseif region(H)==612
      plot(ROImain(H,5),ROImain(H,6),'rd')
   end
end
```

```
%fill zone columns
L=size(ROImain,1);
for H=1:L,
   if region(H)==1316
      if CB3(H)<5 && CB4(H)<5
         zone(H)=1316;
      elseif CB3(H)<5
         zone(H)=13;
      elseif CB4(H)<5
         zone(H)=16;
      end
   elseif region(H)==1417
      if CB3(H)<5 && CB4(H)<5
         zone(H)=1417;
      elseif CB3(H)<5
         zone(H)=14;
      elseif CB4(H)<5
         zone(H)=17;
      end
   elseif region(H)==1518
      if CB3(H)<5 && CB4(H)<5
         zone(H)=1518;
      elseif CB3(H)<5
         zone(H)=15;
      elseif CB4(H)<5
         zone(H)=18;
      end
   elseif region(H)==17
      if CB1(H)<5 && CB2(H)<5
         zone(H)=1700;
      elseif CB1(H)<5
         zone(H)=1;
      elseif CB2(H)<5
         zone(H)=7;
      end
   elseif region(H)==28
      if CB1(H)<5 && CB2(H)<5
         zone(H)=2800;
      elseif CB1(H)<5
         zone(H)=2;
      elseif CB2(H)<5
         zone(H)=8;
      end
   elseif region(H)==39
```

```
        if CB1(H)<5 && CB2(H)<5
            zone(H)=3900;
        elseif CB1(H)<5
            zone(H)=3;
        elseif CB2(H)<5
            zone(H)=9;
        end
    elseif region(H)==410
        if CB1(H)<5 && CB2(H)<5
            zone(H)=4100;
        elseif CB1(H)<5
            zone(H)=4;
        elseif CB2(H)<5
            zone(H)=10;
        end
    elseif region(H)==511
        if CB1(H)<5 && CB2(H)<5
            zone(H)=5110;
        elseif CB1(H)<5
            zone(H)=5;
        elseif CB2(H)<5
            zone(H)=11;
        end
    elseif region(H)==612
        if CB1(H)<5 && CB2(H)<5
            zone(H)=6120;
        elseif CB1(H)<5
            zone(H)=6;
        elseif CB2(H)<5
            zone(H)=12;
        end
    end
end

%concatenate segment(29), zone(30), region(31) columns onto ROImain (in that
order)
ROImain=[ROImain segment zone region];

'calculating angles: Currently out of order'
% angle calculation, will not work if no branch data, CURRENTLY USES 1TD
% AND 2 TD!!
if side==0
else
% define branch line
    % midpoint between B4A and B3A
```

```
xmidBA=(B4A(1,1)+B3A(1,1))/2;
ymidBA=(B4A(1,2)+B3A(1,2))/2;

%branch line point 1

BL1=[xmidBA,ymidBA];

% midpoint between B4B and B3B

xmidBB=(B4B(1,1)+B3B(1,1))/2;
ymidBB=(B4B(1,2)+B3B(1,2))/2;

%branch line point 2

BL2=[xmidBB,ymidBB];

% define feed line
% midpoint between F1B and F2B

xmidFB=(F1B(1,1)+F2B(1,1))/2;
ymidFB=(F1B(1,2)+F2B(1,2))/2;

%feed line point 2

FL2=[xmidFB,ymidFB];

% midpoint between F1C and F2C

xmidFC=(F1C(1,1)+F2C(1,1))/2;
ymidFC=(F1C(1,2)+F2C(1,2))/2;

%feed line point 1

FL1=[xmidFC,ymidFC];

% define feed continuation line
% midpoint between F1D and F2D

xmidFD=(F1D(1,1)+F2D(1,1))/2;
ymidFD=(F1D(1,2)+F2D(1,2))/2;

%continuation line point 1

CL1=[xmidFD,ymidFD];
```

```
    % midpoint between F1E and F2E

       xmidFE=(F1E(1,1)+F2E(1,1))/2;
       ymidFE=(F1E(1,2)+F2E(1,2))/2;

       %continuation line point 1

       CL2=[xmidFE,ymidFE];

% find angles of intersection
    %angle between feed line and branch line (lateral angle, LA)

      LAnumerator = dot((FL2-FL1),(BL2-BL1));
      LAdenominator = (sqrt(((FL1(1)-FL2(1))^2)+(FL1(2)-
FL2(2))^2))*(sqrt(((BL1(1)-BL2(1))^2)+(BL1(2)-BL2(2))^2));
      LAr = acos(LAnumerator/LAdenominator);
      LA = (LAr*180)/pi;

    %angle between feed continuation and branch line (apical angle,AA)

      AAnumerator = dot((CL2-CL1),(BL2-BL1));
      AAdenominator = (sqrt(((CL1(1)-CL2(1))^2)+(CL1(2)-
CL2(2))^2))*(sqrt(((BL1(1)-BL2(1))^2)+(BL1(2)-BL2(2))^2));
      AAr = acos(AAnumerator/AAdenominator);
      AA = (AAr*180)/pi;

    %angle between feed line and feed continuation line (continuation
    %angle, CA)

      CAnumerator = dot((CL2-CL1),(FL2-FL1));
      CAdenominator = (sqrt(((CL1(1)-CL2(1))^2)+(CL1(2)-
CL2(2))^2))*(sqrt(((FL1(1)-FL2(1))^2)+(FL1(2)-FL2(2))^2));
      CAr = acos(CAnumerator/CAdenominator);
      CA = (CAr*180)/pi;

    %calculated continuation angle (360-(AA+LA)) CCA

     CCA = 360 - (AA + LA);

 end

 'building cellwise matrix'
%build cellwise matrix (cellmat)
cellmax=max(ROImain(:,23));
```

```
L=size(ROImain,1); %number of lines in ROImain, one frame corresponds to a
single cell step

%determine max number of steps per cell
%each row of steps matrix corresponds to a single cell in order, ie row 1
%is cell #1, first column is number of steps for that cell, second column
%is the first frame that cell appears and third column is last frame that cell
appears

steps=zeros(cellmax,3);
for H=1:L,
   for i=1:cellmax,
      if ROImain(H,23)==i %go through by cell
         if steps(i,1)==0 %if this is the first step of this cell
           steps(i,2)=ROImain(H,1); %second column records frame number of
first step of cell
         end
         steps(i,1)=steps(i,1)+1; %increment number of steps
         steps(i,3)=ROImain(H,1); %record frame of last step
      end
   end
end

stepmax=max(steps,1);

%build first page
cellmat=zeros(stepmax,13);

%fill matrix with values from ROI per cell
%columns: 1=line, 2=frame, 3=reg 4=x 5=y 6=CB1 7=CB2 13=zone 14=diameter
for H=1:cellmax,
   inc=0;
   cellmat(:,:,H)=0;
   for i=1:L,
      if H==ROImain(i,23)
         ROImainCell=ROImain(i,23);
         inc=inc+1;
         cellmat(inc,1,H)=i;
         cellmat(inc,2,H)=ROImain(i,1);
         cellmat(inc,3,H)=ROImain(i,31);
         cellmat(inc,13,H)=ROImain(i,30);
         if ROImain(i,4)>0
            cellmat(inc,4,H)=ROImain(i,5);
            cellmat(inc,5,H)=ROImain(i,6);
            cellmat(inc,6,H)=ROImain(i,24);
```

```
            cellmat(inc,7,H)=ROImain(i,25);
            cellmat(inc,14,H)=sqrt(((ROImain(i,10)-
ROImain(i,7))^2)+((ROImain(i,11)-ROImain(i,8))^2));
         else
            cellmat(inc,4,H)=ROImain(i,14);
            cellmat(inc,5,H)=ROImain(i,15);
            cellmat(inc,6,H)=ROImain(i,26);
            cellmat(inc,7,H)=ROImain(i,27);
            cellmat(inc,14,H)=sqrt(((ROImain(i,19)-
ROImain(i,16))^2)+((ROImain(i,20)-ROImain(i,17))^2));
         end
      end
   end
end
% remove all empty pages
for H=cellmax:-1:1,
   if cellmat(1,1,H)==0
      cellmat(:,:,H)=[];
   end
end

temp=size(cellmat);
cellmax=temp(3);

'calculating stepwise velocities and shear'
%put previous x,y in cellmat and calculate velocity and stepwise shear
% column 8=prevx 9=prevy 10=velocity 11=shearboundary1 12=shearboundary2
for H=1:cellmax,
   %find maximum number of steps for that cell
   cellstep=steps(H,1);
   for i=2:cellstep,
      cellmat(i,8,H)=cellmat(i-1,4,H);
      cellmat(i,9,H)=cellmat(i-1,5,H);

      if cellmat(i,1,H)==0
      else
      V=sqrt(((cellmat(i,4,H)-cellmat((i-1),4,H))^2)+((cellmat(i,5,H)-cellmat((i-
1),5,H))^2))*60;
      if V==0
        cellmat(i,10,H)=1/(1/60);
      else
        cellmat(i,10,H)=V;
      end

      if cellmat(i,6,H)<=5
```

```
        cellmat(i,11,H)=cellmat(i,10,H)/cellmat(i,6,H);
      end

      if cellmat(i,7,H)<=5
        cellmat(i,12,H)=cellmat(i,10,H)/cellmat(i,7,H);
      end
  end
end
end

'determining origin of branch cells'
%attach branch cells to proper feed cell
%identify feed cells that correspond to branch cells

cellmatch=zeros(cellmax,3);

inc=1;
for H=1:cellmax, %test each cell
   frame1b=0;
   if cellmat(1,3,H)==1316  %if first step is in region 1316
      frame1b=cellmat(1,2,H); %record first frame
      frameL=0;
      for i=1:H,  %for each cell prior
         frameL=max(cellmat(:,2,i)); %record the last frame
         if frameL==frame1b || frameL==frame1b-1 %if the last frame is the same
as the first (or the first minus 1)
            L=size(cellmat,1);
            reglast=0;
            for j=1:L, %find the region in the last frame
               if cellmat(j,3,i)>0
                  reglast=cellmat(j,3,i);
               end
            end
         if reglast==39 || reglast==410  %if the region in the last frame is region 39
or 410
             posdist=sqrt(((cellmat(1,4,H)-cellmat(1,4,i))^2)+((cellmat(1,5,H)-
cellmat(1,5,i))^2));
             cellmatch(inc,:)=[H,i,posdist]; %record the branch cell # the feed cell #
             inc=inc+1;
         end
         end
      end
   end
end
```

```
%check that only one cell feeds each branch cell - assumes that closer cell
%goes down branch

L=size(cellmatch,1);
   for i=L:-1:2,
      if cellmatch(i,1)==cellmatch(i-1,1)
         if cellmatch(i,3) <= cellmatch(i-1,3)
            cellmatch(i,:)=[];
         else
            cellmatch(i-1,:)=[];
         end
      end
   end

%FOR DEBUGGING: cellmat backup before changes
cellmatbackup=cellmat;

%change cell numbers of branch cells to equal corresponding feed cell
L=size(cellmatch,1); %size of cellmatch matrix
X=size(cellmat,1); %number of rows per cell matrix page
linenum=0;
for i=1:L,
   branchcell=cellmatch(i,1);
   feedcell=cellmatch(i,2);
   if feedcell==0
      break
   end
   temp=zeros(X,14);
      j=1;
      while cellmat(j,1,feedcell)~=0,
           temp(j,:)=cellmat(j,:,feedcell);
           cellmat(j,:,feedcell)=0;
           j=j+1;
      end
      H=1;
      while cellmat(H,1,branchcell)~=0,
           temp(j+H-1,:)=cellmat(H,:,branchcell);
           cellmat(H,:,branchcell)=0;
           H=H+1;
      end
      check=size(temp,1);
      inc=linenum;
      while check < X,
         temp(inc,:)=0;
         linenum=inc+1;
```

```
        check=size(temp,1);
    end
    while check>X
        cellmat(X+1,:,:)=0;
        X=X+1;
    end
    cellmat(:,:,feedcell)=temp;
end

'calculating values for cellwise matrix'
regHvel = zeros(9,2); %harmonic average of velocity by region
bulkshear = zeros(9,2); %output bulk shear by region
segvel = zeros(4,2); %output average of velocity by segment
segshear = zeros(4,2); %output bulk shear by segment

%fill region column
for i=1:6,
   regHvel(i,1)=i;
   bulkshear(i,1)=i;
end
for i=7:9,
   regHvel(i,1)=i+6;
   bulkshear(i,1)=i+6;
end

%fill shear column
for i=1:4,
   segvel(i,1)=i;
   segshear(i,1)=i;
end

pages=size(cellmat,3); %number of cells
rows=size(cellmat,1);  %number of steps per cell
VbRavg = zeros(pages,9); %matrix of average velocity per cell by region
VbSavg = zeros(pages,4); %matrix of average velocity per cell by segment

Dreg = zeros(9,2); %matrix of average diameter by region
Dtot17=0; %Dtot*  and Dinc* allow calculation of regional diameters,
Dinc17=0;
Dtot28=0;
Dinc28=0;
Dtot39=0;
Dinc39=0;
Dtot410=0;
Dinc410=0;
```

```
Dtot511=0;
Dinc511=0;
Dtot612=0;
Dinc612=0;
Dtot1316=0;
Dinc1316=0;
Dtot1417=0;
Dinc1417=0;
Dtot1518=0;
Dinc1518=0;

%Dinc* and Dtot* allow calculation of segment diameters

Dtot1=0;
Dinc1=0;
Dtot2=0;
Dinc2=0;
Dtot3=0;
Dinc3=0;
Dtot4=0;
Dinc4=0;

for i=1:pages, %go through each cell, tot* and inc* are for regional velocities tot*
and inc* for region, Stot* and Sinc* for Segment
    Stot1=0;
    Sinc1=0;
    Stot2=0;
    Sinc2=0;
    Stot3=0;
    Sinc3=0;
    Stot4=0;
    Sinc4=0;
    tot17=0;
    inc17=0;
    tot28=0;
    inc28=0;
    tot39=0;
    inc39=0;
    tot410=0;
    inc410=0;
    tot511=0;
    inc511=0;
    tot612=0;
    inc612=0;
    tot1316=0;
```

```
inc1316=0;
tot1417=0;
inc1417=0;
tot1518=0;
inc1518=0;

for j=1:rows,   %go through each row
   if cellmat(j,3,i)==17 && cellmat(j,10,i)>0  %for each cell in the region, take
average only if nonzero

      %region
      tot17=tot17+cellmat(j,10,i);
      inc17=inc17+1;
      Dtot17=Dtot17+cellmat(j,14,i);
      Dinc17=Dinc17+1;
      VbRavg(i,1)=tot17/inc17;

      %segment
      Stot3=Stot3+cellmat(j,10,i);
      Sinc3=Sinc3+1;
      Dtot3=Dtot3+cellmat(j,14,i);
      Dinc3=Dinc3+1;
      VbSavg(i,3)=Stot3/Sinc3;

   elseif cellmat(j,3,i)==28 && cellmat(j,10,i)>0

      %region
      tot28=tot28+cellmat(j,10,i);
      inc28=inc28+1;
      Dtot28=Dtot28+cellmat(j,14,i);
      Dinc28=Dinc28+1;
      VbRavg(i,2)=tot28/inc28;

      %segment
      Stot3=Stot3+cellmat(j,10,i);
      Sinc3=Sinc3+1;
      Dtot3=Dtot3+cellmat(j,14,i);
      Dinc3=Dinc3+1;
      VbSavg(i,3)=Stot3/Sinc3;

   elseif cellmat(j,3,i)==39 && cellmat(j,10,i)>0

      %region
      tot39=tot39+cellmat(j,10,i);
      inc39=inc39+1;
```

```
    Dtot39=Dtot39+cellmat(j,14,i);
    Dinc39=Dinc39+1;
    VbRavg(i,3)=tot39/inc39;

    %segment
    Stot2=Stot2+cellmat(j,10,i);
    Sinc2=Sinc2+1;
    Dtot2=Dtot2+cellmat(j,14,i);
    Dinc2=Dinc2+1;
    VbSavg(i,2)=Stot2/Sinc2;

elseif cellmat(j,3,i)==410 && cellmat(j,10,i)>0

    %region
    tot410=tot410+cellmat(j,10,i);
    inc410=inc410+1;
    Dtot410=Dtot410+cellmat(j,14,i);
    Dinc410=Dinc410+1;
    VbRavg(i,4)=tot410/inc410;

    %segment
    Stot2=Stot2+cellmat(j,10,i);
    Sinc2=Sinc2+1;
    Dtot2=Dtot2+cellmat(j,14,i);
    Dinc2=Dinc2+1;
    VbSavg(i,2)=Stot2/Sinc2;

elseif cellmat(j,3,i)==511 && cellmat(j,10,i)>0

    %region
    tot511=tot511+cellmat(j,10,i);
    inc511=inc511+1;
    Dtot511=Dtot511+cellmat(j,14,i);
    Dinc511=Dinc511+1;
    VbRavg(i,5)=tot511/inc511;

    %segment
    Stot1=Stot1+cellmat(j,10,i);
    Sinc1=Sinc1+1;
    Dtot1=Dtot1+cellmat(j,14,i);
    Dinc1=Dinc1+1;
    VbSavg(i,1)=Stot1/Sinc1;

elseif cellmat(j,3,i)==612 && cellmat(j,10,i)>0
```

```
    %region
    tot612=tot612+cellmat(j,10,i);
    inc612=inc612+1;
    Dtot612=Dtot612+cellmat(j,14,i);
    Dinc612=Dinc612+1;
    VbRavg(i,6)=tot612/inc612;

    %segment
    Stot1=Stot1+cellmat(j,10,i);
    Sinc1=Sinc1+1;
    Dtot1=Dtot1+cellmat(j,14,i);
    Dinc1=Dinc1+1;
    VbSavg(i,1)=Stot1/Sinc1;

elseif cellmat(j,3,i)==1316 && cellmat(j,10,i)>0

    %region
    tot1316=tot1316+cellmat(j,10,i);
    inc1316=inc1316+1;
    Dtot1316=Dtot1316+cellmat(j,14,i);
    Dinc1316=Dinc1316+1;
    VbRavg(i,7)=tot1316/inc1316;

    %segment
    Stot2=Stot2+cellmat(j,10,i);
    Sinc2=Sinc2+1;
    Dtot2=Dtot2+cellmat(j,14,i);
    Dinc2=Dinc2+1;
    VbSavg(i,2)=Stot2/Sinc2;

elseif cellmat(j,3,i)==1417 && cellmat(j,10,i)>0

    %region
    tot1417=tot1417+cellmat(j,10,i);
    inc1417=inc1417+1;
    Dtot1417=Dtot1417+cellmat(j,14,i);
    Dinc1417=Dinc1417+1;
    VbRavg(i,8)=tot1417/inc1417;

    %segment
    Stot4=Stot4+cellmat(j,10,i);
    Sinc4=Sinc4+1;
    Dtot4=Dtot4+cellmat(j,14,i);
    Dinc4=Dinc4+1;
    VbSavg(i,4)=Stot4/Sinc4;
```

```
    elseif cellmat(j,3,i)==1518 && cellmat(j,10,i)>0

        %region
        tot1518=tot1518+cellmat(j,10,i);
        inc1518=inc1518+1;
        Dtot1518=Dtot1518+cellmat(j,14,i);
        Dinc1518=Dinc1518+1;
        VbRavg(i,9)=tot1518/inc1518;

        %segment
        Stot4=Stot4+cellmat(j,10,i);
        Sinc4=Sinc4+1;
        Dtot4=Dtot4+cellmat(j,14,i);
        Dinc4=Dinc4+1;
        VbSavg(i,4)=Stot4/Sinc4;

     end
   end
end

Dreg(1,1)=17; RegVel(1,1)=17;
Dreg(1,2)=Dtot17/Dinc17;
Dreg(2,1)=28; RegVel(2,1)=28;
Dreg(2,2)=Dtot28/Dinc28;
Dreg(3,1)=39; RegVel(3,1)=39;
Dreg(3,2)=Dtot39/Dinc39;
Dreg(4,1)=410; RegVel(4,1)=410;
Dreg(4,2)=Dtot410/Dinc410;
Dreg(5,1)=511; RegVel(5,1)=511;
Dreg(5,2)=Dtot511/Dinc511;
Dreg(6,1)=612; RegVel(6,1)=612;
Dreg(6,2)=Dtot612/Dinc612;
Dreg(7,1)=1316; RegVel(7,1)=1316;
Dreg(7,2)=Dtot1316/Dinc1316;
Dreg(8,1)=1417; RegVel(8,1)=1417;
Dreg(8,2)=Dtot1417/Dinc1417;
Dreg(9,1)=1518; RegVel(9,1)=1518;
Dreg(9,2)=Dtot1518/Dinc1518;

Dseg(1,1)=1; segVel(1,1)=1;
Dseg(1,2)=Dtot1/Dinc1;
Dseg(2,1)=2; segVel(2,1)=2;
Dseg(2,2)=Dtot2/Dinc2;
Dseg(3,1)=3; segVel(3,1)=3;
```

```
   Dseg(3,2)=Dtot3/Dinc3;
   Dseg(4,1)=4; segVel(4,1)=4;
   Dseg(4,2)=Dtot4/Dinc4;


rowsVB=size(VbRavg,1);
   for i=1:rowsVB, %calculate harmonic mean for Velocity and Bulkshear for each
region
       totVb=0;
       incVb=1;
       for j=1:9,
          if VbRavg(i,j)>0
          totVb=totVb+(1/VbRavg(i,j));
          incVb=incVb+1;
          RegVel(j,2)=1/(totVb/incVb);
          bulkshear(j,2)=(8*RegVel(j,2))/Dreg(j,2);
       end
   end
end

rowsSVB=size(VbSavg,1);
for i=1:rowsSVB, %calculate harmonic mean for each segment
       StotVb=0;
       SincVb=1;
       for j=1:4,
          if VbSavg(i,j)>0
          StotVb=StotVb+(1/VbSavg(i,j));
          SincVb=SincVb+1;
          segvel(j,2)=1/(StotVb/SincVb);
          segshear(j,2)=(8*segvel(j,2))/Dseg(j,2);
       end
   end
end

stepshear = zeros(18,2); %output stepwise shear and velocity by zone
%fill zone column
for i=1:18,
   stepshear(i,1)=i;
   zonevel(i,1)=i;
end

WSbZavg = zeros(pages,18); %matrix of average wall shear per cell by zone
VelbZavg = zeros(pages,18); %matrix of average velocity per cell by zone
for k=1:18, %for each feed zone
for i=1:pages, %go through each cell
```

```
totb1=0;  %boundaries 1 and 2 separately totb* for shear Vtotb* for Velocity
 Vtotb1=0;
 incb1=0;
 totb2=0;
 Vtotb2=0;
 incb2=0;
 for j=1:rows,   %go through each row
    if cellmat(j,13,i)>1000
       if cellmat(j,13,i)==1700
          z1=1;
          z2=7;
       elseif cellmat(j,13,i)==2800
          z1=2;
          z2=8;
       elseif cellmat(j,13,i)==3900
          z1=3;
          z2=9;
       elseif cellmat(j,13,i)==4100
          z1=4;
          z2=10;
       elseif cellmat(j,13,i)==5110
          z1=5;
          z2=10;
       elseif cellmat(j,13,i)==6120
          z1=6;
          z2=12;
       elseif cellmat(j,13,i)==1316
          z1=13;
          z2=16;
       elseif cellmat(j,13,i)==1417
          z1=14;
          z2=17;
       elseif cellmat(j,13,i)==1518
          z1=15;
          z2=18;
       end
    else
       z1=cellmat(j,13,i);
       z2=cellmat(j,13,i);
    end
    if k==1 || k==2 || k==3 || k==4 || k==5 || k==6 || k==13 || k==14 ||k==15
       if z1==k && cellmat(j,11,i)>0  %for each shear on boundary 1 in the
region, take average only if nonzero
          totb1=totb1+cellmat(j,11,i);
```

```
            Vtotb1=Vtotb1+cellmat(j,10,i);
            incb1=incb1+1;
            WSbZavg(i,k)=totb1/incb1;
            VelbZavg(i,k)=Vtotb1/incb1;
         end
      end
      if k==7 || k==8 || k==9 || k==10 || k==11 || k==12 || k==16 || k==17 ||k==18
         if z2==k && cellmat(j,12,i)>0  %for each shear on boundary 2 in the
region, take average only if nonzero
            totb2=totb2+cellmat(j,12,i);
            Vtotb2=Vtotb2+cellmat(j,10,i);
            incb2=incb2+1;
            WSbZavg(i,k)=totb2/incb2;
            VelbZavg(i,k)=Vtotb2/incb2;
         end
      end
   end
end

rowsWS=size(WSbZavg,1);
   for i=1:rowsWS, %calculate harmonic mean for each zone
      totWS=0;
      totV=0;
      incWS=1;
      for j=1:18,
         if WSbZavg(i,j)>0
         totWS=totWS+(1/WSbZavg(i,j));
         totV=totV+(1/VelbZavg(i,j));
         incWS=incWS+1;
         stepshear(j,2)=1/(totWS/incWS);
         zonevel(j,2)=1/(totV/incWS);
      end
   end
end
```

SECONDARY DATA ANALYSIS AND OUTPUT

```
%clear old data
clear segvel
clear dboutput
clear RegVel

%move Repaired cells to corrcellmat for finishing
for i=1:pages,
```

```
    if holdcell(1,:,i)==0
    else
      corrcellmat(:,:,i)=holdcell(:,:,i);
        i;
    end
end

%remove 0 steps
for i=1:pages,
    L=size(corrcellmat,1);
    while sum(corrcellmat(1,:,i))==0 && sum(corrcellmat(:,1,i))~=0
        for j=1:L-1,
            corrcellmat(j,:,i)=corrcellmat(j+1,:,i);
        end
    end
end

%put corrected values back in original matrix
cellmat=corrcellmat(:,:,:);

%recheck previous x,y in cellmat
L=size(cellmat);
if cellmax==1
else
cellmax=L(3);
end

%put previous x,y in cellmat and calculate velocity and stepwise shear
% column 8=prevx 9=prevy 10=velocity 11=shearboundary1 12=shearboundary2
cellstep=zeros(cellmax,1);
for H=1:cellmax,
    inc=0;
    %find maximum number of steps for that cell
    stepmax=L(1);
    for j=1:stepmax,
        if cellmat(j,1,H)==0
        break
        else
        inc=inc+1;
        cellstep(H)=inc;
    end
end

    cellmat(1,8,H)=0;
    cellmat(1,9,H)=0;
```

```
    cellmat(1,10,H)=0;

    for i=2:cellstep(H),
        cellmat(i,8,H)=cellmat(i-1,4,H);
        cellmat(i,9,H)=cellmat(i-1,5,H);

        if cellmat(i,8,H)==0
            cellmat(i,10,H)=0;
        else
        V=sqrt(((cellmat(i,4,H)-cellmat((i-1),4,H))^2)+((cellmat(i,5,H)-cellmat((i-
1),5,H))^2))*60;
        if V==0
           cellmat(i,10,H)=1/(1/60);
        else
           cellmat(i,10,H)=V;
        end

        if cellmat(i,6,H)<=5
           cellmat(i,11,H)=cellmat(i,10,H)/cellmat(i,6,H);
        end

        if cellmat(i,7,H)<=5
          cellmat(i,12,H)=cellmat(i,10,H)/cellmat(i,7,H);
        end
    end
end
end

%recalculate vectors used to calculate results

regHvel = zeros(9,2); %harmonic average of velocity by region
bulkshear = zeros(9,2); %output bulk shear by region
segvel = zeros(4,2); %output average of velocity by segment
segshear = zeros(4,2); %output bulk shear by segment

%fill region column
for i=1:6,
    regHvel(i,1)=i;
    bulkshear(i,1)=i;
end
for i=7:9,
    regHvel(i,1)=i+6;
    bulkshear(i,1)=i+6;
end
```

```
%fill shear column
for i=1:4,
   segvel(i,1)=i;
   segshear(i,1)=i;
end

pages=size(cellmat,3); %number of cells
rows=size(cellmat,1);  %number of steps per cell
VbRavg = zeros(pages,9); %matrix of average velocity per cell by region
VbSavg = zeros(pages,4); %matrix of average velocity per cell by segment

Dreg = zeros(9,2); %matrix of average diameter by region
Dtot17=0; %Dtot*  and Dinc* allow calculation of regional diameters,
Dinc17=0;
Dtot28=0;
Dinc28=0;
Dtot39=0;
Dinc39=0;
Dtot410=0;
Dinc410=0;
Dtot511=0;
Dinc511=0;
Dtot612=0;
Dinc612=0;
Dtot1316=0;
Dinc1316=0;
Dtot1417=0;
Dinc1417=0;
Dtot1518=0;
Dinc1518=0;

%Dinc* and Dtot* allow calculation of segment diameters

Dtot1=0;
Dinc1=0;
Dtot2=0;
Dinc2=0;
Dtot3=0;
Dinc3=0;
Dtot4=0;
Dinc4=0;

for i=1:pages, %go through each cell, tot* and inc* are for regional velocities tot*
and inc* for region, Stot* and Sinc* for Segment
       Stot1=0;
```

```
Sinc1=0;
Stot2=0;
Sinc2=0;
Stot3=0;
Sinc3=0;
Stot4=0;
Sinc4=0;
tot17=0;
inc17=0;
tot28=0;
inc28=0;
tot39=0;
inc39=0;
tot410=0;
inc410=0;
tot511=0;
inc511=0;
tot612=0;
inc612=0;
tot1316=0;
inc1316=0;
tot1417=0;
inc1417=0;
tot1518=0;
inc1518=0;

for j=1:rows,   %go through each row
   if cellmat(j,3,i)==17 && cellmat(j,10,i)>0  %for each cell in the region, take
average only if nonzero

      %region
      tot17=tot17+cellmat(j,10,i);
      inc17=inc17+1;
      Dtot17=Dtot17+cellmat(j,14,i);
      Dinc17=Dinc17+1;
      VbRavg(i,1)=tot17/inc17;

      %segment
      Stot3=Stot3+cellmat(j,10,i);
      Sinc3=Sinc3+1;
      Dtot3=Dtot3+cellmat(j,14,i);
      Dinc3=Dinc3+1;
      VbSavg(i,3)=Stot3/Sinc3;

   elseif cellmat(j,3,i)==28 && cellmat(j,10,i)>0
```

```
    %region
    tot28=tot28+cellmat(j,10,i);
    inc28=inc28+1;
    Dtot28=Dtot28+cellmat(j,14,i);
    Dinc28=Dinc28+1;
    VbRavg(i,2)=tot28/inc28;

    %segment
    Stot3=Stot3+cellmat(j,10,i);
    Sinc3=Sinc3+1;
    Dtot3=Dtot3+cellmat(j,14,i);
    Dinc3=Dinc3+1;
    VbSavg(i,3)=Stot3/Sinc3;

elseif cellmat(j,3,i)==39 && cellmat(j,10,i)>0

    %region
    tot39=tot39+cellmat(j,10,i);
    inc39=inc39+1;
    Dtot39=Dtot39+cellmat(j,14,i);
    Dinc39=Dinc39+1;
    VbRavg(i,3)=tot39/inc39;

    %segment
    Stot2=Stot2+cellmat(j,10,i);
    Sinc2=Sinc2+1;
    Dtot2=Dtot2+cellmat(j,14,i);
    Dinc2=Dinc2+1;
    VbSavg(i,2)=Stot2/Sinc2;

elseif cellmat(j,3,i)==410 && cellmat(j,10,i)>0

    %region
    tot410=tot410+cellmat(j,10,i);
    inc410=inc410+1;
    Dtot410=Dtot410+cellmat(j,14,i);
    Dinc410=Dinc410+1;
    VbRavg(i,4)=tot410/inc410;

    %segment
    Stot2=Stot2+cellmat(j,10,i);
    Sinc2=Sinc2+1;
    Dtot2=Dtot2+cellmat(j,14,i);
    Dinc2=Dinc2+1;
```

```
    VbSavg(i,2)=Stot2/Sinc2;

elseif cellmat(j,3,i)==511 && cellmat(j,10,i)>0

    %region
    tot511=tot511+cellmat(j,10,i);
    inc511=inc511+1;
    Dtot511=Dtot511+cellmat(j,14,i);
    Dinc511=Dinc511+1;
    VbRavg(i,5)=tot511/inc511;

    %segment
    Stot1=Stot1+cellmat(j,10,i);
    Sinc1=Sinc1+1;
    Dtot1=Dtot1+cellmat(j,14,i);
    Dinc1=Dinc1+1;
    VbSavg(i,1)=Stot1/Sinc1;

elseif cellmat(j,3,i)==612 && cellmat(j,10,i)>0

    %region
    tot612=tot612+cellmat(j,10,i);
    inc612=inc612+1;
    Dtot612=Dtot612+cellmat(j,14,i);
    Dinc612=Dinc612+1;
    VbRavg(i,6)=tot612/inc612;

    %segment
    Stot1=Stot1+cellmat(j,10,i);
    Sinc1=Sinc1+1;
    Dtot1=Dtot1+cellmat(j,14,i);
    Dinc1=Dinc1+1;
    VbSavg(i,1)=Stot1/Sinc1;

elseif cellmat(j,3,i)==1316 && cellmat(j,10,i)>0

    %region
    tot1316=tot1316+cellmat(j,10,i);
    inc1316=inc1316+1;
    Dtot1316=Dtot1316+cellmat(j,14,i);
    Dinc1316=Dinc1316+1;
    VbRavg(i,7)=tot1316/inc1316;

    %segment
    Stot2=Stot2+cellmat(j,10,i);
```

```
            Sinc2=Sinc2+1;
            Dtot2=Dtot2+cellmat(j,14,i);
            Dinc2=Dinc2+1;
            VbSavg(i,2)=Stot2/Sinc2;

        elseif cellmat(j,3,i)==1417 && cellmat(j,10,i)>0

            %region
            tot1417=tot1417+cellmat(j,10,i);
            inc1417=inc1417+1;
            Dtot1417=Dtot1417+cellmat(j,14,i);
            Dinc1417=Dinc1417+1;
            VbRavg(i,8)=tot1417/inc1417;

            %segment
            Stot4=Stot4+cellmat(j,10,i);
            Sinc4=Sinc4+1;
            Dtot4=Dtot4+cellmat(j,14,i);
            Dinc4=Dinc4+1;
            VbSavg(i,4)=Stot4/Sinc4;

        elseif cellmat(j,3,i)==1518 && cellmat(j,10,i)>0

            %region
            tot1518=tot1518+cellmat(j,10,i);
            inc1518=inc1518+1;
            Dtot1518=Dtot1518+cellmat(j,14,i);
            Dinc1518=Dinc1518+1;
            VbRavg(i,9)=tot1518/inc1518;

            %segment
            Stot4=Stot4+cellmat(j,10,i);
            Sinc4=Sinc4+1;
            Dtot4=Dtot4+cellmat(j,14,i);
            Dinc4=Dinc4+1;
            VbSavg(i,4)=Stot4/Sinc4;

        end
    end
end

Dreg(1,1)=17; RegVel(1,1)=17;
Dreg(1,2)=Dtot17/Dinc17;
Dreg(2,1)=28; RegVel(2,1)=28;
Dreg(2,2)=Dtot28/Dinc28;
```

```
   Dreg(3,1)=39; RegVel(3,1)=39;
   Dreg(3,2)=Dtot39/Dinc39;
   Dreg(4,1)=410; RegVel(4,1)=410;
   Dreg(4,2)=Dtot410/Dinc410;
   Dreg(5,1)=511; RegVel(5,1)=511;
   Dreg(5,2)=Dtot511/Dinc511;
   Dreg(6,1)=612; RegVel(6,1)=612;
   Dreg(6,2)=Dtot612/Dinc612;
   Dreg(7,1)=1316; RegVel(7,1)=1316;
   Dreg(7,2)=Dtot1316/Dinc1316;
   Dreg(8,1)=1417; RegVel(8,1)=1417;
   Dreg(8,2)=Dtot1417/Dinc1417;
   Dreg(9,1)=1518; RegVel(9,1)=1518;
   Dreg(9,2)=Dtot1518/Dinc1518;

   Dseg(1,1)=1; segvel(1,1)=1;
   Dseg(1,2)=Dtot1/Dinc1;
   Dseg(2,1)=2; segvel(2,1)=2;
   Dseg(2,2)=Dtot2/Dinc2;
   Dseg(3,1)=3; segvel(3,1)=3;
   Dseg(3,2)=Dtot3/Dinc3;
   Dseg(4,1)=4; segvel(4,1)=4;
   Dseg(4,2)=Dtot4/Dinc4;


rowsVB=size(VbRavg,1);
   for j=1:9, %calculate harmonic mean for Velocity and Bulkshear for each
region
       totVb=0;
       incVb=1;
       for i=1:rowsVB,
          if VbRavg(i,j)>0
          totVb=totVb+(1/VbRavg(i,j));
          RegVel(j,2)=1/(totVb/incVb);
          bulkshear(j,2)=(8*RegVel(j,2))/Dreg(j,2);
          incVb=incVb+1;
       end
   end
end

rowsSVB=size(VbSavg,1);
for j=1:4, %calculate harmonic mean for each segment
       StotVb=0;
       SincVb=1;
       for i=1:rowsSVB,
```

```
        if VbSavg(i,j)>0
        StotVb=StotVb+(1/VbSavg(i,j));
        segvel(j,2)=1/(StotVb/SincVb);
        segshear(j,2)=(8*segvel(j,2))/Dseg(j,2);
        SincVb=SincVb+1;
      end
   end
end

stepshear = zeros(18,2); %output stepwise shear and velocity by zone
zonevel = zeros(18,2); %initialize zonevel matrix
%fill zone column
for i=1:18,
   stepshear(i,1)=i;
   zonevel(i,1)=i;
end

WSbZavg = zeros(pages,18); %matrix of average wall shear per cell by zone
VelbZavg = zeros(pages,18); %matrix of average velocity per cell by zone
for k=1:18, %for each feed zone
for i=1:pages, %go through each cell

      totb1=0;  %boundaries 1 and 2 separately totb* for shear Vtotb* for Velocity
       Vtotb1=0;
       incb1=0;
       totb2=0;
       Vtotb2=0;
       incb2=0;
       for j=1:rows,   %go through each row
          if cellmat(j,13,i)>1000
             if cellmat(j,13,i)==1700
                z1=1;
                z2=7;
             elseif cellmat(j,13,i)==2800
                z1=2;
                z2=8;
             elseif cellmat(j,13,i)==3900
                z1=3;
                z2=9;
             elseif cellmat(j,13,i)==4100
                z1=4;
                z2=10;
             elseif cellmat(j,13,i)==5110
                z1=5;
                z2=11;
```

```
            elseif cellmat(j,13,i)==6120
               z1=6;
               z2=12;
            elseif cellmat(j,13,i)==1316
               z1=13;
               z2=16;
            elseif cellmat(j,13,i)==1417
               z1=14;
               z2=17;
            elseif cellmat(j,13,i)==1518
               z1=15;
               z2=18;
            end
         else
            z1=cellmat(j,13,i);
            z2=cellmat(j,13,i);
         end
         if k==1 || k==2 || k==3 || k==4 || k==5 || k==6 || k==13 || k==14 ||k==15
            if z1==k && cellmat(j,11,i)>0  %for each shear on boundary 1 in the
region, take average only if nonzero
               totb1=totb1+cellmat(j,11,i);
               Vtotb1=Vtotb1+cellmat(j,10,i);
               incb1=incb1+1;
               WSbZavg(i,k)=totb1/incb1;
               VelbZavg(i,k)=Vtotb1/incb1;
            end
         end
         if k==7 || k==8 || k==9 || k==10 || k==11 || k==12 || k==16 || k==17 ||k==18
            if z2==k && cellmat(j,12,i)>0  %for each shear on boundary 2 in the
region, take average only if nonzero
               totb2=totb2+cellmat(j,12,i);
               Vtotb2=Vtotb2+cellmat(j,10,i);
               incb2=incb2+1;
               WSbZavg(i,k)=totb2/incb2;
               VelbZavg(i,k)=Vtotb2/incb2;
            end
         end
      end
   end
end

rowsWS=size(WSbZavg,1);
   for j=1:18, %calculate harmonic mean for each zone
      totWS=0;
      totV=0;
```

```
        incWS=0;
        for i=1:rowsWS,
            if WSbZavg(i,j)>0
            totWS=totWS+(1/WSbZavg(i,j));
            totV=totV+(1/VelbZavg(i,j));
            incWS=incWS+1;
            stepshear(j,2)=1/(totWS/incWS);
            zonevel(j,2)=1/(totV/incWS);
        end
    end
end

%Data output for Database (dboutput)

dboutput = zeros(18,14); %outputs 1)zone 2)region 3)seg 4)f/b 5)regvel
6)regdiam 7)regshear 8)zonevel 9)zoneshear 10)segvel 11)segdiam
12)segshear 13)feeddiam 14)branchdiam

%fill column 1 - zone
for i=1:18,
    dboutput(i,1)=i;
end

%fill column 2 - region
dboutput(1,2)=17;
dboutput(2,2)=28;
dboutput(3,2)=39;
dboutput(4,2)=410;
dboutput(5,2)=511;
dboutput(6,2)=612;
dboutput(7,2)=17;
dboutput(8,2)=28;
dboutput(9,2)=39;
dboutput(10,2)=410;
dboutput(11,2)=511;
dboutput(12,2)=612;
dboutput(13,2)=1316;
dboutput(14,2)=1417;
dboutput(15,2)=1518;
dboutput(16,2)=1316;
dboutput(17,2)=1417;
dboutput(18,2)=1518;

%fill column 3 - segment %1=feed, 2=junction, 3=fc 4=branch
dboutput(1,3)=3;
```

```
dboutput(2,3)=3;
dboutput(3,3)=2;
dboutput(4,3)=2;
dboutput(5,3)=1;
dboutput(6,3)=1;
dboutput(7,3)=3;
dboutput(8,3)=3;
dboutput(9,3)=2;
dboutput(10,3)=2;
dboutput(11,3)=1;
dboutput(12,3)=1;
dboutput(13,3)=2;
dboutput(14,3)=4;
dboutput(15,3)=4;
dboutput(16,3)=2;
dboutput(17,3)=4;
dboutput(18,3)=4;

%fill column 4 - F/B 1=feed, 2=branch

for i=1:18,
   if dboutput(i,3)==4
      dboutput(i,4)=2;
   else
      dboutput(i,4)=1;
   end
end

%fill column 5 - regvel

dboutput(1,5)=RegVel(1,2);
dboutput(2,5)=RegVel(2,2);
dboutput(3,5)=RegVel(3,2);
dboutput(4,5)=RegVel(4,2);
dboutput(5,5)=RegVel(5,2);
dboutput(6,5)=RegVel(6,2);
dboutput(7,5)=RegVel(1,2);
dboutput(8,5)=RegVel(2,2);
dboutput(9,5)=RegVel(3,2);
dboutput(10,5)=RegVel(4,2);
dboutput(11,5)=RegVel(5,2);
dboutput(12,5)=RegVel(6,2);
dboutput(13,5)=RegVel(7,2);
dboutput(14,5)=RegVel(8,2);
dboutput(15,5)=RegVel(9,2);
```

```
dboutput(16,5)=RegVel(7,2);
dboutput(17,5)=RegVel(8,2);
dboutput(18,5)=RegVel(9,2);

%fill column 6 - reg diameter

dboutput(1,6)=Dreg(1,2);
dboutput(2,6)=Dreg(2,2);
dboutput(3,6)=Dreg(3,2);
dboutput(4,6)=Dreg(4,2);
dboutput(5,6)=Dreg(5,2);
dboutput(6,6)=Dreg(6,2);
dboutput(7,6)=Dreg(1,2);
dboutput(8,6)=Dreg(2,2);
dboutput(9,6)=Dreg(3,2);
dboutput(10,6)=Dreg(4,2);
dboutput(11,6)=Dreg(5,2);
dboutput(12,6)=Dreg(6,2);
dboutput(13,6)=Dreg(7,2);
dboutput(14,6)=Dreg(8,2);
dboutput(15,6)=Dreg(9,2);
dboutput(16,6)=Dreg(7,2);
dboutput(17,6)=Dreg(8,2);
dboutput(18,6)=Dreg(9,2);

%fill column 7 - reg shear (bulk shear)

dboutput(1,7)=bulkshear(1,2);
dboutput(2,7)=bulkshear(2,2);
dboutput(3,7)=bulkshear(3,2);
dboutput(4,7)=bulkshear(4,2);
dboutput(5,7)=bulkshear(5,2);
dboutput(6,7)=bulkshear(6,2);
dboutput(7,7)=bulkshear(1,2);
dboutput(8,7)=bulkshear(2,2);
dboutput(9,7)=bulkshear(3,2);
dboutput(10,7)=bulkshear(4,2);
dboutput(11,7)=bulkshear(5,2);
dboutput(12,7)=bulkshear(6,2);
dboutput(13,7)=bulkshear(7,2);
dboutput(14,7)=bulkshear(8,2);
dboutput(15,7)=bulkshear(9,2);
dboutput(16,7)=bulkshear(7,2);
dboutput(17,7)=bulkshear(8,2);
dboutput(18,7)=bulkshear(9,2);
```

```
%fill column 8 - zone velocity

dboutput(1,8)=zonevel(1,2);
dboutput(2,8)=zonevel(2,2);
dboutput(3,8)=zonevel(3,2);
dboutput(4,8)=zonevel(4,2);
dboutput(5,8)=zonevel(5,2);
dboutput(6,8)=zonevel(6,2);
dboutput(7,8)=zonevel(7,2);
dboutput(8,8)=zonevel(8,2);
dboutput(9,8)=zonevel(9,2);
dboutput(10,8)=zonevel(10,2);
dboutput(11,8)=zonevel(11,2);
dboutput(12,8)=zonevel(12,2);
dboutput(13,8)=zonevel(13,2);
dboutput(14,8)=zonevel(14,2);
dboutput(15,8)=zonevel(15,2);
dboutput(16,8)=zonevel(16,2);
dboutput(17,8)=zonevel(17,2);
dboutput(18,8)=zonevel(18,2);

%fill column 9 - zone shear (stepwise shear)

dboutput(1,9)=stepshear(1,2);
dboutput(2,9)=stepshear(2,2);
dboutput(3,9)=stepshear(3,2);
dboutput(4,9)=stepshear(4,2);
dboutput(5,9)=stepshear(5,2);
dboutput(6,9)=stepshear(6,2);
dboutput(7,9)=stepshear(7,2);
dboutput(8,9)=stepshear(8,2);
dboutput(9,9)=stepshear(9,2);
dboutput(10,9)=stepshear(10,2);
dboutput(11,9)=stepshear(11,2);
dboutput(12,9)=stepshear(12,2);
dboutput(13,9)=stepshear(13,2);
dboutput(14,9)=stepshear(14,2);
dboutput(15,9)=stepshear(15,2);
dboutput(16,9)=stepshear(16,2);
dboutput(17,9)=stepshear(17,2);
dboutput(18,9)=stepshear(18,2);

%fill column 10 - Segment velocity
```

```
for i=1:18,
   for j=1:4,
      if dboutput(i,3)==segvel(j,1)
        dboutput(i,10)=segvel(j,2);
      end
   end
end

%fill column 11 - segment diameter

for i=1:18,
   for j=1:4,
      if dboutput(i,3)==Dseg(j,1)
        dboutput(i,11)=Dseg(j,2);
      end
   end
end

%fill column 12 - segment shear (bulk)

for i=1:18,
   for j=1:4,
      if dboutput(i,3)==segshear(j,1)
        dboutput(i,12)=segshear(j,2);
      end
   end
end

%fill column 13 - feed diam and column 14 branch diam

dboutput(:,13)=D;
dboutput(:,14)=d;

excel=ones(L(1),1);
excel=[excel,cellmat(:,:,1)];
for XL=2:cellmax,
   temp=ones(L(1),1);
   temp=temp*XL;
   temp=[temp,cellmat(:,:,XL)];
   excel=[excel;temp];
end

dlmwrite('cellmatrix',excel, ',');
```